

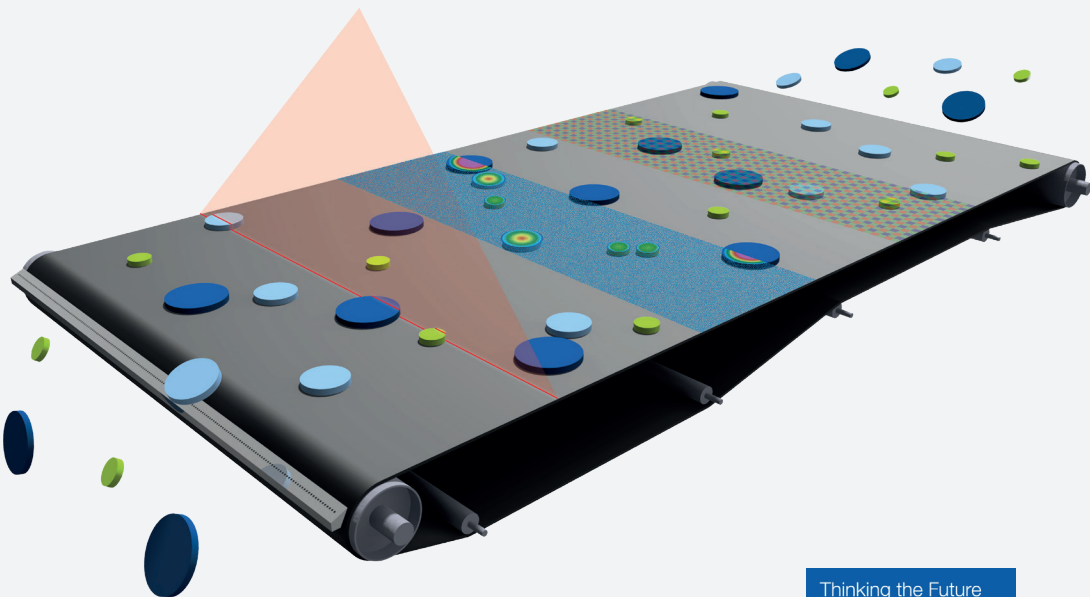


# SBSC 2022

9<sup>th</sup> Sensor-Based Sorting & Control

Kathrin Greiff,  
Hermann Wotruba,  
Alexander Feil,  
Nils Kroell,

Xiaozheng Chen,  
Devrim Gürsel,  
Vincent Merz (eds.)



**Kathrin Greiff, Hermann Wotruba,  
Alexander Feil, Nils Kroell, Xiaozheng Chen,  
Devrim Gürsel, Vincent Merz (eds.)**

**9th Sensor-Based Sorting & Control 2022**

Shaker Verlag  
Aachen 2022

**Bibliographic information published by the Deutsche Nationalbibliothek**

The Deutsche Nationalbibliothek lists this publication in the Deutsche Nationalbibliografie; detailed bibliographic data are available in the Internet at <http://dnb.d-nb.de>.

This book is available under the license CC-BY.  
Creative Commons Attribution 4.0 International License  
(<https://creativecommons.org/licenses/by/4.0/legalcode>)



Printed in Germany.  
Print-ISBN 978-3-8440-8516-7  
PDF-ISBN 978-3-8440-8545-7  
<https://doi.org/10.2370/9783844085457>

Shaker Verlag GmbH • Am Langen Graben 15a • 52353 Düren  
Phone: 0049/2421/99011-0 • Telefax: 0049/2421/99011-9  
Internet: [www.shaker.de](http://www.shaker.de) • e-mail: [info@shaker.de](mailto:info@shaker.de)



**SBSC** 2022

**9<sup>th</sup> Sensor-Based Sorting & Control**  
April 13<sup>th</sup> - 14<sup>th</sup>, 2022, Aachen

**Scientific Direction:**

Prof. Dr. rer. nat. Kathrin Greiff; Prof. Dr.-Ing. Hermann Wotruba; Dr.-Ing. Alexander Feil; Nils Kroell, M. Sc.;  
Dr.-Ing. Xiaozheng Chen; Devrim Gürsel, M. Sc.; and Vincent Merz, M. Sc. (eds.)

A joint conference of Department of Anthropogenic Material Cycles (ANTS) and the Unit of Mineral Processing (AMR) of RWTH Aachen University.  
April 13. – 14., 2022 in Aachen, Germany.



# Preface

---

Dear participants of the SBSC 2022,

A key task for us and future generations will be to use finite resources more mindfully and sustainably. Both in mining and recycling, it is equally important that the efficiencies of processing procedures and chains are improved regarding recovery, yield, and product quality. In the last four decades, sensor technology has provided important development impulses for this in the aforementioned industries as well as in other industries such as the agricultural and food industries and is being used in more and more industrial applications. These developments were presented at the previous SBSC events and intensively discussed among the expert audience.

Developments in processing increasingly complex and larger amounts of data suggest that the current sorting function of sensors in plants can be combined with digital material flow characterization, and sorting performance can be improved in the future. These advancements can be enabled by the interplay of different sensors, the use of digital markers, and the enhanced description options through, for example, machine and deep learning.

A digital description of material flows could make personnel- and cost-intensive physical sampling largely superfluous in the future. Data information can also make processes scalable and thus allow an evidence-based evaluation of processes, which in many cases is not yet possible or only possible at great expense. If relevant input and output variables are measurable in real time, processes could be controlled according to these characteristics, and up- and downstream processes could be evaluated. In this way, considerable optimization potentials can be expected in terms of technical, economic, and ecological aspects.

To better utilize the potentials of sensor technology in the future, more attention must also be paid to the aspect of material flow management. In particular, the difficult handling of non-bulk materials requires technical innovations to achieve improved sorting results. However, once the challenges of material flow management and sensor-based material flow characterization have been solved, the already great

importance of sensor technology in the process plants of a then more sustainable industry will continue to increase, that seems certain.

These and other topics will await us at SBSC 2022. We look forward to exchanging ideas with you again after a break of four years!

Hermann Wotruba, Kathrin Greiff, Alexander Feil, Nils Kroell,  
Xiaozheng Chen, Devrim Gürsel, and Vincent Merz

# Content

---

<b>Preface</b> . . . . .	<b>.5</b>
<b>Content</b> . . . . .	<b>.7</b>
<b>Circular Economy Empowered by Data</b> . . . . .	<b>11</b>
Johannes Jacoby, Christian Korsten, Felix Flemming	
<b>Relevance and challenges of plant control in the pre-processing stage for enhanced sorting performance</b> . . . . .	<b>17</b>
Bastian Küppers, Sabine Schlögl, Nils Kroell, Verena Radkohl	
<b>Assessment of sensor-based sorting performance for light-weight packaging waste through sensor-based material flow monitoring: Concept and preliminary results</b> . . . . .	<b>35</b>
Nils Kroell, Tobias Dietl, Abtin Maghmoumi, Xiaozheng Chen, Bastian Küppers, Alexander Feil, Kathrin Greiff	
<b>Quantifying the Delabelling Performance using Sensor-based Material Flow Monitoring</b> . . . . .	<b>55</b>
Sabine Schlögl, Bastian Küppers	
<b>Challenges faced during a near-infrared-based material flow characterization study of commercial and industrial waste</b> . . . . .	<b>71</b>
Kerstin Kleinhans, Bastian Küppers, Juan Carlos Hernández Parrodi, Kim Ragaert, Jo Dewulf, Steven De Meester	
<b>Increase throughput and sorting quality with flow control</b> . . . . .	<b>85</b>
Stefan Heinrichs, Raphael Stein, Andreas Roper Yearwood, Nico Schmalbein	
<b>Sensor-based sorting and the Circular Economy</b> . . . . .	<b>99</b>
Mathilde Robben, Daniel Swaab, Jens-Michael Bergmann	
<b>Sorting of Construction and Demolition Waste for coarse fractions</b>	<b>105</b>
Sebastian Müller, Anette Müller, Ines Döring, Ulrich Palzer	



<b>Systematic Determination of the Influence of Factors Relevant to Operating Costs of Sensor-based Sorting Systems . . . . .</b>	<b>113</b>
Jan Ludwig, Merle Flitter, Georg Maier, Albert Bauer, Marcel Reith-Braun, Robin Gruna, Harald Kruggel-Emden, Thomas Längle, Jürgen Beyerer	
<b>SenSoRe: A sensor-based testbed for sorting and innovative recycling . . . . .</b>	<b>133</b>
Louise Hagesjö, Méline Gilbert Gatty, David Malmström, Jonas Petersson	
<b>Latency evaluation of an FPGA-based sorting system . . . . .</b>	<b>143</b>
Simon Wezstein, Michael Stelzl, Michael Heizmann	
<b>Material Value Estimation for Recycling of Waste Printed Circuit Boards (WPCBs) by a Deep-Learning-assisted Approach on X-Ray Images . . . . .</b>	<b>161</b>
Markus Firsching, Steffen Rürger, Wladislaw Benner, Malte Vogelgesang, Alexander Ennen	
<b>Artificial Intelligence-based Particle Size Prediction for Solid Waste Particles . . . . .</b>	<b>179</b>
Lisa Kandlbauer, Karim Khodier, Renato Sarc	
<b>INSTAnT</b>	
<b>Innovative sensor technology for optimised material recovery from bottom ash treatment . . . . .</b>	<b>187</b>
Liesbeth Horckmans, Roeland Geurts, Wenzhi Liao, Kris Broos, Karen De Boeck, Auriane De Coster, Peter Segers, Denis Van Loo, Kay Johnen, Alexander Feil, Lisa Höflechner	
<b>Deep-Learning-based Aluminum Sorting on Dual Energy X-Ray Transmission Data . . . . .</b>	<b>199</b>
Steffen Rürger, Jann Goschenhofer, Ayush Nath, Markus Firsching, Alexander Ennen, Bernd Bischl	
<b>Rapid GEOSCAN fully penetrative analysis enabling bulk diversion . . . . .</b>	<b>219</b>
Luke Balzan, Henry Kurth	
<b>The impact of mixing and scale on the bulk ore sorting potential of a panel cave mine . . . . .</b>	<b>235</b>
Mahir Can Cetin, Bern Klein, Stefan Nadolski	

**Mineral process sampling and analysis using X-ray computed tomography – a feasibility test results on cassiterite ore. . . . 237**

Christopher Robben, Pedro Condori, Gerhard Zacher, Andreas Staude,  
Aysa Moslemiyekan, Kim Esbensen

**New Protocols for Pre-Concentration Sampling and Testing . . . . 253**

Bob McCarthy, Adrian Dance

**Laser sensors enable robotic sorting for tool alloys recycling. . . . 273**

Cord Fricke-Begemann, Frederik Schreckenber, Martin Geisler,  
Michaela Lindemann

**Importance of Sensor Based Sorting to Sound Metals Recycling . 281**

Shuji Owada

**Sorting of post-consumer aluminium scrap using Laser-Induced Breakdown Spectroscopy (LIBS) and machine learning . . . . 291**

Simon Van den Eynde, Dillam Jossue Diaz-Romero, Bart Engelen,  
Alexander Eckert, Luc Waignein, Jörn Vandewalle, Isiah Zaplana, Jef Peeters



# Circular Economy Empowered by Data

Johannes Jacoby<sup>1\*</sup>, Christian Korsten<sup>2</sup>, Felix Flemming<sup>3</sup>

<sup>1</sup>TOMRA Sorting GmbH, TOMRA Recycling, Mülheim-Kärlich, Germany

<sup>2</sup>TOMRA Sorting GmbH, TOMRA Mining, Wedel, Germany

<sup>3</sup>TOMRA Sorting GmbH, TOMRA Sorting Digital, Mülheim-Kärlich, Germany

\* Corresponding Author: Otto-Hahn-Straße 2-6, 56218 Mülheim-Kärlich, Germany,  
Johannes.Jacoby@tomra.com

---

Keywords: Sensor-based Sorting, Digitalization, Data, Circular Economy, Performance Optimization, Sustainability

## Abstract

With the demand for more sustainability in the mining and in the waste and metal recycling industry, process operators are searching for possibilities to improve efficiencies and sorting purity. Sensor-based sorters have been playing a key role in the automation of those industries for the last 20 years. However, in terms of connectivity and digitalization it is still in its early phase. By embracing technology and digitalizing processes, the recycling and mining industry can improve its effectiveness by monitoring input, removing unwanted material, and improving sorting output.

Already today these sensor-based sorters generate a vast amount of data about the scanned material that is not yet used to its full potential, thus, connectivity and digitalization are identified as key part of the solution. Additionally, new sensors and technologies such as camera-based deep learning provide solutions for unsolved sorting problems, as well as data sources with new levels of details. The available data will have a positive impact on the performance of individual machines, overall processes, and the whole value chain. Improved data transparency will be key to establish a functioning market for recyclates and plastic waste feedstock. It will

also help operators of mines to improve their sustainability by transparently and continuously monitoring the quality of the retrieved material and thereby optimize the mining operation further.

In the future, large groups of digitally connected machines will communicate and report production data across the value-chain and the globe. Leveraging collected data and advanced analytics, new sorting technologies and processes will be developed to improve sorting efficiency and boost final material recovery and purity positively impacting the sustainability of the mining and recycling industry.

## **1 Introduction**

Today's recycling and mining industries consist of complex processes where the optimal operation relies heavily on experience. While the feedstock coming from the mine is more consistent in particle size and material composition, the feedstock into a typical waste sorting plant varies strongly and in a stochastic manner. Optimizing such complex processes requires typically a three-step approach.

First, one needs to visualize the current operation. While in classical process automation scheme, this means certain process quantities, like pressures, temperatures, or motor speeds, in a recycling application the added complexity of the material composition needs to be considered. For mining applications, the grade or particle size distribution of the material might be of interest. In this step, the data collection already needs to start, as it builds the fundament for the final step.

Second, once the process is visualized and monitored, one can start to stabilize the process. In this step, the basic understanding of different relations between various quantities will become evident. Process anomalies can be detected and will be handled.

Only when the process runs stable, the third and final step can be addressed. In this step, the process will be optimized based on the previously collected process information and machine data. System control Algorithms will be able to close feedback loops and optimize the overall operation of the process. With this final step, the experience of the operators is not replaced, but enriched by data driven approaches.

The above-described steps are required, regardless, if the optimization of an individual machine, a whole process, or even the full value chain is considered. Obviously, the complexity increases as the number of elements or parties involved increases, but without transparency one will not arrive at a stable operation and without a stable operation, the optimization of the whole will be out of reach. Digitalization is the key enabler of such optimizations, and the sensor-based sorter is the major source of data providing detailed information on the material being processed, in the mining and recycling industry.

## **2 Optimize Sorter Performance**

As one of the main value drivers in the sorting process, the optimal performance of each individual sorter is essential. Considering the sorter itself, topics like a reduction of downtime by predicting maintenance needs will optimize the sorters availability (TOMRA, 2020). Improving the sorting performance itself, by utilizing the data obtained from a second sorter that runs in a sequence, or by additional sensor technology, e.g., cameras combined with image recognition based on deep learning methods as feedback mechanism, provides already a big potential due to the variability of the input material (Streifinger et al., 2022).

Already today, the existing sorters in the process can serve as data sources. While they were originally not design to act as such, it is only little effort, to extend their capabilities and make the data available. A digital twin of the sorter can already enable the prediction of anomalies and thereby add further value beyond the sorting itself.

## **3 Optimize Process Performance**

Considering now, that data from multiple sorters within the process is available, one can start to combine this information and optimize the performance of the whole process, across the different sorters. This requires communication to be established between the different elements in the process, first and foremost the sorters. They act as both, active element, separating the material, and as a sensor providing information on the material going through the process. Whatever the target function might be, a certain purity of the sorted product, or a desired throughput through the process, one can now start to have self-optimizing and adaptive processes.

The output becomes stable and predictable in quantity and quality, despite the fact, that the input material is fluctuating in its composition. It is an extension of the optimization of the individual sorter described before, as now in the combination of multiple sorters, the complexity but also the flexibility increases.

## **4 Optimization of the Value Chain**

Focusing on the recycling of plastic, there is only about 2% of material in a closed loop today (Ellen MacArthur Foundation, 2017). Most of the virgin plastic produced and used every year ends up either in the environment, in landfills, or in incineration. Yet, the consumers increase their pressure onto the big consumer brands, as the public awareness rises, combined with legislation, which enforces higher recycling rates (ReSociety, 2021) (EU Directive, 2018). The challenge we observe today, is a lack of transparency. It is unclear how much material of what quality is available where. It goes back again to the first step described earlier – Visualize. Today, there is only very limited information available, which for sure is not sufficient to close the loop for more material (ReSociety, 2021).

Data will help in this picture. Not from just one sensor-based sorter, but from all sensor-based sorters. Imagining all this information on material quantities, but also reliable qualities would be available, one could establish a stable supply and demand relationship, connecting the recycling industry with the virgin plastic producers to use more recyclates instead of virgin material. This data on product quantity and quality is generated continuously in a fully automated process, without the need for manual samples being considered representative for the full batch. It will generate trust and is the basis for a stable production.

Once such transparency on data is available, a stable market for recyclates can be established and the value chain will start to optimize itself. The recycling process can be optimized based on short term market needs and provide the right quality at the right time for the following process steps like compounding. Waste collection could be optimized in such a way to provide the right infeed material at the right time. Communities get quantifiable feedback on how to improve the sorting at the source. Alternatively, one could also imagine that the recycling process adopts itself much faster to the incoming material composition.

## 5 Conclusion

Considering sensor-based sorters not only as sorting devices in the mining or recycling process, but as valuable data sources, there are plenty of opportunities to optimize the sorter itself, the process around it, but also the full value chain. In this sense, data transparency becomes a fundamental requirement to change our linear economy to a circular economy. Digitalization is the technology to make data available, which in turn empowers the circular economy.

## References

- TOMRA (2020) Digitalization – Connect to Enhance Productivity in the Recycling Industry, <https://solutions.tomra.com/digitalization-ebook>
- Streifinger, F., Flemming, F., & Sama, V. (2022) *KI besitzt großes Potential für die Sortierung von Lebensmittelverpackungen*, Kunststoffe, 01/2022, Carl Hanser Verlag
- Ellen MacArthur Foundation (2017) *The New Plastics Economy*, p. 27, <https://ellenmacarthurfoundation.org/the-new-plastics-economy-rethinking-the-future-of-plastics>
- ReSociety (2021) *Holistic Resource Systems*, <https://www.resociety.net/browse-white-papers/holistic-resource-systems>
- EUDirective2018/852(2018), Official Journal of the European Union, p.147 <https://eur-lex.europa.eu/legal-content/EN/TXT/PDF/?uri=CELEX:32018L0852&from=DE>





# **Relevance and challenges of plant control in the pre-processing stage for enhanced sorting performance**

Bastian Küppers<sup>1\*</sup>, Sabine Schlögl<sup>2</sup>, Nils Kroell<sup>3</sup>, Verena Radkohl<sup>1</sup>

<sup>1</sup>STADLER Anlagenbau GmbH, Altshausen, Germany

<sup>2</sup>Montanuniversität Leoben, Chair of Waste Processing Technology and Waste Management (AVAW), Leoben, Austria

<sup>3</sup>RWTH Aachen University, Department of Anthropogenic Material Cycles (ANTS), Aachen, Germany

\*Corresponding Author: Humboldtstraße 11, 46236 Bottrop, Germany, [bastian.kueppers@w-stadler.de](mailto:bastian.kueppers@w-stadler.de)

---

Keywords: sensor-based material flow monitoring, plant control, sorting performance

## **Abstract**

To increase recycling rates many technological improvements can be made within sorting (processing and sorting on article basis) and recycling (processing and sorting on particle basis) of waste. This paper discusses such technological improvements, focussing on the potential of pre-processing (pre-shredding, screening, air and ballistic separation) in sorting plants. For this purpose, the general structure of state-of-the-art sorting plants is briefly introduced.

Material flow characteristics such as input material composition or volume flow, have high impact on the performance of such sorting plants and are discussed accordingly. By adjusting parameters such as shredder speeds or screen cuts, these characteristics can be set to adjust the plant in accordance with variations in the input material. Such adaptations can only be made if the material flow data is reliable and available in nearly real-time (e.g., through built-in sensors). The related challenges in data acquisition, data analysis, and plant control are discussed.

Finally, a case study is presented to demonstrate the potential of adaptive plant control: Through data derived from near-infrared sensors the load of two processing

lines could be adjusted, resulting in significantly increased plant performance: Yield of product fractions from 3D-/heavy processing lines could be increased by 3-15 wt%.

## 1 Introduction

Member states of the European Union have implemented different collection and recycling systems for various types of packaging wastes to achieve environmental benefits through (a) minimizing/avoiding littering and landfilling of packaging wastes and (b) substituting primary raw materials with the obtained recyclates from recycling. Compared to other end-of-life options such as incineration, mechanical recycling of packaging waste is advantageous because of the achieved energy savings and reduced greenhouse gas emissions. (European Union, 2018; Ragaert et al., 2017; Perugini et al., 2005; Astrup et al., 2009)

Since (mechanical) recycling of packaging wastes is environmentally advantageous, a higher material recirculation is encouraged on a political level (Circular Economy Action Plan; Packaging and Packaging Waste Directive). For example, the new EU Packaging Directive is being discussed, which is demanded to include requirements for minimum recycling contents of 30 wt% for plastic packaging by Plastics Europe. (Grüner Punkt; 2021)

State-of-the-art material recirculation of packaging materials is achieved in three steps: (i) collection of packaging wastes, (ii) pre-sorting (production of pre-concentrates on an article basis), and (iii) recycling (washing, sorting, and processing into a product – mostly on particle/flake basis), see Fig. 1. Type, extend and performance of each step, from waste collection over pre-sorting up to recycling, is highly relevant for maximising the recycling of valuable materials, i.e., keeping more packaging in closed material cycles.



Fig. 1: Relevance of collection-, pre-sorting and recycling-performance (80% exemplary performance) for the overall achieved recycling performance

As can be seen in Fig. 1, each step, from collection to recycling, contributes to the overall recycling quota, resulting in approximately 50% recycling rate for any article, if the performance of each step is 80%. According to the Pareto principle, each of the three steps should be improved equally, to achieve maximum improvement of overall recycling rate. Such overall improvements in the value chain inhibit the increased losses in certain steps, that cannot be regained through improvements in downstream steps (e.g., in the recycling process).

In case of the collection of waste this can be particularly achieved by political/organisational measures, e.g., by introducing a deposit system for a certain packaging, through the provision of dustbins in public places to prevent littering or encouraging optimized waste separation through public campaigns.

Pre-sorting and recycling performance are mostly driven by technological improvements. However, certain aspects such as quality control of product fractions are to this day often handled manually. (Kranert et al., 2017)

In the past, most technological advances in pre-sorting have been made through improvements and expansions in sensor-based sorting (SBS) cascades, as increased processing power of computers allowed for more sophisticated sorting algorithms, resulting in improved performances of optical sorting machinery—primarily near-infrared (NIR)-based sorters for the sorting of (plastic) packaging wastes.

However, all sorting machinery, in particular optical sorters, require an even material feed, ideally with a limited particle size ratio (ratio of maximum to minimum particle size). Therefore, comprehensive pre-processing of collected waste is of utmost importance to achieve high pre-sorting performance in waste sorting plants. (Feil et al., 2018; Feil et al., 2019 Feil et al., 2021)

In the present paper, the overall design of such a sorting plant is explained to discuss various parameters that can be adjusted in pre-processing, allowing for increased sorting performance of downstream processing lines that are mostly comprised of (optical) sorting machinery. Subsequently, the potential and challenges of using sensors for adjustments in the pre-processing of waste is discussed, ending with an example of sensor-based adaptive plant control in pre-processing, resulting in improved sorting performance of downstream sorting technology.

## 2 Structure of sorting plants

In most sorting plants, the input waste is delivered to an input storage. This can comprise of, e.g., simple boxes made of concrete blocks or underground bunkers. From here the input material is fed to the sorting plant by means of wheel loaders, cranes, or with similar machinery. The sorting system itself can be divided in two sections: (i) pre-processing stage and (ii) sorting stage (Feil et al., 2021).

In pre-processing, the waste stream is treated to allow for optimal sorting of valuables, residues, and impurities in downstream sorting lines. For this purpose, mostly pre-shredders (this also includes bag/bale openers), sieves, air classifiers, and ballistic separators are utilised.

- **Pre-shredding** allows for opening of bales, breaking up agglomerates and clamped materials, limitation of maximum particle size, and selective shredding for material enrichment in different particle size fractions. Additionally, pre-shredders dose the material to the sorting plant, creating a material stream, potentially displaying fluctuations. In sorting plants of lightweight packaging wastes (LWP), most often bag openers are installed.
- Most often the pre-shredder is followed by one or multiple **sieving stages**. In LWP sorting plants, most often drum screens are utilised for screen cuts of approx.  $\geq 40$  mm. Depending on the size of such plants, about four screen cuts must be implemented through drum screens in the screening stage. Finer screen cuts (about 20 mm) are usually implemented as vibratory sieves. Despite the separation of oversize and fine impurities the screen cuts are chosen to enrich certain materials in specific particle size ranges (to capitalise on the selective shredding, up-stream) and to create material flows with sizes that fit to the processing lines that follow the screening stage. Additionally, the performance of down-stream machinery is optimal when limited particle size ratios (1:3 to 1:4) are present in all processing lines (Feil et al., 2021).
- Often **air classifiers** are positioned as the first processing units in the processing lines after the screening stage, while **ballistic separators** are implemented afterwards (Kleinhans et al., 2020). In such cases, the air classifiers are used to produce relatively clean film/2D/light fractions, while the ballistic separators must ensure high purities in the 3D/heavy fractions,

potentially also serving as an additional screening stage, depending on the chosen paddle mesh. Nonetheless, both machine types can also be used separately from each other, always with the goal of separating 2D/light and 3D/heavy fractions (Möllnitz et al., 2020). This enriches valuable materials in both fractions and reduces the volume of 3D material flows additionally, allowing for increased throughput rate and performance in the 3D processing lines as the 2D material is reduced. Valuable fractions in the 3D lines are ferrous and non-ferrous metals as well as various plastic fractions and beverage carton.

In each processing line of the sorting stage, several sorting machines are implemented, usually after air classification. Those units are characterised by the fact that they separate specific material types, in contrast to pre-processing units mentioned above, which prepare (at most enrich) certain material. Sorting machines and their primary products are:

- Magnets – Production of ferrous product;
- Eddy current separators – Production of non-ferrous metal product;
- Optical sorters (predominantly NIR- but also induction- and colour- based sensors) – Production of pre-products such as PP, PE, PET, PS, beverage carton, Paper, RDF. (Kleinhans et al., 2020)

Such sorting machines (mostly optical sorters) can also be used as cleaners, further enriching the respective product fractions created beforehand to reach increased product qualities. Other optical sorters are used as scavengers, obtaining valuables from residue streams that were lost by upstream sorting units. Sorting machinery, that is used to create a product fraction out of a mixed material stream are defined as roughers. (Feil et al., 2021)

Many product streams undergo manual quality control during which valuable materials are recirculated to the process, while residues can be specifically passed to the residues fraction.

## 2.1 Relevance of material flow characteristics for plant performance

To adjust a sorting plant a multitude of parameters can be set, depending on the combination/design of processing stages/machinery used within a process. The available parameters can be set to affect the following main material flow characteristics:

- The **material composition** highly affects the performance of any processing unit, as the behaviour of any particle type differentiates in any pre-processing unit. For example, films are much more prone to remaining at its particle size during pre-shredding and tends more to be pulled through a screen mesh. Additionally, the likelihood to be entrained into any product of a sorting machine is substantially higher than for heavy three-dimensional particles. Accordingly, the adjustment of any material composition bears high potential for alterations in machine performance. (Küppers, Schlögl, et al., 2020; Küppers, Seidler, et al., 2020)
- The **particle size range** affects the performance of any processing and sorting machine. While, e.g., high amounts of very fine material in an otherwise rather coarse material stream, compared to the screen cut, improve the performance of screens (such particles are much more prone to pass the mesh immediately), especially for sensor-based sorting these fines often result in reduced yield and/or purity, thus reduced sorting performance. If such fines are magnetic, these particles can hardly be removed by an over belt magnet, while they tend to remain in an eddy current field, where they cannot only hinder the discharge of non-ferrous metals but also constitute a risk to the durability of this machine type.
- The **volume flow** constitutes one of the most important factors for the dimensioning of shredders, sieves, air classifiers, magnet separators, and eddy current separators. Accordingly, the adjustment of this characteristic in any plant and processing line allows for manipulation of machine and plant specific performance adaption (Curtis et al., 2020). The volume flow can be tied to other characteristics, as the input composition: If, e.g., the bulk density of the input is reduced, due to a change in material composition (e.g., higher share of film), this causes an increased input volume flow, which in turn reduces, the performance of built-in sieves, as those machines are designed for specific volume flows. Such a sieving performance reduction can result

in shifts of the volume flow in all downstream processing lines, evoking the performance of all processing machines to change.

- The **area flow** is defined as the flow of projected object area as seen by a sensor, mounted over a conveyor belt. This characteristic is mostly important for optical sorters as classification and thus separation performance is highly dependent of the size of the specific area flow (Curtis et al., 2020). Ideally, the occupation density (area on a belt that is occupied by material) does not exceed 30 area-%. The higher the occupation density (and the closely linked area flow), the lower the performance (yield and product purity) of any optical sorter in most cases (Küppers, Schlögl, et al., 2020; Küppers, Seidler, et al., 2020; Kroell et al., 2022). This is due to the increased probability of false classification of objects and the resulting reduced sorting performance that persists at increased occupation densities.

## **2.2 High-impact parameters in sorting plants**

In sorting plants, several parameters can be adjusted to improve the performance of such a plant. In general, the significance of these parameters is linked to the point in the processing line, where they can be set. The earlier this can happen, the higher the impact on the whole processing line is as all downstream machinery is affected by such parameters. Additionally, changes (positive or negative) in such parameters multiply with each machine, since the reduced or increased performance of each unit negatively or positively affects the performance of the following one. Hereafter, several of potential high-impact parameters are described.

- **Composition of input material.** As single plants are often fed with materials from several collection systems, the input composition can vary strongly, e.g., from day to day or from shift to shift. Each processing plant is designed for a specific input composition. Limited fluctuations can occur while the full functionality of the plant is still ensured. However, extreme fluctuations in the input composition can affect the performance of single machines, processing lines or of the whole plant. Accordingly, mixing two input materials of different compositions can allow for improved plant performance, while processing of such input materials separately might inhibit reaching a plants full potential.



- Rotational speed in pre-shredders. Pre-shredders have several parameters like size of the discharge grate, speed of crushing tools or interval size for changes in direction of crushing tools. If the crushing tools are located on several shafts the speed and interval changes might be controlled independently from each other to allow not only for the right amount of particle reduction but also generating reduced volume flow fluctuations (Feil et al., 2019).
- Screen cuts. In sieves, the selected screen cut is the most obvious parameter for plant control. Despite its obvious purposes (creating material streams with specified particle size ranges, and enrichment of certain material fractions) the most important function of a screen is the split of the in going volume flow into output streams that have the right size for downstream processing lines and built-in sorting machinery. By using a progressive mesh size and splitting the resulting sieve underflow in accordance with the dimensions of downstream processing lines a suitable volume flow split can be achieved. In a multitude of LWP sorting plants movable, bi-directional belts are positioned under drum screens, allowing for this adjustment of the screen cut.
- Air flow in air classifiers. The selected air flow significantly affects the selectivity of air classifiers. Depending on the air flow the material composition and the correlating bulk density in light and heavy fraction are manipulated significantly (Pretz et al., 2020). This way the load on processing lines for light and heavy material is adjusted, as both, volume and area flow, are affected likewise. Regarding the material composition in light and heavy processing lines, this results in changes regarding the share of film and 3D plastics in each line. Borderline objects, like food trays that are characterised by properties which can be associated with light *and* heavy fraction objects (e.g., trays for cheese packaging that contain a film-like lid). Those are shifted from one output fraction to another, when resetting the parameter “air flow” in an air classifier.
- Paddle angle in ballistic separators. The parameter “paddle angle” affects the selectivity of ballistic separators similarly to the air flow in air classifiers. However, the underlying mechanisms of a ballistic separator are different to those of an air classifier. Contrary to popular belief, ballistic separators not only split two-dimensional from three-dimensional objects. Additionally, to the shape of an object the ductility, flexibility, elasticity, and weight of an object affects the separation into the 2D or 3D fraction. On ballistic separators,

typical borderline objects are foams (from mattresses), beverage cartons, and cardboard boxes. The steeper the paddle angle, the more of the incoming material flow is yielded into the 3D fraction and vice versa.

The potential of the afore mentioned parameters is often not capitalised on by many plant operators. This is due to the high complexity modern sorting plants exhibit. Accordingly, most plants constitute a black box and only a limited number of parameters is controlled manually (e.g., rotational speed of the shredder for throughput adjustment). Automated plant adaptations could exploit such unused potentials if their control could be monitored in near-real time and assessed adequately.

### **3 Challenges in plant control**

As described above, the adjustment of parameters bears high potential for continuous plant optimisation. However, several challenges must be overcome to enable an automated plant control. These challenges are related to

- the sensors used to obtain material flow and machinery data,
- the process control algorithm that is used to transform the data into an automated response (parameter adaptation), and
- the actuators, directly affecting the operating principle of a pre-processing or sorting machine. (Khodier et al., 2019)

The reliability of data derived from a sensor is dependent on (i) the type of measurand (e.g., volume, area, material composition), (ii) the machine that is controlled, (iii) the desired effect that is to be attained, and (iv) its overall validity. The type of measurand derived from a sensor (e.g., volume flow) is relevant as it may be used to adjust the respective volume flow dependent parameter (e.g., screen cut). However, this parameter might be set with the aim to change a different target value (e.g., area flow) that is more relevant for the performance of downstream optical sorters. Accordingly, the basic information that can be derived from sensor data must at least correlate with the target value (in this case the area flow). An example for such a correlation is given in Fig. 2., displaying volume and occupation density (or area flow) at the same position in a process line for light weight packaging sorting.

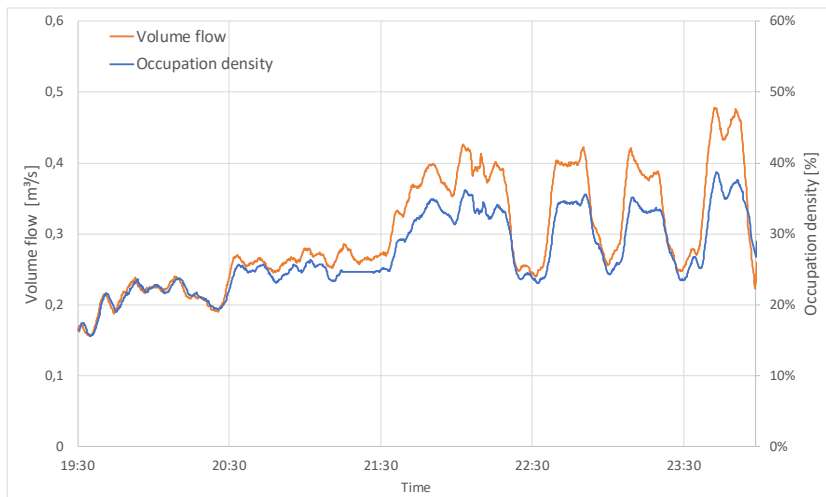


*Fig. 2: Comparison between occupation density (strongly correlated with area flow) and volume flow on a belt conveyor*

As depicted in Fig. 2., a high correlation between occupation density and volume flow can be observed. However, the extent of changes in one measurand is not directly transferable to the other one. For this case, one can expect that the correlation between both measurands is sufficient as long as the occupation density is low enough to keep object overlay to a minimum when comparing data before 21:30 with data after this point in time. Additionally, changes in the input composition might lead to a change in the proportion of occupation density to volume flow. How strong and how stable the correlation between measurand and target value must be, must be decided on a case-by-case basis. Ideally, the measurand type directly complies with the target value and correlation is strong. The overall validity of a measurand is dependent on the suitability for the application (a certain NIR-sensor may be ideally suited for assessing the share of paper in a material stream but not for differentiation of plastic types), on the quality/versatility of the sensor itself but also on the environmental conditions. For example, in a dusty environment a volume flow sensor that is less precise but generates more stable data is better suited for volume flow monitoring than a very precise sensor that is strongly affected by a dusty environment. Especially in the waste/recycling sector this can entail case specific selection of different sensors for similar or even identical tasks.

The algorithms used for process control include the raw data pre-processing (deriving usable data from detected signals – for NIR-sensors this might result in normalization, smoothing and deriving the raw data). The resulting compressed data, in form of, e.g., false colour pixels, volumetric information, can then be further processed, to compensate for systematic misidentifications, handling error values, or weighting the data stream (e.g., transforming a pixel-related sensor measurements into mass-based material flow characteristics [Kroell et al., 2021] or emphasizing certain material classes). Additionally, volumetric and areal information can be used to allow for object recognition which can strongly impair or improve the validity of data, depending on the circumstances (material presentation to the sensor, material characteristics, etc.) and algorithm. Obviously, the utilisation of sensor data from built-in optical sorters represents an attractive opportunity to capitalise on data that is otherwise used for sorting purposes only. Here the problem is, that the main focus of the algorithms in such sorting machines is correct classification and separation of eject and reject material. This does not mean, that the data generated throughout this process is reliable for the monitoring and assessment of a material stream.

With this pre-processed data the actual control algorithm can be realized, e.g., based on threshold transgression, steady adjustment of the measurand allowing for maximal approximation to a target value, or alike. The timeframe in which such adaptations must be induced by the algorithm must be tailored to the application at hand. For example, screen cut changes in an upstream sieve every second based on strongly fluctuating data that is received by the sensor 30 seconds afterwards, cannot be used effectively. Accordingly, moving averages could be applied to smoothen the highly fluctuating volume data and adequate control cycle times would allow for sensible screen cut adaptations.

Despite the aforementioned three main challenges, a comprehensive understanding regarding interdependencies of parameters, target values, and machine requirements for optimal performance are imperative to implement any form of adaptive plant control. Additionally, the costs of any adaptive plant control and its impact/potential must be appropriately interrelated.

## 4 Case study on adaptive screen cut control

In the following, we present preliminary results from a case study on adaptive screen cut control in a LWP sorting plant. Sensor-based area flow control was implemented in the mid-coarse and mid-fine processing lines during regular operation time. Access to the sorting plant for these trials was provided by the company PreZero.

For data acquisition, two hyperspectral-imaging NIR-sensors (Helios EQ32 [EVK Kerschhagl GmbH; Raaba, Austria]) operating in the wavelength range of about 1050 nm to 1.700 nm were utilized. Each NIR-sensors measures one acceleration of a sensor-based unit for sorting out beverage cartons in the (i) mid-coarse and (ii) mid-fine processing line, respectively, i.e., the pre-conditioned material flows after air classification and ferrous separation. Based on the classified NIR-data (false-colors) the occupation density, i.e., the area share of the acceleration belt that is occupied with material is calculated, which is directly linked to the area flow (occupied area per time unit).

The movable belt under the drum screen (Fig. 3) was adjusted to various positions to assess the effect of this parameter with regard to the split of the area flow optimally between the mid-coarse and mid-fine processing line. The area flow was chosen as the evaluation criterion, as both processing lines were mostly equipped with optical sorters which in turn classify the material stream based on areal information. Accordingly, the parameter to be adjusted is the screen cut, while the correlating target values are the occupation densities (or area flows) in the downstream processing lines. The chosen belt positions for screen cut adjustments are shown in Fig. 3.

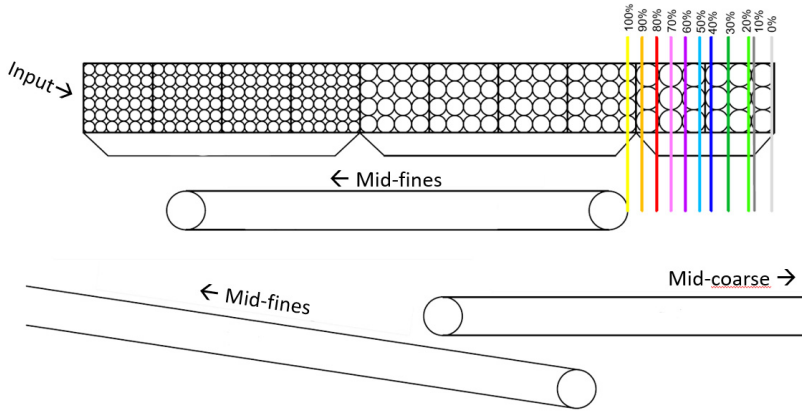


Fig. 3: Positions of moveable conveyor under drum screen for screen cut adaptation between mid-coarse and mid-fines

The occupation density, as monitored by the NIR-sensors, at each position is displayed in Fig. 4. The boxplots (divided in quartiles) illustrate the occupation density fluctuations in each line.

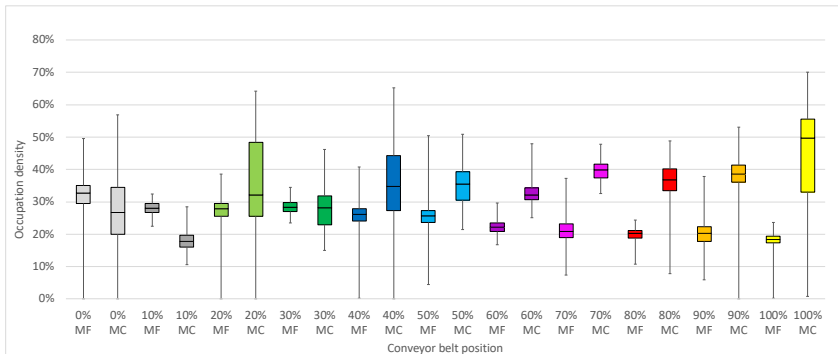


Fig. 4: Occupation density in mid-fine (MF) and mid-coarse (MC) lines in dependence of conveyor belt position (positions in Fig. 3 are colour coded accordingly)

One can see that the occupation densities on both lines differ strongly (on average by 31% - MC: 50% and MF: 19%) difference at conveyor belt position 100%, while the equilibrium (at about 29%) is reached at movable conveyor position 30%. Between positions 100% and 70% no significant change with regard to the occupation densities can be recorded. From positions 70% to 40%, however, noticeable convergence of the occupation densities in both lines (40%→35% in mid-coarse and 21%→27%) can be observed. A steady but slow convergence to equilibrium can be noted between 50% and 20-30% position. Below 20% the occupation densities diverge noticeably.

To assess the impact of this parameter (screen cut) the yield of several product fractions in the heavy line of the plant was measured at position 100% for one month and compared to the yield of those product fractions, when operating at 20% position for one month. Results show significantly improved yield (3 wt% to 15 wt%) for the product fractions generated from the heavy/3D material flows, produced at the 20% position compared to the yield at the 100% position.

Both test phases were conducted in summer, to reduce the effect of changing humidity during these months. However, since the depicted trials were conducted during normal operation of the plant certain external effects (changes in input composition, holiday season, etc.) cannot be fully excluded. During these test months changes were made in the 2D/light processing lines, which is, why neither improvements nor a decline in those processing lines can be traced back to these changes. Nonetheless, it is reasonable to hypothesise that similar effects can be expected in the 2D/light processing lines if the material distribution of these material streams changed equivalently.

It may be assumed that a near real-time adaptive screen cut control would allow even higher improvements in plant performance, as temporal fluctuations could be potentially compensated. Nonetheless, such a control circuit poses a complex challenge in which not only two processing lines of a sorting plant must be observed but rather the effect on all output fractions (yield and purity) should be part of such a function. This is because the focus (purity vs. yield) regarding the sorting algorithms in all optical sorters highly affects what is affected by an adapted screen cut. A fixed prediction regarding the benefit for a process flow can barely be made in advance. Especially as the preceding operation of any plant leaves only a certain potential for improvement.

## **5 Conclusion**

In this paper, the potential and challenges in adaptive plant control for waste sorting plants was discussed. While a multitude of parameters in several pre-processing and sorting machines can be adapted, overlooked high-impact parameters seem to be located in the pre-processing stage of a sorting plant. The accurate adaptation of a sorting plant based on sensor data is subject to the stability and accuracy of sensors and process control algorithm. Prerequisite to all efforts regarding adaptive plant control is comprehensive knowledge regarding the quantitative influence such parameters have for all process lines in a processing plant.

The potential of one high-impact parameter was shown by a case study on adaptive screen cut control. Two NIR-sensors were applied to assess the area flows in two parallel processing lines by means of the detected occupation densities on speed belts. Results show significant improvements of the plant performance in the heavy/3D processing lines: By optimising the screen cut based on the acquired sensor data to achieve even occupation densities in both processing lines, the yield of all 3D product fractions could be increased by 3 wt% to 15 wt%.

## **References**

- Astrup, T., Fruergaard, T., Christensen, T.H., 2009. Recycling of plastic: accounting of greenhouse gases and global warming contributions. *Waste management & research* 27, 763–772. <https://doi.org/10.1177/0734242X09345868>
- Circular Economy Action Plan. [https://ec.europa.eu/environment/strategy/circular-economy-action-plan\\_de](https://ec.europa.eu/environment/strategy/circular-economy-action-plan_de)
- Curtis, A., Küppers, B., Möllnitz, S., Khodier, K., Sarc, R., (2020). Real time material flow monitoring in mechanical waste processing and the relevance of fluctuations. <https://doi.org/10.1016/j.wasman.2020.10.037>
- European Union, 2018. European Parliament and Council Directive 94/62/EC of 20 December 1994 on packaging and packaging waste.



- Feil, A., Coskun, E., Bosling, M., Kaufeld, S., & Pretz, T. (2019). Improvement of the recycling of plastics in lightweight packaging treatment plants by a process control concept. *Waste Management & Research: The Journal of the International Solid Wastes and Public Cleansing Association, ISWA*, 37(2), 120–126. <https://doi.org/10.1177/0734242X19826372>
- Feil, A., Pretz, T. (2018). Ungenutzte Potenziale in der Abfallaufbereitung. In: *Recy & DepoTech Conference 2018*. Leoben (Austria).
- Feil, A., Kroell, N., Pretz, T., & Greiff, K. (2021). Anforderungen an eine effiziente technologische Behandlung von Post-Consumer Verpackungsmaterialien in Sortieranlagen. *Müll Und Abfall*, 21(7), 362–370. <https://doi.org/10.37307/j.1863-9763.2021.07.04>
- Grüner Punkt, 2021: New EU packaging directive on its way. <https://www.gruener-punkt.de/en/company/news/details/new-eu-packaging-directive-on-its-way>
- Khodier, K., Curtis, A., Sarc, R., Lehner, M., O’Leary, P., Pomberger, R. (2019). Smart solid waste rocessing plant: vision and pathway. *ISWA world congress 2019*
- Kleinhans, K., Hallermans, M., Huysveld, S., Thomassen, G., Ragaert, K., Can Geem, K.M., Roosen, M., Mys, N., Dewulf, J., De Meester, S. (2020). Development and application of a predictive modelling approach for household packaging waste flows in sorting facilities. *Waste Management* 120 (2021) 290–302. <https://doi.org/10.1016/j.wasman.2020.11.056>
- Kranert, M. (2017). Einführung in die Kreislaufwirtschaft. <https://doi.org/10.1007/978-3-8348-2257-4>
- Kroell, N., Dietl, T., Maghmoumi, A., Chen, X., Küppers, B., Feil, A., Greiff, K. (2022) Assessment of sensor-based sorting performance for lightweight packaging waste through sensor-based material flow monitoring: Concept and preliminary results. *Sensor-based Sorting and Control 2022*.
- Kroell, N., Chen, X., Maghmoumi, A., Koenig, M., Feil, A., Greiff, K. (2021). Sensor-based particle mass prediction of lightweight packaging waste using machine learning algorithms *Waste Management* 136 (2021) 253-265. <https://doi.org/10.1016/j.wasman.2021.10.017>

- Küppers, B., Seidler, I., Koinig, G. R., Pomberger, R., & Vollprecht, D. (2020). Influence of throughput rate and input composition on sensor-based sorting efficiency. *Detritus*(9), 59–67. <https://doi.org/10.31025/2611-4135/2020.13906>
- Küppers, B., Schlögl, S., Friedrich, K., Lederle, L., Pichler, C., Freil, J., Pomberger, R., & Vollprecht, D. (2020). Influence of material alterations and machine impairment on throughput related sensor-based sorting performance. *Waste Management & Research*. <https://doi.org/10.1177/0734242X20936745>
- Möllnitz, S., Küppers, B., Curtis, A., Khodier, K., Sarc, R., (2020). Influence of pre-screening on down-stream processing for the production of plastic enriched fractions for recycling from mixed commercial and municipal waste. *Waste Management*, <https://doi.org/10.1016/j.wasman.2020.10.007>
- Packaging and Packaging Waste Directive: <https://eur-lex.europa.eu/legal-content/EN/TXT/?uri=CELEX:01994L0062-20150526>
- Perugini, F., Mastellone, M.L., Arena, U., 2005. A life cycle assessment of mechanical and feedstock recycling options for management of plastic packaging wastes. *Environmental Progress* 24, 137–154. <https://doi.org/10.1002/ep.10078>.
- Pretz, T., Raulf, K. and Quicker, P. (2020). Waste, 4. Recycling. *Ullmann's Encyclopedia of Industrial Chemistry*. [https://doi.org/10.1002/14356007.o28\\_o05.pub2](https://doi.org/10.1002/14356007.o28_o05.pub2)
- Ragaert, K., Delva, L., van Geem, K., 2017. Mechanical and chemical recycling of solid plastic waste. *Waste Management (New York, N.Y.)* 69, 24–58. <https://doi.org/10.1016/j.wasman.2017.07.044>



# Assessment of sensor-based sorting performance for lightweight packaging waste through sensor-based material flow monitoring: Concept and preliminary results

Nils Kroell<sup>1\*</sup>, Tobias Dietl<sup>1,2</sup>, Abtin Maghmoumi<sup>1</sup>, Xiaozheng Chen<sup>1</sup>, Bastian Küppers<sup>2</sup>, Alexander Feil<sup>1</sup>, Kathrin Greiff<sup>1</sup>

<sup>1</sup>Department of Anthropogenic Material Cycles, RWTH Aachen University, Aachen, Germany

<sup>2</sup>STADLER Anlagenbau GmbH, Altshausen, Germany

\* Corresponding Author: Wüllnerstr. 2, D-52062 Aachen, Germany,

nils.kroell@ants.rwth-aachen.de

---

Keywords: sensor-based material flow monitoring, sensor-based sorting, sorting performance, post-consumer lightweight packaging waste, plastic recycling

## Abstract

*Background:* Sensor-based sorting (SBS) units are a crucial part of lightweight packaging (LWP) waste sorting plants. Compared to sorting trials under technical lab conditions, significantly lower sorting performances are observed in many LWP sorting plants. One reason for this discrepancy is assumed to be the insufficient material flow representation under real sorting conditions. *Aim:* This paper aims to quantitatively determine how material flow presentation influences the performance of SBS units on the example of LWP waste. *Method:* In a case study, near-infrared (NIR) sensors were used to monitor the input, eject and drop fraction of an industrial-scale, NIR-based SBS unit at different throughputs. *Result:* Preliminary results show that higher occupation densities and insufficient material singling lead to significantly a lower sorting performance both in terms of purity of the eject fractions and yield of eject materials. *Conclusion:* The findings suggest that much of the discrepancy

between theoretically possible and practically achieved LWP sorting performance can be explained by suboptimal material flow presentation. Optimized material flow presentation thus might offer considerable, but so far largely untapped, optimization potentials in LWP sorting.

## **1 Introduction**

Global plastic production has grown from 2 Mt to 380 Mt between 1950 and 2015 (Geyer et al., 2017) and is expected to double again over the next 20 years (European Commission, 2018). The current production, usage, and end-of-life disposal of plastics cause severe environmental damages, e.g., greenhouse gas (GHG) emissions (Zheng & Suh, 2019) and pollution of global ecosystems (Jambeck et al., 2015). Plastic recycling and the substitution of primary by recycled plastics can significantly lower the environmental impacts of plastics (Astrup et al., 2009; Perugini et al., 2005). For example, substituting 1 Mg of primary plastic with recycled plastic achieves GHG savings between 0.9 Mg and 2.2 Mg CO<sub>2</sub>e (Turner et al., 2015).

Germany is the largest producer of post-consumer plastic waste in Europe and generated about 5.35 Mt/a post-consumer plastic wastes in 2019; the majority (59 wt%) of which is collected as post-consumer lightweight packaging (LWP) waste with an amount of 3.16 Mt/a (Conversio Market & Strategy GmbH, 2020). After collection, LWP waste is firstly sorted by LWP sorting plants into pre-concentrates and a remaining sorting residue. Pre-concentrates are further refined into secondary raw materials by specialized recycling plants and then re-enter the anthropogenic material cycle (Feil & Pretz, 2020). Although several improvements were introduced to LWP sorting (Feil et al., 2021), the overall performance of LWP sorting in Germany remains unsatisfactory: In 2019, only about 19 wt% of post-consumer plastic waste could be converted into recyclates, and only 8 wt% were used to substitute virgin material (Conversio Market & Strategy GmbH, 2020).

Considerable material losses towards energy recovery occur both during the collection with about 30 wt% as well as in sorting and recycling plants with about 35 - 40 wt% each of the respective inputs (Kuchta, 2020). As high material losses in recycling plants are partly caused by insufficient purity of pre-concentrates (Dehoust & Christiani, 2012), technical optimization of LWP sorting plants plays a key role in improving the performance of post-consumer plastic recycling.

## 1.1 State of the art and challenges in LWP sorting

In LWP sorting plants, the input material flow is firstly preconditioned (liberation, sieving, wind-shifting, ballistic separation) before ferrous and non-ferrous metals as well as beverage cartons are sorted out. The preconditioned material flow then enters the heart of any modern LWP sorting plant: A sensor-based sorting (SBS) cascade typically containing more than 20 SBS units to sort the material flow into the desired preconcentrates. (Feil et al., 2021)

SBS units in LWP sorting are almost exclusively *belt sorters*, i.e., the material flow is presented on acceleration belts ( $v \approx 3$  m/s) to the sensor. Compressed air nozzle bars are then used to sort the material flow in a *drop* and *eject* fraction, depending on the chosen sorting recipe. Common target fractions in SBS for LWP are polypropylene (PP), polyethylene (PE), polyethylene terephthalate (PET), polystyrene (PS), beverage cartons (BC), and paper & cardboard (PPC). As all target fractions of SBS in LWP have distinct near-infrared (NIR) spectra, NIR-based sorters are primarily used in LWP-sorting. (Feil et al., 2021; Feil & Pretz, 2020)

Modern SBS equipment can, according to manufacturers, achieve technical efficiencies of  $\geq 95$  wt% under laboratory and pilot plant conditions (4R Sustainability, 2011). However, the actual achieved product purities and observed material losses fall far short of these expectations (see above).

One main reason for the poor sorting results in industrial-scale LWP sorting is assumed to be the inadequate material flow presentation to the SBS unit (Feil et al., 2019): For optimal sorting results, material flows have to be presented as a *singled monolayer* to the SBS units. If particles overlap or touch each other, false-negative (material supposed to end in the eject fraction ends in the drop fraction) or false-positive (vice versa) sorting results occur, which lead to lower yield and purities, respectively. Two physically plausible mechanisms for false sorting results are:

- (M1) False sorting decisions due to overlapping:** All sensors currently applied in LWP sorting are *surface measurement technologies*. Thus, in the case of overlapping, only the material on top is considered in the sorting decision, leading to false-negative or false-positive sorting decisions, depending on the material on top. Additionally, mixed spectra (NIR) or colors (VIS) can lead to false sorting decisions in case the material on top is (semi-)transparent.

- (M2) Entrainment of drop particles:** In the case of overlapping or touching particles, turbulence of air valves can lead to false-positive material ejects (especially for light material fractions such as films).

## **1.2 Addressed research gap**

This study aims to quantitatively determine how the material flow presentation influences the sorting results and how much of the discrepancy between theoretically possible and real-world observed sorting results can be explained by insufficient material flow presentation to SBS units in LWP sorting plants.

Recent studies have shown that the material throughput strongly influences the SBS performance of chute sorters in lab-scale (Küppers, Schlögl, et al., 2020; Küppers, Seidler, et al., 2020). However, the results are only partly transferable to industrial-scale SBS units since (i) LWP sorting is almost exclusively performed on belt sorters with significantly different feeding characteristics, (ii) the investigated working width (500 mm) is significantly lower compared to industrial applications (influence of boundary areas), and (iii) the characteristics of the investigated test material (idealized plastic chips) are not comparable with real-world post-consumer wastes. Additionally, investigations with industrial SBS equipment (Curtis et al., 2021) show that the throughput fluctuations hamper SBS performance but are limited to comparing two scenarios (fluctuating and non-fluctuating throughput).

One limitation of current SBS research is that existing performance assessment methods are based on manually determining the composition and quantity of eject and drop fractions (i.e., manual sorting), which is time- and cost-intensive. Therefore, only a small number of data points can be determined, limiting the statistical confidence of obtained results. Furthermore, sorting results are only available once the sorting trial is finished and therefore cannot be measured time-resolved and are limited to batch-wise trials. To overcome these limitations, we propose a new assessment method based on sensor-based material flow monitoring (SBMM), in which additional sensors are used to determine the composition and quantity of the eject and drop fractions.

## 2 SBS performance assessment based on SBMM

In the proposed assessment methodology, additional sensors are used to monitor (i) the material flow presentation on the acceleration belt and (ii) the sorting result, i.e., quantity and composition of the eject and drop fraction (Figure 1).

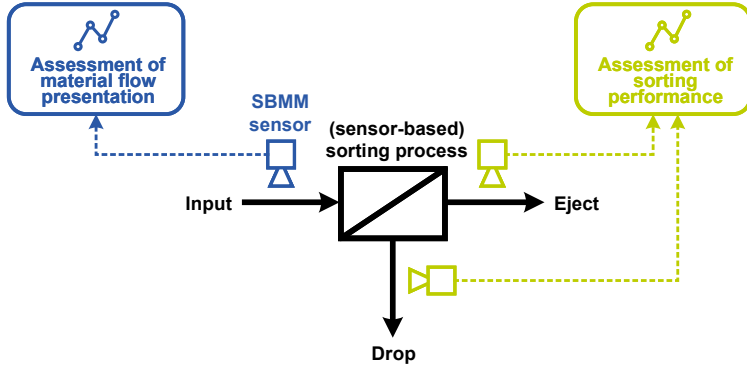


Figure 1: Concept for SBS performance assessment through SBMM.

### 2.1 Assessment of material flow presentation

To describe the material flow presentation on the acceleration belt quantitatively, this section define different material flow presentation indicators.

**Occupation density (OD).** Traditional assessment of material flow presentation of acceleration belts is based on the *occupation density* (OD), which describes the share of the acceleration belt area that is covered by material (Küppers, Schlögl, et al., 2020):

$$OD = \frac{\dot{A}_{\text{covered}}}{\dot{A}_{\text{belt}}} \quad (1)$$

Where  $\dot{A}_{\text{belt}}$  is the *area flow* (projected area per time unit as presented to the sensor) of the acceleration belt, which is a function of belt speed ( $v_{\text{belt}}$ ) and belt width ( $b_{\text{belt}}$ ) (Eq. (2)), and  $\dot{A}_{\text{covered}}$  is the area flow of belt area that is covered by material.



$$\dot{A}_{\text{belt}} = v_{\text{belt}} * b_{\text{belt}} \quad (2)$$

The OD can be calculated deterministically without prior knowledge about the material flow. However, as shown exemplarily in Figure 2, the OD neglects the material distribution on the conveyor surface (e.g., overlapping), which may influence the sorting result (see Mechanism M1, Section 1.1).

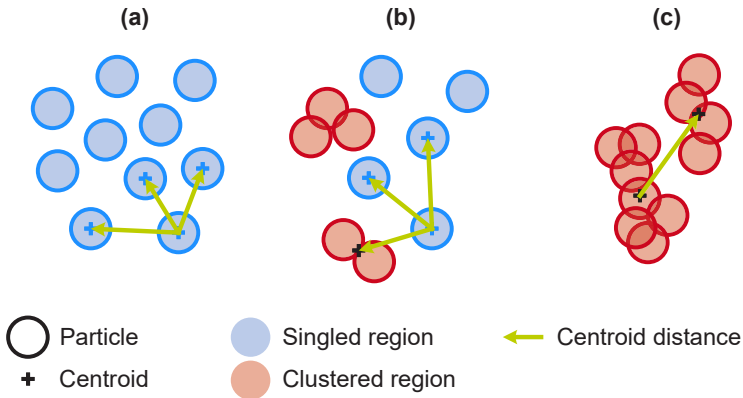


Figure 2: Exemplary material distributions with similar ODs, but (a) high, (b) medium, and (c) low particle singling.

**Singling ratio (SR).** To overcome the limitations of the occupancy density indicator, we propose a new indicator, the *singling ratio* (SR). To determine the SR, we classify all associated, covered areas (*regions*) into (i) *singled regions* (regions that contain only one particle) and (ii) *clustered regions* (regions that contain two or more touching or overlapping particles), cf. Figure 2. The SR then describes the percentage of covered area that is singled:

$$SR = \frac{\dot{A}_{\text{singled}}}{\dot{A}_{\text{singled}} + \dot{A}_{\text{clustered}}} = \frac{\dot{A}_{\text{singled}}}{\dot{A}_{\text{covered}}} \quad (3)$$

A SR of 1 indicates perfect singling, while a SR of 0 means that all particles touch or overlap with at least one other particle.

**Particle distances.** While the SR describes the singulation of the material flow, it ignores the proximity to nearby regions, which may influence the sorting result (see Mechanism M2, Section 1.1). Different metrics can describe the distance between regions on a conveyor surface. Here, we use the Euclidian centroid-to-centroid distance between a given region  $i$  and its neighbor region  $j$ , where  $x$  and  $y$  are the coordinates of the respective centroid and region  $j$  is the  $k$ -th nearest neighbor of region  $i$ :

$$CD_k(i, j) = \sqrt{(x_i - x_j)^2 + (y_i - y_j)^2} \quad (4)$$

On a material flow level, the distances of all  $n$  regions in a given evaluation area result in a distribution of individual centroids distances, which can be summarized through statistical indicators such as the arithmetic mean:

$$\overline{CD}_k = \frac{1}{n} \sum_{i=1}^n CD_{k,i} \quad (5)$$

## 2.2 Assessment of sorting performance

In any SBS task, particles can be divided into target (index  $T$ ) and non-target particles (index  $nT$ ). Optimal sorting is defined by maximizing target and minimizing non-target particles in the eject fraction.

Four different sorting results can occur: (i) target material ends in the eject fraction ( $\dot{m}_{T,eject}$ ; true positive [TP]), (ii) target material ends in the drop fraction ( $\dot{m}_{T,drop}$ ; false-negative [FN]), (iii) non-target material ends in the drop fraction ( $\dot{m}_{nT,drop}$ ; true negative [TN]), and (iv) non-target material in the eject fraction ( $\dot{m}_{nT,eject}$ ; false-positive [FP]). Thus, the sorting result can be interpreted as a 2 x 2 confusion matrix:

$$\text{Confusion matrix: } \begin{bmatrix} \dot{m}_{T,eject} (TP) & \dot{m}_{nT,eject} (FP) \\ \dot{m}_{T,drop} (FN) & \dot{m}_{nT,drop} (TN) \end{bmatrix} \quad (6)$$

Commonly, two indicators are used to evaluate the sorting task (Feil et al., 2016): *Purity* (Eq. (7)) describes the share of the target fraction in the eject fraction, i.e., evaluation of the first confusion matrix row.

$$c_{w,eject} = \frac{\dot{m}_{T,eject}}{\dot{m}_{eject}} = \frac{\dot{m}_{T,eject}}{\dot{m}_{T,eject} + \dot{m}_{nT,eject}} \quad (7)$$

*Yield* (Eq. (8)) describes how much of the target fraction from the input material flow is sorted into the eject fraction, i.e., evaluation of the first confusion matrix column.

$$R_w = \frac{\dot{m}_{T,eject}}{\dot{m}_{T,input}} = \frac{\dot{m}_{T,eject}}{\dot{m}_{T,eject} + \dot{m}_{T,drop}} \quad (8)$$

Although purity and yield are of high practical importance, both indicators must always be considered to evaluate the sorting performance. To obtain a single performance indicator, we propose to unite purity and yield into the  $F_1$ -score, which is the harmonic mean of both values (Tharwat, 2021):

$$F_1 = 2 \cdot \frac{c_{w,eject} \cdot R_w}{c_{w,eject} + R_w} \quad (9)$$

$F_1$ -scores range between 0 and 1. An  $F_1$ -score of 1 indicates a perfect sorting performance ( $c_{w,eject}$  and  $R_w=1$ ), while the  $F_1$ -score becomes zero if purity or yield become zero.

In cases where purity and yield are not of equal importance, it is possible to weigh both indicators through a factor  $\beta$  in the  $F_\beta$ -score (Eq. (10)), which leads to yield being weighted  $\beta$ -times more than purity (Tharwat, 2021).

$$F_\beta = (1 + \beta^2) * \frac{c_{w,eject} \cdot R_w}{(\beta^2 \cdot c_{w,eject}) + R_w} \quad (10)$$

### **3 Case study: Material and methods**

In a case study, we tested the technical feasibility of our assessment method with an industrial scale SBS unit using real-world LWP waste.

#### **3.1 Test setup**

The developed test setup consists of a state-of-the-art, industrial-scale NIR-based SBS unit with a total working width of 2000 mm, an acceleration belt speed of 3 m/s, and an air nozzle bar with 12.5 mm nozzle distance operated at 5.5 bar air pressure. For the sorting trials, the effective working width was reduced to 1000 mm to enable high occupation despite the limited transport capacity of the upstream conveyors. The sorter was programmed to actively sort out PET, while all other materials were supposed to end in the drop fraction. The sorting recipe came directly from the SBS manufacturer, represented an industry-standard sorting recipe used in several LWP sorting plants, and was not further modified or adapted for the sorting trials.

A first additional NIR sensor (NIR-1) recorded the acceleration belt. After the SBS unit, the drop and eject fraction then fell on separate conveyor belts respectively (width:  $b = 830$  mm, belt speed:  $v = 1.2$  m/s), where both material flows were captured by a second NIR sensor (NIR-2). Afterward, the NIR-2 recordings were digitally split into eject and drop recordings. To simulate a continuously working sorting plant, eject and drop material flows were mixed and entered a material loop before being fed again to the SBS unit. Inside the material loop, a modified ballistic separator and several belt transfers ensured a material flow homogenization before re-entering the SBS units.

The used NIR sensors were EVK HELIOS EQ32 sensors from EVK Kerschhagl GmbH (Raaba, Austria) working in the wavelength range of 930 nm – 1700 nm with a spectral resolution of 3.1 nm at an acquisition frequency of 450 Hz. An analysis recipe (Figure 3a) containing spectral references for the material classes PET, PP, PE, PS, BC, and PPC was developed and loaded on both NIR sensors. The NIR sensors classify each pixel based on the analysis recipe, and the resulting false-color images (Figure 3b-d) were recorded using a self-developed recording software for subsequent data analysis.

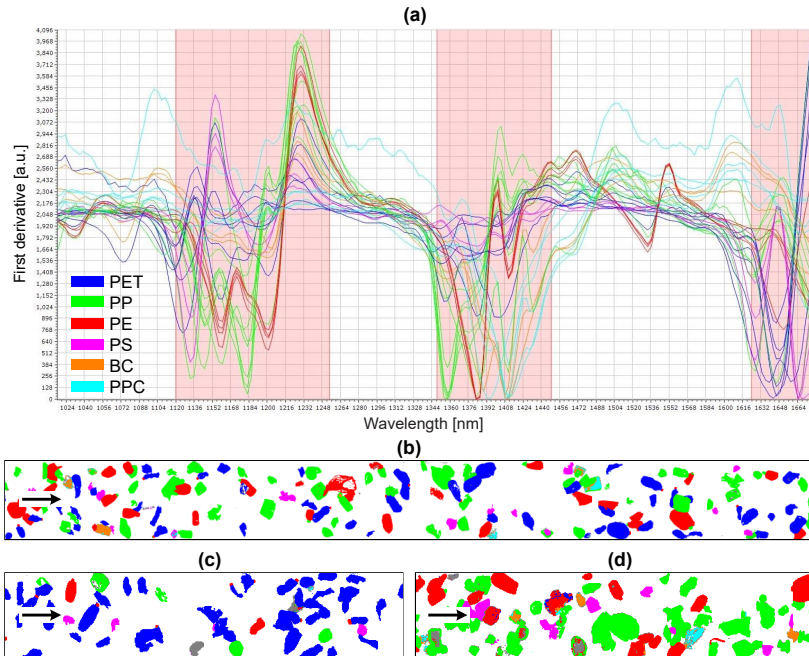


Figure 3: (a) NIR recipe and resulting false-color images (red marked areas are used for spectral classification) of (b) acceleration belt (NIR-1), (c) eject, and (d) drop belt (NIR-2). Grey: unclassified material.

### 3.2 Material and experimental procedure

The investigated test material is LWP waste from Maribor (Slovenia). To simulate a realistic 3D plastic fraction typical for SBS applications in LWP sorting, we preconditioned the material flow before the trials with a ballistic separator to remove 2D materials and fines (< 45 mm) and an eddy current and magnetic separator to remove ferrous and non-ferrous metals, respectively. To achieve material flow with a certain percentage of eject material (in this case PET), pure PET and non-PET fractions were generated firstly. For the PET fraction, post-consumer PET bottles were used as the source material. To ensure proper classifiability of each bottle and to exclude false discharges due to poor classifiability of certain bottles (e.g., full-sleeve bottles), the PET fraction was delabeled with the STADLER Delabeler

(Küppers et al., 2019) to generate a pure post-consumer PET fraction and exclude the influences of labels and sleeves on the sorting result. A non-PET 3D plastic fraction was generated by sorting out all PET contents from the preconditioned LWP waste prior to the sorting trials. Subsequently, a PET content of 30 wt% was set for the test material by mixing defined amounts of the PET and non-PET fraction.

Different material flow presentations were simulated by gradually increasing the throughput in 16 throughput steps. The throughput increases were achieved by adding a defined amount of additional test material to the material loop in each step. After a buffer time of 5 minutes to equilibrate the material loop, the sorting results were monitored for 10 minutes (equivalent to about 3.5 material cycles) for each throughput step.

### **3.3 Data evaluation**

The subsequent data analysis was implemented in Python 3.8. First, all images were spatially calibrated to obtain results in metric units. Second, the material flow composition and OD were determined and aggregated to a sampling rate of 15 Hz. Third, each region was classified into singled and clustered regions, and centroid distances were determined. After that, the SR was determined, and the centroid distances were resampled by evaluating the image in chunks of 1/15 s length in conveying direction. To reduce the artifacts of individual particles and obtain information on the material flow level, all results were smoothed by a 1s moving average.

The sorting performance indicators (Eq. (11)-(13)) were then calculated by comparing the area flows per material class:

$$c_{\text{PET,eject}}^* = \frac{\dot{A}_{\text{PET,eject}}}{\dot{A}_{\text{eject}}} [\text{px}\%] \quad (11)$$

$$R_{\text{PET}}^* = \frac{\dot{A}_{\text{PET,eject}}}{\dot{A}_{\text{PET,eject}} + \dot{A}_{\text{PET,drop}}} [\text{px}\%] \quad (12)$$

$$F_{1\text{PET}}^* = 2 \cdot \frac{c_{\text{PET,eject}}^* \cdot R_{\text{PET}}^*}{c_{\text{PET,eject}}^* + R_{\text{PET}}^*} [\text{px}\%] \quad (13)$$

For a mass-based process evaluation, these area-based indicators have to be transformed into mass-based indicators (Kroell et al., 2021), which we plan to address in future work. Since the grammages of the investigated material groups are in a similar order of magnitude, we neglect this effect for the first demonstration of technical feasibility and report the preliminary results in pixel percent (px%), cf. Eq. (11) – Eq. (13).

## 4 Case study: Preliminary results and discussion

### 4.1 Discrimination of singled and clustered regions

To determine if the classification into singled and clustered regions based on the NIR-1 recordings (false-color images) is technically feasible, we manually classified  $n = 1,000$  randomly sampled regions. The resulting dataset contained  $n = 632$  (63.2%) singled,  $n = 335$  (33.5%) clustered regions, and  $n = 33$  (3.3%) regions that could not be classified unambiguously (which were excluded from the labeled dataset).

For an initial classifier, we extracted the two features (i) *impurity* (share of all except the most common material classes and unclassified material of a particle) and (ii) *projection area* of each region and split the dataset into 75% training and 25% test data. Figure 4 shows the distribution of impurities and projection areas between the singled and clustered regions.

Based on the training data, we determined two thresholds (i)  $\tau_{\text{impurity}} = 12$  px% (optimal threshold between singled and clustered regions, see Figure 4a) and (ii)  $\tau_{\text{area}} = 1,000$  cm<sup>2</sup> (maximum projection area of singled clustered incl. 10% buffer for different particle positions). Based on these thresholds, we constructed a simple if/else classifier:

$$RT = \begin{cases} \text{"clustered"}, & \text{if } I_{\text{region}} \geq \tau_{\text{impurity}} \text{ or } A_{\text{region}} \geq \tau_{\text{area}} \\ \text{"singled"}, & \text{else} \end{cases} \quad (14)$$

Where  $I_{\text{region}}$  and  $A_{\text{region}}$  are the impurity and projection area of a region respectively, and  $RT$  is the region type. Figure 4c shows that this simple classifier already achieves a classification accuracy of 92.3% and can sufficiently discriminate singled from clustered regions (Figure 4d).

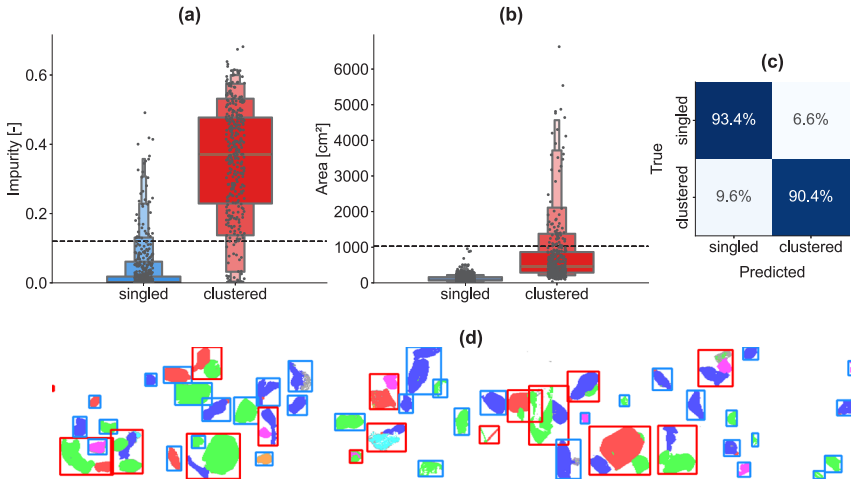


Figure 4: Identification of clustered regions. (a) Distribution of material impurities per region type, (b) distribution of projection areas per region type, (c) confusion matrix of region type classification based on impurity and projection area thresholds (dashed line in [a] and [b]) and or-conjunction on the test set, (d) exemplary false-color image with identified regions (blue: singled, red: clustered).

The classification accuracy can likely be improved by incorporating more features, extending the training data set, and applying sophisticated machine learning (ML) models. Especially convolutional neural networks (CNNs) could be promising for this classification task.

## 4.2 Interrelation between material flow presentation indicators

Based on the discrimination of singled and clustered regions, the SR was calculated, and Figure 5a shows the interrelation between OD, SR and relative throughput. As one would expect, the OD increases with increasing relative throughput, while the SR decreases. Two segments can be identified: For ODs between 0% and about 20%, the SR stays roughly constant. For ODs above about 20%, the SR decreases with increasing belt occupation.

The centroid distances (Figure 5b) decrease with increasing OD, i.e., regions move closer together. However, at ODs above about 30%, increased region distances can be observed. This effect can be very likely be traced back to the formation of more clustered regions (cf. Figure 5a) at higher ODs: As the clustered regions have



larger projection areas than singled particles, the centroid distances increase with lower SRs and higher ODs.

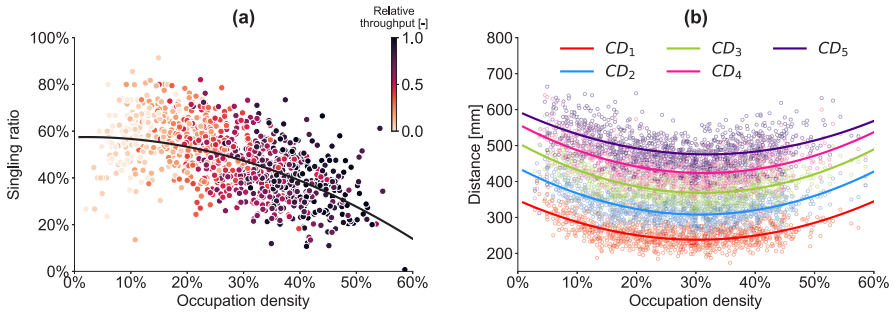


Figure 5: Interrelation between (a) OD and SR for different relative throughputs and (b) OD and centroid distances.  $CD_i$ : centroid distance to  $i$ -th nearest neighbor. (1s moving average; scatterplot for better visualization limited to a random selection of 1,000 data points each)

These findings show that the SR can be a useful metric to assess the material flow presentation besides the OD. However, as all sorting trials were conducted on the identical acceleration belt and with identical material flow guidance, the additional advantage of SR over the OD can currently only be estimated to a limited extent.

Furthermore, the preliminary SBMM data indicates that the presentation of post-consumer LWP as a singled monolayer to SBS units is indeed challenging: Even at the lowest investigated throughputs (mean OD: 8.8%), only about half of the covered area (mean SR: 52.4%) was classified as singled.

In contrast, the centroid-to-centroid distances seem to be of limited use for describing the particle proximity at higher ODs due to the formation of clusters. Here, region distances that describe the distances between individual region borders could be a potential improvement.

### 4.3 Influence of material flow presentation on sorting performance

Figure 6 shows the interrelation between the material flow presentation (assessed by the OD and SR) and different sorting performance metrics (purity, yield, -score). As depicted in Figure 6a, the sorting performance decreases linearly with increasing OD from about 91.6 px% purity and 98.7 px% yield at 8.8% OD to about 74.2 px% purity and 97.0 px% yield at 42.6% OD.

For the investigated SBS unit, a 12.2-fold steeper decrease of the purity with increasing OD (slope: -0.49) compared to the yield (slope: -0.04) can be observed. Accordingly, Figure 6b shows an increased sorting performance for higher SR. Here, the purity increases 12.5 times steeper than the purity with increasing SR. As graphically shown in Figure 6, the -score can be a useful performance metric to combine purity and yield.

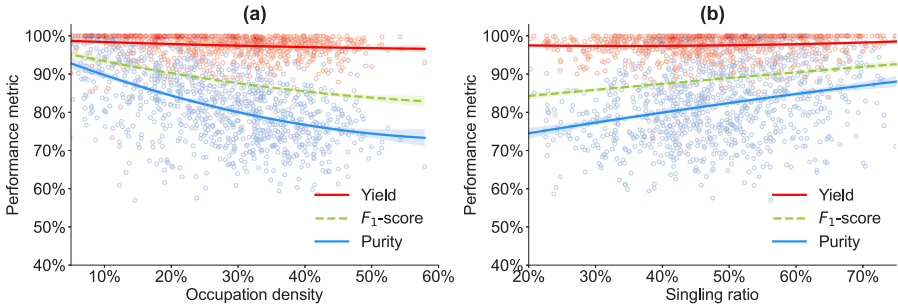


Figure 6: Influence of (a) OD and (b) SR on sorting performance. (5s moving average; scatterplot for better visualization limited to a random selection of 1,000 data points each)

The significantly reduced sorting performance of SBS units due to suboptimal material flow presentation (high OD) is consistent with related research (Curtis et al., 2021; Küppers, Schlögl, et al., 2020; Küppers, Seidler, et al., 2020). In contrast, a quantitative comparison of our findings with the results of Küppers, Seidler, et al. (2020) highlights the significant influence of individual SBS units, machine settings, and material flows on the obtained transfer function (quantitative relation between material flow presentation or throughput and sorting result): While Küppers, Seidler, et al. (2020) report a decreased yield of on average -0.76% per 1% additional OD, the yield of our investigated SBS unit decreased with only -0.04% per 1% additional OD. A possible explanation for this is that in state-of-the-art SBS equipment, the weighting of purity and yield can be adjusted in the sorter settings, and changing these weightings would directly affect the slope of the purity and yield in the obtained transfer function. Moreover, the sorting results are influenced by the characteristics of the underlying sorting engine and the input material. It would thus be interesting to compare the sorting performance as assessed through the -score for different SBS settings or different SBS units in future work.

## 4.4 Limitations

It is essential to note that the obtained purity and yield values cannot be directly transferred to plant scale LWP sorting due to (i) the pixel-based performance assessment (cf. Section 3.3) and (ii) the removal of articles with limited sortability (cf. Section 3.2). The first limitation (pixel-based assessment) results in underestimating the sorting performance, as, e.g., PE bottle caps on PET bottles are counted as target material in traditional (particle-based) sorting assessment, but as non-target material in our pixel-based assessment method. The second limitation causes overestimating of the sorting performance, as articles with limited sortability would cause additional sorting errors. Here, a direct comparison of the SBMM- and pixel-based sorting assessment with traditional (particle-based) performance assessment would be of great value.

## 5 Conclusion and outlook

In conclusion, our case study shows that an automatic assessment of (sensor-based) sorting processes is technically feasible and offers significant advantages over state-of-the-art assessment methods, e.g., in terms of reduced time and cost expenditure, a higher statistical significance of the results, and greater flexibility and detail of data evaluation. The introduced indicators singling ratio and particle distances enable a more nuanced description of the material flow presentation and demonstrate the difficulty of singling post-consumer LWP wastes on acceleration belts.

Our results show that increased belt occupation significantly linearly reduces the sorting performance of SBS equipment in terms of lower purity, yield, and overall sorting performance ( $F_1$ -score). These preliminary findings suggest that much of the discrepancy between theoretically possible and practically achieved LWP sorting performance can be explained by suboptimal material flow presentation.

In future work, we plan to extend the sorting trials to different material flow compositions and further improve the developed assessment method. Furthermore, the hypothesis that large parts of the discrepancy between theoretically possible and practically achieved LWP sorting performance can be explained by suboptimal material flow presentation shall be investigated in SBMM trials at plant scale. If this hypothesis is validated, optimized material flow presentation offers considerable,

but so far largely untapped, optimization potential in LWP sorting and could largely contribute to a loss-minimized plastic recycling in general.

## Acknowledgments

This work was supported by the German Federal Ministry of Education and Research (BMBF) within the program „Resource-efficient circular economy - plastics recycling technologies (KuRT)“ under the project ReVise (grant no. 033R341).

## References

- 4R Sustainability, I. (Ed.). (2011). *Demingling the mix: An assessment of commercially available automated sorting technology*.
- Astrup, T., Fruergaard, T., & Christensen, T. H. (2009). Recycling of plastic: Accounting of greenhouse gases and global warming contributions. *Waste Management & Research*, 27(8), 763–772. <https://doi.org/10.1177/0734242X09345868>
- Conversio Market & Strategy GmbH. (2020). *Stoffstrombild Kunststoffe in Deutschland 2019*.
- Curtis, A., Küppers, B., Möllnitz, S., Khodier, K., & Sarc, R. (2021). Real time material flow monitoring in mechanical waste processing and the relevance of fluctuations. *Waste Management (New York, N. Y.)*, 120(1), 687–697. <https://doi.org/10.1016/j.wasman.2020.10.037>
- Dehoust, G., & Christiani, J. (2012). *Analyse und Fortentwicklung der Verwertungsquoten für Wertstoffe: Sammel- und Verwertungsquoten für Verpackungen und stoffgleiche Nichtverpackungen als Lenkungsinstrument zur Ressourcenschonung*. <http://www.uba.de/uba-info-medien/4342.html>
- European Commission (Ed.). (2018). *A European Strategy for Plastics in a Circular Economy*. <https://eur-lex.europa.eu/legal-content/EN/TXT/?uri=COM:2018:28:FIN>

- Feil, A., Coskun, E., Bosling, M., Kaufeld, S., & Pretz, T. (2019). Improvement of the recycling of plastics in lightweight packaging treatment plants by a process control concept. *Waste Management & Research*, 37(2), 120–126. <https://doi.org/10.1177/0734242X19826372>
- Feil, A., Kroell, N., Pretz, T., & Greiff, K. (2021). Anforderungen an eine effiziente technologische Behandlung von Post-Consumer Verpackungsmaterialien in Sortieranlagen. *Müll Und Abfall*, 21(7), 362–370. <https://doi.org/10.37307/j.1863-9763.2021.07.04>
- Feil, A., & Pretz, T. (2020). Mechanical recycling of packaging waste. In *Plastic Waste and Recycling* (pp. 283–319). Elsevier. <https://doi.org/10.1016/B978-0-12-817880-5.00011-6>
- Feil, A., van Thoden Velzen, E. U., Jansen, M., Vitz, P., Go, N., & Pretz, T. (2016). Technical assessment of processing plants as exemplified by the sorting of beverage cartons from lightweight packaging wastes. *Waste Management (New York, N.Y.)*, 48, 95–105. <https://doi.org/10.1016/j.wasman.2015.10.023>
- Geyer, R., Jambeck, J. R., & Law, K. L. (2017). Production, use, and fate of all plastics ever made. *Science Advances*, 3(7), e1700782. <https://doi.org/10.1126/sciadv.1700782>
- Jambeck, J. R., Geyer, R., Wilcox, C., Siegler, T. R., Perryman, M., Andrady, A., Narayan, R., & Law, K. L. (2015). Marine pollution. Plastic waste inputs from land into the ocean. *Science (New York, N.Y.)*, 347(6223), 768–771. <https://doi.org/10.1126/science.1260352>
- Kroell, N., Chen, X., Maghmoumi, A., Koenig, M., Feil, A., & Greiff, K. (2021). Sensor-based particle mass prediction of lightweight packaging waste using machine learning algorithms. *Waste Management (New York, N.Y.)*, 136, 253–265. <https://doi.org/10.1016/j.wasman.2021.10.017>
- Kuchta, K. (2020). Bewertung des Recyclingprozesses von Kunststoffverpackungen. In O. Holm, E. Thomé-Kozmiensky, D. Goldmann, & B. Friedrich (Chairs), *Recycling- und Sekundärrohstoffe*, Berlin.

- Küppers, B., Chen, X., Seidler, I., Friedrich, K., Raulf, K., Pretz, T., Feil, A., Pomberger, R., & Vollprecht, D. (2019). Influences and consequences of mechanical delabeling on PET recycling. *Detritus*, 6(0), 39–46. <https://doi.org/10.31025/2611-4135/2019.13816>
- Küppers, B., Schlögl, S., Friedrich, K., Lederle, L., Pichler, C., Freil, J., Pomberger, R., & Vollprecht, D. (2020). Influence of material alterations and machine impairment on throughput related sensor-based sorting performance. *Waste Management & Research*. Advance online publication. <https://doi.org/10.1177/0734242X20936745>
- Küppers, B., Seidler, I., Koinig, G. R., Pomberger, R., & Vollprecht, D. (2020). Influence of throughput rate and input composition on sensor-based sorting efficiency. *Detritus*(9), 59–67. <https://doi.org/10.31025/2611-4135/2020.13906>
- Perugini, F., Mastellone, M. L., & Arena, U. (2005). A life cycle assessment of mechanical and feedstock recycling options for management of plastic packaging wastes. *Environmental Progress*, 24(2), 137–154. <https://doi.org/10.1002/ep.10078>
- Tharwat, A. (2021). Classification assessment methods. *Applied Computing and Informatics*, 17(1), 168–192. <https://doi.org/10.1016/j.aci.2018.08.003>
- Turner, D. A., Williams, I. D., & Kemp, S. (2015). Greenhouse gas emission factors for recycling of source-segregated waste materials. *Resources, Conservation and Recycling*, 105, 186–197. <https://doi.org/10.1016/j.resconrec.2015.10.026>
- Zheng, J., & Suh, S. (2019). Strategies to reduce the global carbon footprint of plastics. *Nature Climate Change*, 9(5), 374–378. <https://doi.org/10.1038/s41558-019-0459-z>



# Quantifying the Delabelling Performance using Sensor-based Material Flow Monitoring

Sabine Schlögl<sup>1\*</sup>, Bastian Küppers<sup>2</sup>

<sup>1</sup>Montanuniversität Leoben, Chair of Waste Processing Technology and Waste Management (AVAW),  
Leoben, Austria

<sup>2</sup>STADLER Anlagenbau GmbH, Altshausen, Germany

\* Corresponding Author: Franz-Josef-Str. 18, 8700 Leoben, Austria; [sabine.schloegl@unileoben.ac.at](mailto:sabine.schloegl@unileoben.ac.at)

---

Keywords: SBMM, SBQC, Delabelling, NIR, plastic packaging waste

## Abstract

The aim of the presented trials is to quantify the delabelling performance by using sensor-based material flow monitoring (SBMM). To evaluate the usability of SBMM for that task, the material was analysed before and after the delabelling process for every batch of samples both with an NIR sensor and by manual sorting. The samples were taken from plants in Belgium and Germany, to create a variety of labelled PPW-objects. The examined objects have been covered with different types (e.g., full sleeve, half sleeve, adhesive labels) and materials (mono- or multi-layered plastics). Based on the results of these trials regarding fullsleeve PET-bottles, sensor-based quality control (SBQC) could further be developed and then implemented in a sorting plant after a delabelling process, to ensure the delabelling performance and thus enhance the success of the following sensor-based sorting steps.



# 1 Introduction

The amount of plastic packaging waste (PPW) in Europe has been increasing over the past decades. Germany, the largest producer of PPW in Europe, generated 3.24 Mio. Mg of PPW in 2018, which is equivalent to an increase of 10% compared to 2009. In Austria the increase in that time span was 3%, in Belgium 6%. Although the total amount of PPW in Austria and Belgium is significantly lower than in Germany (AT: 302.000 Mg and BEL: 347.000 Mg in 2018), the demand for higher recycling rates in combination with increasing numbers of PPW stresses the need for technical innovation in the sorting and recycling process (European Commission, 2021; Directive 2018/852).

In addition, the design of plastic packaging creates challenges for the waste management industry. One example are labels, which cover a part of the product and thus hinder the correct classification of such articles through sensor-based sorting (SBS) machinery. A trend of enlarged labels for marketing reasons resulted in an increasing number of full body and bigger adhesive in the last decade. These labels can be made of a variety of different plastics or even paper. As the resulting near-infrared (NIR) spectra of labelled objects usually differs from the ones of the unlabelled objects, reduced yield and product purity in sorting plants and a resulting lower chance for recycling is the consequence (Cotrep, 2019; Gomes, 2014; Hüttler, 2021; Pomberger, 2021).

An approach to deal with that problem is to use a delabelling device, which separates the labels from the waste object (e.g., a plastic bottle). If the removal of labels is successful, the material of the object is then easily detected by SBS. An additional benefit of delabeling is the absence of ink or colour additives in the resulting material flow, which might even improve the level of recycling, as some colours cannot be removed completely in the recycling process (Hüttler, 2021). One example for a problematic colour additive is titanium dioxide ( $\text{TiO}_2$ ) which is commonly used in white objects (Loaeza et al., 2021). If the bottles are both coloured and covered with a label a separation by colour is impossible without a delabelling step. The general functionality of the “Label Remover” of STADLER Anlagenbau GmbH for separating labels from PET bottles was shown by Küppers et al. (2019).

To ensure a continuously persisting delabelling performance, sensor-based material flow monitoring (SBMM) methods can be used. One use case is the detection of malfunctions, which can be caused by necessary maintenance work like the

exchange of blunt blades. As a consequence of this, or due to special challenges caused by the input material, the amount of labels in the output stream can be too high. This can be quantified on-time with sensor-based quality control (SBQC). Immediate measures like physical changes to the process (e.g., changing blades, changing the distance of rotor, and stator knives) or using sensor-based process control (SBPC) in the form of a material re-feed to a point prior to the delabelling step are the possible consequences.

The results in the following show an excerpt of trials with labelled PPW material from different European countries. The challenges and possibilities of quantifying the delabelling performance with SBMM are exemplarily shown for manually sorted labelled PET-material using an NIR-sensor.

## 2 Material and Methods

The PET-material for these trials consists of manually picked full-sleeve bottles of two different PPW sorting plants in Belgium and Germany. The total number of bottles was 479, with 416 coming from Belgium and 63 from Germany. The type of bottles in each sample can be seen exemplarily in Fig. 1:



Fig. 1: Input material: PET-bottles from Belgium (left) and Germany (right).

As the grade of labelling differed in the input material it was quantified by manually sorting all objects and categorizing it in “No label”, “Partly delabelled” and “Complete label”. The term “label” in this work includes all kinds of labels and sleeves independent of the material of the label or type of processing. The number of objects in each category can be seen in Tab. 1. Both samples originally did

not contain objects of non-PET-material. An interesting detail was the share of specific products in the samples. For instance, 26% of the full-sleeve PET-bottles in the Belgian sample consisted of the packaging of a popular drink from the brand “Cécémel”.

Tab. 1: Number of input object manually sorted by grade of labelling.

	No label	Partly delabelled	Complete label	Total
PET_Belgium	376	38	2	416
PET_Germany	40	22	1	63
Total	416	60	3	479

The trials were conducted in pilot plant scale in the “Test and Innovation Centre” of STADLER. The test setup consisted of a screw conveyor followed by an ascending conveyor belt. The NIR-sensor (Type: EVK Helios EQ32, wavelength range: 930 – 1700 nm [EVK DI Kerschhagl GmbH, Raaba, Austria]) was mounted over the conveyor belt. The material then either passed the delabelling step and was directly discharged or was fed into the “Label Remover” followed by a ballistic separator to separate fines, labels (2D) and delabelled PET-bottles. The delabelling steps can be seen in the flowchart in Fig. 2.

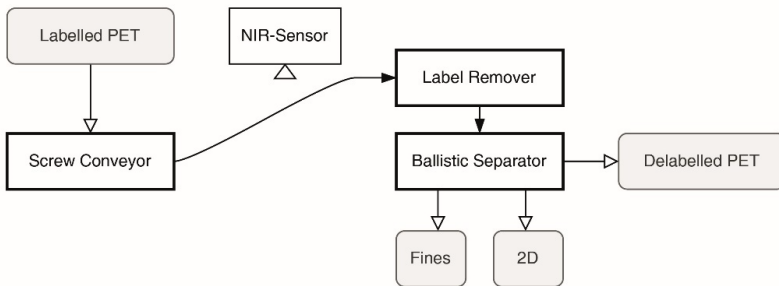


Fig. 2: Flowchart of test setup (“Delabelling phase”).

A scheme and a picture of the STADLER “Label Remover” can be seen in Fig. 3. Technical details and the fundamental functionality can be found in Küppers et al. (2019).

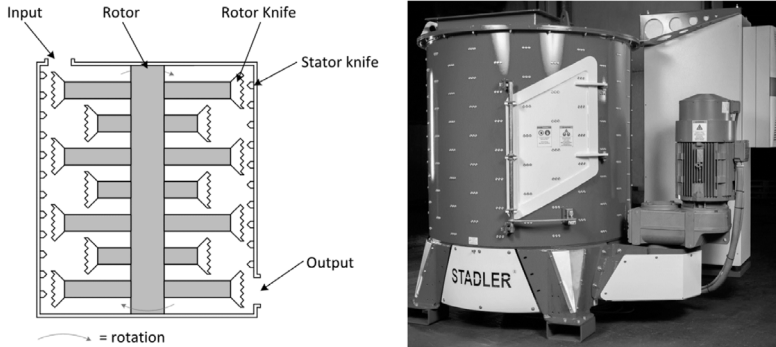


Fig. 3: Scheme and picture of the STADLER “Label Remover” (Küppers et al., 2019).

After manually sorting the input to determine the grade of labelling the material was mixed again to ensure an even distribution of all types of objects. To determine the delabelling performance, the material was scanned before and after delabelling. As only one NIR-Sensor was used the test setup was changed for the analysis phases to scan the material multiple times without it entering the “Label Remover”. After the first analysing phase the material was delabelled (“delabelling phase”) followed by the second analysing phase. After the second analysing phase, the material was manually sorted once by grade of labelling and once by colour.

In both analysing and delabelling phases, the samples were fed into to screw conveyor using a wheel loader. When passing the NIR-sensor the number of pixels of each material (e.g., PET, PET with label, PE, etc.) was recorded. Usually, the analysing phase consisted of five repetitions of recording the pixel data per time unit for the entire material flow plus one repetition of scanning and saving the raw data of the stream to help with the subsequent interpretation of the collected data.

For the German PET, the first analysing phase only consisted of two repetitions due to time limitations. To improve the data under those circumstances and to exclude material loss, as the sample was rather small (63 bottles in total) the material was

not fed through the screw conveyor and put through the whole pilot plant but put on the conveyor belt manually before the sensor and collected directly after. The following steps did not differ from the Belgian material.

As there are multiple conveyor belts between the input and the output of the pilot plant some material loss was unavoidable. This was aimed to be quantified by weighing input and output fractions (3D-material, 2D-material, fines). The output fractions of PET\_Belgium are shown exemplarily in Fig. 4. The fine fraction of the PET-input consisted mainly of broken or small caps (Fig. 4-B) and smaller pieces of shredded labels (Fig. 4-C). Nevertheless, the majority of labels (both shredded and complete) ended up in the 2D-material together with some bigger caps.

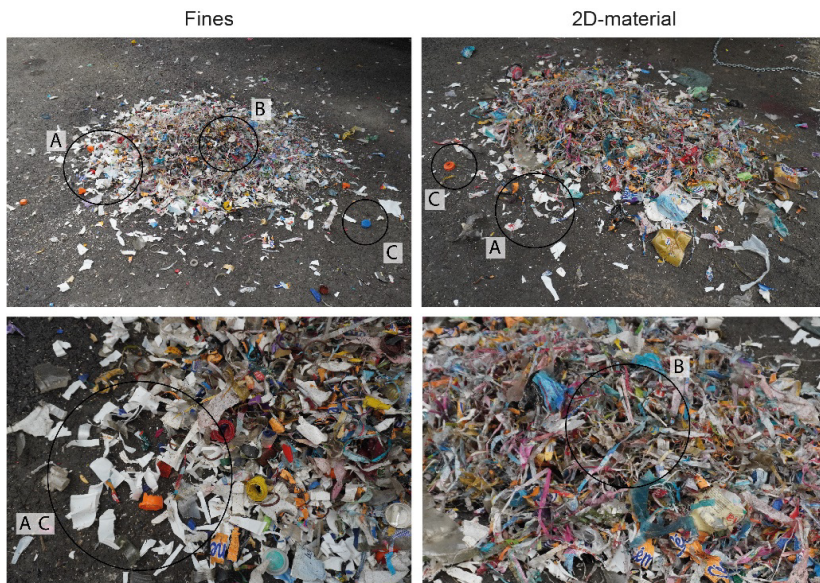


Fig. 4: Output material of PET\_Belgium: Fines (left) and 2D-material (right).  
A: shredded PS contaminants, B: shredded labels, C: caps

It was not possible to clean the pilot plant after analysing and delabelling phases of each sample to exclude the possibility of contamination with remains of former trials. These contaminations can contain material of samples of PS, PE, and PP with different types of labels. In Fig. 4, a relevant amount of shredded parts of white

PS-cups can be seen in both fines and the 2D-fraction (Fig. 4-A), although more of these contaminants were found in the fine fraction. These remained from prior tests with PS-material.

The used teach-in for the trials was designed specifically for the PET input material and tested multiple times with various objects to attain the best possible results. The teach-in includes the definition of background (conveyor belt) and the manually added material classes and their allocated reference spectra. The material classes for these trials differentiate between PET, PE, paper and cardboard (“PPK”), PS, PP, PET\_Mix-Sleeve, PE\_Label and PET\_Label. A distinction of PP and PP\_Label was not feasible due to a limited number of possible material classes. Fig. 5 shows an excerpt of the teach-in:

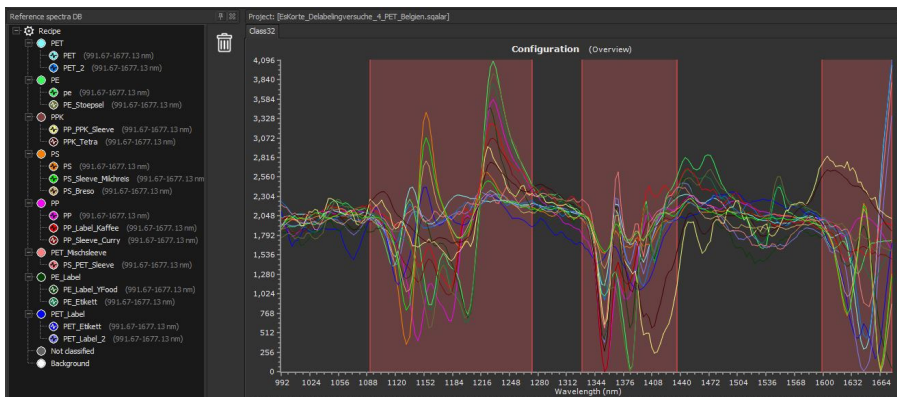


Fig. 5: Excerpt of the Teach-In for PET-material including material classes (left) and reference spectra (right).

The red areas in Fig. 5 show the spectral ranges which are used for classification. The chosen sections are 1092 - 1273 nm, 1330 - 1436 nm and 1599 - 1677 nm. More settings are listed in the following table:

Tab. 2: Chosen settings within the teach-in.

Setting	Value
Wavelength range	220 pixel
Spatial range	232 pixel
Exposure time	450 $\mu$ s
Frame rate	447 Hz
Background: Dynamics of Spectra	< 270

The size of pixels is depended of working width, spatial range, belt speed and frame rate. In particular the pixel width results from the ratio of working width (approx. 700 mm) to the number of spatial pixels monitoring the conveyor belt (“spatial range”). The pixel length is depended on belt speed (0,83 m/s) and frame rate of the sensor.

### 3 Results and Discussion

#### 3.1 Analysis of false color images

An excerpt of the live false colour image of the delabelled material flow can be seen in Fig. 5. The light blue pixels are classified as PET while the dark blue pixels are classified as PET with a PET-label (“PET\_Label”). The picture shows an occasional systematic misclassification of PET-material as PET\_Label in particular on the edges or at the base of the bottles. This can be explained by the general phenomenon of refraction on edges as well as remaining liquids or the thicker wall strength of the bases of PET-bottles. Although a certain level of misclassification cannot be avoided the overall results have been satisfying both for the labelled and delabelled PET-bottles.

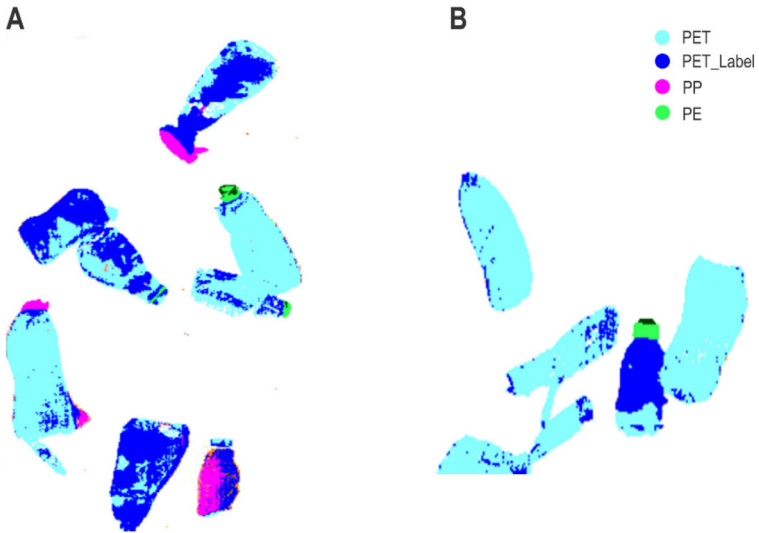


Fig. 6: False color image of the labelled (A) and delabelled (B) material flow.

An interesting detail of the delabelled material flow are the missing caps on many bottles (apparent by the missing pink and green pixels in the false colour image in Fig. 1-B), which have been separated from the bottles during the delabelling process. As they have been sorted into fines or the 2D-fraction they can't be seen in the false color images of the delabelled objects in the analysing phase. In Fig. 7 the missing caps are marked exemplarily in photos of the manually sorted fractions "Partly delabelled" and "No label". In these photos a high number of bottles with missing caps is observable.





Fig. 7: Pictures of manually sorted “Partly delabelled” (left) and “No label” (right) material after delabelling. A: Exemplary bottles without caps.

### 3.2 Analysis of NIR pixel data

Comparing NIR pixeldata of the material flow before and after delabelling an increase of PET-pixels is evident. For the Belgian material, the share of PET-pixels increased on average by 40 percentage points (pp.) while the German increase was 35 pp. (See Fig. 8: Black shares).

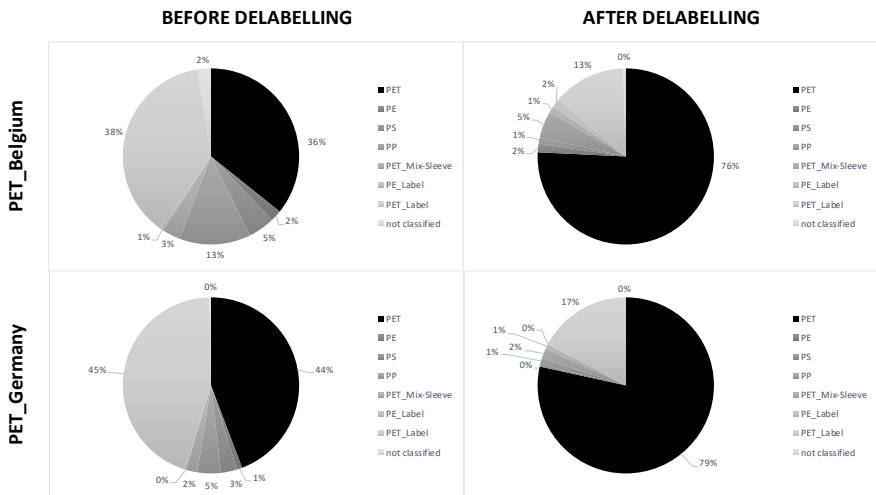


Fig. 8: Mean shares of detected pixels before (left) and after (right) delabelling of Belgian (up) and German (down) PET-material (PET: black).

As the removal of labels increases the unimpaired surface area of PET-bottles the detection of more PET-pixels is the immediate consequence. The share of “PET\_Label” decreased from 38% to 13% for the Belgian and from 45% to 17% for the German material. This was the highest reduction on pixel shares of all material classes of labels. This implies that the majority of labels were made of PET.

Looking into the repeatability of these results Fig. 9 shows the total amount of pixels per trial. One trial represents one repetition in the analysing phase. For PET\_Belgium the coefficient of variation was 3.3% before delabelling and 3.6% after delabelling. For PET\_Germany the affiliated numbers are 0.0% and 6.0%. Considering the low number of objects (63) in the German sample these results show a high reliability on NIR sensor data in this context.

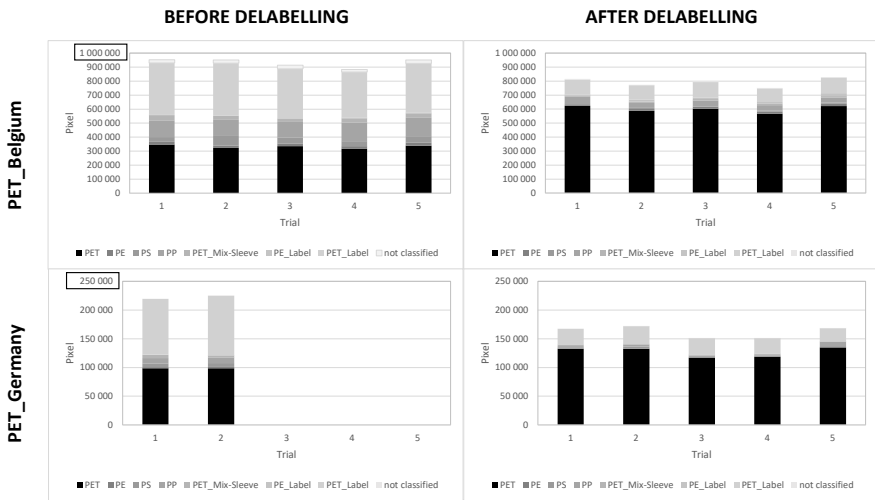


Fig. 9: Total number of detected pixels before (left) and after (right) delabelling of Belgian (up) and German (down) PET-material (PET: black).

Another finding concerns the total amount of pixels before and after delabelling. For both the Belgian and the German material a significant loss of pixels can be detected. The main reason for this effect is the separation of caps during the delabelling process (see Fig. 5) and the separation of PP-labels which were classified as PP (as they are assigned to the same material class). This is implied in the NIR-data by the reduction of about 83,000 PP-pixels for the Belgian material and a reduction of about 6,500 PP-pixels for the German material and was validated

by visual inspection of the raw data. The biggest shift in monitored false colour pixels was found from PET\_Label to PET. The second biggest change occurred in the reduction of PP-pixels.

It is notable that there is a significant difference of total pixels between the two samples which can be explained with differing sampling sizes (PET\_Belgium: 416, PET\_Germany: 63). The average number of pixels per bottle was 2,242 for PET\_Belgium and 3,536 for PET\_Germany. This systematic difference can be attributed to different consumer behaviours and varying packaging designs in both countries resulting in different objects collected in the two countries as, e.g., 26 % of the Belgian material are “Cécémel”-bottles which are rather small compared to the average size of German bottles. Therefore, the SBMM-data appears to be plausible and reliable regarding the total amount of pixels as well.

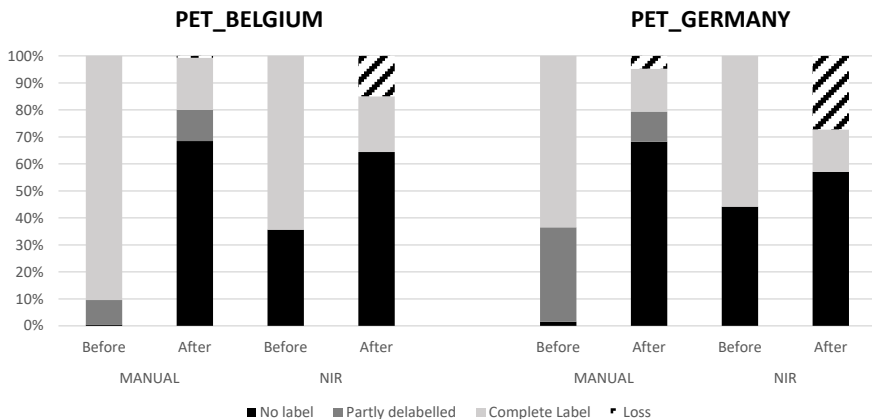


Fig. 10: Comparison between manual sorting and NIR-data including losses before and after delabelling for Belgian (left) and German (right) material (Black: No Label or PET pixel share, Light grey: Complete Label or sum of non-PET pixel shares).

The sensor data was further validated by a comparison with the results of manual sorting. Fig. 10 shows shares of NIR-data as PET and non-PET particles and shares of manually sorted objects classified by grade of labelling (“No label”, “Partly delabelled”, “Complete label”). To enable the comparison the hypothesis states that a bottle without a label consists of 100 % PET. A bottle with a complete label on the other hand is comparable to non-PET-pixels. Both object and pixel shares include

losses caused by delabelling, sorting the material in the ballistic separator or losses within the pilot plant (striped areas in Fig. 10).

The results of manual sorting confirmed the usability of the “Label Remover” for full-sleeve PET-bottles: 80% of the 416 bottles of PET\_Belgium were fully or at least partly delabelled (see black and dark grey shares in Fig. 10) with just 1% loss of objects. The increase of “No label”-bottles was 68 pp. For the German input material (63 bottles) the affiliated numbers are 79% with 5% losses and an increase of 67 pp. In both 3D-output fractions no contaminations with non-PET objects were found.

The corresponding NIR-data showed an increase from 36% to 64% for PET Belgium which equals an increase of 27 pp. with losses of 15%. This increase is significantly lower than the value in manual sorting (68 pp.) which might be explained by the fact that both partly and completely labelled objects in fact show some PET-surface area at least on the bottom of objects. This results in a higher value before delabelling than the presented hypothesis implies. Comparing only the information for delabelled bottles (Fig. 10: “After”) the correlation of manual sorting and NIR data is better: 69 % (“No label”) and 63 % (“PET”) for PET\_Belgium. The same principle can be observed within the PET\_Germany data with 68 % (“No label”) and 57 % (“PET”).

To improve that correlation the average share of PET-pixels of partly and completely labelled objects is needed. However, the results show that the increase of PET-pixels due to the increased exposed surface area caused by the delabelling process can be detected successfully without having any information about the characteristics of the input material.

Lastly, the delabelled bottles were classified by colour. The number of bottles in each category can be seen in Tab. 3. The majority of all delabelled bottles consisted of clear PET (93 %), the rest was dominated by white PET (6%).

Tab. 3: Number of delabelled bottles sorted by colour.

	clear	white	brown	green
PET_Belgium	396	26	3	0
PET_Germany	56	2	0	1
Total	452	28	3	1

These results emphasise the importance of high-quality delabelling processes to enable the separation of white PET-bottles as their colour additives hinder the possibilities of recycling.

## 4 Conclusion

The demanded higher recycling rates of the European Union stress the need of innovation in the waste management industry. To improve the chances for recycling of commonly used labelled objects the industrial use of delabelling machinery is a possibility. To enable a consistently high delabelling performance sensor-based material flow monitoring (SBMM) can be used in a sorting plant, enhancing the success of the following sensor-based sorting steps.

This work presented the following findings for manually picked full-sleeve PET-bottles from PPW sorting plants in Belgium and Germany:

- The delabelling causes a shift in the NIR pixel data from detected “PET\_Label” pixels to “PET” pixels due to the increased exposed surface of the PET-bottles after removing labels.
- The total number of PP pixels decreases through the delabelling process which is caused by the removal of PP-caps and labels classified as PP. This separation of non-PET-material from the PET-stream might increase the chances for a high-level recycling
- The coefficient of variation among repeated sensor recordings was low (0% to 6%) for both input materials which shows the reliable analysis of the material using an NIR-sensor.
- A lower average number of pixels per bottle was detected for Belgian material. This was validated with the results of manual sorting which revealed

differences in the samples from Belgium and Germany caused by different consumer behaviours and varying packaging designs.

- The correlation between sensor data and results of manual sorting works better for delabelled objects. Nevertheless, the increase of delabelled objects is evident in the NIR-data in form of an increase of the total number of PET-pixels as well as PET-shares for both materials.
- The delabelling process revealed that 7 % of all examined bottles contained colour additives (6 % even potentially problematic white additives).

Overall, the results demonstrate the feasibility of using sensor-based quality control (SBQC) to evaluate the delabelling performance concerning full-sleeve PET-material. Regardless, future research could continue to explore the possibilities and challenges of using sensor-data to quantify the delabelling of other materials such as PE, PP, or PS. Furthermore, the potential of object-based instead of pixel-based analysis could be reviewed.

## **Funding**

The authors disclosed receipt of the following financial support: The project “EsKorte” was funded by the Austrian Research Promotion Agency within the program “Production of the Future” under grant agreement 877341.

## References

- Cotrep (2019) Recyclability of plastic packaging. Comité Technique pour le Recyclage des Emballages Plastiques (COTREP) <https://www.cotrep.fr/content/uploads/sites/3/2019/02/cotrep-guidelines-recyclability.pdf>
- European Commission (2021) Packaging waste by waste management operations. Eurostat. Online Data Code: ENV\_WASPAC
- European parliament and the council of the European union (2018) Directive (EU) 2018/852 of 30 May 2018 amending Directive 94/62/EC on packaging and packaging waste.
- Gomes, T., Hurley, R.A., Duchowski, A., Darby, D., & Ouzts A. (2014) The effect of full body versus partial body graphic labelling on beverage Packaging. *Packaging Technology and Science*. 2014. 27: 933 – 943. DOI: 10.1002/pts.2070
- Hüttler, M. (2021) Circular Design of plastic packaging – A comparative analysis. Master Thesis in the Master’s Program “Management in Polymer Technologies” of Johannes Kepler University Linz.
- Küppers, B., Chen, X., Seidler, I., Friedrich, K., Raulf, K., Pretz, T., Feil, A., Pomberger, R., & Vollprecht, D. (2019). Influences and consequences of mechanical delabelling on PET recycling. *Detritus*. DOI: 10.31025/2611-4135/2019.13816.
- Loeza, D., Cailloux, J., Santana Pérez, O., Sánchez-Soto, M., & Maspoch M.L. (2021) Impact of Titanium Dioxide in the Mechanical Recycling of Post-Consumer Polyethylene Terephthalate Bottle Waste: Tensile and Fracture Behavior. *Polymers* 2021: 13(2), 310. DOI: 10.3390/polym13020310
- Pomberger R. (2021) Über theoretische und reale Recyclingfähigkeit (About theoretical and real recyclability). *Österreichische Wasser- und Abfallwirtschaft (ÖWAV)*. 73: 24–35. DOI: 10.1007/s00506-020-00721-5

# Challenges faced during a near-infrared-based material flow characterization study of commercial and industrial waste

Kerstin Kleinhans<sup>1,4</sup>, Bastian Küppers<sup>2</sup>, Juan Carlos Hernández Parrodi<sup>2</sup>, Kim Ragaert<sup>3</sup>, Jo Dewulf<sup>4</sup>, Steven De Meester<sup>1\*</sup>

<sup>1</sup>Laboratory for Circular Process Engineering (LCPE), Department of Green Chemistry and Technology, Faculty of Bioscience Engineering, Ghent University, Kortrijk, Belgium

<sup>2</sup>Stadler Anlagenbau GmbH, Altshausen, Germany

<sup>3</sup>Circular Chemical Engineering (CCE), Faculty of Science and Engineering, Maastricht University, The Netherlands

<sup>4</sup>Sustainable Systems Engineering (STEN), Department of Green Chemistry and Technology, Faculty of Bioscience Engineering, Ghent University, Ghent, Belgium

\* Corresponding Author: Steven De Meester, [steven.demeester@ugent.be](mailto:steven.demeester@ugent.be)

---

Keywords: non-household waste, ballistic separation, material flow monitoring, C&I waste, sensor-based, near-infrared, waste characterization

## Abstract

To gain better insight into the composition and recycling opportunities of commercial and industrial (C&I) waste, a sensor-based material flow characterization (SBMC) study was conducted at a C&I waste sorting facility. The 2D and 3D fractions from ballistic separation were monitored so that the material composition of both fractions could be determined. While previous studies and studies in the literature have mainly focus on the SBMC results, this paper will highlight the challenges encountered during the measurement that have a potential impact on the results. The focus in this regard will be on non-NIR related challenges, SBMC preparation challenges, and classification challenges.



# 1 Introduction

To meet the European Union's ambitions to increase recycling rates further and thus move closer to a circular economy (European Commission, 2020), waste streams that do not originate from households, such as commercial and industrial (C&I) waste, must also be taken into account for recycling. In comparison to household waste, only little information on the composition of C&I waste is available in scientific literature even though its potential for high recovery rates has been documented in previous studies, especially for the plastics fraction (Kleinhans et al., 2021).

To fill this knowledge gap and pave the way for improved recovery rates for C&I waste, a series of near-infrared (NIR)-assisted material flow measurements were conducted at a C&I waste sorting facility in Vantaa, Finland. Better knowledge of the composition of C&I waste will help evaluate the potential for prevention or reuse and can assist in the development of innovative, targeted waste management solutions.

While the typical use of sensor technology is material classification for sensor-based sorting, this and previous studies (Hernández Parrodi et al., 2021; Küppers et al., 2019a) show the optimization possibilities that arise when sensors are used not only for sorting, but also for sensor-based material flow characterization (SBMC). In addition, SBMC enables real-time material flow monitoring of the current material composition and plant downtimes, but the various challenges of applying SBMC at plant scale have rarely been discussed in depth.

In this case study, the 2D and 3D fractions from ballistic separation were monitored, allowing us to determine the material composition of both fractions, and thereby quantifying the separation performance of the ballistic separation process. In the respective process line, further separation is realized with state-of-the-art NIR sorting technology. The material fractions wood, cardboard, high-density polyethylene (HDPE), clear polyethylene (PE) film, and colored PE film are recovered. With the monitoring in this study, also the amounts of recovered polypropylene (PP), polyvinyl chloride (PVC), polyethylene terephthalate (PET) and expanded polystyrene (EPS) were quantified to get a better understanding of the composition of non-household plastics.

The encountered challenges throughout this project are the focus of the present article. These challenges can be grouped into non-NIR related challenges, challenges in preparatory work for SBMC and classification challenges. Aim of

this research is to point out the possible the influences of these challenges on the results of SBMC on the example of conducted C&I monitoring.

## **2 Material and Methods**

This case study has taken place in a sorting facility in Vantaa, Finland that belongs to the Remeo Oy group and operates two lines: one construction and demolition (C&D) and one C&I waste sorting line. The measurements have taken place during 18 – 20 October 2021 in the C&I line, of which a simplified layout can be found in Fig. 1. The C&I line operates on average 15 Mg/h and recovers PE film, HDPE, wood, cardboard, ferrous and non-ferrous metals, solid recovered fuel (SRF) and inert fractions.

As shown in Fig. 1, the SBMC took place after the ballistic separation, this means that the input material has already been shredded (to < 300 mm), sieved, and ferrous and non-ferrous metals have been extracted via magnetic and eddy current separators. Furthermore, the ballistic separator was equipped with 80 mm paddle holes to produce another fine fraction in addition to the 2D and 3D fractions. After the ballistic separation, several downstream NIR sorting steps are applied to produce the desired output fractions.

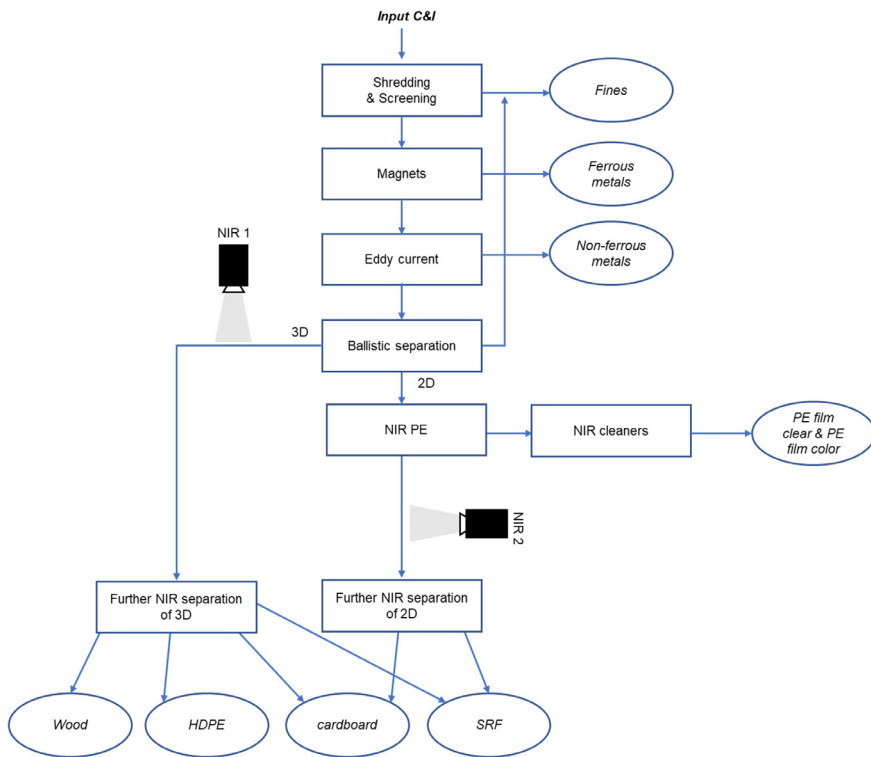


Fig. 1: Simplified flowsheet of the studied C&I line (square shapes stand for separation equipment, oval shapes stand for products)

Similar to previous studies (Hernández Parrodi et al., 2021), two hyper-spectral-imaging NIR sensors (Helios EQ32 from EVK Kerschhaggl GmbH, Raaba, Austria) with a possible spectral range of ca. 930 nm – 1700 nm were used for the material flow monitoring. Halogen lamps (each 400 W covering 300 mm working width) were utilized as emitters and positioned as displayed in Fig. 2 (two lamps on the 2D line and four lamps on the 3D line).

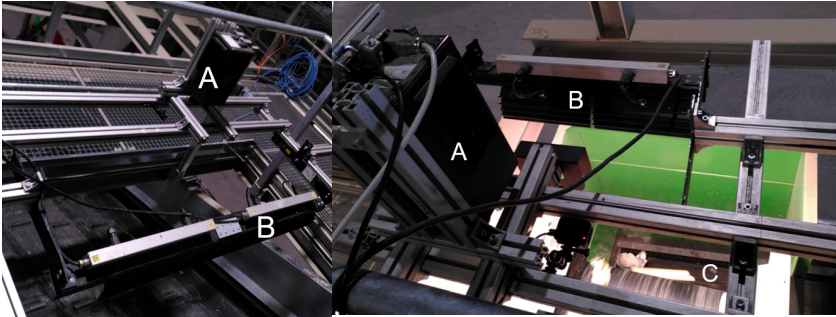


Fig. 2: Test setup in the sorting plant (left: 2D line, right: 3D line),  
A: NIR sensor, B: Lamps, C: Conveyor belt handover

## 2.1 NIR-Analysis

The analysis of the measured NIR spectra was based on a classification recipe that translates the raw spectra into classified data. Further, this recipe links every spatial pixel with 220 spectral information (spectral pixels) and derives, smoothens, and normalizes it to generate stable material-specific spectra. The black conveyor belts constituted the background showing low intensity and dynamics compared to the detected objects. The spectra of different material types of substances (see Fig. 3 and Fig. 4) were defined in the analysis recipe, distinguishing the material classes PVC, PE, PP, EPS, PET, cardboard, wood, and inert. Detected materials whose specific spectrum is not part of the analysis concept are classified as „unknown“ or were wrongly detected as another material if they had a similar spectrum. Only the wavelength ranges marked in transparent red (see Fig. 3 and Fig. 4) were used to classify the different material classes, since these were the ranges that are most important for distinguishing the spectra between the material classes.

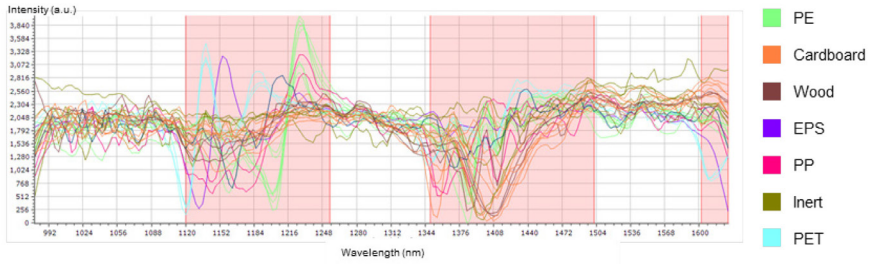


Fig. 3: Used analysis recipe (first derivative, smoothed) for the 2D fraction

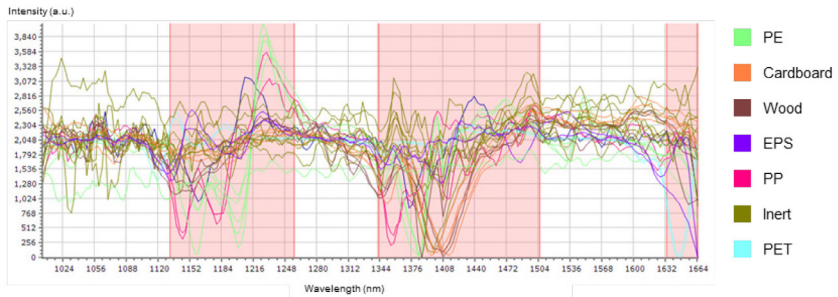


Fig. 4: Used analysis recipe (first derivative, smoothed) for the 3D fraction

The interpreted spectra can be assigned to the measured pixels so that false-color images, as shown in Fig. 5, can be generated.

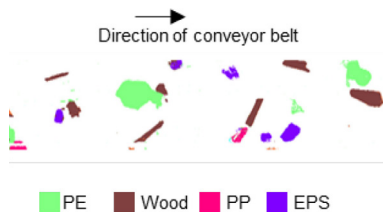


Fig. 5: Example false-color image of the 3D line

## 3 Encountered challenges

Although SBMC offers many opportunities, there are some challenges that influence the validity and the accuracy of the measurements.

### 3.1 Non-NIR related challenges

#### *Fire safety*

Proper lighting is of utmost importance in SBMC, but if lamps are used, as in our case with several 400W lamps, one must be aware of fire hazard. To prevent the lamps from shining on a standing belt and overheating of the black surface, the lamps were controlled via a built-in belt speed monitoring device and switched off when the belt stopped. Furthermore, it is important to choose a sufficient distance to the belt to avoid that waste items, especially film material, might be touching the lamps and could be melted or ignited. Additionally, in case there is a significant dust build-up on the lamps, it is important to clean them frequently as this represents a fire hazard as well. Whereas this does not directly influence the SBMC, one must be aware of the maintenance effort. However, it is possible that dust adhesion on the glass of the lamps might have a slight influence on the measurement, as specific wavelengths may not be detected because they are absorbed by the dust, which is an inert material.

#### *Data transfer*

To enable real-time flow monitoring, a stable connection to a server that stores the data must be provided. During this and previous studies, we have found that having a connection, e.g., to an LTE or Wi-Fi network or using Ethernet cables, is not always possible at every location in a sorting facility, but it is a prerequisite for real-time monitoring.

### 3.2 Challenges in preparatory work for SMBC

#### *Spectral range selection*

The choice of the spectral range to be evaluated greatly influences the classification accuracy. Whereas it is desired to not lose spectral regions that hold important information to distinguish the desired material classes, it should be noted that scaling effects can occur if high absorbance is measured at the margin of the measuring range. For example, a PP spectrum, as reported in previous studies

(Küppers et al., 2019b), shows a high intensity in the raw spectrum between 1000-1150 nm, if this region is included for classification, all other peaks are scaled down, also those that might be interesting to distinguish from other material classes. This might lead to misclassifications if spectra of different material classes cannot be adequately distinguished anymore. In case other classification algorithms are used different effects can occur.

Moreover, the choice of the range to distinguish the spectra is important and should always be made according to the composition of the waste stream and the goal of the classification. If necessary, individual ranges can also be weighted differently to improve the classification, effects of this depends on options of the postprocessing software.

### *Recipe creation*

When adding spectral information of sample material to the classification recipe, it is important that a representative selection of items from the waste stream is made, paying attention to the variability of certain waste items. This means, for example, that a dry and a wet version of a waste item, or an item with a label or sleeve made of a different material, should be included in the desired classification. This will result in adding a variety of spectra for each material class. This preparatory work can greatly impact the accuracy and reliability of the SBMC and should therefore be carried out thoroughly.

### *Background definition*

In this study, a further challenge for classification was the attached dirt on the 2D and 3D line and conveyor belt cleats on the 2D line (see Fig. 6). Although it was possible to adjust the classification recipe to correctly classify both conditions as background, it was necessary to add additional classification rules, e.g., PET is still classified as PET despite low intensity. As a result of this recipe adaption, false classification of some PET pixels as background, or vice versa, might occur.

It is important to find a good balance between not recognizing cleats and not compromising the recognition of waste items to avoid further systematic errors in the SBMC, e.g., recognizing dirt on the belt as inert material. Therefore, it is necessary to handle the background definition and additional classification rules, if any, with care. This problem is more pronounced with low belt occupancy.

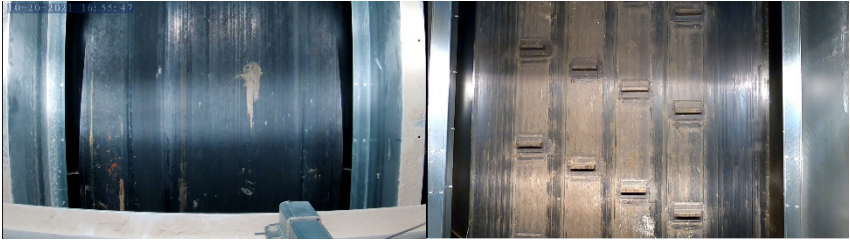


Fig. 6: Photo impressions of the conveyor belts at the location of measurement (left: 2D, right: 3D with cleats)

### Object recognition

The main challenge for classification is also the material flow presentation to the NIR sensor, especially the spatial singling of individual particles. In our study the 3D line had a better object singling, which resulted in less to no touching and overlapping of the waste items. On the 2D line, on the other hand, small debris accumulations occurred frequently and overlays were often seen (see Fig. 7). This is also confirmed by the mean occupation density of approximately 12% on the 3D and 42% on the 2D line. An improved material flow presentation can be achieved by measuring after conveyor belt transfer points or through the use of speed belts.

In general, SBMC can be performed on object or pixel basis. Using object-based SBMC can be useful, e.g., for sorting purposes to control air valves, but is not necessarily useful for material flow monitoring purposes. In particular, the use of SBMC at suboptimal locations in a sorting system, e.g., locations with increased material overlay due to low bandwidth, belt speed, or high throughput, can benefit from pixel-based material flow analysis.



Fig. 7: Photo impressions of object singling on the 2D (left) and 3D (right) line



### 3.3 Classification challenges

#### *Systematic misrepresentation due to overlays*

Due to the overlays, there is a systematic error in recognition of the overlaid objects, as only the surface is scanned. This underestimation cannot always be assigned to a specific material class. However, it can be discussed that due to density differences, lighter materials may be found more often at the top of the overlays. In case a transparent plastic film is part of an overlay, it is also possible that parts of the underlying material are detected, the question to what extent the film and the underlying material are correctly detected would need systematic studies to be assessed. The same effect could also occur in other materials, e.g., in the 3D stream with transparent PET, so systematic studies in both 2D and 3D streams would be of interest.

#### *Carbon-black plastics*

In addition, visual control noted that the 2D line contained significant amounts of black film that were not previously removed at the PE film NIR-sorter. As commonly known, carbon-black items cannot be detected via NIR technology, therefore, this fraction was not monitored in this study. According to our visual analysis, the majority of black items were film materials from garbage bags, assuming these are mainly made of PE we might have an underestimation of PE in the flow monitoring of the 2D line.

#### *False classification of dust adhesions*

A previous study by Parrodi Hernández et al. (2021) showed the potential of SBMC for monitoring inert materials. In our study, we added several spectra of inert material to the NIR recipe, but no large amounts of inert material could be observed in the 2D nor in the 3D stream. However, our measurements showed a fraction of inert material (see Fig. 8). This was because attached dirt on the waste objects is classified as inert pixels. Thus, we acknowledge this as a systematic error and an overestimation of inert material.

#### *Pulp-based materials*

A further issue in this study was the limited classification results of the pulp-based materials wood and cardboard. Both materials were noted to be partly misclassified as the other, especially in the 2D line where the waste items were less separated. This negatively influences the validity and accuracy of the SBMC for the material classes cardboard and wood. We noted that this effect was less prominent on days

with less dust in the air (see Fig. 8). The reason for the lower dust content was rainfall, which increased the moisture content of the waste items, affecting detection quality as reported in previous studies (Küppers et al., 2019b).

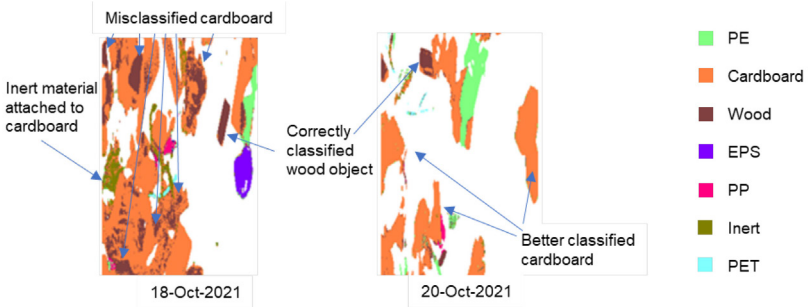


Fig. 8: False color images to show differences in detection quality related to dust content and further systematic errors

### Light overexposure/ direct reflectance

We encountered that, while measuring EPS, we might have a systematic underestimation of pixels. Due to its white color, EPS has a high reflectance and is therefore often partly not recognized (see Fig. 9). This effect could also occur, when monitoring shiny objects, e.g., metal parts.

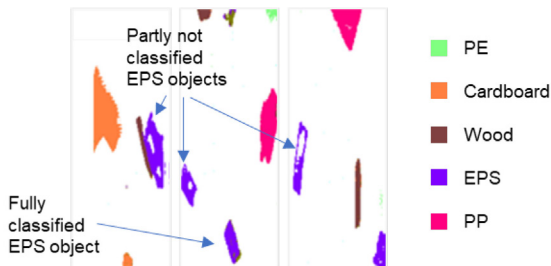


Fig. 9: Screenshots of false color images with differently classified EPS (purple) on the 3D line

Another cause for this error could be a suboptimal white calibration. The white calibration was performed with the help of white tiles placed on the conveyor belt.

Since the tiles are very flat, the maximum brightness from the sensor's point of view is set approximately to the height of the conveyor belt. Therefore, white 3D objects may not be fully detected, as they exceed the maximum brightness. This effect would be even more pronounced with, e.g., trough conveyors or rising conveyor belts with cleats and should be kept in mind while performing the white calibration.

Fig. 10 shows some examples of challenges for the white calibration and the light exposure in general. To be able to perform SBMC independently of ideal situations, like a speed belt with good object separation, one is confronted with for instance different types of conveyor belts, high belt occupancy, overlays, and different sizes of waste items. In the case of high belt occupancy or bigger 3D objects, it might happen that the waste items hinder ideal light exposure, see case (b) in Fig. 10. In addition, white calibration might be challenging on non-straight conveyor belts (see situation c) and d) in Fig. 10), as the focus point of the lamps calibrated via a white tile might not match the real location of the waste items. The items might lie higher or lower depending on the type of belt. This might influence the measured intensity and therefore cause missing pixels or lead to misclassification.

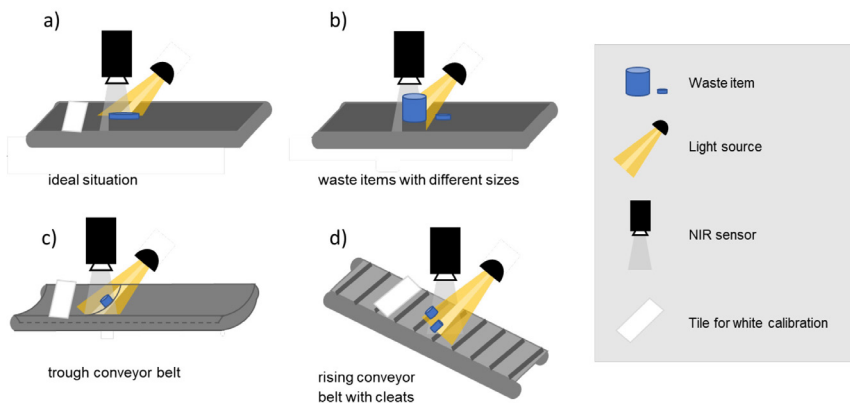


Fig. 10: Challenges for white calibration and light exposure

## 4 Conclusion

This paper discussed the challenges of SBMC of a three-day long (18-20 October 2021) measurement campaign on a C&I sorting line in Vantaa, Finland, after ballistic separation. The tests carried out as part of this study showed that real-time monitoring in C&I sorting systems using NIR sensors is possible, and can be used to create a new data set that can determine the composition of C&I waste.

Various challenges have been identified, ranging from non-sensor related matters, like fire safety or data transfer, to preparatory work for SBMC and classification difficulties. Although some of these challenges might limit the validity and accuracy of the flow monitoring, the potential of this technology outweighs the drawbacks in a significant manner. The potential includes real-time flow monitoring, quality assessment, and the possibility to set the basis for future applications to optimize and control sorting equipment. To do this, it is important to be able to measure under suboptimal conditions (e.g., overlays, dust problems, different belt types and speeds, or varying throughput rates), which was demonstrated to be possible in this and previous case studies.

## Acknowledgements

We thank the Interreg 2 Seas program *PlastiCity* that is co-funded by the European Regional Development Fund under subsidy contract No. 2S05-021 and the province of East-Flanders, Belgium, for funding this research. Furthermore, we thank the staff from Remeo Oy Vantaa and STADLER Anlagenbau GmbH for their support during the tests.

## References

- European Commission, 2020. A new Circular Economy Action Plan For a cleaner and more competitive Europe COM/2020/98.
- Hernández Parrodi, J.C., Kroell, N., Chen, X., Dietl, T., Pfund, E., Küppers, B., Nordmann, C., 2021. Near-Infrared-Based Material Flow Monitoring of Construction and Demolition Waste Nahinfrarot-basierte Stoffstromüberwachung von Bau- und Abbruchabfällen, in: Mineralische Nebenprodukte Und Abfälle. Berlin : Thomé-Kozmiensky Verlag GmbH, pp. 92–111.

- Kleinhans, K., Demets, R., Dewulf, J., Ragaert, K., De Meester, S., 2021. Non-household end-use plastics: the 'forgotten'plastics for the circular economy. *Curr. Opin. Chem. Eng.* 32, 100680. <https://doi.org/https://doi.org/10.1016/j.coche.2021.100680>
- Küppers, B., Hernández Parrodi, J.C., García López, C., Pomberger, R., Vollprecht, D., 2019a. Potential of sensor-based sorting in enhanced landfill mining. *Detritus* 8, 24–30.
- Küppers, B., Schloegl, S., Oreski, G., Pomberger, R., Vollprecht, D., 2019b. Influence of surface roughness and surface moisture of plastics on sensor-based sorting in the near infrared range. *Waste Manag. Res.* 37, 843–850. <https://doi.org/10.1177/0734242X19855433>

# **Increase throughput and sorting quality with flow control**

Stefan Heinrichs<sup>1\*</sup>, Raphael Stein<sup>1</sup>, Andreas Roper Yearwood<sup>1</sup>, Nico Schmalbein<sup>1</sup>

<sup>1</sup>STEINERT GmbH, Cologne, Germany

\* Corresponding Author: Widdersdorfer Str. 329-331, 50933 Cologne, Germany,  
stefan.heinrichs@steinert.de

---

Keywords: process control, throughput, sensor-based-sorting, flow control, automation, product quality, M2M communication

## **Abstract**

The ideal mass throughput of sensor-based sorting units is usually an economic compromise between product quality and productivity. If the mass throughput is too high, the quality of the sorted products does not meet the requirements, while low throughputs result in insufficient production rates.

Although it is desirable to constantly feed the sorting unit with this ideal throughput, practical applications often suffer from significant throughput fluctuations, especially when treating non-bulk materials. With an unregulated feed, a sorting unit is often operated alternately with a too high or a too low throughput. This can usually be explained by an uneven material discharge from the upstream dosing hopper, caused by the material behaviour on the feeding unit. Because of factors such as the filling level of the bunker and partial blockages due to interlocking parts, the material discharge is not constant over time despite constant conveying parameters.

In order to minimize this effect, STEINERT has developed a regulation concept which significantly reduces the throughput fluctuations by continuously regulating the bunker. State-of-the-art camera technology permanently records the current material discharge from the dosing bunker. Utilizing this data, the conveying parameters of the dosing bunker can constantly be adjusted according to the current

situation to generate a more consistent material flow. In addition, the material flow can be adapted to the needs of the downstream sensor-based-sorter. This control circuit clearly homogenizes the material discharge from the dosing bunker and consequently also the throughput of the sorting unit. This approach allows a significant increase in the average throughput of the sorting unit. The system positively impacts on technical and organizational processes, which also contribute to the increased throughput, such as the timely refilling of the bunker. Additionally positive effects on the achieved product qualities have been observed, due to the reduction of overfeeding.

## **1 Introduction**

Ongoing development work leads to a constant shift in the limits of what is feasible. Much of what is considered state-of-the-art today was unthinkable a short time before. In the sensor-based sorting of bulk goods and non-bulk goods, the requirements for the sorting goals to be achieved are shifting ever further. With the relation of product quality and product yield, there is a high priority for the maximum throughput to be achieved, in order to keep the operating costs per processed tonnage low. This publication is not about improving one technical parameter of a sorting machine itself, but about improving the performance of a sorting process as a whole. As a producer of sorting equipment with over 130 years of experience, STEINERT sees itself as a provider of technical solutions for various raw material industries. The following technological concept can be of advantage in the mechanical processing of primary resources as well as in the secondary resources like waste and metal recycling.

The material infeed to a sorter can be measured and controlled by using existing data points in combination with additional data recorded by sensors outside the sorter itself. Efficient material feed control significantly improves the technical limitations of a sorting process like strongly fluctuating throughput rates. With flow control sorting processes can be brought closer to the ideal operating conditions.

## **2 Current feeding of sorting processes**

Functional units in mechanical treatment plants can be categorized into comminution, screening and sorting processes, which are connected by conveyors. In most plants sorting happens in-line after at least one comminution and a screening step. The amount of sorting steps in a row depends on the desired level of sorting depth.

Plants that aim for a high sorting depth produce a lot of intermediate products with small quantities. These intermediates usually need to be re-processed on a multi-sensor unit that is operated in a batch mode as the economics do not allow an own sorting machine per material due to low quantities. These multi-use sorting machines are often built as a stand-alone process with its own peripheral equipment like an own hopper that feeds the material to the sorting unit. The batch process is often used to cover a high variance of different tasks and materials.

Another case are short sorting lines for specified material streams that run in-line without further conditioning, e.g., comminution. These process lines are typically loaded discontinuously by a wheel loader. As a starting point for continuous processing, a hopper or bunker feeder is commonly in use. In common systems different options to design a bunker feeder are available, like vibratory feeders with either electro-magnetic or imbalanced drives, belt or chain conveyors or walking floor conveyors.

To reach constant operating conditions close to ideal throughput, continuous feeding is of key interest, which is true for bulk material as well as for non-bulk material like scrap metals. Practical applications often suffer from significant throughput fluctuations, especially when treating non-bulk materials. The sorting unit is then operated alternately with a too high and a too low throughput. This can usually be explained by an uneven material discharge from the upstream dosing hopper, as depicted in Fig. 1.

The graph shows the material throughput in a sensor-based sorting machine arranged subsequently to a dosing hopper recorded with a 3D-recognition system. In the diagram, four feeding cycles of one bunker can be identified, which start when the bunker is filled by a wheel loader and emptied over the time with constant conveying parameters. The diagram shows that during operation, the feeder creates a very uneven material distribution to the following sensor-based sorter. At the beginning of each cycle the material flow is far above the targeted ideal throughput. During emptying the achieved throughput is constantly decreasing. The



graph drops to zero when the feeder is empty. The filling level of the feeder has to be visible for the operators, in order to perform on time re-filling cycles. Between start and end of each cycle, the throughput shows a clear trend of too much material at the beginning and too little material discharged at the end.

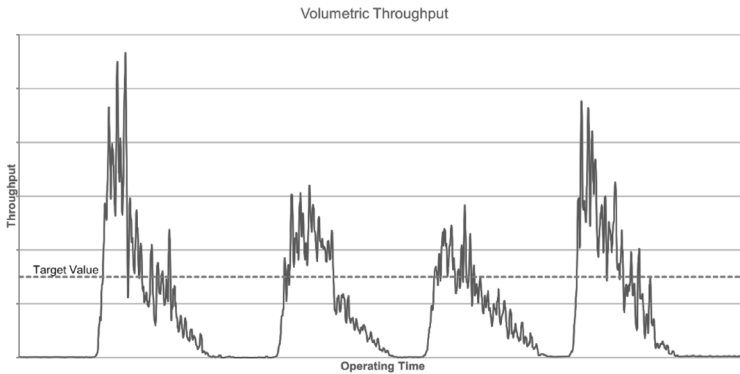


Fig. 1: Uneven material discharge of a non-regulated bunker

## 2.1 Processing dependencies

Once the loading of a sensor-based-sorting machine exceeds the ideal operating point, the quality of the sorting products decreases. With too much material on the belt the sorting process cannot be sufficient due to increased object collisions or overlapping pieces, which subsequently leads to a disturbed detection, increasing number of false classifications and interferences in the discharging area using compressed air. As a result of these inefficiencies the product qualities are decreasing because more impurities are transferred into the product fraction. Also, the recovery of target material into product stream is decreasing, as the number of lost pieces into the residual fraction is proportional to the overload.

On the other hand, feeding a sorting machine below the ideal level means a loss of operating capacity. The potential amount of material being processed efficiently cannot be reached and it also cannot be compensated by feeding above the ideal level as described before. In an economical evaluation, the unused capacity will significantly impact on the operating costs (measured in €/t).

In terms of product quality, the average daily production is affected by the different operating states through the day. On market sale, the mixed product must admit deductions on the target price, which will impact on the revenues, as well.

## **2.2 Impacts on conveying**

The conveying speed of a vibration conveyor depends on several factors like vibration amplitude, vibration frequency, material layer height, inclination of the conveyor trough, friction generated by the lining material and characteristics of the feeding material. As most of the conveying parameters can be seen as constant, the material height in the bunker and therefore the weight of the filling that is lasting on the vibrating trough is changing while emptying. The impact of the changing material weight is depending on the installed drive of the vibration conveyor, which can be either electromagnetic or imbalance drives. Electromagnetic driven vibration conveyors are less robust against such changing conditions.

Another significant impact on the conveying behavior are the characteristics of the feeding material. Especially non-bulk material tends to build partial blockages due to interlocking pieces. While bulk material like gravel generally has a similar shape, it is also easy to define a specific particle size distribution, non-bulk materials vary a lot due to the shape and therefore it becomes challenging to even define a particle size. In an auto shredder residue (ASR) material almost every imaginable shape can be found. There can be flat sheets, longish pieces, wires, wire balls, deformed sheets, stripes, bars, balls or foils. Besides the shape, the material composition can vary a lot as well. Common ASR material consists of different non-ferrous metals, ferrous metals, stainless steel, wood, rubber, plastics and minerals, such as stones or ceramics. Consequently, a high variance of the specific particle weight can be observed for non-bulk materials, which impacts the specific conveying behavior.

Another significant influencing factor in operating a sorting plant at ideal capacity is human behavior. Defining the optimal operating point with regards to the throughput is often done based on optical estimation of the operator at single points and is therefore highly subjective. A readjustment of the feeding parameters is often based on some observations over a short period of time, which most likely does not lead to an improvement in long term. By knowing Fig. 1, any readjustment based on one point in time cannot lead to an enhancement of the full discharging cycle.

To use the sorter to capacity the material supply must be steady, and the bunker must never be emptied completely. In some plants it occurs that a hopper is not refilled right on time due to organizational reasons. Without monitoring the filling level of the bunker, this can happen several times a shift, which means unused operation capacity and therefore monetary losses.

### **3 Optimizing the material feed**

Running a mechanical sorting machine close to the ideal operation point requires steady operating conditions. One key aspect of optimization is to continuously transfer resting feedstock in a bunker to an even feed and thereby achieve a throughput that balances productivity and quality. Depending on the material properties the technical challenge to reach and maintain an even material flow is high.

#### **3.1 Technical set-up**

As our observations have shown, the hopper is the key element regarding the actual throughput that arrives at a sorter. Therefore, there is a need for a technical installation that monitors the material stream that leaves the hopper. This monitoring must happen right at the discharge of the hopper or very close to the hopper on a subsequent conveyor.

As described by (Römisch, 2011, p.187), a volume flow on a continuous conveyor system can be described as a product of the cross-sectional area ( $A$ ) and the velocity ( $v$ ) of the material.

In the described set-up, a 3D camera is used to record aforementioned values. Optical flow calculations provide a sufficiently accurate information on the volume flow that is moving through the observed area. This information is sent to a control unit, where a controller algorithm translates the deviation from the targeted volume flow into a change in hopper speed, which is transmitted as an analogue signal to the frequency controller of the hopper drives or as a digital signal into another control unit, e.g., via a standardized bus system.

Fig. 2 shows the control loop model of “flow control”. The upper part of the figure shows the control loop at the hopper, where the 3D-camera records the previously explained measured volume flow (actual value) and compares it constantly to a set target volume flow (setpoint). In order to reach the setpoint, the hopper speed is then regulated.

The hopper control loop furthermore receives constant validation from the sensor-based sorter (sbs). In a second control loop, the measured volume flow (actual value) is compared to an ideal volume flow (setpoint). A deviation from the ideal flow in the sensor-based sorting unit is translated into an in- or decrease to the target volume flow at the hopper.

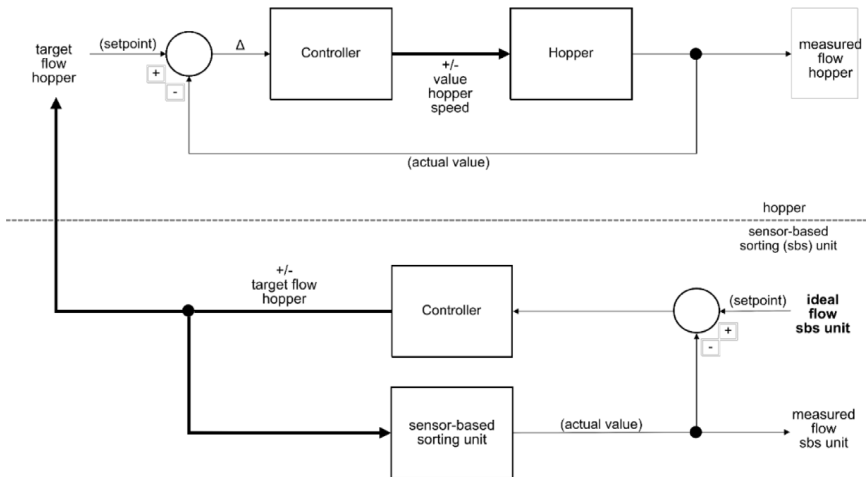


Fig. 2: “Flow control” - control loop model

As can be seen from the description of the control loop, the evaluation of the volume flow in the sorting machine happens ‘close to sorting’ and is decisive for the short-term control of the feeder (distant to sorting). Both units transfer data and signals with direct machine-to-machine (M2M) communication. Applied direct M2M communications are of advantage as no vertical signal exchange to a higher-level control system is necessary. The essential signal exchange stays horizontal between the involved units.

As keeping the material flow steady is the main target, the system also has to deal with different situations. An empty hopper discharge can have two reasons: (A) the bunker is empty or (B) the material has blocked the upstream funnel. For case (A) the system must recognize that the hopper is empty in order to prevent a continued increase of the feeder speed due to automated regulation. In case (B) the blocked material needs to be liberated by a spontaneous shaking at high drive speed. To recognize the fill level of the infeed bunker, the system is equipped with additional sensors.

Another use case for level metering is to indicate when to refill the hopper to ensure a continuous operation. This information can either be forwarded to a control room to start other processes or to a machine operator to manually refill the system, for example using a wheel loader.

The volume flow measuring module with the 3D camera itself can also be installed on a conveying system independently from a feeder. This would enable the detection of volume flows at almost any point in a treatment plant to monitor also other processing machines like crushers, screens or non-sensor-based sorters like eddy-current separators.

If the volume flow needs to be regulated, the system has to be installed on or close to a bunker. STEINERT offers either a fully equipped bunker feeder or the option of retrofitting an existing bunker. The retrofitting option depends on some technical and organizational requirements, which are described below.

### **3.2 Technical and organizational conditions**

In order to add the flow control system to an existing processing plant, the layout and equipment is required to match several conditions. To be controlled by the flow control system, the bunker's conveying speed needs to be adjustable via an electrical input signal. The range of this control should be enough to eliminate blockages in the bunker on the one end and completely stop conveying at the other end. Bunkers with magnetic vibrating hoppers offer larger flexibility, due to their wide range of control and the fact, that they can be adjusted very precisely and react quickly to rapid changes in the input signal (Schubert, 1984, p. 378).

Positioning of feeding devices and the sensor-based sorter also has a huge impact on the performance of the flow control system. As described in chapter "Technical

set-up“, the flow control system uses the volume flow measured at the bunker and at the sensor sorter and combines these measurements to continuously set the bunker speed to its optimal value. Short distances between those two points of measurement are favorable while long distances result in a slow responding system. However, with the feedback from the sorter, the usual deficit of long distances can be partially compensated.

Regarding the input material, it is crucial, that the individual pieces can be separated and do not stick together. Especially high contents of wires and cables in the input material tend to create clusters of material which decrease the performance of the flow control system significantly. In cases with a large quantity of such material, the feeding of a process with liberated material requires other solutions, such as additional comminution to liberate material and create steady material flows. The flow control system has originally been designed for particle sizes above 4 mm, but first tests have also shown a good performance at smaller size ranges for certain input materials. Some recognition systems often suffer when the material surface is shiny, e.g., for stainless steel. In all tests carried out, the described system showed a high robustness towards shiny surfaces.

Furthermore, it is important to provide a proper training to equipment operators, working with these systems daily. As for any technical installation that is operated in harsh environmental conditions like treatment plants it is crucial to maintain the equipment properly. Especially cleaning the system as well as conducting the necessary maintenance steps should be included into a company's modus operandi to keep the flow control system operational and in ideal conditions.

## **4 Improving production and qualities**

Regulating the material flow to run a sorting machine close to an ideal operating point impacts on both, the achievable sorting qualities and the production of a material processing facility.

### **4.1 Impacts on sorting qualities**

The three key parameters of a recycling sorting process, as described by (Bunge, 2011), are recovery rate, product quality and throughput rate. In Fig. 3 this interdependency is depicted.

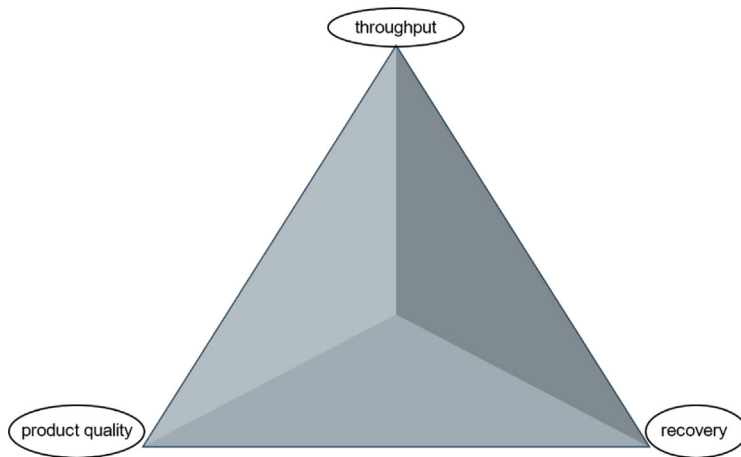


Fig. 3: Qualitative sorting dependencies

A high level of all three parameters is obviously desirable. However, the parameters influence each other. Shifting the focus to one of the parameters has a negative influence on the others. For example, very high product qualities can only be achieved when throughput rates are kept low to have an optimal object singulation on the belt and accepting losses in recovery by ignoring material compounds at the same time.

While recovery rate and product quality can be influenced in a sensor sorter itself, e.g., by changing sorting algorithms or compressed air settings, the throughput rate needs to be controlled before entering the sensor-based sorter.

To optimize all three parameters, an additional system like “flow control” is necessary to achieve an optimal sorting state and thereby high economic feasibility. “Flow control” automatically adjusts the material flow rate as predetermined by a process engineer and the plant operator according to the desired sorting target. Not only finding an ideal throughput rate but also assuring that this rate is achieved constantly, is an important factor to constantly achieve high product quality and recovery rates.

Scrap and waste streams are generally very heterogenous and thus in many cases difficult to convey and discharge. Especially automotive shredder residues (ASR) or

cable-rich input materials often tend to clog hopper outlets. In manually controlled systems, it can take a long time until blockages are noticed by the operator and the hopper speed is manually increased to unclog the material.

Fig. 4 shows a statistic of a volume flow rate generated in a STEINERT KSS sensor sorter. The material sorted was an ASR material. The graph shows two states of operation. First state from approx. 5:30 to 7:25 am shows manual operation by the plant operator controlling the hopper speed from a control cabinet. The second state begins at around 7:25 am when “flow control” was activated for automated operation.

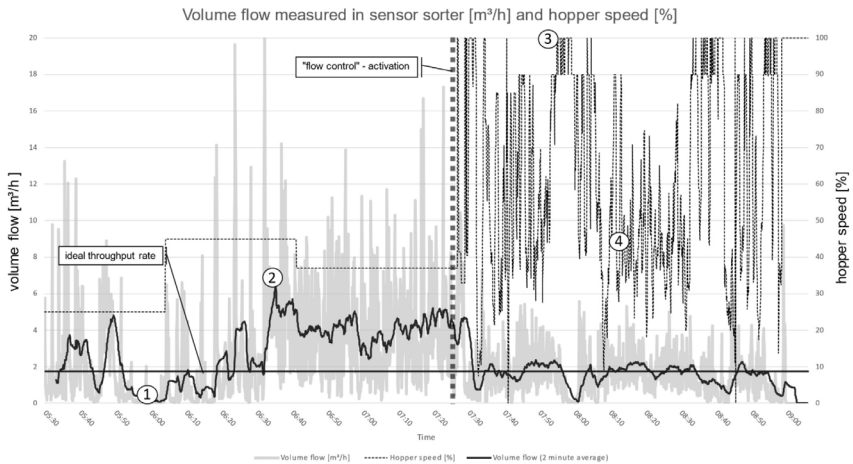


Fig. 4: Volume flow in sensor sorter and hopper speed

A few interesting states can be observed in Fig. 4. At around 5:50 am there is a decrease in volume flow for around 30 minutes that has been caused by a blockage in the hopper outlet (1). With manually increased hopper speed, the blockage was removed at 6:20 am. However, this increased hopper speed later on leads to a higher flow that was either not seen or misinterpreted by the plant operator leading to a volume flow that, at its peak, is more than three times higher than the ideal operating point (2).

With “flow control” activated blockages are detected immediately and the hopper speed is increased automatically to the maximum (3). Idle time with no or only low



throughput entering the machine is thus reduced significantly. While operating, “flow control” does small adjustments keeping the machine operating at the predetermined ideal operating point (4), which impacts positively on the sorting qualities, as well. The level of regulation cycles underlines the necessity for constant monitoring of the material feed, which proves the necessity for a system as described.

## **4.2 Impacts on production**

In recycling processes, sensor-based sorters usually are the most expensive sorting equipment (compared to screening, magnetic sorters, etc.) with regards to both acquisition and operating costs. It is hence desirable, to especially operate sensor sorters at full capacity and thus reduce processing costs.

Sensor-based sorters are often used as stand-alone applications for multiple input materials. “Flow control” also offers more advantages here, as it is fully integrated with the sensor-based sorter software. A customized sorting program can be stored together with a customized “flow control” program resulting in optimized controls for the three key parameters throughput rate, recovery rate and product quality for every input material.

The filling measurement inside the bunker provide the plant operator with information on the material quantity that is available to the plant. This data can either be sent to the control room or can be linked to visual indicators, like a traffic light system, to give information on the necessity to add material. Assuring the system is constantly filled with input material and thus operated without idle times, furthermore, decreases overall processing costs.

## **4.3 Installations**

The first application of “flow control” has been installed in a STEINERT line sorting system (LSS) equipped with either a LIBS sensor for aluminium sorting or XRF sensors for heavy metal scrap sorting. Line sorting systems have the highest requirements for a constant infeed as the input material needs to be isolated into a single file. Peaks in the machine infeed result in an overlapping of objects and thus in poor sorting results. Since line-based sorting systems are immanently lower in capacity than standard belt sorters, it is even more crucial to run them at their ideal operating point.

“Flow control” was later successfully implemented with other STEINERT belt (KSS) and chute (CHUTECH) sensor sorters and is now in operation at various sites. Furthermore, existing hopper and sensor sorters in operation were retrofitted with the 3D-camera module and a software upgrade. Many different types of infeed material and particle sizes down to 4 mm were successfully controlled.

## **5 Conclusion**

The introduced system can make a difference in achieving production targets of mechanical treatment plants. Regulating the material feed to a sensor-based sorter is an important parameter to reach constant production conditions and subsequently improved and steady sorting qualities.

At the same time the overall throughput can be increased due to a reduction of underutilization and systems running idle. As shown before demanded quality goals do not allow a compensation of lost production time by running higher throughput rates. The targeted full capacity can only be reached by operating machines on a constant level. The automated regulation system supports to avoid production losses.

The installation positively impacts also on the operating procedures on site for two reasons. Firstly, the operator gets the information when the bunker needs to be refilled, which normally has to happen by visual inspection. Secondly, the operator does not need to regulate the conveying speed manually, as the system regulates the material flow automatically. The necessity to monitor the feeding equipment by the operator while interrupting other tasks becomes obsolete. Therefore, the daily workload of staff can be reduced.

The system is available and can be offered for different plant configurations. Retrofitting of an existing bunker in combination with a STEINERT sensor-based-sorter is possible as well as a fully new installation including an automatically regulated bunker.

Possible routes for further development are applications of the system for more complex processing lines and extend it to systems that are not controlled by complex routines, such as magnets, eddy currents or other mechanical processing equipment. The application of additional sensors for such approaches have already been tested positively.

## **References**

Bunge, R. (2012). *Mechanische Aufbereitung* (1. Auflage). Wiley-VCH Verlag.

Römisch, P. (2011) Stetigförderer. In: *Materialflusstechnik*. Vieweg+Teubner Verlag.  
[https://doi.org/10.1007/978-3-8348-8196-0\\_6](https://doi.org/10.1007/978-3-8348-8196-0_6)

Schubert, H. (1984). *Aufbereitung fester mineralischer Rohstoffe Band III* (Second edition). VEB Deutscher Verlag für Grundstoffindustrie.

# **Sensor-based sorting and the Circular Economy**

Mathilde Robben<sup>1\*</sup>, Daniel Swaab<sup>2</sup>, Jens-Michael Bergmann<sup>3</sup>

<sup>1</sup>TOMRA GmbH Mining, Wedel, Germany

<sup>2</sup>TOMRA GmbH, Circular Economy, Mülheim-Kärlich, Germany

<sup>3</sup>TOMRA GmbH Mining, Wedel, Germany

\* Corresponding Author: Feldstraße 128, 22880 Wedel, Germany, mathilde.robben@tomra.com

---

Keywords: Sorting, Green Mining, Circular Economy, Energy transition

## **Abstract**

Climate change, environmental pollution, resource scarcity, global population growth are amongst the defining issues of the 21<sup>st</sup> century. Approaching them by transitioning to a circular economy is one of the central challenges of our time.

Making the shift from linear to circular while building thriving economies requires decreasing the environmental impact of extracting raw materials radically, reducing the use of primary resources, designing waste-free products, including recyclable materials, and implementing technologies to ensure the system is regenerative. Sensor-based sorting solutions have proven their worth, as a ground-breaking technological innovation, in both the primary and secondary resource industry.

Further technology development is essential to approach circularity, but technology alone is not enough to create a circular economy: public policy, consumer engagement, and collaboration across the complete value chain are necessary too.

# **1 Introduction**

Today, we follow the linear economy. Resources are extracted from the earth; raw materials are processed to create products and the products are disposed of after use. A shift is made in how we think about the use of minerals and metals from a production-disposal mentality towards ongoing use and re-use underpinned by a transition to renewable energy resources, the circular economy.

As the world addresses the environmental challenges of our time and the recycling industry and consumer goods companies dominate the conversations on this, the mining industry has an important contribution to make, as a major producer of minerals and metals, as well as a big consumer of energy.

Mining companies need to find ways to maximize the efficiency of their operations to cut back on the use of water and other limited resources while reducing waste and the total impact on the environment as much as possible.

The total inventory of resources in use by humankind is ever-increasing, both in mass as well as in diversity. Even in case, the circle can be closed with high recycling rates there will always stay a need for primary resources. However, this can be seen as an opportunity for the mining industry to re-think the way it fulfils this essential role with minimum impact on the environment and without losing sight of profitability. The primary resources entering the circle should be extracted in the most sustainable way.

## **2 The role of sensor technology**

Technology plays an essential role in achieving the ambitious aim of a circular economy. It is necessary to employ state-of-the-art approaches that push boundaries. Sensor-based technology in reverse vending equipment recovers material and enables a clean look recycling of for example beverage containers and sensor-based sorting solutions have proven their worth in both the primary and secondary resource industry.

Sorting is implemented in the fields of waste management and recycling, where it can be used to increase precision and streamline processes. It is used as large-scale industrial technology to sort mixed waste into different material types. This optimizes yield and quality of recyclable materials such as plastic, metals and paper.

The importance of recycling is not just for material purposes, but also for a reduction in emissions associated with production.

- One metric ton of recycled plastic feedstock on average offsets greenhouse gas emissions equivalent to 1.9 t CO<sub>2</sub> (<https://systemiq.earth/breakingtheplasticwave/>).
- If we sort and recycle one tonne of mixed waste before sending it to landfills, we could save 0.309 t CO<sub>2</sub> emissions.
- If we sort and recycle one tonne of mixed waste before sending it to incinerators, we could save 0.349 t CO<sub>2</sub> emissions.
- By collecting and sorting mixed waste materials before they are burned or tossed into landfills, we can avoid up to 730 million t of CO<sub>2</sub> emissions by 2030.

Sensor-based sorting technologies can also significantly reduce the environmental impact of mining operations and, at completion, contribute to rehabilitating the site. They also enable much more efficient use of resources. Implementing sorting may result in a smaller footprint for the mining operation, the need to use specific chemicals in beneficiation plants to be reduced, and the ore recovery to be maximized. These solutions bring the dual benefits of greater sustainability and better profitability for the mining company.

### **3 Potential value add of sorting in mining**

Sensor-based sorting technology is in comparison to other mineral processing techniques a technology that uses little resources such as water and chemicals per ton of product. The average energy consumption of the equipment is around 0.5 kWh/ per ton of feed. No water is needed as a sorting medium, only occasionally for material preparation. The sorters can be containerized and the footprint is relatively small.

In mining and processing, there are three areas for sorting to have a positive impact on the environmental footprint.

- ROM waste removal, i.e. reducing energy, water, chemicals use by using sorting to reduce the barren material which needs to be processed.
- Extension of the life of mine, as lower grade material can be upgraded and thus be economically processed.
- Re-processing marginal dumps.

According to a study conducted by the IEA (IEA, Key World Energy Statistics 2020 Report) mining consumes up to 4% of global energy production annually. An estimated 50-75% of the energy used is for the liberation/comminution of ore and minerals only, making grinding the most energy-intensive part of the production cycle. Considering that grinding is the most energy-intensive part of the production cycle, implementing sorting in the early stages of processing reduces waste material and shrinks the carbon footprint while increasing profitability.

In the table below an overview is given on estimated average savings caused by sorting.

Tab. 1: Estimated environmental and productivity value add of sensor-based sorting

Effect of sensor-based sorting	Environment	Cost & productivity	Savings
<b>Decreased energy consumption</b> Transport, pumping & dewatering, disposals	X	X	15 kWh saved per ton of material & 2% to 3% of the world energy consumption is used for crushing, screening, <b>and milling</b>
<b>Decreased water consumption</b> Cooling, transport in the process	X	X	3 to 4 m <sup>3</sup> water saved per ton of material
<b>Reduced carbon footprint</b>	X	X	CO <sub>2</sub> /Green counter, 7.5 kg per ton of material sorted

Effect of sensor-based sorting	Environment	Cost & productivity	Savings
<b>Decreased Transport cost</b>		X	Costs down €0.30/ton/km
<b>Chemical usage decrease</b> Flotation reagents, acid for leaching and cyanide	X	X	A few grams up to a few kilos per ton
<b>Reduced tailings</b> Fine particles	X	X	3 m <sup>3</sup> tailings volume per ton (2 m <sup>3</sup> material plus 1 m <sup>3</sup> water)
<b>Productivity increase</b> De-bottleneck conventional process		X	Per ton of waste 1 additional ton of ore production
<b>Lifetime of mine increased</b>	X	X	30-50% longer life of a mine
<b>Waste into value</b> Create sellable product	X	X	The coarse waste rejected can be sold (for a low price)
<b>Reduced cut-off grade</b> Higher dilution in the mine, process marginal dumps		X	30-50% more reserves
<b>Legislation</b>		X	Up to 3 years quicker approvals



## **4 Conclusion**

There are economically viable solutions available today that can accelerate the path towards a circular economy and a green mining industry. Sensor-based sorting solutions are proven in both the recycling and the mining industry. The synergies of the applications in both industries are not only the technical similarity of the equipment but also the achievement of environmental improvements.

The mining industry must contribute to the approach of the circular economy. Beyond efficient operation and resource management in extracting primary resources, it is necessary to curtail excessive consumption and ensure products are designed to be reused, and once at the end of life, easily recycled. This means the roles of all actors along the value chain, including the industries and the customers, have to be considered, so that holistic and integrated recovery and recycling systems can be developed and tested.

A combined effort, support, and willingness to collaborate from government, industry bodies, and the public will be required to help achieve circularity. The perfect time to start to make the future more sustainable is now -with the technologies available and proven.

# Sorting of Construction and Demolition Waste for coarse fractions

Sebastian Müller<sup>1\*</sup>, Anette Müller<sup>2</sup>, Ines Döring<sup>3</sup>, Ulrich Palzer<sup>4</sup>

<sup>1,2,3,4</sup>IAB — Weimar Institute of Applied Construction Research, Über der Nonnenwiese 1, Weimar 99428, Germany

\* Corresponding Author: Über der Nonnenwiese 1, 99428 Weimar, Germany, s.mueller@iab-weimar.de

---

Keywords: construction demolition waste, CDW, recycling, brick, concrete, gypsum, building rubble mix, sorting, free-fall, sensor-based, near infrared NIR, colour detection

## 1 Sorting systems in the recycling economy

Attendant with the rapid development of computer technology and significant advances in sensor engineering, the development of sensor-supported sorting processes has been observed since the mid-1980s. In waste processing, the introduction of sensor-based processes began with the sorting of waste glass on channel sorters. Since then, the performance of the machines and equipment has been continuously improved. Today, the detectors used range from visual spectroscopy to X-ray fluorescence spectroscopy. The particle size range in which the sensor-based processes are applied is also steadily further developed. The lower limit currently stands at 1 mm for sorting ceramics, porcelain and stones from waste glass [1; 2]. But there are also examples of the optical sorting of large and heavy fragments with a mass up to 2 kg [3]. In the recycling economy, sensor-based sorting is indispensable today – for example for the recovery of secondary raw materials from mixed plastics or for the separation of recyclables from mixed paper waste. It forms the basis for the realization of material cycles. In contrast, sensor-based sorting is still found only rarely in the recycling of Construction Demolition Waste (CDW), although it is the only process offering the possibility to separate different types of mineral construction materials. As a key player in sensor-based sorting, OptoSort GmbH has developed “Apollo”, a freefall sorter. Its efficiency in

sorting construction waste has been analyzed by the company IAB Weimar gGmbH in wide-ranging sorting and separation tests. The results are presented here refer to the detection of components in CDW with the help of near-infrared (NIR) technology and the separation of the mixes based on this. Colour sorting as another option that can be realized with the “Apollo” or the combination of the two detection options is currently undergoing tests.

## 2 Features of the sorter

The “Apollo” freefall sorter (Fig. 1) is a “channel machine” in accordance with the classification introduced by Pretz and Julius [4]. A vibrofeeder is first used for the singularization and uniform distribution of the recycle that is fed over the entire 600 mm working width of the sorter. From there, the stream of material is transferred to an inclined channel, where it is further accelerated and the particles singled. During freefall of the feed below this channel, the particles are inspected. The

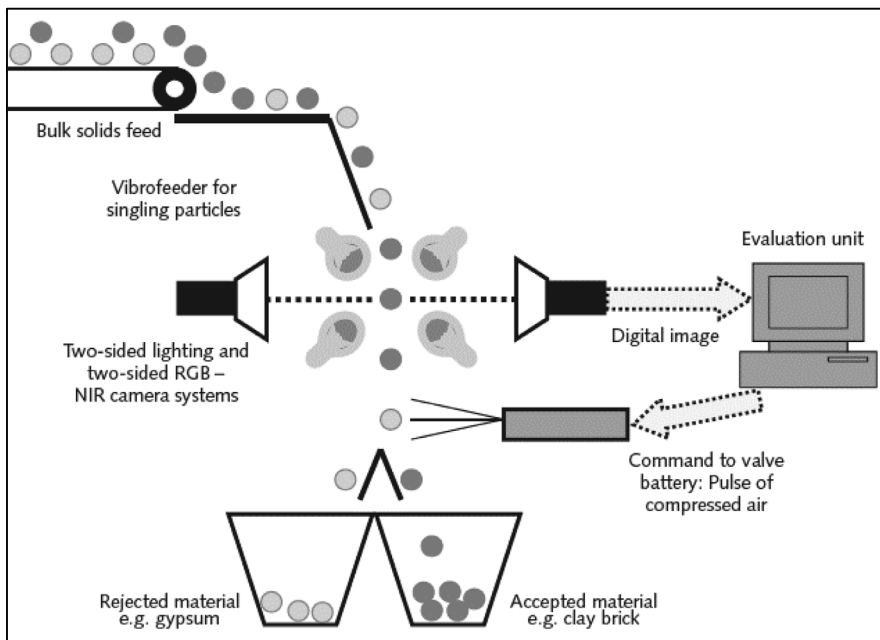


Fig. 1: Schematic showing the freefall sorter, ©OptoSort GmbH, IAB Weimar gGmbH

For inspection, it is possible to combine colour detection and hyperspectral NIR technology with each other. Sensors arranged on both sides of the material stream scan two opposite surfaces of each particle. This setup is essential for sorting construction waste, making provision for the fact that coarse particles in construction waste can consist of several components. For example, layers of mortar or gypsum often stick to wall construction materials, and these cannot be detected with only one-sided detection. The technical layout of the individual machine groups in the recycling test centre at IAB Weimar gGmbH begins with feed of the mix to be sorted on the “Material feed” level (Fig. 2). From there, the material is transferred on the vibrofeeder to the “Sorting machine” level. The materials are identified in the freefalling stream of material, with colour recognition and hyperspectral near-infrared (NIR) scanning being performed individually or in combination with each other. In either case, sensors on the two sides of the material stream scan two opposite particle surfaces. Depending on the scanning results, at the “Material discharge” level, the particles are either discharged by means of compressed air as “rejects” or leave the sorter in freefall as “accepts”. To minimize the consumption of compressed air, generally the material present in smaller concentrations in the feed mix is “blown out” of the material stream. The sorter is suitable for sorting particle sizes from 8 mm to 75 mm with a maximum particle size ratio of 1:4. For example, 8/32 mm or 16/64 mm fractions can be sorted [5].

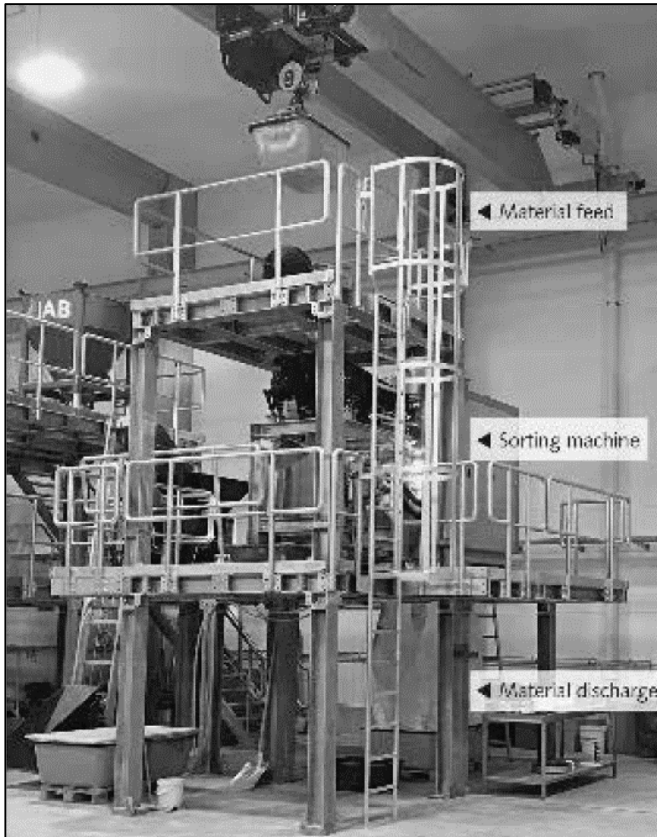


Fig. 2: "Apollo" freefall sorter at its installation site, ©IAB Weimar gGmbH

### 3 Results of selected sorting tests

In the processing of CDW, different sorting tasks must be combined. On the one hand, it may be necessary to remove impurities from a mixture of CDW to make it usable for defined applications. Frequently occurring mineral impurities include gypsum or lightweight building materials like autoclaved aerated concrete. As a non-mineral impurity, wood can also be contained, because this cannot generally be removed completely with conventional dry sorting techniques. On the other hand, the recovery of useful materials from CDW is often required. For example, the recovery of unmixed brick particles from building rubble is of great interest because

these can be used in vegetation technology. For recycled aggregates, which are needed in the production of R-concretes, a defined composition must be maintained. With the help of sensor-based sorting, the composition can be selectively modified to meet relevant specifications. In the extraction of raw materials for the production of construction materials, their extraction is mostly controlled such that starting materials meeting requirements are produced. Where raw materials are becoming scarce, as apparent in the gypsum industry, sorting can help to selectively control the composition of previously unusable raw materials so as to make these usable for subsequent production of construction materials.

### 3.1 Removal of gypsum from a building rubble mix

The starting material was a mix of building rubble consisting of brick, concrete and gypsum in the size range 22.4/63 mm. The gypsum content, which made up 4.9 wt% of the material makes on the one hand recycling impossible and on the other hand landfilling required. Prior to the sorting process, the NIR spectra of the construction materials to be separated were captured (Fig. 3) and the sorting program taught to detect these materials. Around 60 kg of the mix for separation has passed the sorter.

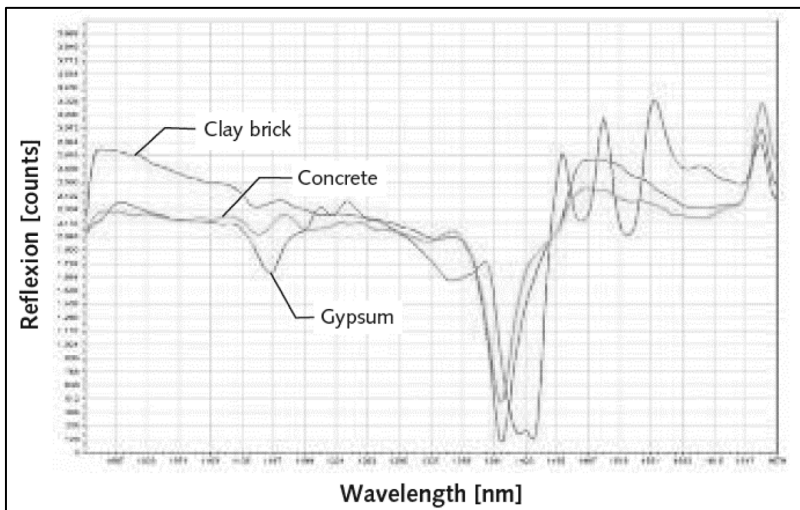


Fig. 3: First derivative of NIR spectra for brick, concrete and gypsum ©IAB Weimar gGmbH

The gypsum content remaining in the product after it had passed through the sorting machine was determined by means of visual inspection based on manual sorting analysis. The result of machine sorting is shown (Fig. 4) that the gypsum content could be reduced considerably. With the remaining 0.4 wt% gypsum in the accepted product discharged on freefall, application of the product in unbound base courses in road construction is possible [6].

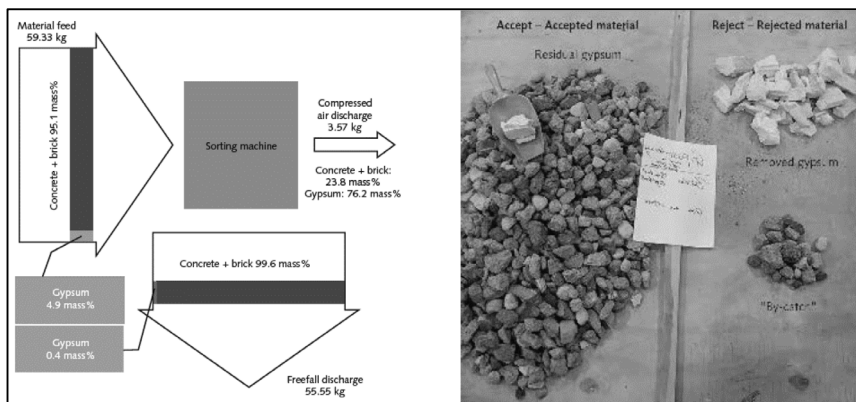


Fig. 4: Sorting result for the separation of gypsum from mixed construction rubble, ©IAB Weimar gGmbH

### 3.2 Separation of a brick-concrete mix

The starting material was a mix of building rubble consisting of brick and concrete. In this case, concrete was the impurity to be detected by means of NIR sensors and then discharged with the help of compressed air. The feed mix was a 22.4/63 mm fraction, which corresponds to a particle size ratio of around 1:3. The NIR spectra were used as the feature (Fig. 3). The brick content in the starting mix accounted for 81.7 wt%. The content of concrete was 18.3 wt%. With sorting, the brick content could be increased to 97.6 wt%. 2.4 wt% concrete remained as “bycatch” in the product (Fig. 5). Accordingly, the brick content could be increased considerably compared to that in the starting material. As a result, use of the recovered sorted material for greening roofs would be possible.

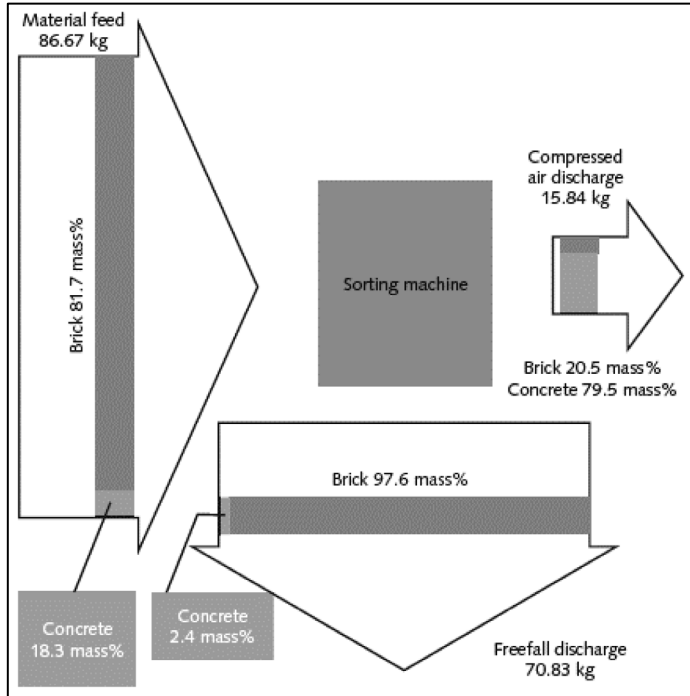


Fig. 5: Sorting result for the separation of brick and concrete, ©IAB Weimar gGmbH

## 4 Conclusion

In this paper a report on sorting tests on mineral CDW with the “Apollo” freefall sorter is presented. The standout feature of this sorter is the pairs of sensors arranged on two sides of the free falling material stream. In this way opposite particle surfaces are scanned so that any adhesions or coatings can be detected. Identification of the particles are based on NIR spectra. For this purpose, the spectra of phenotypical representatives of the components are first captured, and then used to teach the sorting program to detect these materials. The aims of the mechanical sorting tests presented here are the reduction of gypsum from CDW and the extraction of single-variety bricks. The results show that the aims can be achieved.



## References

- Bayer, 1996, Altglasaufbereitung: Farbsortierung und vollautomatische Qualitätskontrolle in Theorie und Praxis. Glastechnische Berichte. Glass Sci. Technol. Vol. 69, Nr. 1, S. N1–N.7.
- Dornauer et al. 2017, Möglichkeiten und Anwendungen neuester VIS/NIR-Sortierer in der Aufbereitung von Sekundärrohstoffen. [www.vivis.de/phocadownload/Download/2016.../2016\\_RuR\\_611-620\\_Dornauer.pdf](http://www.vivis.de/phocadownload/Download/2016.../2016_RuR_611-620_Dornauer.pdf) vom 06.04.2017
- Coppers & Duddek 2008, Optische Sortierung großer und schwerer Teile. Gesteinsperspektiven. Heft 7, S. 46–49.
- Pretz & Julius, 07–08/2008, Stand der Technik und Entwicklung bei der berührungslosen Sortierung von Abfällen. Österreichische Wasser- und Abfallwirtschaft. Heft 07–08/2008, S. 105–112.
- Müller et al. 05/2021 Tests on a freefall sorter, Sensor-based sorting of mineral waste and raw materials AT MINERAL PROCESSING Volume 62, S. 48-55
- Beuth-Verlag, 2017, DIN 4226-101: Rezyklierte Gesteinskörnungen für Beton nach DIN EN 12620 – Teil 101: Typen und geregelte gefährliche Substanzen. DIN Deutsches Institut für Normung, Berlin

# **Systematic Determination of the Influence of Factors Relevant to Operating Costs of Sensor-based Sorting Systems**

Jan Ludwig<sup>1</sup>, Merle Flitter<sup>1</sup>, Georg Maier<sup>1,\*</sup>, Albert Bauer<sup>2</sup>, Marcel Reith-Braun<sup>3</sup>, Robin Gruna<sup>1</sup>, Harald Kruggel-Emden<sup>2</sup>, Thomas Längle<sup>1</sup>, Jürgen Beyerer<sup>1,4</sup>

<sup>1</sup>Fraunhofer IOSB, Karlsruhe, Germany, Institute of Optronics, System Technologies and Image Exploitation

<sup>2</sup>Mechanical Process Engineering and Solids Processing (MVTA), TU Berlin, Germany

<sup>3</sup>Intelligent Sensor-Actuator-Systems Laboratory (ISAS), Karlsruhe Institute of Technology (KIT), Germany

<sup>4</sup>Vision and Fusion Laboratory (IES), Karlsruhe Institute of Technology (KIT), Germany

\* Corresponding Author: Fraunhoferstr. 1, 76131 Karlsruhe, Germany, [georg.maier@iosb.fraunhofer.de](mailto:georg.maier@iosb.fraunhofer.de)

---

Keywords: Design of Experiments, Sensor-based Sorting, Operational Costs

## **Abstract**

Within the next decade, the recycling rates of all waste streams in the European Union are to be consistently increased (EU, 2018). Sensor-based sorting plays a crucial role in achieving those aims. However, the composition of the operating costs of sensor-based sorting systems (SBS), which are made up of compressed air and electricity costs, for example, has not yet been adequately investigated. The main cause is the massive experimental effort required to investigate these costs. In this paper, we propose a systematic approach for determining the operating costs of SBS systems by using Design of Experiments (DoE). For this purpose, experiments are carried out to investigate whether the methodology of DoE is applicable to the use case of SBS. The resulting models are validated with statistical measures and additional experimental runs. For comparability of the results, two different materials, namely construction and demolition waste as well as plastic flakes, with grain sizes between 0 - 10 mm are investigated. With the presented approach high

coefficients of determination of the regression models are reached. Consequently, the results show that precise regression models can be derived with reduced effort.

## **1 Introduction**

In various industries, such as minerals, food and waste processing, sensor-based sorting (SBS) systems have become indispensable. In the recycling sector, such systems have found application for more than 20 years (Bilitewski & Härdtle, 2013). Within the next decade, the recycling rates of all waste streams in the European Union are to be consistently increased (EU, 2018). SBS systems play a key role to achieve these official regulations while maintaining high fraction purities, which are mandatory for an efficient circular economy.

With SBS systems, high volumes of waste can be sorted automatically. However, an important aspect for sorting plant operators to stay competitive is to optimize their present sorting processes. Regarding German and Italian material recovery facilities, where the economic success greatly depends on gate or sorting fees (Cimpan, 2016; Gadaleta et al., 2020) or evaluating existing, separate waste collection and recycling systems. This study mitigates the current pervasive scarcity of data on process efficiency and costs by documenting typical steps taken in a techno-economic assessment of MRFs, using the specific example of lightweight packaging waste (LWP), it is important to be aware of the cost drivers of these processes.

Research has tended to focus on the techno-economic assessment of recycling processes, where the specific costs of SBS systems are treated as a black box. In (Cimpan, 2016) or evaluating existing, separate waste collection and recycling systems. This study mitigates the current pervasive scarcity of data on process efficiency and costs by documenting typical steps taken in a techno-economic assessment of MRFs, using the specific example of LWP the authors conduct a techno-economic assessment of different material recovery facilities and describe that 2/3 of the total energy consumption of the recovery process are connected to sorting and refining. Precisely because of the high share of energy consumption in the recovery process, the links between sorting and refining process parameters and the resulting costs must be understood. In turn, this enables the modeling of the subsystem and thus provides the basis for a cost-optimization. Additionally,

a realistic profitability assessment of application of SBS systems is not possible without knowledge about the cost model of such systems.

The techno-economic assessment of sorting plants gives important insights about economic aspects like revenues and economies of scale but is often based on constant values for the energy consumption of different components (Cimpan, 2016; Gadaleta et al., 2020) or evaluating existing, separate waste collection and recycling systems. This study mitigates the current pervasive scarcity of data on process efficiency and costs by documenting typical steps taken in a techno-economic assessment of MRFs, using the specific example of LWP. With the use of models for the energy consumption of subsystems, a model with higher granularity can be established. Therefore, in this work, we combine the results of previous works which investigate the influence of process parameters on SBS systems with results of techno-economic assessments of sorting plants.

In this paper, we propose a systematic approach for determining the operating costs of SBS systems by using Design of Experiments (DoE). For this purpose, experiments are carried out to investigate whether the methodology of DoE is applicable to the use case of SBS. Three factors that are supposed to have a significant impact on the electricity and compressed air consumption of an SBS system are analyzed in a response surface design. For the assessment of the applicability of this method to various scenarios, two different materials, namely construction and demolition waste (CDW) as well as plastic flakes, with grain sizes between 0 - 10 mm are investigated. With this systematic and transferable method, precise models of the energy consumption of the SBS system are derived and validated by analysing coefficients of correlation. Additionally, validation runs are conducted to validate the models' predictions.

Related works focusing on the influence of process parameters of SBS systems that are referred to in this work include (Küppers et al., 2020, 2021). There, the influence of the parameters occupation density and eject fraction ratio on the sorting efficiency is investigated with lab scale experiments. In (Möllnitz et al., 2020), the authors analyze the influence of pre-screening on the sorting process of mixed municipal solid waste and mixed commercial waste, including an SBS system. A recent work which investigates the implementation of SBS systems in CDW processing is (Vegas et al., 2015) guaranteeing optimal technical and environmental performance, are required for high-grade construction applications such as concrete. The main problem constituents causing a decrease in the quality

of recycled aggregates to be used in high grade applications are: organic material, gypsum and autoclaved aerated concrete (AAC). There, the authors analyze the potential of SBS systems in CDW sorting and derive specific costs between 0,80 and 1,50 € / t. Works which perform a techno-economic assessment of sorting plants with different capacities can be found in (Cimpan, 2016; Fleischhacker, 2011; Gadaleta et al., 2020; Oliveira Neto et al., 2017; Porten & Feltes, 2014; Rudolph et al., 2020; Gadaleta et al., 2020; Oliveira Neto et al., 2017; Porten & Feltes, 2014; Rudolph et al., 2020).

On this basis, we create a systematic procedure for modeling the specific costs connected to SBS systems. Therefore, in the following section we introduce the experimental setup and materials used for the experiments. As a next step, the concept of DoE is presented and applied to the system. The results are then analyzed and evaluated based on statistical measures. Lastly, the results are summarized, and the principal conclusions are drawn.

## **2 Methods**

In the following section, the equipment and materials used in the experiments are depicted. Furthermore, the concept of DoE is explained in general and the process of applying DoE to the investigated SBS system is described.

### **2.1 Equipment**

The sorting system analyzed in this work is a laboratory-scale SBS system with a line-scan camera, a conveyor belt 140 mm wide, and pneumatic separation. The pneumatic resolution is 5 mm. To guarantee stable and reproducible feeding, a vibrating feeding tray is used. The system was developed for demonstration, research, and development purposes with state-of-the-art components.

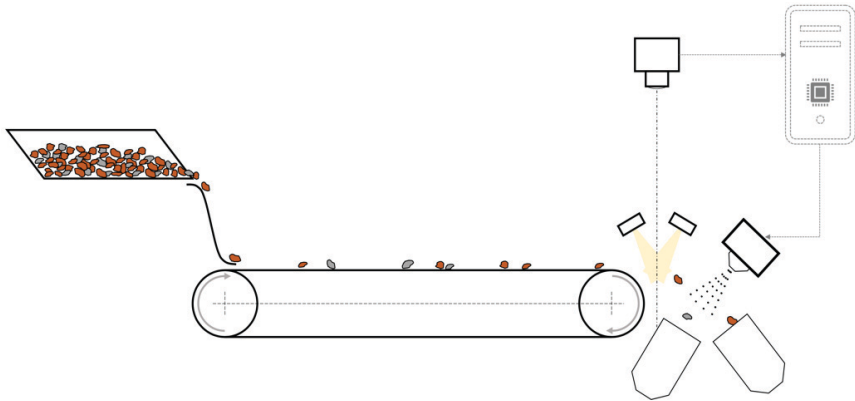


Fig. 1: Schematic depiction of the sorting procedure of the investigated SBS system

The sorting procedure is schematically depicted in Fig. 1. Starting from a vibrating feeder, the material is fed onto a conveyor belt. By utilizing a slide between vibrating feeder and conveyor belt, the particles in the material stream are separated by pre-acceleration for better detectability. A line-scan color camera is used to scan the particles after exiting the conveyor belt. Lastly, a binary separation is enabled by ejecting particles with impulses of compressed air.

## 2.2 Materials

The materials used for the experiments are CDW as well as mixed plastic flakes with grain sizes between 0 - 10 mm (see Fig. 2). The CDW is a mixture of clay- and sand-lime-brick and thus has higher average particle weight (0.184 g) than the plastic flakes (0.037 g). Each experimental run is conducted with 1000 g of CDW or 250 g plastic flakes, respectively. In the experiments with CDW, sand-lime-particles are handled as the eject fraction. In those with plastic flakes, blue particles are ejected. By analyzing different materials, the applicability of the approach to other scenarios in the field of SBS is assessed.



Fig. 2: Three particle size classifications (0 mm — 4.0 mm, 4.0 mm — 5.4 mm, and 5.4 mm — 10.0 mm) for the materials CDW (left) and plastic flakes (right)

### 3 Description of Design of Experiments

Generally, analyzing a system with continuous variable parameters is complex and expensive. Exemplary parameters of an SBS system are *feed rate*, *particle size*, *particle shape*, *eject fraction ratio* as well as the *operating pressure* and the *splitter position* (Gülcan & Gülsoy, 2017; Küppers et al., 2020, 2021) a better understanding of this method is required concerning general properties and mineral sorting applications. To date, optical sorting has been widely studied in terms of industrial applications and performance evaluation particularly in mineral processing. Nevertheless, process optimization requires better understanding of qualitative and quantitative figures based on real life sorting. To identify the influence of parameters on the quality of a system, approaches like trial-and-error or one-factor-at-a-time (OFAT) are expensive. Therefore, in this work, an approach for analyzing the running costs of an SBS system by using DoE is depicted. Due to the large number of factors influencing these costs, this established method for an efficient analysis of processes is necessary. Methods for the systematic analysis and subsequent optimization of a system based on multiple target figures are described in (Siebertz et al., 2017) in detail, as are all the steps mentioned below.

Initially, the system is delimited, which means process parameters are identified and *target figures*, with which the assessment of the system's quality is possible, are chosen. Intuitively, the experimental effort increases with the number of additional parameters. From the set of parameters, a subset is chosen for conducting the

experiments. Those parameters in the subset are called *factors*. For each *factor*, the settings to test, which are called *levels*, are determined in advance. This is necessary to create the experimental design.

Target figures are continuous measurement values that measure the system's quality. For these target figures, regression models are later generated based on the experimental data obtained. These models can be used for further purposes like optimization or continuous prediction within the design space.

After delimiting the system, an *experimental design* is generated. For this purpose, many established experimental designs can be used from packages in Python and R. Additionally, specific statistics and DoE-software like *Design Expert*, *Minitab* and *SPSS Statistics* offer DoE-functions. There is also the possibility to create individual designs as described in (Siebertz et al., 2017) and realized in (Khodier et al., 2021). According to (Siebertz et al., 2017), this is mostly applied in the areas of chemistry and process engineering because not every combination of factors is executable. In this case, the individual design is created based on statistical criteria from which the person responsible can choose. The theoretical basis behind this procedure is explained in (Siebertz et al., 2017). The potential of the usage of individual designs is depicted in (Khodier et al., 2021), where real-scale experiments in waste processing were conducted. Therefore, two continuous factors are investigated on 11 or 5 levels respectively and one categorical factor with three different characteristics. In a full-factorial design, this would result in 165 runs ( $n_{\text{runs}} = 11 \cdot 5 \cdot 3$ ) but could be reduced to 32 experimental runs with the use of a D-optimal design. In the case of (Khodier et al., 2021), this minimization is necessary because of the high costs connected to conducting real-scale experiments.

According to (Siebertz et al., 2017), the mathematical basis of the reduction of the experimental designs is pairwise orthogonality of the setting-vectors of each factor. A setting-vector represents all the settings of one factor in the design. That way, multiple factors can be modified between experiments and their effects on the target figures can be estimated separately. This reduces the expense and enables an analysis of variances (ANOVA) for determining the significance of the factors' effects. An ANOVA includes hypothesis tests for determining whether a factor has a significant effect on the target figures.

The correctness of the ANOVA and the resulting regression model depends on three assumptions, which must be validated after calculation of the regression



model. One must confirm that the model's residuals are independent, normally distributed and have constant variance. To enable optimal preconditions for the validity of those assumptions, three different concepts, namely randomization, replication, and blocking, can be used.

Randomization refers to the randomness of the running order in the experimental design. By randomizing, systematic effects, for instance the pollution of the camera lens, can be uniformly distributed on the experiments. Without this, the effect of factors, whose levels are varied only in the last few runs of a design, would be affected stronger than those in the first runs.

Replication is important to be able to estimate the dispersion of measurements. Therefore, the whole design can be repeated.

The last concept described in (Siebertz et al., 2017) is blocking. Blocking should be used if the experimental runs of the design can be grouped into subgroups, that are conducted under different conditions which are expected to influence the target figures. That way, the blocking information can be considered for the analysis.

The fundamental principle of an ANOVA is to test differences among means in grouped data. Therefore, the total sum of squares (TSS) of the measurements of one target figure is separated into two parts, namely the sum of squares within groups (SSW) and the sum of squares between groups (SSB). According to (Siebertz et al., 2017), the equation  $TSS=SSW+SSB$  holds true. Intuitively, if the SSW is small and the SSB is high, the factor is likely to influence the target figure.

Lastly, with a hypothesis test, it is investigated if the share of that is explained by the is high enough to reject the null hypothesis with a high certainty. The null hypothesis claims that the factor does not have a significant effect on the target figure. Two errors, namely the type 1 and type 2 error, exist for this test. Type 1 is the error of assuming the factor has an effect, although it does not, and type 2 is the error of assuming the factor does not have an effect, although it does. Therefore, two upper limits for the risk of a wrong decision must be defined in advance. The significance level  $\alpha$  defines the maximally acceptable risk for a type 1 error and  $\beta$  for a type 2 error. The decision, whether the null hypothesis is rejected, is based on the p-value, which is the probability that the variance between groups is not caused by the factor's effect. If  $p < \alpha$  holds, the risk for a type 1 error is smaller than the acceptable risk and the factor is considered to have a significant effect. As a

last step, the tree assumptions mentioned above must be validated by analyzing the corresponding plots as described in (Siebertz et al., 2017). ANOVA is hence used as a preliminary step for the regression of the target figures. Factors which are not considered to have a significant effect are excluded and not modeled in the respective regression model.

For each factor with a significant effect, the effect can be modeled with a regression model. Lastly, these individual models are aggregated to a multiple regression model of the target figure. If all effects are modelled linearly, the model is referred to as a multiple linear regression model.

## **4 Application to the SBS system**

To apply this knowledge on the present problem, the SBS system is delimited first. Target figures which are closely linked to the operational costs of an SBS system are selected, namely *compressed air consumption*, *electricity consumption of the valves* and *purity of the reject fraction*. The compressed air consumption is used for estimating the necessary power of the compressor unit. The consumption of compressed air is measured in liters with a flow meter (Festo SFAM-62-3000I-M-2SA-M12) for each experimental run. The electricity consumption of the valves is expected to have a small influence on the running cost but is not a constant electricity consuming part of the SBS system. The electricity consumption is calculated with an application that documents the frequency and duration the valves are being activated for in each run. Additionally, the purity of the reject fraction is considered as a target figure. The associated regression model, however, is not necessary for estimating the costs related to the SBS system.

Regarding these target figures, the influence of factors is investigated. In (Küppers et al., 2020) the occupation density of the conveyor belt is shown to have a significant effect on the sorting quality of the system. For designing an optimal sorting process, the throughput must be considered (Cimpan, 2016) or evaluating existing, separate waste collection and recycling systems. This study mitigates the current pervasive scarcity of data on process efficiency and costs by documenting typical steps taken in a techno-economic assessment of MRFs, using the specific example of LWP. The throughput rate can be mapped linearly to the occupation density of the conveyor belt. This is why the correlation between the occupation density and the target figures is analyzed within the scope of this work. The eject-fraction ratio in

the material stream is likely to be correlated with the operational costs of an SBS system, too. The more eject particles are contained in the stream, the higher is the expected consumption of electricity. Although this seems obvious, the correlation of this factor to the operational/electricity costs has not been investigated yet. Another factor that is expected to have an influence on the operational costs is the particle size of the material. The particle size directly influences the duration of compressed air impulses. For larger particles, the duration of the impulses is typically higher than for smaller ones.

With three factors, a face-centered Central-Composite-Design can be used (Siebertz et al., 2017). This design is a combination of a 2-level factorial design and additional orthogonal combinations originating from the center point, which can be seen in Fig. 3. Therefore, each factor is investigated on three levels, leading to an experimental plan containing 15 experiments. Additionally, five replicate runs of the center point run are conducted to enable a lack-of-fit-test (LOF), which tests if the model fits well throughout the design space and thus describes the correlation between the factors and target figures correctly. Therefore, the variation of the center points is tested against the variation between the actual and predicted values, also referred to as residuals. If the variation of the residuals is significantly larger than the variation of the replicated center point measurements, the model does not fit the data well, potentially. This results in a total sum of 20 experiments for each material.

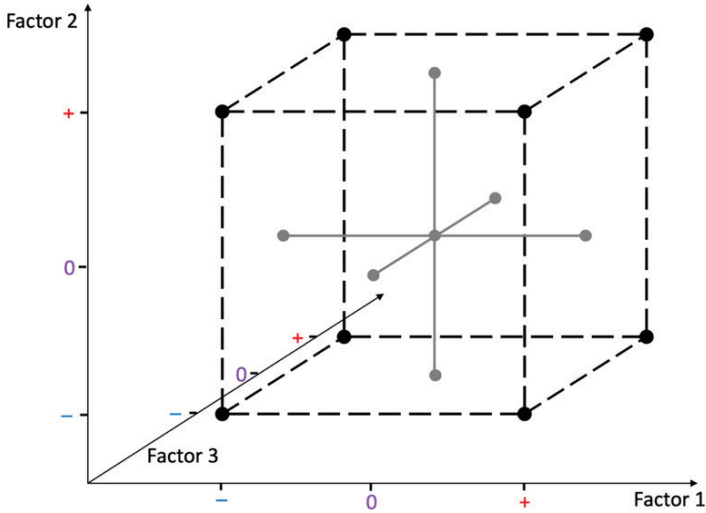


Fig. 3: Visualization of a face-centered central composite design

Important preparatory actions are to randomize the order of the runs in the experimental plan and to determine the number of replications necessary for minimizing the risks of false conclusions. For this system,  $\alpha=0.05$  and  $\beta=0.2$  are chosen as reasonable risks as they are common values in the literature (Siebertz et al., 2017). The risks influence the number of necessary runs. Due to the low variance of the target figures in replicate runs, which are experiments with the same factor settings, the experimental plan does not have to be repeated to reach the preconditions for the risks named above. This variance is determined in preliminary tests. In this case, blocking is not needed, because all experiments are conducted under the same conditions.

The three factor levels of each factor must be determined. In our case, all three factors are numeric. Hence, the influence of every factor can be included into the regression model continuously.

In preliminary tests, the highest feasible *occupation density* was determined at 10 %. Additionally, the idea is to examine a large design space. Therefore, the lower limit of the occupation density of 1 % and an upper limit of 10 % is chosen. The three factor levels are depicted in Fig. 4.

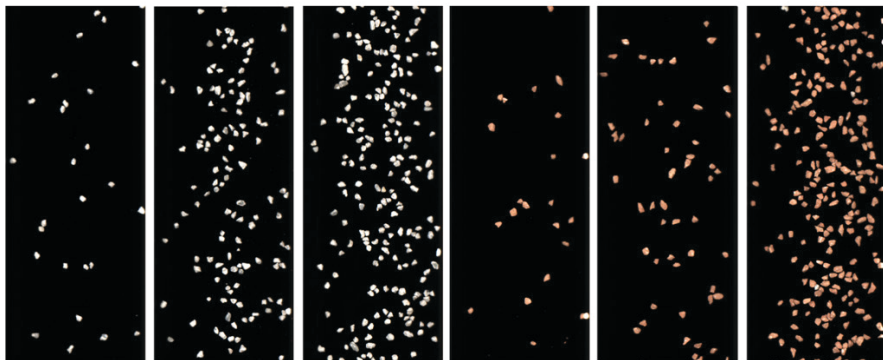


Fig. 4: Occupation densities (1 %, 5.5 %, 10 %) of the medium particle size with sand-lime particles on the left and clay particles on the right.

In terms of the *particle size*, both materials are screened into three different fractions. The resulting fractions are 0 mm — 4.0 mm, 4.0 mm — 5.4 mm, and 5.4 mm — 10.0 mm and are shown in Figure 2.

Lastly, levels for the factor *eject-fraction ratio* must be determined. The upper limit is chosen to be 20 %, whereas the lower limit is set to 5 %. The resulting factor levels are shown in Tab. 1.

Tab. 1: Factor levels

	Factor levels		
	--	0	+
<b>Occupation density</b>	1 %	5.5 %	10 %
<b>Particle size</b>	2 mm	4.85 mm	7.7 mm
<b>Eject fraction ratio</b>	5 %	12.5 %	20 %

The approach for the analysis of the measurements after conducting the experimental design is the same for both materials. Therefore, only the procedure for the analysis of the experiments with CDW is presented. Exemplary for all three target figures, the ANOVA results of the compressed air consumption is depicted in Table 2. After

the collection of data within the experiments, the ANOVA is applied. Therefore, the probability  $p$  for every effect or interaction of a factor not to be significant is calculated and those with a  $p$ -value higher than  $\alpha$  are eliminated from the model. In the following, the three factors occupation density, particle size and eject-fraction ratio are referred to as  $A$ ,  $B$ ,  $C$ , respectively.

The fact that  $A^2$ , the quadratic effect of the occupation density, is not eliminated from the model is caused by the principle of hierarchical integrity (Siebertz et al., 2017). Since the interaction of  $A^2$  and  $C$  is significant,  $A^2$  must be respected in the regression model.

Tab. 2: ANOVA table for the target figure compressed air consumption

Source	Sum of Squares	Degrees of Freedom	Mean Square	F-value	p-value	
<b>Model</b>	0.0652	8	0.0082	89.85	<0.0001	significant
A-Occupation dens.	0.0272	1	0.0272	299.8	<0.0001	
B-Particle size	0.0173	1	0.0173	190.34	<0.0001	
C-Eject fr. ratio	0.0011	1	0.0011	12.18	0.0051	
AB	0.0020	1	0.0020	22.22	0.0006	
AC	0.0027	1	0.0027	29.23	0.0002	
$A^2$	0.0000	1	0.0000	0.1231	0.7323	
$C^2$	0.0011	1	0.0011	12.40	0.0048	
$A^2C$	0.0005	1	0.0005	4.97	0.0476	
<b>Residual</b>	0.0010	11	0.0001			
Lack of Fit	0.0009	6	0.0002	13.49	0.0059	significant
Pure Error	0.0001	5	0.0000			
<b>Cor Total</b>	0.0662	19				

The validation of the ANOVA assumptions is conducted by confirming that the residuals are independent, normally distributed and have constant variance. Therefore, different plots are used. The independence of the residuals is confirmed by analyzing the residuals-vs-run-plot, which depicts the residuals at each run in

the ascending run order. If trends exist in this plot, independence of the residuals cannot be confirmed. With the data obtained in the experiments, no such trends are found in any of the residuals-vs-run-plots. To confirm the assumption of normally distributed residuals, the normal plot of residuals is used. For all the models, no significant deviation of a normal distribution can be found in this plot. Therefore, the assumption of normally distributed residuals is validated. Lastly, the residuals-vs-predicted plot must be analyzed to confirm the assumption of constant variance in the experimental space. The representation of the residuals in the plot does not contradict this assumption. With this analysis, the ANOVA-assumptions are validated, and the model's quality must be assessed.

## 5 Results

Figure 5 shows the model for the target figure compressed air consumption for CDW. The respective mathematical description is depicted in eq. (1).

$$\begin{aligned} Q(a, b, c) = & (0.152 - 0.004 \cdot a + 0.008 \cdot b - 0.012 \cdot c + 0.001 \cdot a \cdot b \\ & + 0.0007 \cdot a \cdot c + 0.001 \cdot a^2 + 0.0003 \cdot c^2 \\ & - 0.0001 \cdot a^2 \cdot c)^{-2} \end{aligned} \quad (1)$$

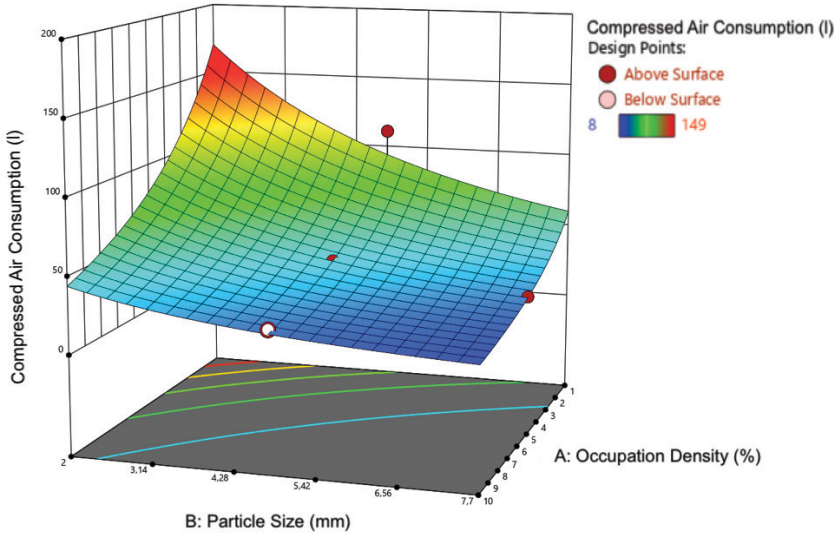


Fig. 5: Regression model for the occupation density in l per kg CDW

On average, sorting the plastic flakes consumes 2.64 times more energy for the valves and 1.96 times more compressed air for the same amount of material compared to CDW. This can be explained by the lower average particle weight of the plastic flakes.

The activation duration of the valves is reduced for the sorting of plastic flakes, which leads to a reduction of the average air consumption per activation by 46 % compared to the sorting of CDW. The sorting quality is not affected by this and lies between 89.48 % and 99.57 % for the plastic flakes. For the sorting of CDW, the values lie between 91.92 % and 99.67 %.

In the case of the center point measurements of the experiments with both materials, the energy consumption of the valves amounts to 1 % of the energy consumption for generating the compressed air. Therefore, the model for the energy consumption of the valves will not be discussed further.



For CDW, the compressed air consumption decreases with higher occupation density from 90 l/kg to 30 l/kg, which is caused by higher share of overlapping particles. With rising particle size, the compressed air consumption decreases from 80 l/kg to 30 l/kg. Compared to that, the main effect of the eject-fraction ratio causes a rise in compressed air consumption from 30 l/kg to 40 l/kg. The courses of these main effects are like the effects calculated for the plastic flakes.

For the assessment of regression models quality, the coefficient of determination  $R^2$  is frequently used. In DoE-software, three variants of this coefficient, which can be seen in eq. (3) and (4), are listed by default.

$R^2$  is a measure between 0 and 1 for the correlation between the model's predictions and the measurements. If the model fits the data perfectly,  $R^2$  equals 1. A problem about this is that this measure does not consider whether parameters with low effect are respected in the model. Therefore,  $R^2_{adj}$  is used. As depicted in eq. (3), the number of measurements and model parameters are respected. If parameters, which are not significant enough, are added to the model,  $R^2_{adj}$  decreases and the effect of overfitting can be detected. Additionally,  $R^2_{pred}$  shows how well the model predicts new data in the design space. For that, the model is built on all measurements of the experimental design except one. This process is repeated for each measurement and the residuals of the predictions to the real values are aggregated as predicted residual sum of squares (PRESS).  $R^2_{adj}$  and  $R^2_{pred}$  should be within 0.2 of each other to exclude overfitting (Siebertz et al., 2017).

$$R^2 = 1 - \frac{\text{Sum of squares}_{\text{residuals}}}{\text{Sum of squares}_{\text{total}}} = 1 - \frac{\sum_{i=0}^n \sum (y_i - \hat{y}_i)^2}{\sum_{i=0}^n \sum (y_i - \bar{y})^2} \tag{2}$$

$\hat{y}_i$  = prediction  $i$  of the regression model,  
 $n$   $\hat{=}$  Number of datapoints

$$R^2_{adj} = 1 - \frac{\text{Sum of squares}_{\text{residuals}}/(n - K)}{\text{Sum of squares}_{\text{total}}/(n - 1)} \tag{3}$$

$K$   $\hat{=}$  Number of factors,  
 $n$   $\hat{=}$  Number of datapoints

$$R^2_{pred} = 1 - \frac{\text{PRESS}}{\text{Sum of squares}_{\text{total}}} \tag{4}$$

For conducting the LOF, five repetitions of the center point setup are conducted. The LOF test is significant for the CDW models, which implies the model potentially does not fit the data. In this case, this is caused by the fact that the center point data is nearly identical. For experiments with high occupation density and low particle size the experiments show more variation. Therefore, the variation of the center point data is not representative for the variation in the experimental space.

In 4 of the 6 models,  $R^2_{pred}$  reaches values over 0.9, which shows that the models predict points well within the design space (see Tab. 3). Furthermore, the quality of the predictions of the regression models is assessed with validation runs. The measurements of those runs all lie within the 95 % confidence interval for each model.

In 5 of 6 cases, the deviation of  $R^2_{adj}$  and  $R^2_{pred}$  are significantly smaller than 0.2 so no overfitting effects are present. The high deviation of  $R^2_{adj}$  and  $R^2_{pred}$  of the model for the purity of the eject-fraction for plastic flakes could be traced back to higher variance in the measurements caused by air turbulences, which affect the light-weight plastic particles more than the heavier CDW particles.

All three factors are shown to have a significant effect on the target figures. It must be highlighted that the energy consumption of the valves is marginal compared to the energy consumption for generating compressed air.

Tab. 3: Quality measures of the regression models

	<b>Energy cons. valves</b>	<b>Compressed air cons.</b>	<b>Purity of eject fraction</b>
<b>CDW</b>			
$P_{LOF}$	0.0002	0.0047	0.0029
$R^2_{adj}$	0.9658	0.9726	0.9771
$R^2_{pred}$	0.8618	0.9149	0.9057
<b>Plastic flakes</b>			
$P_{LOF}$	0.1355	0.2442	0.1288
$R^2_{adj}$	0.9959	0.988	0.9413
$R^2_{pred}$	0.9795	0.9672	0.7517

## 6 Conclusion

The identification of specific characteristics of the operating costs related to SBS has not been subject to recent literature. Therefore, in this work an approach for modeling the influence of multiple parameters on the consumption of electricity and compressed air of an SBS system was proposed.

The results of our study show, that precise regression models can be derived with reduced effort compared to methods like trial-and-error or OFAT. The choice of a response surface design resulted in 15 experimental runs. The method for analysis of the experimental data was ANOVA. By using two different materials for the execution and analysis of the experiments, the applicability of the presented procedure was assessed. Due to high coefficients of determination of the regression models ( $R^2$ ,  $R^2_{\text{adj}}$  and  $R^2_{\text{pred}}$ ) and the confirmation of the models' predictions with validation runs, the applicability of DoE to model SBS consumption was shown in this contribution. Thus, especially in real scale experiments where the number and duration of experiments should be reduced, this approach can be used.

All the factors investigated in the experiments, namely occupation density, particle size, eject-fraction ratio, have a significant effect on the three target figures. The distances between factor levels are a good compromise between investigating a large experimental space and precise modeling of the target figures.

## Acknowledgement

IGF project 20354 N of research association Forschungs-Gesellschaft Verfahrens-Technik e.V. (GVT) was supported by the AiF under a program for promoting the Industrial Community Research and Development (IGF) by the Federal Ministry for Economic Affairs and Energy on the basis of a resolution of the German Bundestag.

## References

- Bilitewski, B., & Härdtle, G. (2013). *Abfallwirtschaft*. Springer Berlin Heidelberg. <https://doi.org/10.1007/978-3-540-79531-5>
- Cimpan, C. (2016). Techno-economic assessment of central sorting at material recovery facilities—The case of lightweight packaging waste. *Journal of Cleaner Production*, 11.

- Directive (EU) 2018/852 of the European Parliament and of the Council of 30 May 2018 amending Directive 94/62/EC on packaging and packaging waste (Text with EEA relevance)
- Fleischhacker, S. (2011). *Stoffliche Verwertung von Abfällen- Einsatz der Nahinfrarot- Sortiertechnik im Bereich von Gewerbeabfällen*. 120.
- Gadaleta, G., De Gisi, S., Binetti, S. M. C., & Notarnicola, M. (2020). Outlining a comprehensive techno-economic approach to evaluate the performance of an advanced sorting plant for plastic waste recovery. *Process Safety and Environmental Protection*, 143, 248–261. <https://doi.org/10.1016/j.psep.2020.07.008>
- Gülcan, E., & Gülsoy, Ö. Y. (2017). Performance evaluation of optical sorting in mineral processing – A case study with quartz, magnesite, hematite, lignite, copper and gold ores. *International Journal of Mineral Processing*, 169, 129–141. <https://doi.org/10.1016/j.minpro.2017.11.007>
- Khodier, K., Feyerer, C., Möllnitz, S., Curtis, A., & Sarc, R. (2021). Efficient derivation of significant results from mechanical processing experiments with mixed solid waste: Coarse-shredding of commercial waste. *Waste Management*, 121, 164–74. <https://doi.org/10.1016/j.wasman.2020.12.015>
- Küppers, B., Schlögl, S., Friedrich, K., Lederle, L., Pichler, C., Freil, J., Pomberger, R., & Vollprecht, D. (2021). Influence of material alterations and machine impairment on throughput related sensor-based sorting performance. *Waste Management & Research: The Journal for a Sustainable Circular Economy*, 39(1), 122–129. <https://doi.org/10.1177/0734242X20936745>
- Küppers, B., Seidler, I., Koinig, G. R., Pomberger, R., & Vollprecht, D. (2020). Influence of Throughput Rate and Input Composition on Sensor-Based Sorting Efficiency. *Detritus*, 9, 59. <https://doi.org/10.31025/2611-4135/2020.13906>
- Möllnitz, S., Küppers, B., Curtis, A., Khodier, K., & Sarc, R. (o. J.). *Influence of pre- screening on down-stream processing for the production of plastic enriched fractions for recycling from mixed commercial and municipal waste*. 9.

- Oliveira Neto, R., Gastineau, P., Cazacliu, B. G., Le Guen, L., Paranhos, R. S., & Petter, C. O. (2017). An economic analysis of the processing technologies in CDW recycling platforms. *Waste Management*, *60*, 277–289. <https://doi.org/10.1016/j.wasman.2016.08.011>
- Porten, M., & Feltes, J. (2014). Probleme, Kosten und Tipps zur Anschaffung von Sortieranlagen. *Das deutsche Weinmagazin*, *14*. <https://www.dwm-aktuell.de/probleme-kosten-tipps-anschaffung-sortieranlagen>
- Rudolph, N., Kiesel, R., & Aumnate, C. (2020). *Einführung Kunststoffrecycling: Ökonomische, ökologische und technische Aspekte der Kunststoffabfallverwertung*.
- Siebertz, K., van Bebber, D., & Hochkirchen, T. (2017). *Statistische Versuchsplanung*. Springer Berlin Heidelberg. <https://doi.org/10.1007/978-3-662-55743-3>
- Vegas, I., Broos, K., Nielsen, P., Lambertz, O., & Lisbona, A. (2015). Upgrading the quality of mixed recycled aggregates from construction and demolition waste by using near-infrared sorting technology. *Construction and Building Materials*, *75*, 121–128. <https://doi.org/10.1016/j.conbuildmat.2014.09.109>

# SenSoRe: A sensor-based testbed for sorting and innovative recycling

Louise Hagesjö<sup>1\*</sup>, Mélina Gilbert Gatty<sup>1</sup>, David Malmström<sup>1</sup>, Jonas Petersson<sup>1</sup>

<sup>1</sup>Swerim, Material analysis and process monitoring, Stockholm, Sweden

\* Corresponding Author: Isafjordsgatan 28A, SE-164 40 Kista, Sweden, [louise.hagesjo@swerim.se](mailto:louise.hagesjo@swerim.se)

---

Keywords: LIBS, testbed, innovative sorting, non-ferrous metals, plastics, machine learning

## Abstract

For the industry to be able to obtain efficient sorting of different types of material flows, a testbed has been developed in Sweden: SenSoRe – Sensors and sorting for innovative recycling. This has been done in a consortium consisting of representatives along the recycling chain: research institutes, sensor manufacturers, system manufacturers, recyclers, and production industry. The purpose of the testbed is for actors to test, develop and/or combine different sensors on material flows and have possibility to use different analysis methods for e.g., quantification or classification. SenSoRe then serves as a link between the initial lab-development and the final industrial implementation. A strength with the testbed is the possibility to test large flows of materials, which is important when e.g., training models for development of machine learning (ML) approaches. Another strength with the testbed is its consortium with actors in production, recycling and research, while still being an open and neutral platform. The technique LIBS (laser-induced breakdown spectroscopy) is suitable for analysis in harsh industrial environments and can in principle detect all elements in the periodic table, it has thus served as a central technique for the development of the testbed. Two of the pilot tests based on the machine learning algorithm SIMCA (Soft Independent Modelling of Class Analogies) are presented, where the first pilot test concerns quality control of non-ferrous (NF) fractions at a Swedish recycling company, and the other investigated black plastic sorting. Results of both pilot tests show that analysis of LIBS data based on SIMCA

could potentially provide online-sensors increased quality and sorting of both NF-metals and plastic materials at recycling plants. These pilot tests show the technical usefulness of the SenSoRe project, and its benefit with actors in both the sensing and recycling industry represented.

## **1 Introduction**

Laser-induced breakdown spectroscopy (LIBS) is a fast, contactless and flexible technique for chemical analysis of materials. The measurements mainly provide information about the elemental composition, but some molecular information can also be obtained. Measurements can be carried out off-line or on-line without pre-treatment of sample materials and on all aggregation states of a material (Noll et al., 2012). LIBS has started to be developed for being used industrially for sorting on refractories and for identification of steel blooms (Noll et al., 2018). The metals research institute Swerim (former Swerea KIMAB) has a long experience in LIBS and is conducting research to develop, improve and implement LIBS in industry. In 2016, Swerim and a project consortium consisting of research institutes, sensor manufacturers, system manufacturers, recyclers, and production industry got granted financial support from Vinnova (Sweden's innovation agency) for developing and establish a testbed for recycling with sensors. The background is a general need to implement new techniques in industry for more efficient sorting of different types of material flows and a testbed with an infrastructure to simulate industry conditions can be beneficial before implementing in industry.

## **2 The testbed SenSoRe – Sensors and sorting for innovative recycling**

The testbed SenSoRe – sensors and sorting for innovative recycling, was officially launched in May 2019 with financial support for a 5-year-period until Dec 2021. The testbed includes both competence and physical facilities, where the competence part consists of a sharing knowledge and know-how among the project consortium with research institutes, sensor manufacturers, system manufacturers, recyclers and production industry. The idea is to provide a participating actor with an enhanced network and a neutral platform for an innovative meeting place. Besides, the testbed should be open and flexible, thus not limited to specific interests of participating actors. The physical part of the testbed mainly consists of an infrastructure located

at Swerim, with a conveyor belt, having the flexibility to attach different sensors, run with different speeds (from 3,4 cm/s to 6 m/s) and circulate different types of materials (see Fig. 1). This lab environment simulates a real conveyor belt application for material sorting at recycling facilities. The physical part also includes other test-labs in the project consortium and modular parts with sensors, adapted to be implemented in industry.



*Fig. 1: A physical infrastructure part of the testbed with a LIBS equipment installed and material circulating on the conveyor*

In the development of the testbed, there have been pilot tests and shorter studies done with the aim to get relevant examples to show the possibility within the testbed. Since LIBS is suitable for analysis in harsh industrial environments (Noll et al., 2018), it has served as one of the central techniques in the development of the testbed infrastructure. Two of the pilot tests were quality control of non-ferrous metals and identification and classification of black plastics, which are further presented.

## **2.1 Pilot test 1: Quality control of non-ferrous metals**

The use of LIBS for online analysis of shredded metal fractions has in the recent years reached attention amongst the recycling industry (Legnaioli et al., 2020). It has the possibility to classify the scrap pieces by their metal and alloy type directly at the conveyor belt, including identification of light elements such as aluminium and magnesium, which makes it an interesting complement to online XRF. The main benefits for recyclers are continuous quality control of shredded metal scrap and classification of scrap pieces for subsequent sorting. With this pilot test, the



possibility of using LIBS as an online quality control of shredded non-ferrous (NF) fractions was tested and evaluated at a recycling facility.

One of the initial steps was to use the testbed to try different positionings of the LIBS-equipment to see how best detection could be achieved on a continuous flow of material (e.g., to get the best hit-rate). The conclusion was that the best detection would be hitting the samples at the end of the conveyor, with a horizontal detection, see Fig. 2. The LIBS equipment used has been developed in collaboration with RISE and is a further development of equipment previously published (Noharet et al., 2015 & Gurell et al., 2011). A dedicated software for displaying the relative content of the identified metal alloys was also developed in connection to the trials of the testbed.

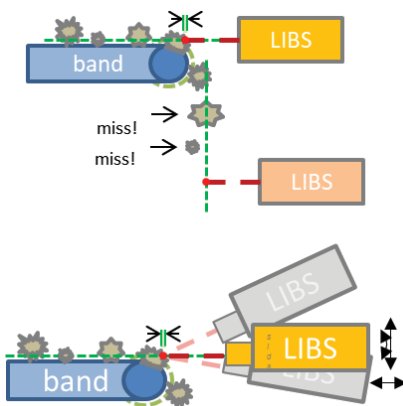


Fig. 2: Schematic view of different configuration tests, resulting in a detection horizontally on the samples. The top configuration shows tests with detection on falling material, the configuration at the bottom shows test with different angles on the flow of material.

The prototype was then tested and implemented at the recycling facility for continuous measurement for 4 days at the conveyor end, just before separation. Since the analysis was only done on a spot in the middle of the belt, around 10% of the samples were detected by the LIBS-sensor. The aim was to see if it could be assumed an even distribution along the width of the belt and thus give representative results in the analysis. The complete batch of materials were collected and later analyzed separately with an XRF-equipment.

The LIBS-analysis used the supervised machine learning algorithm, SIMCA (Soft Independent Modelling of Class Analogies) for classification in the different metals: Cu, Brass, Al, Stainless steel, Zn, Pb and an unknown class. The algorithm was trained on known samples in the testbed before the installation at the recycling facility. SIMCA is in general a suitable method for handling unknown samples, not found in the test set, and to classify them according to a “unknown” class. The result can be seen in Fig. 3, where the LIBS analysis with SIMCA is compared to the XRF measurement of the same batch. The results show overall reasonable resemblance between the two methods and thus that the LIBS point-measurement could be representative for the entire batch.

The LIBS-prototype could also detect a change in metal class distribution when there was a change to another batch of scrap, which showed an increased fraction of Zn and decreased fraction of Cu. This can be seen in Fig. 4. This distribution was also expected from the supplier of that batch.

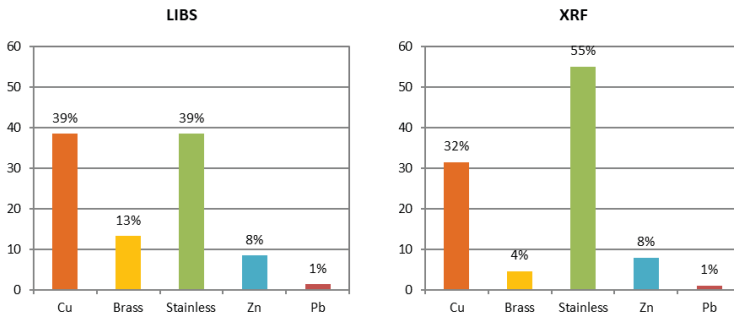


Fig. 3: Histograms showing LIBS analysis using SIMCA for classification of a batch (left) and XRF analysis of the same batch (right). The analysis shows the distribution of the samples classified in the different metals. The histograms are re-normalized to not show unknown.

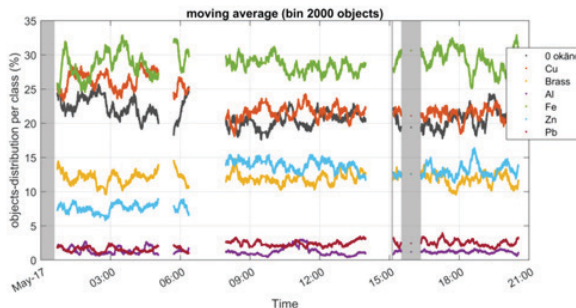


Fig. 4: Between 06:35 and 07:45 there was a change of scrap from another batch which showed an increase in Zink and a decrease in Copper content (from 26 to 22 % and 8 to 14 % respectively). This was expected from that batch.

## 2.2 Pilot test 2: Identification and classification of black plastics

Recently, interest in the applicability of the LIBS technique for plastic sorting has been raised, especially for black plastics, due to limitations of the existing technologies based on NIR spectroscopy and X-ray fluorescence (XRF). Several groups have demonstrated that LIBS can be used to identify different types of polymers (Lui et al., 2019). LIBS spectral data from polymers provide complex information and a classical spectral analysis based on element line identification is not sufficient to distinguish the different polymers. Instead, machine-learning algorithms for LIBS data-analysis has been successfully applied to distinguish plastics (Vinicius et al., 2017 & Shameen et al., 2006). However, most studies considered a small sample set and clean plastic fractions with LIBS measurements carried out off-line in controlled lab environments. Plastic scrap materials encountered at recycling plants often contain various additives, which in addition to dust, perturb the LIBS spectra and thus become more challenging to classify. This makes it important to have a large representative training set and test set of samples to ensure that the ML-algorithm is based on signals originated from the material of interest and hence increase robustness of the analysis.

In the pilot test, series of LIBS measurements were performed on clean recycled plastics and on real plastic scrap with the testbed infrastructure, simulating conditions for plastics sorting at industrial recycling facilities. This provided an extensive sample set of several independent measurements on different black

plastics including polypropylene (PP), polyethylene (PE), polystyrene (PS), acrylonitrile butadiene styrene (ABS), medium-density polyethylene (MPE) and polyvinyl chloride (PVC). A schematic view of the experimental set up and a photo of the on-line LIBS prototype used in this study for identification of the plastics is shown in Fig 5.

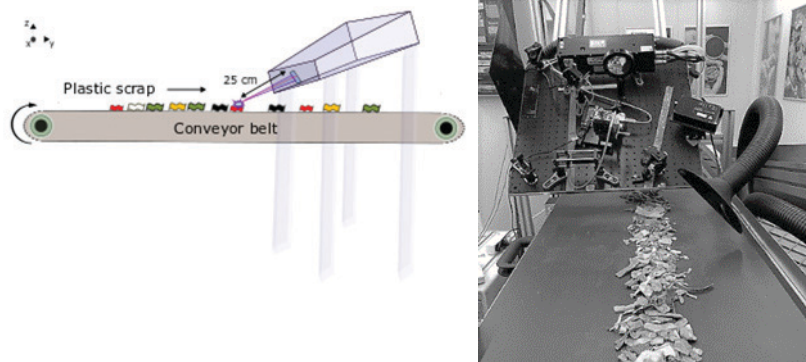


*Fig. 5: Schematic of the experimental set up for LIBS measurements (left). Plastic scrap and LIBS prototype used in this study mounted on the automatic conveyor belt to simulate conditions for sorting at industrial recycling facilities (right).*

The supervised machine learning algorithm, SIMCA was used to classify the polymers. First, the algorithm was trained for all reference classes of plastics. Then, the scrap plastics was introduced as a test set for the algorithm to predict the class of those samples, based on the training set. For the two scenarios, the performance of the algorithm in terms of classification accuracy was used as metric and calculated through dividing the number of correctly classified samples by the total number of samples in the class. In Fig. 6, the result is presented for both the reference samples and the scrap samples, with an average of over 80 % classification accuracy with respect to the plastic type, both for the reference material and the scrap material. Fig. 7 compares the LIBS spectra of a sample of clean recycled PS after extrusion and a sample of PS from recycling facilities. There are clear spectral differences that may arise from e.g., additives and dust. Hence, it demonstrates the importance of large and representative sample sets to identify element specific features and to avoid the risk of models built on spectral features that are not specific for the plastic of interest (i.e., overfitting).

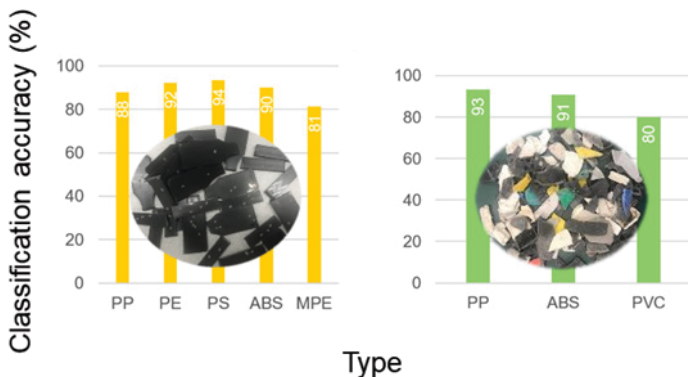


Fig. 6: Classification accuracy (%) for the reference samples (left) and the real scrap samples (right)

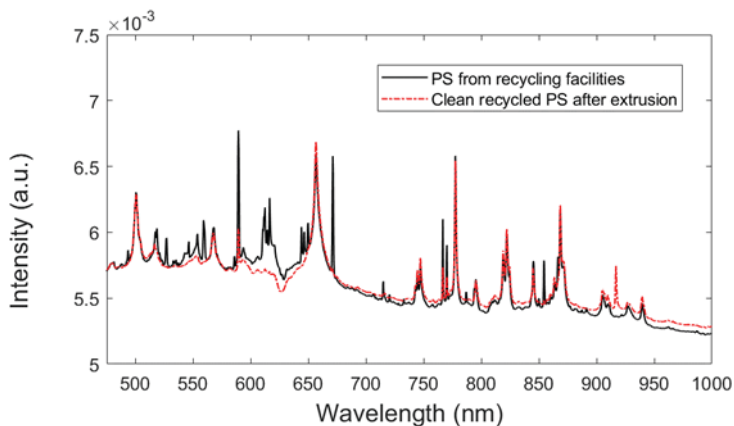


Fig. 7: Comparison of the LIBS spectra of a clean sample of PS and a real scrap sample of PS from recycling facilities

The analysis of the LIBS data based on supervised ML algorithms could potentially provide online-sensors for increased sorting of black plastic materials at recycling plants. Further improvement in classification accuracy can likely be achieved by higher sampling frequency (e.g., use of pulsed laser with repetition rate > 10 Hz) and the next steps from here would be to do field tests at industrial recycling facilities.

### 3 Conclusion

Overall, there is a great usefulness with an industrial-like testbed as SenSoRe, where the two pilot tests show the benefit of testing setup and large material flow in industrial-like conditions and the success of using results from lab-scale trials to install and measure in-situ in industry. It can also be concluded that analysis of LIBS data based on SIMCA provide accurate quality control for non-ferrous metals at a recycling facility and could potentially provide online-sensors for increased sorting of plastic materials at recycling plants. Though there is a great usefulness with SenSoRe for actors in recycling and sensor development, it is hard to build a business around it and the testbed need continued financial support to be able to develop further.

### References

- Gurell, J., Bengtson, A., Falkenström, M., Hansson, B.A.M. (2011). Laser induced breakdown spectroscopy for fast elemental analysis and sorting of metallic scrap pieces using certified reference materials. *Spectrochimica Acta Part B: Atomic Spectroscopy*. 74-75, p. 46-50.
- Legnaioli, S., Campanella, B., Poggialini, F., Pagnotta, S., Harith, M. A., Abdel-Salamb, Z. A., Palleschi, V. (2020). *Industrial applications of laser-induced breakdown spectroscopy: a review*. *Analytical Methods*, 12, 1014
- Lui, K., Tian, D., Li, C., Li, Y., Yang, G., Ding, Y. (2019). *A review of laser-induced breakdown spectroscopy for plastic analysis*. *Trends in Analytical Chemistry*. 110., p. 327-334.
- Noharet, B., Sterner, C., Irebo, T., Gurell, J., Bengtson, A., Vainik, R., Karlsson, H., Ily, E. (2015). *A compact LIBS system for industrial applications*. *Proceedings of SPIE - The International Society for Optical Engineering*.
- Noll, R. (2012). *Laser-Induced Breakdown Spectroscopy: Fundamentals and Applications*. Berlin Heidelberg: Springer.
- Noll, R., Fricke-Begemann, C., Connemann, S., Meinhardt, C., Sturm, V. (2018). *LIBS analyses for industrial applications – an overview of developments from 2014 to 2018*. *Journal of Analytical Atomic Spectroscopy*. 33(6), 945-956.

Shameen, K.M.M., Choudhari, S.K., Bankapur, A., Kulkarni, S.D., Unnikrishnan, V.K., George, S.D., Kartha, V.B., Santhosh, C. (2006). *A hybrid LIBS-Raman system combined with chemometrics: an efficient tool for plastic identification and sorting*. Analytical and Bioanalytical Chemistry. 2. 385., p. 256-262.

Vinicius, C.C, Aquino, F.W.B., Paranhos, C.M., Pereira-Filho, E.R. (2017). Identification and classification of polymer e-waste using laser-induced breakdown spectroscopy (LIBS) and chemometric tools. Polymer Testing. 59., p. 390-395.

# Latency evaluation of an FPGA-based sorting system

Simon Wezstein<sup>1\*</sup>, Michael Stelzl<sup>2</sup>, Michael Heizmann<sup>3</sup>

<sup>1</sup>MSTVision GmbH, R&D, Mainz, Germany

<sup>2</sup>MSTVision GmbH, Management, Mainz, Germany

<sup>3</sup>Karlsruhe Institute of Technology, Institute of Industrial Information Technology, 76187 Karlsruhe, Germany

\* Corresponding Author: Am Schinnergraben 65, 55129 Mainz, Germany, [simon.wezstein@mstvision.de](mailto:simon.wezstein@mstvision.de)

---

Keywords: latency, FPGA-based sorting, system optimization, frame grabber, VisualApplets, line scan

## Abstract

This contribution addresses the latency evaluation of a fully field programmable gate array (FPGA) implemented sensor-based sorting application. The FPGA design is modified to provide timing insights from camera trigger to image processing to actuator signaling. In addition, the signals of the valve are captured with an oscilloscope, providing its voltage, current and the nozzle pressure. A matrix camera is placed in the process side view to track the object. For reproducibility, black plastic balls (diameter: 6 mm, mass: 0.12 g) are used to carry out 659 single experiments. The sorting design is specified to have system latencies under 1 ms. Our measurements show that this is the case for the whole image processing chain, with approx. 200  $\mu$ s latency, but not for the actuator signaling, with approx. 1.8 ms latency.



# 1 Introduction

In the field of sensor-based sorting with line scan cameras, three performance measures of processing are important in addition to recognition performance: latency, jitter, and throughput. Detecting small defects requires high-resolution imaging that leads to a high data rate. In comparison to ore sorting, image processing poses a bottleneck if the detection of small defects is required, e.g., in plastic pellets sorting (Robben & Wotruba, 2019). The distance between scan and separation can be minimized through low processing latency and jitter (Fig. 1). A minimal distance leads to less oversorting due to less accumulation of unexpected material shifts and tumbling (Stelzl, 2019).

The field programmable gate array (FPGA) integrated sorting design by MSTVision GmbH was developed in 2018. Its specification comprises 1 ms or less overall latency, including image processing and actuator triggering. The design uses an 8192 px Camera Link line scan camera, running at a line frequency of 100 kHz. This results in a throughput of roughly 820 MB/s. (Stelzl, 2019)

The main motivation of this contribution is to get a detailed overview of the whole system latency, from camera triggering to object movement. The test setup is explained in detail in Section 2.

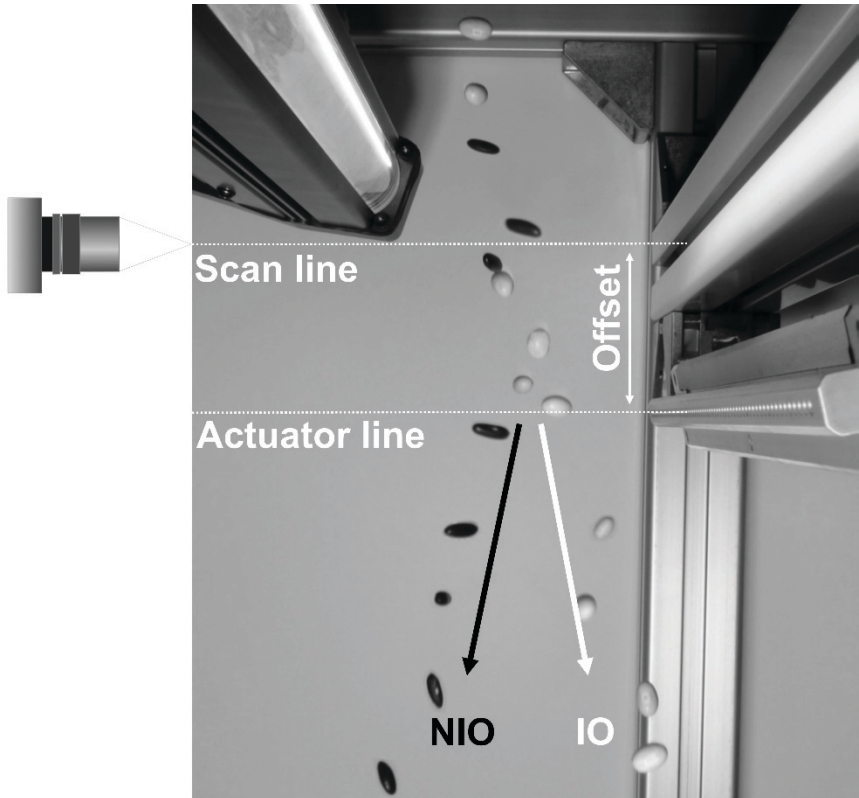


Fig. 1: Side view into the sorting process of plastic balls. Black balls are separated from white balls. The distance between scan line and actuator line is ca. 7 cm. Modified version from (Stelzl, 2019)

## 2 Setup and Methods

A full-scale sorting system with undefined bulk material is not suitable for detailed timing assessment. An experimental setup was designed to obtain controlled conditions for a single experiment. To overcome unavoidable variations each experiment is carried out repeatedly. The overall timing assessment is done by automatically running single object experiments with three splitted data acquisition systems. A line scan system is used to run the sorting application. An area scan system is used to track the falling object. An oscilloscope is used to measure the timing of the valve and its controller. With these three systems, it is possible to

capture all relevant timings. A programmable logic controller (PLC) is used to run the object dispenser and to start the image acquisition. A detailed description is contained/presented in the Section 2.3.

The timing analysis of the process is divided in multiple stages: (1) Camera triggering: width, period; (2) camera image transfer: delay to trigger end, duration, period; (3) image preprocessing with segmentation; (4) object detection; (5) actuator timing; (6) valve controller; (7) valve current; (8) pressure; and (9) object movement.

## **2.1 FPGA image processing**

All FPGA processing in this contribution has been developed with Basler (formerly Silicon Software) VisualApplets. VisualApplets enables graphical development of image processing applications on/for Basler frame grabbers. (Basler AG, 2022)

## **2.2 MSTVision high speed sorting**

The MSTVision high speed sorting system is entirely built in VisualApplets (Section 2.1). It is built for Basler microEnable 5 VCL Camera Link frame grabbers and allows to process the Camera Link bandwidth with 10 taps at 85 MHz clock. The actuators are controlled with a direct bus connection from the frame grabber to the valve control board. The specification is 1 ms overall latency, which is the latency between detecting the last line of an object to the earliest possible actuator signal. The used frame grabber, camera, and lens (Section 2.4) are the same as in (Stelzl, 2019). The offset between camera scan line and the middle of the nozzle is 70 mm +/- 4 mm in the test setup (Fig. 1). Fig. 2 shows the basic operation principle of the system. For this contribution, the original FPGA design has been extended to deliver the relevant timing insights. The actuator timing block refreshes the bus output every 1 ms. The precision and interval of actuator delays depend on the user definable timebase. Here we use a 1.66  $\mu$ s timebase, and the delays are set according to our mechanical setup (delay: 9000 timer increments, 15 ms; width: 4000 timer increments, 6.7 ms).

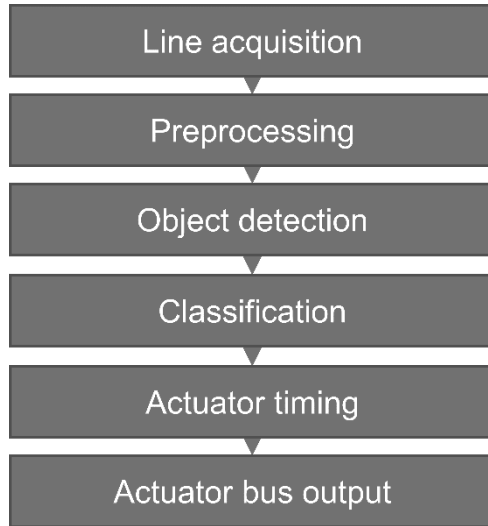


*Fig. 2: Basic system diagram*

### **2.3 Measurement concept**

The measurement principle is to dispense single plastic balls with 6 mm diameter and 0.12 g mass to fall through the line scan system which runs the modified MSTVision sorting application. After passing the line scan camera, it is pneumatically shot after a specified delay to change its trajectory, as it would occur in a sorting scenario. The modified design collects various timing stats for offline diagnosis in the FPGA. The collected timing information comprises:

- Camera trigger rising and falling edge,
- Camera line first and last pixel received,
- Camera line first and last pixel processed,
- Object detected,
- Actuator bus telegram first and last element processed.

Every time the FPGA sends a bus telegram with an activated actuator, a pulse signal with 0.5 ms width is emitted on one frame grabber digital output connected to the oscilloscope, too.

In parallel an area scan camera observes the process from the side. This enables the tracking of the ball trajectory. In Fig. 4 and 5 images of the two cameras are shown. Both camera systems are operated in transmitted light setups.

To achieve the possible data merging afterwards, the two systems share the same world clock, whose frequency is 601 kHz. For distortion correction, the camera is calibrated.

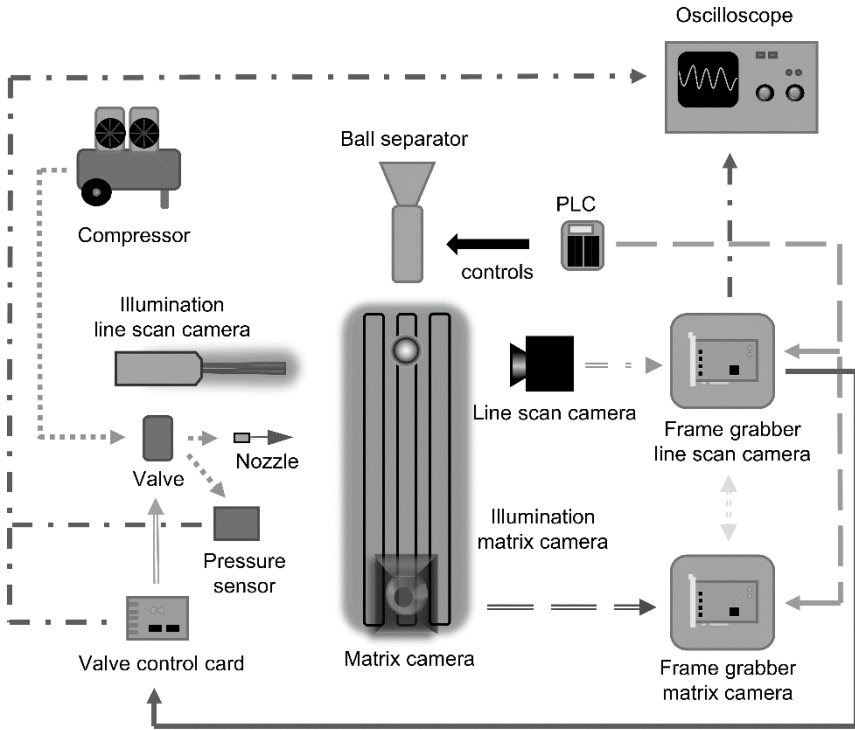
The oscilloscope has four inputs:

1. Frame grabber signal “active telegram”,
2. Valve controller output voltage,
3. Valve current via a shunt resistor,
4. Pneumatic pressure in the hose connecting valve and nozzle.

With the frame grabber signal (1) a data merge into the world clock domain is enabled. This allows to track single valve activations to the object seen in the camera images. The valve controller output, which is the valve voltage, is used to trigger the oscilloscope.

A PLC is used to control the whole process. A mechanical unit for feeding, separating, and dispensing of the balls is PLC controlled. The two frame grabbers are enabled by the PLC with a digital signal, which starts acquiring images.

All grabbed images, actuator values and oscillograms are stored on SSDs. The mentioned timing information of the two camera systems is embedded in the images provided from the frame grabbers. The machine runs fully automatic, enabling the collection of big datasets to compensate mechanical variations using statistical methods.



**Caption:**









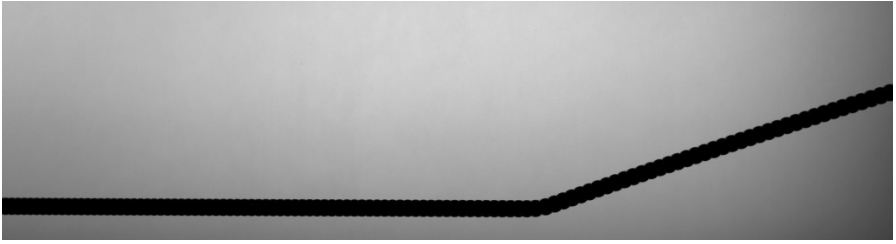
	Actuator bus		Valve power
	Analog		Camera Link
	Digital IO		CoaXPRESS
	Pneumatic		World clock

Fig. 3: The measurement setup



*Fig. 4: Global minimum image of all images of one sample captured by the area scan camera. This shows the trajectory of a single ball falling and being shot in the system. Left to right: Falling direction, Bottom to Top: Direction to the line scan camera.*



*Fig. 5: Cropped image of the line scan camera showing a falling ball. The line scan frequency is higher as it should to get quadratic pixels, therefore the object looks elliptic.*

## 2.4 System components

The test setup consists of the components listed in Tab.1-3.

Tab. 1: Line scan system components

Component	Model/Configuration
<b>Frame grabber</b>	Basler (formerly Silicon Software) microEnable 5 VCL
<b>Valve controller</b>	MSTVision MSTMatrix32-Board
<b>Valve</b>	SMC SX11F-AG
<b>Nozzle</b>	Single nozzle with 1.5 mm diameter
<b>Camera</b>	Teledyne e2v Eliixa Plus EV71YC2MCL8005-BA1 (8192x1 pixels, 100 kHz line frequency)
<b>Lens</b>	Myutron LSF5028-F
<b>Line light</b>	MTD BL 350-B-D5-M16r-Ta

Tab. 2: Area scan system components

Component	Model/Configuration
<b>Frame grabber</b>	Basler imaWorx CXP-12 Quad Basler boA1936-409cmHSP
<b>Camera</b>	(1920x512 pixels, 1 kHz trigger frequency)
<b>Lens</b>	Linos MeVis-C 25 mm 1:1.6
<b>Lighting</b>	Array of Schott HB-LED line lights + diffusor

Tab. 3: Oscilloscope system components

Component	Model/Configuration
<b>Oscilloscope</b>	Pico Technology PicoScope 2406B (4 Channels, 8 Bit, 1 GS/s)
<b>Pressure sensor</b>	Keller PA-21PHB/10 bar
<b>Current sensor</b>	0.1 Ohm Shunt resistor

### 3 Results

This section shows the results of the measurements with the setup and methods described above. The results are shown in the chronological order of the process. At last, the data is merged to show the complete timing context of the process.



### 3.1 Camera timing with triggering and image transfer

The process begins with the camera triggering. In the MSTVision design, the line scan triggering is done via the Camera Link CC1 signal, where its period determines the line frequency, and the width determines the exposure time. The camera runs at 100 kHz line frequency with 6  $\mu\text{s}$  specified exposure time. After the triggering, the line sensor readout begins. After the line readout, the data transfer via Camera Link starts after an unknown delay. As the camera is configured with Camera Link Deca mode at 85 MHz pixel clock, the expected transfer time is 9.64  $\mu\text{s}$ . The expected transfer period is the same as the Trigger: 10  $\mu\text{s}$ . The “Trigger to full transfer” time describes the time from Trigger start to receiving the last pixel of a line. It is the sum of trigger period, transfer delay and transfer period. The measured values (Tab. 4, a) are within expectation...

### 3.2 Image preprocessing and segmentation

After line triggering and line acquisition the image preprocessing and segmentation takes place. They require some lines to be buffered as there are two-dimensional kernel operations implemented. The expected delay is a multiple of the transfer period, it is measured from acquiring the first line pixel to the availability of the first processed pixel of this line. The processing time is the timespan from the first to the last processed pixel of a line. With taking parallel processing into account, the expected value is ca. 8.2  $\mu\text{s}$  excluding unknown latencies. The processing period is the time between the beginning of two consecutive lines, its expected value is 10  $\mu\text{s}$ . Its measured value (Tab. 4, b) is 10.0  $\mu\text{s}$  but with a standard deviation of 1.12  $\mu\text{s}$ , which is rather large compared to the other values. The minimum value is 8.37  $\mu\text{s}$ , the maximum value 15.0  $\mu\text{s}$ . As the image acquisition is steadily running, the variation is either caused by waiting cycles in the processing and segmentation pipeline or by waiting cycles in the object detection pipeline. The mean value is within expectation, which explains why the system is always capable to process the incoming data.

### 3.3 Object detection

With the preprocessed lines, the object detection is carried out. Its timing latency (Tab. 5, a) is the time stamp of the object subtracted by the interpolated time stamp of the last and first pixel of the preprocessed line. The mean value is 23.1  $\mu\text{s}$  with a standard deviation of 3.52  $\mu\text{s}$ .

### 3.4 Actuator timing

The actuator timing latency is measured from the object detection time stamp to the actuator processing end time stamp (Tab. 5, b). For this measurement, a separate dataset is recorded, where the output delays are set to zero. Additionally, the dataset of the working setup is evaluated, too. The value range is approx. 1 ms, which is explained by the 1 ms polling period. The zero delay values are within expected values. The working setup's value range has an offset of 1 ms, which effects that the valve triggers too early. This behaviour is currently not explainable and further investigation has to be done, although it never posed a problem in real world deployments. The sample count is 297 and 586 respective.

### 3.5 Valve controller

The valve controller timing is measured with the oscilloscope data from the frame grabber pulse to the beginning of the voltage output to the valve (Tab. 5, c). Two dedicated measurement series are used, one with a 64 actuators telegram and one with a 32 actuator telegram set, their sample count is 904 and 586 respective. Example signals are plotted in Fig. 6.

With nearly identical value ranges and their histograms (Fig. 6) it seems that the controller has an internal polling cycle similar to that value, while the difference between the measurement series,  $40.8 \mu\text{s}$ , seems to be the bus cycle time for a set of 32 actuators.

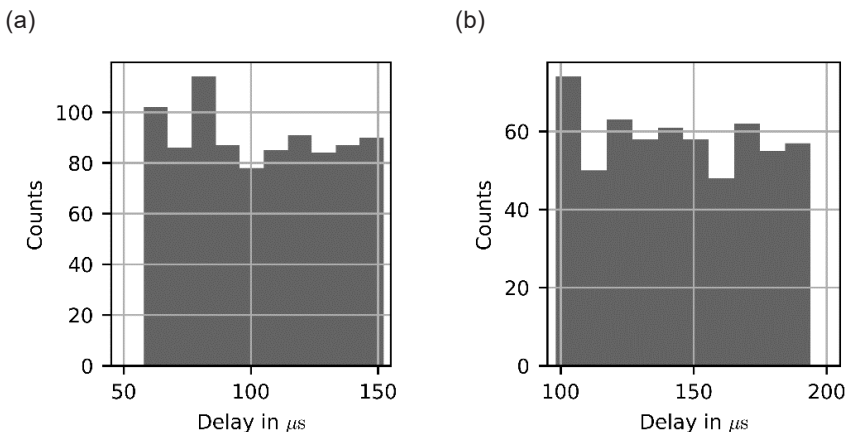


Fig. 6: (a): Histogram of valve controller latencies in 32 actuator setup. (b): Histogram of valve controller latencies in 64 actuator setup.

### **3.6 Valve current**

The valve current latency is measured with the oscilloscope data from the beginning/end of the voltage output (Fig. 7, second subplot) to the valve current exceeding/subceeding a current threshold of 0.5 A (Tab. 5, d). An example signal is plotted in Fig. 7, third subplot. The sample count is 986. Energizing the coil needs a longer time than deenergizing, by a factor of ca. 7. The relative variation is inverse to the energizing/deenergizing time by ca. 1/6, which is explainable by the different slew rates.

### **3.7 Pressure**

The nozzle pressure is measured with the oscilloscope data from the beginning of the voltage output to the valve to the point of exceeding a pressure threshold of 0.25 bar (Tab. 5, e). The pressure off delay has a bigger value range compared to the pressure on delay. The reason is that there are some measurements which have only 1 ms of power on period. This results in a lower peak pressure thus also in a shorter pressure decay. The sample size is 986.

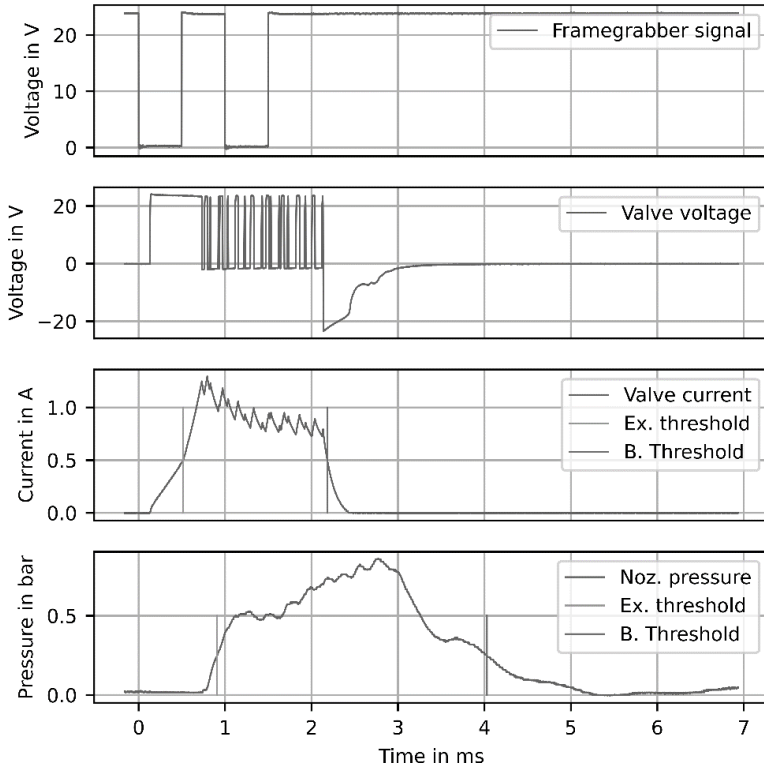


Fig. 7: Example plot of the recorded oscillograms, low pass filtered. The frame grabber sets the output high for two consecutive bus cycles (1ms each), the resulting pressure pulse is about 4 ms long while the controller output (second and third Plot) turns the valve on for ca. 2 ms.

### 3.8 Object movement

The latency of the beginning of the object movement is measured from the beginning of the pressure pulse to the starting time of object movement (Tab. 5, f). The starting time of object movement is determined by two least squares line fits, one on all observations before turning the valve on and the other on all observations after turning the valve on (Fig. 8). From the line fits, the deflection angle is calculated, too. The transfer to world coordinates is done with all objects bounding box sizes. The matrix camera angle was adjusted before, its difference

from an ideal orthogonal setup is considered negligible. The sample size is 659 single experiments.

All data is merged in one timing context, with the trigger time stamp of the first object’s camera line. The trajectories shown in Fig. 8 look as expected, except some samples with low deflection angles. These samples are either misdirected in x- or y-axis (Fig. 9, Fig. 10).

Tab. 4: Timing values for Section 3.1 and 3.2, all values in  $\mu\text{s}$ . The sample count is denoted as  $N$ . \*) The calculated standard deviation of multiple values is lower than one FPGA clock cycle (8.0 ns), which implies to add the standard deviation of the corresponding continuous uniform distribution with the width of one clock cycle period (6.48 ns).

	<b>Expected</b>	<b>Mean</b>	<b>Std*</b>	<b>N</b>
(a) Camera timing with triggering and image transfer (Section 3.1)				
<b>CC1 period</b>	10.0	10.0	0.0	25680836
<b>CC1 width</b>	6.0	6.0	0.0	25680836
<b>Transfer delay</b>	-	27.5	7.842e-3	25680062
<b>Transfer time</b>	9.64	9.64	3.973e-3	25680836
<b>Transfer period</b>	10.0	10.0	7.614e-3	25680062
<b>Trigger to full transfer</b>	43.1	43.2	7.839e-3	25680836
(b) Image preprocessing and segmentation (Section 3.2)				
<b>Processing delay</b>	-	129.8	0.865	25665356
<b>Processing time</b>	8.2	8.35	50.8e-3	25680062
<b>Processing period</b>	10.0	10.0	1.12	25660721

Tab. 5: Timing values for Section 3.3 to 3.8, all values in  $\mu\text{s}$

	<b>Min</b>	<b>Mean</b>	<b>Std</b>	<b>Max</b>	<b>Max-Min</b>
(a) Object detection (Section 3.3)					
<b>Obj. detection</b>	12.7	23.1	3.52	36.7	24.0

	Min	Mean	Std	Max	Max-Min
(b) Actuator timing (Section 3.4)					
<b>0 delay</b>	13.7	516	277	1004	990
<b>Working del.</b>	13.7e3	14.2e3	292	14.7e3	1001
(c) Valve controller (Section 3.5)					
<b>Delay 32 act.</b>	57.9	104	27.4	152	94.4
<b>Delay 64 act.</b>	98.2	145	28.0	194	95.8
(d) Valve current (Section 3.6)					
<b>Del. current on</b>	382	384	1.28	392	10.3
<b>Del. current off</b>	44.4	55.8	7.12	102	57.9
(e) Pressure (Section 3.7)					
<b>Del. pressure on</b>	768	778	3.09	787	19.0
<b>Del. pressure off</b>	1091	1888	62.6	1942	851
(f) Object movement (Section 3.8)					
<b>Movement delay</b>	8.34e3	9.04e3	324	10.8e3	2.41e3

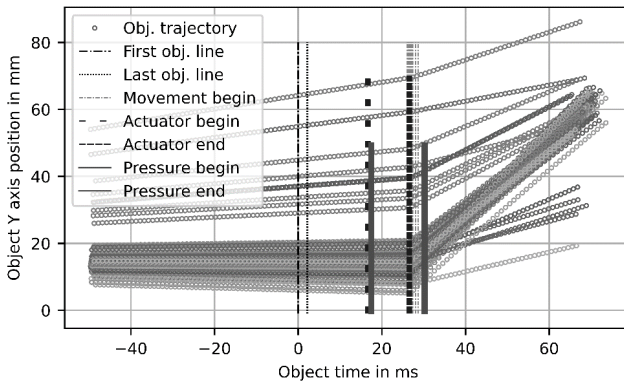


Fig. 8: Merged experimental data with object trajectories and time marks for several process steps. The thickness of the horizontal lines results from the deviation of measurements relative to the first object scan line.

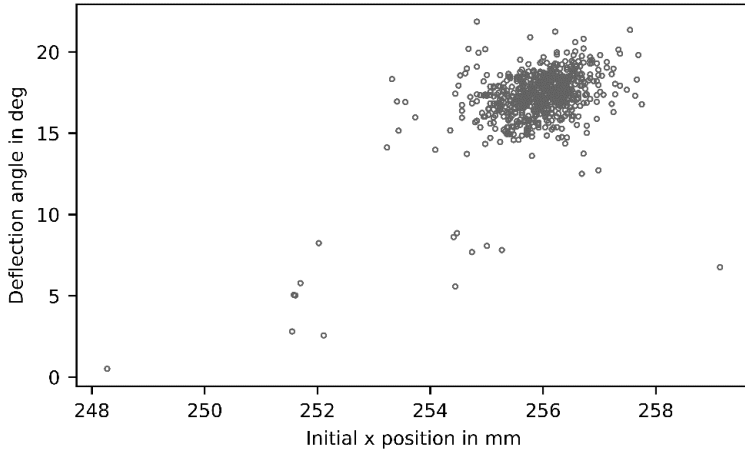


Fig. 9: The deflection angle observed with the corresponding x position. The x axis is the position in the scan line.

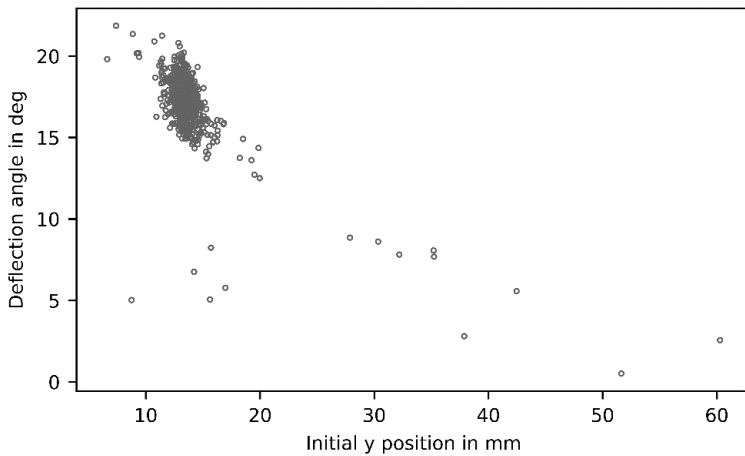


Fig.10: The deflection angle observed with the corresponding y position. The y axis is the position towards the line scan camera.

## **4 Conclusion**

The developed measurement concept has proven to deliver reproducible system timing insights of practical interest. With the described system, approx. 1 TB of raw data was acquired and processed afterwards. It was identified that the main latency and jitter contributor of the system is the actuator control chain, after classification until the pressure rises, with over 1 ms jitter and over 1.8 ms latency. These values are at least one order of magnitude higher than the sum of the other values. Several improvement options exist: optimization of the actuator timing module, valve controller board and pneumatic setup.

The measurement concept of single experiments proved to provide interesting timing insights. Whereas the image acquisition, processing and object detection latencies are well below the 1 ms specification, the actuator latency and jitter are not. For latencies below 1 ms the polling cycle should be reduced. In addition, an offset between set actuator delay and real actuator delay could be observed, it is a constant offset. Future development in this technology should address this issue. In future work, the impact of the valve itself needs to be put in focus as well the system characteristics under high load scenarios. The developed measurement system and environment will help us to test and benchmark our future improvements which include better latencies for actuator control and the implementation of more complex image processing, including convolutional neuronal networks.

## **References**

- Robben, C., & Wotruba, H. (2019). Sensor-Based Ore Sorting Technology in Mining - Past, Present and Future. *Minerals*, 9(9), 523.
- Stelzl, M. (2019). Minimale Responsezeit. *Materialsortierung mit FPGA-Framegrabber und Trigger Boards*. Downloads Sorting | MSTVision. Retrieved October 11, 2021, from <https://mstvision.de/downloads-sorting/>.
- Basler AG (2021). VisualApplets grafische FPGA-Programmierung | Basler. Retrieved January 23, 2022, from <https://www.baslerweb.com/de/produkte/framegrabber-portfolio/visualapplets/>.





# Material Value Estimation for Recycling of Waste Printed Circuit Boards (WPCBs) by a Deep-Learning-assisted Approach on X-Ray Images

Markus Firsching<sup>1\*</sup>, Steffen Ruger<sup>1</sup>, Wladislaw Benner<sup>2</sup>,  
Malte Vogelgesang<sup>2,3</sup>, Alexander Ennen<sup>1</sup>

<sup>1</sup>Fraunhofer IIS, Fraunhofer Institute for Integrated Circuits IIS, Division Development Center X-Ray Technology EZRT, Furth, Germany

<sup>2</sup>Fraunhofer IWKS, Fraunhofer Research Institution for Materials Recycling and Ressource Strategies, Alzenau, Germany

<sup>3</sup>Technische Universitat Darmstadt, Institut IWAR SuR, Darmstadt, Germany

\* Corresponding Author: Fraunhofer EZRT, Flugplatzstr. 75, 90768 Furth, Germany,  
markus.firsching@iis.fraunhofer.de

---

Keywords: PCB, WPCB, X-ray imaging, XRT, sorting, WEEE, recycling, deep neural networks, machine learning

## Abstract

Prior to actual metallurgical extraction, the value of individual entire Waste Printed Circuit Boards (WPCBs) can currently only be estimated roughly by optical inspection by a human or with very high effort (e.g. ICP analysis). At the moment, no system is available that can estimate the monetary value of WPCBs online. We introduce a sorting method for the automated evaluation and sorting of WPCBs based on the predicted value of each individual WPCB. The system acquires dual energy X-ray images (DE-XRT) from the WPCBs on a conveyor belt. These images are pre-processed and fed into a deep neural network. The system calculates the value of each WPCB based on features in the DE-XRT images. Furthermore, XRT is a more robust imaging technique in the context of application in dirty/soiled environments.

For the purpose of machine learning, a representative database is indispensable for model training and evaluation. Therefore, our first step was to generate such a machine-readable data and label base from real-world WPCBs, starting with a sample of 104 individual WPCBs. The next steps include the acquisition of the X-ray images and the chemical analysis of the components to obtain the concentrations of the valuable metals. This information provides the ground truth for the calibration of the model that predicts the actual value of the WPCB.

Our approach is based on the detection of components that contain valuable materials like ICs (integrated circuits), BGA/PGAs (ball grid/pin grid arrays), TCs (tantalum capacitors), connectors and others. For training and evaluation of our database we followed the established evaluation scheme in machine learning. The data is split into three individual sets, namely training, validation and test. Validation is used to tune the training process of the model and to validate its performance. Once that final model is found the test data serves as its independent final evaluation.

Our research shows good results in the detection of value-bearing components from single WEEE WPCBs. The achieved scores on the harmonic mean of recall and precision for the four component classes IC, TC, connector and BGA/PGA are 87.83 %, 82.54 %, 79.25 % and 88.89 %.

## **1 Introduction**

The value of Waste Printed Circuit Boards (WPCBs) from Waste of Electrical and Electronic Equipment (WEEE) differs greatly due to high variance in the content of valuable elements (mostly gold and tantalum). In the recycling process, the value of complete WPCBs can currently only be approximated roughly before the actual metallurgical recovery. Especially the value of a larger batch can only be extrapolated based on a few random samples and visual examination by human experts which is time consuming and error-prone. This situation is unsatisfactory for both buyers and sellers of WPCBs. A fully automated evaluation and, if requested, sorting of the WPCBs is desirable.

There are first scientific publications on detecting the components on PCBs (Mallaiyan Sathiaselvan, Paradis, Taheri, & Asadizanjani, 2021) and value estimation of WPCBs (Silva, Júnior, Azevedo, Oliveira, & Fernandes, 2021). However, both are based on visual images of the (W)PCBs instead of X-ray images.

For (W)PCBs populated with components on both sides, this approach can only provide incomplete information, as only one side can be analyzed at the same time when using images based on visible light. This limitation also applies for all other types of imaging using a type of radiation that is not penetrating the object, but only providing an image of the surface (reflected light imaging). Examples include, but are not limited to, near infrared, ultraviolet and terahertz.

## 2 Measurements and Methods

Our general approach was to scan the WPCBs on a conveyor belt to acquire dual energy X-ray transmission (DE-XRT) images. The next step was to detect the components of value for the recycling based on these X-ray images using state of the art deep neural networks. In our case we selected the component classes integrated circuits (ICs), tantalum capacitors (TCs), ball and pin grid arrays (BGAs/PGAs) and connectors, which we expect to have the highest material value (i.e. predominantly gold and tantalum). We have developed a model to predict the value of the WPCB for the recycling based on those components. The component based model allows flexible adaption to the requirements of the user of such a system.

### 2.1 Measurements

**X-ray imagery:** 104 WPCBs were scanned on a conveyor belt in our lab set up at a speed of 0.45 m/s (27 m/min). The X-ray images were acquired using a Comet MXR225/HP11 X-ray tube operating at 100 kV with 15 mA and a Hamamatsu C10800 dual energy line detector with a pixel pitch of 0.4 mm. Fig. 1 shows a visual example of a WPCB and its resulting DE-XRT data as grayscale images.

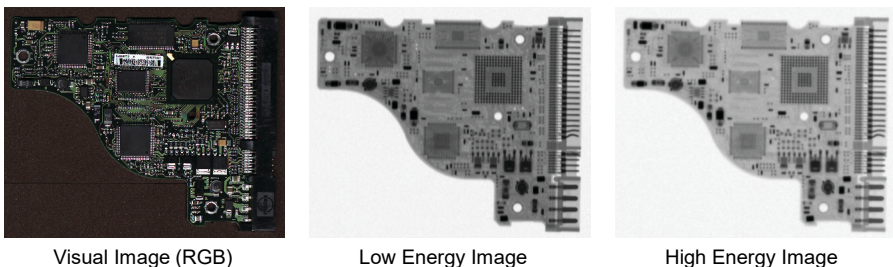


Fig. 1: A WPCB sample visualized in RGB (left) and DE-XRT (center and right) domain

**Value estimation:** The distribution of valuable material of components of each class was determined by inductively coupled plasma optical emission spectrometry (ICP-OES analysis) of a random sample of 10 ICs, 7 BGA/PGAs, thickness measurements of gold coatings on connectors using REM and literature values for tantalum content in tantalum capacitors. Each selected component class is presented in Fig. 2.

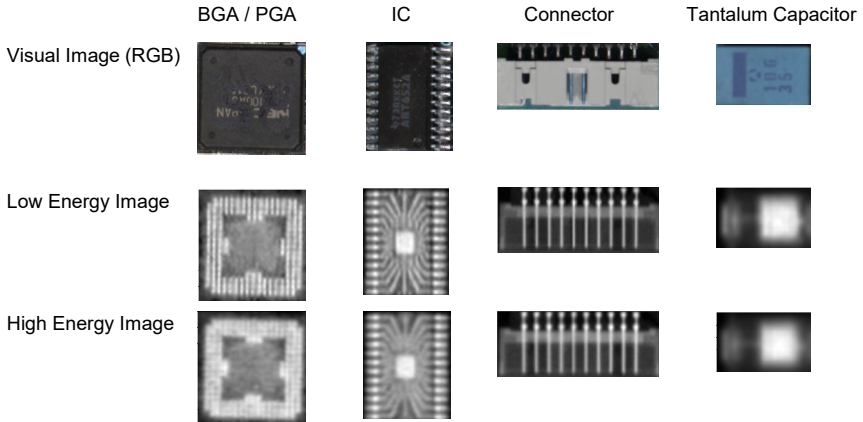


Fig. 2: Visualization of one example of the component classes (BGA/PGA, IC, connector and TC (tantalum capacitor)) each presented in visual and DE-XRT data domain

## 2.2 Preparation

In a first step of image pre-processing, the X-ray images were normalized (division by the unattenuated intensity  $I_0$ ) and logarithmized (applying the negative natural logarithm) leading to a pixel value according to the following formula:

$$V = -\log\left(\frac{I}{I_0}\right) \tag{1}$$

The value is then scaled to fit into the value range of standard image data formats. The example for the resulting image of WPCB ID 063 is shown in Fig. 3.

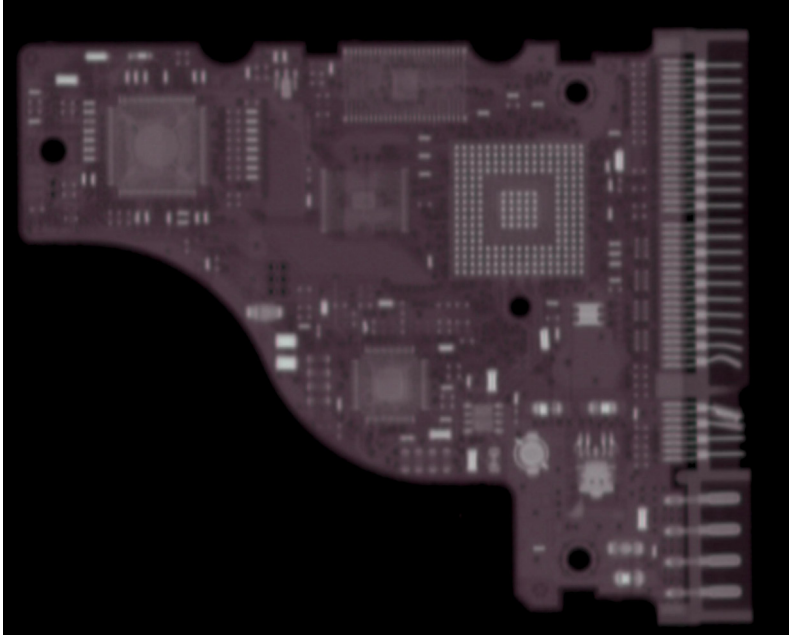


*Fig. 3: Preprocessed X-ray image (WPCB-ID 063)*

### **2.3 Database**

In total, the X-ray images of 104 WPCBs were acquired with the proposed measurement scheme. The components on the individual WPCBs were annotated manually according to the four component classes (ICs, BGAs/PGAs, tantalum capacitors and connectors) in the images with reference to visual images of the respective WPCB.

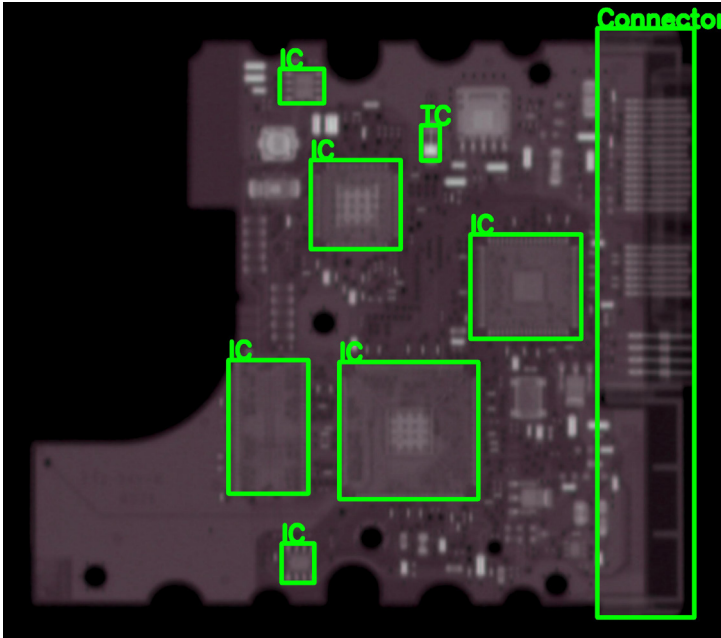


Fig. 4: Ground truth labels of WPCB ID 065

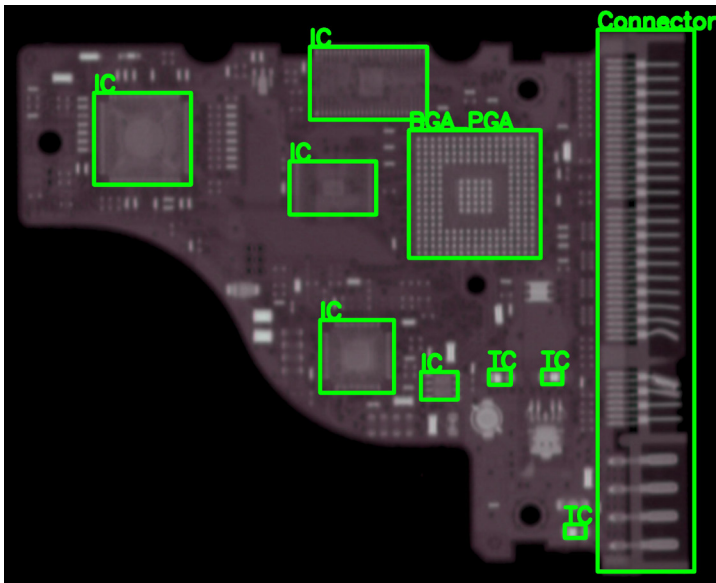


Fig. 5: Ground truth labels of WPCB ID 063

In machine learning consistent and representative data and labels are crucial. To fulfil this criterion a subset of 77 WPCBs are selected for our studies after an observation of inconsistent annotations in 27 WPCBs. This was necessary due to the fact that representative annotations are time-consuming. The components of 77 WPCBs resulted in a total of 1516 annotated components. Two examples of the ground truth labels are shown in Fig. 4 and Fig. 5 (ID 065 and 063). The occurrence number of each component class in the entire data set is shown in Tab. 1.

The sample WPCB were randomly split into three categories according to the standard procedure in deep learning applications:

1. A training set: It is used to train the machine learning model.
2. A validation set: It is used to validate the performance of the training process during the training.
3. A test set: After a model is trained, this set is used to finally evaluate the performance of this model with samples not seen by the model.



Tab. 1: Quantity of available component classes in the data sets for training, validating and testing

Sets	Component classes			
	IC	TC	Connector	BGA/PGA
Training	733	201	197	22
Validation	67	32	34	7
Test	122	69	28	4
<u>Sum</u>	<u>922</u>	<u>302</u>	<u>259</u>	<u>33</u>

The individual data sets are composed of 55 WPCBs for model training and 11 WPCBs each in the validation and test set.

## 2.4 Deep Learning Model

The prediction of the component classes on the WPCBs is a typical object detection task. We use the object detection network YOLO (you only look once) that shows state-of-the-art results for real time object detection in visual images and videos (Redmon, Divvala, Girshick, & Farhadi, 2016)(Bochkovskiy, Wang, & Liao, 2020; Redmon, Divvala, Girshick, & Farhadi, 2016; Redmon & Farhadi, 2017, 2018). The YOLO approach expresses the object detection task as a regression problem for spatially separation of bounding boxes with a class probability assignment to each of the boxes. This is realized with a single neural network that predicts bounding boxes and class probabilities directly from an input image (end-to-end). Using a single shot architecture is not only beneficial for the prediction speed of detecting objects, it also ensures that the model can implicitly encode contextual information about classes and their appearance during training.

Similar to other state-of-the-art models for object detection, the YOLO architecture can be separated into two parts: a backbone, which is used for extraction of relevant features and a head that final predicts the sizes and locations of bounding boxes with its class assignments of objects (Bochkovskiy et al., 2020). The deep neural network model mainly consists of convolutional layers that are combined with other type of layers and mechanism that the development in recent years found to be helpful for accurate detection. In the following, the used operations and the detailed architecture of the model (shown in Tab. 2) are presented:

**Conv:** The basic operation is the convolutional layer that applies a 2D convolution on a given input followed by a batch normalization (Ioffe & Szegedy, 2015) and a SiLU activation function (Elfving, Uchibe, & Doya, 2018).

**Focus:** The focus operation is proposed in YOLOv5 as first stage for processing the given input. It down samples the spatial dimensions of the given input by a factor of two with different sampling steps and is applied four times. The results are concatenated to an output that consists of four times larger channel dimension and a two times smaller spatial dimension and is finally processed with the Conv operation. This accelerates the speed for training and inference, while preserving the results of the affected operations.

**C3:** Furthermore, an operation denoted as C3 is proposed in YOLOv5, which is mainly composed of three Conv operations from which one is followed by a possible cascading of a bottleneck residual block (He, Zhang, Ren, & Sun, 2016). This bottleneck processes a given input through a Conv operation with a  $1 \times 1$  kernel followed by another Conv operation with  $3 \times 3$  kernels and adds those results to its input.

**SPP:** To become robust to arbitrary images sizes deformations, a spatial pyramid pooling (SPP) operation (He, Zhang, Ren, & Sun, 2015) with max pooling and kernel sizes set to 5, 9 and 13 is applied. This SPP operation follows the scheme proposed in YOLOv3 (Bochkovskiy et al., 2020; Redmon & Farhadi, 2018) that processes a given input via Conv with a  $1 \times 1$  kernel before applying a SPP operation and finally processes a Conv operation on the concatenated output.

**Upsampling:** The upsample operation processes a given input by enlarging the spatial dimension by factor of two with a nearest interpolation mode.

**Detection:** And finally, the detection operation for bounding box and one-hot encoded class predictions (in our case for four different components) are assigned in different grid cells.

Tab. 2: Summary of the used object detection model

	<b>Operations</b>	<b>Filters</b>	<b>Size</b>	<b>Stride</b>
<b>Backbone</b>	1. Focus	32	3 × 3	1
	2. Conv	64	3 × 3	2
	3. C3 with 1x bottleneck	64		
	4. Conv	128	3 × 3	2
	5. C3 with 3x bottleneck	128		
	6. Conv	256	3 × 3	2
	7. C3 with 3x bottleneck	256		
	8. Conv	512	3 × 3	2
	9. SPP	512	1 × 1	1
	10. C3 with 1x bottleneck no residual connection	512		
	11. Conv	256	1 × 1	1
<b>Head</b>	12. Upsampling			
	13. Concatiation with o. o. 7			
	14. C3 with 1x bottleneck no residual connection	256		
	15. Conv	128	1 × 1	1
	16. Upsampling			
	17. Concatiation with o. o. 5			
	18. C3 with 1x bottleneck no residual connection	128		
	19. Conv	128	3 × 3	2
	20. Concatiation with o. o. 15			
	21. C3 with 1x bottleneck no residual connection	256		
	22. Conv	256	3 × 3	2
	23. Concatiation with o. o. 11			
	24. C3 with 1x bottleneck no residual connection	512		
	25. Detection based on o. o. 18, 20 and 24			

\*o. o. = operation output

In total the model consists of 283 layers and 7,071,633 parameters.

The configuration of the training process with the proposed WPCB data set was set to 2000 epochs, a batch size of 8 and input image dimensions of 640 × 640 pixels in

which the corresponding WPCB samples are centred and rescaled to the required dimensions. Furthermore, data augmentation strategies are used and randomly applied for each iteration step. We use standard methods like scale, translate and flip for tackling geometric distortions. For dealing with distortions in the colour space of the image, adjustments to hue, saturation and brightness are added. In addition Mosaic data augmentation is applied, which processes four image mosaics instead of one single image (Bochkovskiy et al., 2020).

During training the model performances are validated with the validation data and the model parameters are stored when performances increases. The final model is evaluated with the test data which was not included in the training and validation process and is - until the test evaluation - unseen from the model.

## 2.5 Value model

The value model is the part of the system that calculates a value for a specific WPCB based on the output of the object detection system (in this case the YOLO network) and a number of parameters that are set by the end-user. For example, these parameters could be the daily rates for the high value materials like gold and tantalum, the recovery rate in the subsequent recycling processes, average content of high value material in each component class or the size of the overall WPCB and the components.

Using this approach, the method allows a very flexible adaption to different circumstances in the recycling process and allows a realistic value estimation even in different applications. A simple example of what the value estimation looks like is as follows. Every detected component from a given class contributes to the total value with an amount that is specific to that class. The resulting total value is the sum over all component classes:

$$v_{tot} = \sum_i n_i v_i \quad (2)$$

where  $v_{tot}$  is the total value of the WPCB,  $n_i$  is the number of detected components of class  $i$  and  $v_i$  is the mean value of a component of class  $i$ . The mean value per component is known from the chemical analysis of a representative sample set for all component classes.

In our test set that was analysed by ICP, we found a mean gold content for ICs of 0.457 mg per piece, for BGA/PGAs of 4.71 mg per piece and for connectors of 0.914 mg per piece. With a gold price of 1516 € per troy ounce (31.1 g) in October 2021, the price per mg is 4.87 ct (€). This results in an average value of 2.2 ct per IC, 22.9 ct per BGA/PGA and 4.4 ct per connector. The mean mass for an analysed whole TC was 767 mg. Market price for one kilogram of waste tantalum capacitors in October 2021 is about 25 €/kg (Sauer, 2022). This results in an average value of 1.9 ct per TC.

### **3 Results**

In this section the achieved performance scores of the object detection model are shown first, followed by the estimated value of the WPCBs from the value model based on the given predicted input of the component classes. All results are obtained from the test set.

The absolute numbers of true and predicted component classes can be seen in the Fig. 6. For evaluation of the object detection model, the harmonic mean of recall and precision (F1 score) is selected as performance score. It takes the amount of correct predicted component classes with respect to their absolute amount into account and also considers the number of wrongly predicted classes with respect to the correct predicted ones (model precision).

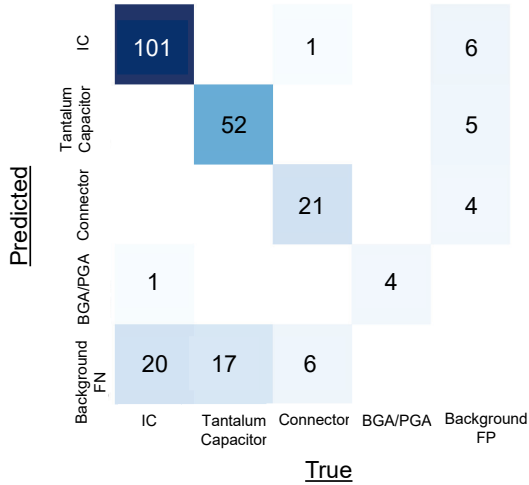


Fig. 6: Confusion matrix

The resulting F1 scores for the four component classes IC, TC, connector and BGA/PGA are 87.83 %, 82.54 %, 79.25 % and 88.89 %.

Based on these results, the value model is estimating an overall test set value of 4.62 €. From the mean value per piece in every component class derived from ICP and the announced price model in Section 2.4, the total value of the test set is 4,93 €. In Tab. 3 the estimated component class values are presented and faced with the underlying value of the test set components.

Tab. 3: Target and estimated value of the component classes

Component class	IC	TC	Connector	BGA/PGA	Total value
<b>Target value</b>	2.44 €	1.31 €	0.28 €	0.90 €	4.93 €
<b>Estimated value</b>	2.16 €	1.08 €	0.25 €	1.13 €	4.62 €

In the following a detailed example for two WPCBs are given. The prediction of components with our model in the WPCBs ID 063 and 065 is shown in Figure 7 and Figure 8.

When compared with Fig. 4 and Fig. 5, the performance of the component detection model can be seen. With ID 065, only one IC (bottom center) was missed and one false IC was detected (bottom right), all other components were detected correctly. In ID 063, all components were detected correctly. The detected components and the actual value estimation is performed as can be seen in Table 3. WPCB ID 065 shows the same quantity for all component classes even although not all components were detected correctly. Specifically, one IC in the lower left corner was not detected, while the model mistakenly detected an IC in the lower right corner. Thus, the total number of IC did not change.

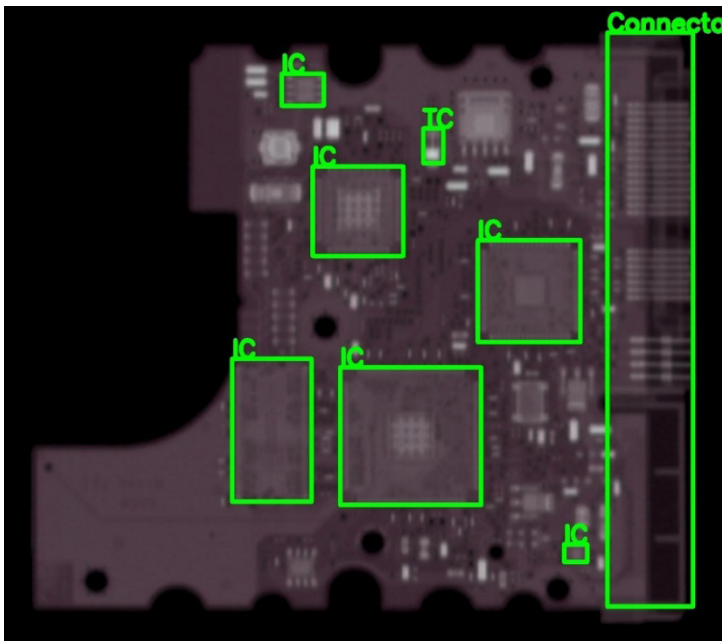


Fig. 7: Predicted Components WPCB ID 065

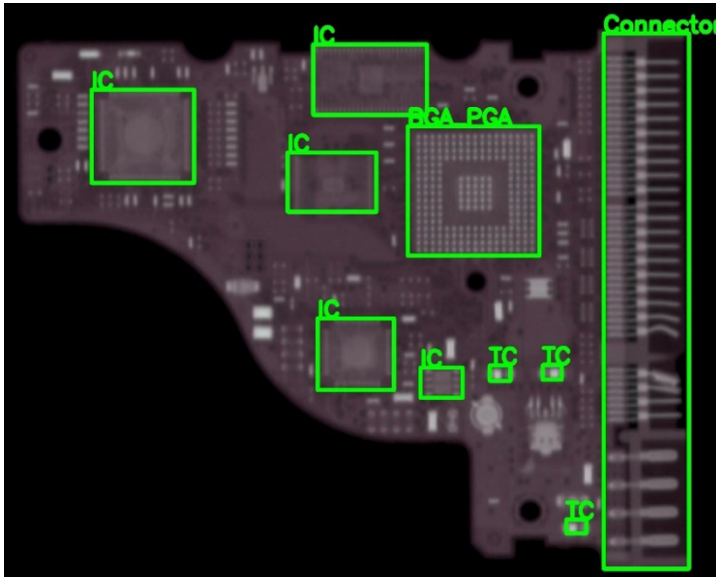


Fig. 8: Predicted components WPCB ID 063

Tab. 4: Total value estimation in €-cents of an example WPCB ID 065

Component	Detected quantity	Ground truth quantity	Value per unit	Predicted value
IC	6	6	2.2 ct	13.2 ct
TC	1	1	1.9 ct	1.9 ct
BGA/PGA	0	0	22.9 ct	0 ct
Connector	1	1	1.0 ct	4.4 ct
<u>Total Value</u>				<u>19.5 ct</u>



Tab. 5: Total value estimation in €-cents of an example WPCB ID 063

Component	Detected quantity	Ground truth quantity	Value per unit	Predicted value
IC	5	5	2.2 ct	11.0 ct
TC	3	3	1.9 ct	5.7 ct
BGA/PGA	1	1	22.9 ct	22.9 ct
Connector	1	1	1.0 ct	4.4 ct
<u>Total Value</u>				<u>44.0 ct</u>

## 4 Conclusion and outlook

Despite the relatively small sample number for training, the model showed good detection performance of the component classes. The statistical analysis of the object detection in the test sample set, i.e. the samples that were previously unseen by the prediction model is shown in the test. The achieved scores on the harmonic mean of recall and precision for the four component classes IC, TC, connector and BGA/PGA are 87.83 %, 82.54 %, 79.25 % and 88.89 %. With that performance in component detection and the statistical knowledge gained from the chemical analyses, the value prediction model provides the possibility to estimate the value of every single WPCB in the material stream. In Figure 6 the absolute numbers of true and predicted component classes can be seen, which leads to an overall test set value of 4.93 € resulting from IC worth 2.44 €, TC worth 1.31 €, connectors worth 0.28 € and BGAs/PGAs worth 0.90 €. The prediction achieves in total a worth of 4.62 € resulting from IC worth 2.16 €, TC worth 1.08 €, connectors worth 0.25 € and BGAs/PGAs worth 1.83 € for the test set with the above mentioned performance scores of the harmonic mean of recall and precision.

For an advanced value estimation, we are currently developing methods based on the size and weight of the components and the concentration of the high value materials rather than their number to account for the size variation within a component class. Furthermore, we are planning to include the dual energy X-ray analysis using the basis materials decomposition (Firsching, Nachtrab, Uhlmann, & Hanke, 2011) in future, which is able to provide additional material information.

## References

- Bochkovskiy, Alexey, Wang, Chien-Yao, & Liao, Hong-Yuan Mark. (2020). Yolov4: Optimal speed and accuracy of object detection. *arXiv preprint arXiv:2004.10934*.
- Elfwing, Stefan, Uchibe, Eiji, & Doya, Kenji. (2018). Sigmoid-weighted linear units for neural network function approximation in reinforcement learning. *Neural Networks*, 107, 3-11.
- Firsching, M, Nachtrab, F, Uhlmann, N, & Hanke, R. (2011). Multi - Energy X - ray Imaging as a Quantitative Method for Materials Characterization. *Advanced Materials*, 23(22 - 23), 2655-2656.
- He, Kaiming, Zhang, Xiangyu, Ren, Shaoqing, & Sun, Jian. (2015). Spatial pyramid pooling in deep convolutional networks for visual recognition. *IEEE transactions on pattern analysis and machine intelligence*, 37(9), 1904-1916.
- He, Kaiming, Zhang, Xiangyu, Ren, Shaoqing, & Sun, Jian. (2016). *Deep residual learning for image recognition*. Paper presented at the Proceedings of the IEEE conference on computer vision and pattern recognition.
- Ioffe, Sergey, & Szegedy, Christian. (2015). *Batch normalization: Accelerating deep network training by reducing internal covariate shift*. Paper presented at the International conference on machine learning.
- Mallaiyan Sathiaseelan, Mukhil Azhagan, Paradis, Olivia P., Taheri, Shayan, & Asadizanjani, Navid. (2021). Why Is Deep Learning Challenging for Printed Circuit Board (PCB) Component Recognition and How Can We Address It? *Cryptography*, 5(1), 9. doi:10.3390/cryptography5010009
- Redmon, Joseph, Divvala, Santosh, Girshick, Ross, & Farhadi, Ali. (2016). *You only look once: Unified, real-time object detection*. Paper presented at the Proceedings of the IEEE conference on computer vision and pattern recognition.
- Redmon, Joseph, & Farhadi, Ali. (2017). *YOLO9000: better, faster, stronger*. Paper presented at the Proceedings of the IEEE conference on computer vision and pattern recognition.
- Redmon, Joseph, & Farhadi, Ali. (2018). Yolov3: An incremental improvement. *arXiv preprint arXiv:1804.02767*.

Sauer, Florian (2022, January 24). [personal communication]. MAIREC Edelmetallgesellschaft mbH.

Silva, Leandro H. de S., Júnior, Agostinho A. F., Azevedo, George O. A., Oliveira, Sergio C., & Fernandes, Bruno J. T. (2021). Estimating Recycling Return of Integrated Circuits Using Computer Vision on Printed Circuit Boards. *Applied Sciences*, 11(6), 2808. doi:10.3390/app11062808

# Artificial Intelligence-based Particle Size Prediction for Solid Waste Particles

Lisa Kandlbauer<sup>1\*</sup>, Karim Khodier<sup>1</sup>, Renato Sarc<sup>1</sup>

<sup>1</sup>Montanuniversitaet Leoben, Department of Environmental and Energy Process Engineering, Chair of Waste Processing Technology and Waste Management, Leoben, Austria

\* Corresponding Author: Franz-Josef-Strasse 18/I (LS Abfallverwertungstechnik/-wirtschaft), 8700 Leoben, Austria, lisa.kandlbauer@unileoben.ac.at

---

Keywords: real-time metrology, artificial intelligence, particle size prediction, particle descriptors, mixed commercial waste, waste management

## Abstract

Knowing particle size distributions from streams inside waste treatment plants is crucial for dynamically controlling a plant to achieve better process performance and improved output streams. Here, an existing dataset of particle-describing parameters extracted from single-particle images was used, and particle sizes were predicted for the fractions paper & cardboard and wood in the size classes (in mm) 10–20, 20–40, 40–60, 60–80 and > 80 based on the classification algorithms RUSBoosted Trees and Bilayered Neural Network. The results show that the correct classification rate for a material fraction depending on the model type is between 64% and 82%.

## 1 Introduction

A current research vision for mechanical waste treatment plants is the “Smart Waste Factory Network”, which – among other aspects – deals with dynamic process control (Sarc et al., 2021). The concept of a dynamically regulated waste treatment plant is a viable method for future plant operation and the generation of optimized output streams. Hence, ideal feeding of the individual machines in the

plant is required. Therefore, knowing the material-specific particle size distribution (PSD) is a key factor. Usually, PSDs in the waste management sector are determined by screening analyses of representative samples; sorting analyses are implemented mainly by manual sorting. These analyses lead to a high personnel and time expenditure and are usually only carried out for specific questions (e.g., the description of the material quality (regards material composition and PSD) for subsequent recycling processes). In addition, the time delay until the results from this method are obtained does not allow its utilization for process control since the material has already left the plant and can no longer be influenced by it.

To enable a beneficial influence of the particle size of material streams in near real-time, a trinity of three requirements needs to be fulfilled, according to Khodier et al. (2019): controllable actuators – especially in dosing devices like shredders (Feil and Pretz, 2018) – such as shredder gap widths or their shaft rotation speed, which were investigated by Khodier et al. (2021), optimization algorithms, as well as methods for real-time metrology. To determine PSDs, individualizing particles is expected to be necessary to make their geometry accessible to sensors. Furthermore, some conversion is needed, from what the sensor detects to actual particle weights. An approach is made through databases of surface weights, which is part of research activities from Kroell et al. (2021), Weissenbach and Sarc (2021, 2022) and Wünsch et al. (2015). The reliable determination of the behaviour of particles in a screen, based on 2-dimensional sensor information, was already investigated by Kandlbauer et al. (2021). Here, a large number of particles with known material and particle size class was collected from screening analyses using drum screens (screen cuts in mm: 10, 20, 40, 60, 80) with additional manual sorting into five material classes (wood (wo), plastic 2D and 3D, paper/cardboard (p&c), residuals). These particles were subsequently photographed with an RGB camera on a conveyor belt and processed in binary images resulting in over 11,000 RGB images of individual particles (see Figure 1 for an example). The images were used to calculate various shape descriptors, later used in a Partial Least Squares (PLS) Regression Model, to predict the particle size based on the image data only. Depending on the material, the method resulted in a correct classification for individual particle sizes between 15% (paper & cardboard) and 100% (3D plastics). This work investigates Artificial-Intelligence- (AI) based approaches for determining particle size from the available shape descriptors.



Fig. 1: Example of the used images: original RGB image (left), greyscale image (middle), and binary image (right) of singlified waste particle (Kandlbauer et al. 2021)

## 2 Materials and Methods

For processing the already available data (11 descriptors, see Kandlbauer et al. 2021 for more details), MATLAB® 2021a was used as the programming environment, particularly the Machine Learning and Statistics Toolbox and the Classification Learner App. All models were trained with 10-fold cross-validation to obtain meaningful results. For first comparisons with the results from Kandlbauer et al. (2021) the models RUSBoosted Trees and Bilayered Neural Network (see Matlab 2022a, 2022b) were tested in a first approach and presented in the contribution here, but additional models are of interest for further research. To make the results comparable with the numbers reached with the method from Kandlbauer et al. (2021), the same number of particles was used for training and testing the algorithms. For a detailed description see chapter 2.4 in Kandlbauer et al. (2021). Here, it must be mentioned that a different number of particles is available for each material-specific particle size class (see Kandlbauer et al. 2021, Table 3). The results are presented as the share of correctly/false classified particles for each particle size class.

## 3 Results

Results for the models Bilayered Neural Network and RUSBoosted Trees are presented in Tab. 1 (fraction p&c) and Tab. 2 (fraction wo).

For the overall correct classification (all five particle size classes combined) of the material fraction p&c, the Bilayered Neural Network model achieves a classification

accuracy of 82%, and the RUSBoosted Trees model 64%. The overall performance (all five particle size classes combined) for the AI-based models is 75% in both cases. Additional AI-based classification models and material fractions are investigated at the moment to determine similarities and differences between the results coming from the PLS regression and AI-based classification models. Also, AI-based regression models are considered.

To understand and explain abnormalities in the results from the classification (e.g., for p&c 60 mm – 80 mm), relations between the individual descriptors/images need to be investigated in future work. Nevertheless, the presented method shows a promising way for real-time metrology of particle sizes of mixed commercial waste for the future. Especially for the size classes 20 mm – 60 mm (p&c), the new models can be seen as a suitable prediction method since the PLS performed below 20% (Kandlbauer et al., 2021) in these cases, which indicates that these particle size classes are not well distinguishable from each other with the used method.

Tab. 1: Results for the fraction paper&cardboard for different classification models (values in %, particle size classes in mm). Note: bold numbers show the share of the correctly classified objects.

		to 10–20	to 20–40	to 40–60	to 60–80	to > 80
<b>Bilayered Neural Network</b>	<b>from 10–20</b>	<b>87</b>	13	0	0	0
	<b>from 20–40</b>	6	<b>90</b>	2	0	2
	<b>from 40–60</b>	0	4	<b>25</b>	1	70
	<b>from 60–80</b>	0	1	5	<b>3</b>	91
	<b>from &gt; 80</b>	0	0	2	1	<b>97</b>
<b>RUSBoosted Trees</b>	<b>from 10–20</b>	<b>93</b>	7	0	0	0
	<b>from 20–40</b>	7	<b>88</b>	5	0	0
	<b>from 40–60</b>	0	7	<b>68</b>	21	4
	<b>from 60–80</b>	0	2	23	<b>49</b>	26
	<b>from &gt; 80</b>	0	1	14	25	<b>60</b>

Tab. 2: Results for the fraction wood for different classification models (values in %, particle size classes in mm). Note: bold numbers show the share of the correctly classified objects.

		to 10–20	to 20–40	to 40–60	to 60–80	to > 80
Bilayered Neural Network	from 10–20	<b>92</b>	8	0	0	0
	from 20–40	4	<b>90</b>	5	1	0
	from 40–60	0	4	<b>73</b>	19	4
	from 60–80	0	1	21	<b>63</b>	15
	from > 80	0	0	7	22	<b>71</b>
RUSBoosted Trees	from 10–20	<b>93</b>	7	0	0	0
	from 20–40	5	<b>87</b>	8	0	0
	from 40–60	0	10	<b>73</b>	16	1
	from 60–80	0	3	21	<b>63</b>	13
	from > 80	0	1	7	20	<b>72</b>

## 4 Conclusions

Compared with the results from Kandlbauer et al. (2021), the tested AI-based models result in a better classification for p&c in the size classes 20 mm – 60 mm, where the PLS model just reached a correct classification of max. 18%. If considering the particle sizes > 60 mm, the PLS model reaches a higher correct classification rate. Comparing the results for the fraction wood, the differences between the PLS model and the AI-based models are not as substantial as for p&c. However, overall the results from Kandlbauer et al. (2021) lead to higher accuracy for this specific material fraction. Additional algorithms are tested at the moment to be compared with the already available results to determine a suitable method for sensor-based particle size distribution in waste treatment processes for mixed solid waste.



## **Acknowledgement**

Partial funding for this work was provided by: The Center of Competence for Recycling and Recovery of Waste for Future (acronym ReWaste F) (contract number 882 512) under the scope of the COMET – Competence Centers for Excellent Technologies – financially supported by BMK, BMDW and the federal state of Styria, managed by the FFG.

## **References**

- Feil, A., Pretz T., 2018. Ungenutzte Potentiale in der Abfallaufbereitung, Proceedings of the 14th Recy & DepoTech, 153-160.
- Kandlbauer, L., Khodier, K., Ninevski, D., Sarc, R., 2021. Sensor-based Particle Size Determination of Shredded Mixed Commercial Waste based on two-dimensional Images. Waste Management 120: 784-794. <https://doi.org/10.1016/j.wasman.2020.11.003> .
- Khodier, K., Curtis, A., Sarc, R., Lehner, M., O’Leary, P., Pomberger, R., 2019. Smart Solid Waste Processing Plant Vision and Pathway, Conference Contribution ISWA world congress 2019.
- Khodier, K., Feyerer, C., Möllnitz, S., Curtis, A., Sarc, R., 2021. Efficient derivation of significant results from mechanical processing experiments with mixed solid waste: Coarse-shredding of commercial waste, Waste Management 121, 164-174, <https://doi.org/10.1016/j.wasman.2020.12.015>.
- Kroell, N., Chen, X., Maghmoumi, A., Koenig, M., Feil, A., Greiff, K., 2021. Sensor-based particle mass prediction of lightweight packaging waste using machine learning algorithms, Waste Management 136, 253-265, <https://doi.org/10.1016/j.wasman.2021.10.017>.
- Matlab, 2022a. Ensemble Algorithms, <https://de.mathworks.com/help/stats/ensemble-algorithms.html>, last access: 11.02.2022.
- Matlab, 2022b. Choose Regression Model Options, <https://de.mathworks.com/help/stats/choose-regression-model-options.html>, last access: 11.02.2022.

- Sarc, R., Curtis, A., Kandlbauer, L., Khodier, K., Lorber, K.E., Pomberger, R., 2019. Digitalization and intelligent robotics in value chain of circular economy oriented waste management – a review. *Waste Management* 95: 476–492. <https://doi.org/10.1016/j.wasman.2019.06.035>.
- Weissenbach T., Sarc, R., 2021. Investigation of particle-specific characteristics of non-hazardous, fine shredded mixed waste, *Waste Management* 119, 162-171, <https://doi.org/10.1016/j.wasman.2020.09.033>.
- Weissenbach T., Sarc, R., 2022. Particle-specific characterization of non-hazardous, coarse-shredded mixed waste for real-time quality assurance, *Journal of Environmental Management* 301, <https://doi.org/10.1016/j.jenvman.2021.113878>.
- Wünsch, C., Illykh, G., Borisov, D., 2015. Determination of waste compositions by the identification of fraction specific material surfaces by near-infrared-technology and the allocation of appropriate basis/surface weights. *Proceedings Sardinia 2015, Fifteenth International Waste Management and Landfill Symposium*. CISA Publisher. Cagliari 2015.



# **INSTAnT Innovative sensor technology for optimised material recovery from bottom ash treatment**

Liesbeth Horckmans<sup>1\*</sup>, Roeland Geurts<sup>1</sup>, Wenzhi Liao<sup>1</sup>,  
Kris Broos<sup>1</sup>, Karen De Boeck<sup>2</sup>, Auriane De Coster<sup>2</sup>, Peter Segers<sup>2</sup>,  
Denis Van Loo<sup>3</sup>, Kay Johnen<sup>4</sup>, Alexander Feil<sup>4</sup>, Lisa Höflechner<sup>5</sup>

<sup>1</sup>VITO, Sustainable Materials, Mol, Belgium

<sup>2</sup>Suez Treatment & Recycling - Valomac, Grimbergen, Belgium

<sup>3</sup>Tescan-XRE, Gent, Belgium

<sup>4</sup>RWTH, ANTS, Aachen, Germany

<sup>5</sup>TOMRA Sorting GmbH, Mülheim-Kärlich, Germany

\* Corresponding Author: Boeretang 200, 2400 MOL, Belgium, Liesbeth.horckmans@vito.be

---

Keywords: bottom ashes, sensor-based sorting, artificial intelligence, machine learning

## **Abstract**

Within the European Union, approximately 500 Waste-to-Energy plants are currently in use that generate approximately 19 Mt/year of bottom ash. The metals contained within are only partly recovered by magnetic and eddy current separation. The ERA-MIN2 project INSTAnT developed innovative sensor-based characterization technology to enhance (metal and mineral) resource recovery from these bottom ashes. Due to the exterior dust layer, traditional surface-based sensor techniques are inadequate to accurately identify particle composition.

The INSTAnT characterization technology uses a combination of dual-X-ray transmission and 3D laser triangulation sensors to get in-depth knowledge of the particles. After alignment and segmentation, various features including mass,

density, atomic number and shape are determined. Subsequently, the data is processed by a machine learning model to classify particles in 6 classes (glass, ceramic, slag, ferrous metal, Al, Cu), with an overall accuracy of > 90 %. However, the preparation of representative training fractions proved a key issue to ensure applicability of the model to new unseen bottom ashes. Overlap in the training fractions complicates the particle classification.

Furthermore, INSTAnT applied the CombiSense Chute machine to separate glass from the mineral fraction of bottom ash for better valorisation, with a resulting purity of > 98 % (for slag) and 80 % (for glass).

## **1 Introduction**

Within the European Union, approximately 500 Waste-to-Energy plants are in use that generate approximately 19 Mt/year of bottom ash per year (CEWEP, 2018). Bottom ashes are the incombustible residual part of the incinerated waste, and contain 80-85 m % mineral fraction and 10-12 m % metals, including 2-5 m % non-ferrous metals (of which 2/3 aluminium) (CEWEP, 2017). Recovery of metals from bottom ashes is beneficial both from an economic and environmental perspective, due to the inherent value of the metals and the greenhouse gas emission savings by replacing virgin metal production.

State-of-the-art bottom ash treatment plants use a combination of physical separation techniques to recover the metals and produce clean mineral fractions for use in construction. Typically, the process sieves the incinerated bottom ash in several size fractions, followed by magnetic separation to recover ferrous metals, and Eddy current separators to sort out non-ferrous metals. About 80 % of the metals embedded in the bottom ash are thus recovered (CEWEP, 2017), with significant portions of (NF) metals lost particularly in the fine particle range. The efficiency of the treatment steps is determined based on representative sampling and chemical analysis of the output streams, which is a costly and time-consuming process. Due to the long lag time between sampling and analysis, continuous process steering to optimize metal recovery is not possible. Surface-based sensor techniques are inadequate to accurately identify particle composition because of the exterior dust layer.

The ERA-MIN 2 INSTAnT project (2018-2021) developed an innovative sensor-based characterization technology (Characterise-to-Sort, CtS) for bottom ashes, based on machine learning. With this non-destructive technology, continuous inline analysis of the composition is possible, enabling improved steering of the process plant and higher value recovery. In addition, sensor-based sorting technologies were applied for glass separation to increase the valorisation potential of the mineral fraction.

## **2 Characterise-to-Sort (CtS) technology**

The CtS technology (patent application PCT/EP2020/087063) uses a combination of dual energy X-ray transmission (DE-XRT), 3D laser triangulation (3DLT) and RGB imaging (colour camera) to determine a wide range of parameters e.g. mass, shape, composition, etc. on individual particle level (<https://vimeo.com/545185006>). Classification models are constructed based on this data, using advanced image processing algorithms and machine learning.

To train the model, learning fractions were prepared for six target classes from the different output streams: glass, ceramic and slag from the mineral fraction, ferrous metals, and Al and Cu from the non-ferrous metals. At least 500 particles were handpicked for each of the 3 size fractions (4-8, 8-20 and 20-40 mm) of the output streams of the Suez bottom ash treatment plant VALOMAC, located in Grimbergen, Belgium.

The learning fractions were scanned at a belt speed of 20 mm/s. The materials were fed using a vibrating feeder to ensure optimal spreading of the particles. Calibration of the sensors is executed prior to each scan. For each learning fraction, the materials were separated in 3 sets: TRAIN (used for training the model), VALIDATE (used to optimize the model) and TEST (used to determine model accuracy, “unseen” by model).

Custom-made alignment and segmentation algorithms were developed and applied. A large array of (hand crafted) features are extracted for each particle related to e.g. mass, volume, density, shape, chemical composition (average atomic number). Classification models were trained employing both hand-crafted and machine learned feature sets (deep learning, CNNs). Fig. 1 shows an example of the scan results for the 4-8 mm training fractions. As this figure shows, identification based on

visual information is impossible due to the strong similarity of the different particles. The information on density and chemical composition gained from the DE-XRT is indispensable in the classification of bottom ash particles.

When applying the model to the unseen TEST particles, an overall accuracy of 90 % is reached (Fig.2). The accuracy for glass is lower (77 %) due to confusion with the chemically similar ceramic and Al fractions, and impure (overlapping) training fractions (notice e.g. green specks of Cu-particles in the Al fraction in Fig. 1). The impurities in the training fractions are due to the difficulty in visually identifying the proper class during handpicking.

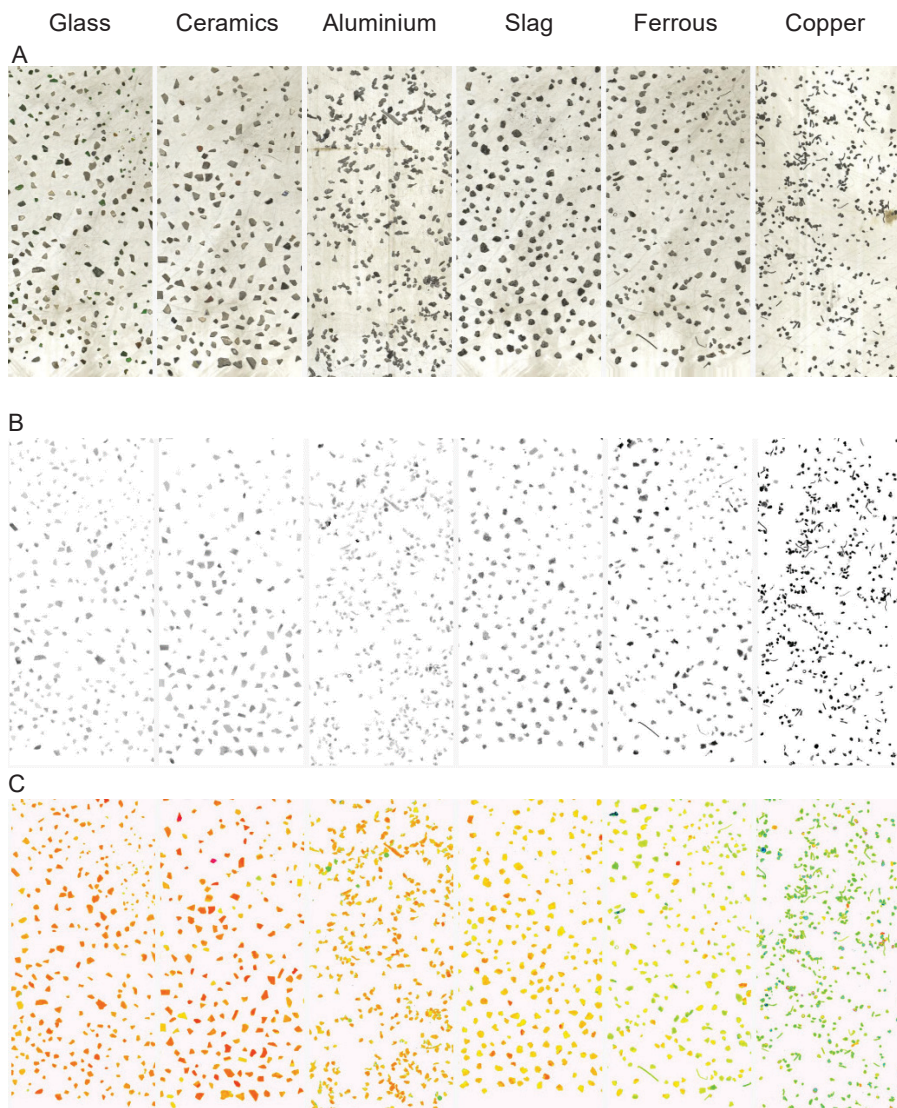


Fig. 1: Training fractions, 4-8 mm. A) Colour scan, resolution 0.25 mm, B) dual energy X-ray transmission scan, total energy, resolution 100  $\mu$ m, C) Average atomic number DE-XRT, resolution 100  $\mu$ m



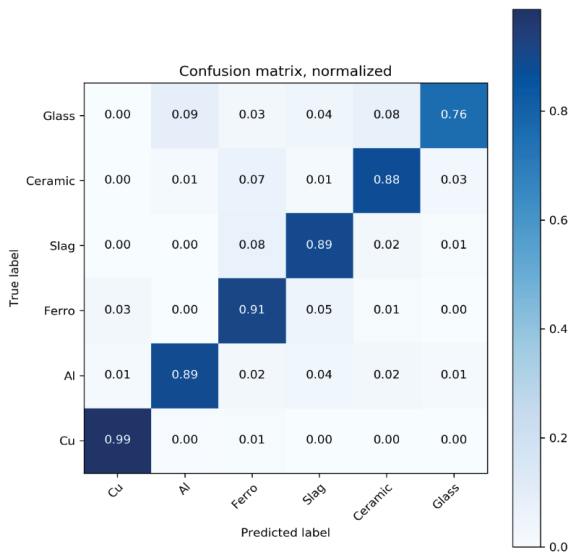


Fig. 2: Confusion matrix of INSTAnT bottom ash classification model

When the model was applied to new samples taken from production, accuracy dropped significantly. Analysis showed that the new samples were much coarser than the training fractions, most likely due to preferential handpicking of larger particles. As such, the training fraction were not representative of the whole production, causing the model to underperform. This shows that the preparation of pure, non-overlapping (mutually exclusive) training fractions that are representative for the target stream, also on a longer term, is crucial for the development of machine learning models. The presence of material composites, often found in bottom ashes (and other materials), poses an additional problem.

### 3 Glass separation

The mineral fraction of bottom ashes contains a certain amount of glass due to the presence of glass in the input (household) waste that is incinerated. The maximum amount of glass allowed in aggregates for concrete in Belgium is determined by the European standard for concrete EN 206-1 (NBN 2016) and its Belgian annex (NBN B 15-001 (BNB, 2018), while limitations for other uses are listed in the Belgian

national regulation for aggregate quality, PTV 406 (COPRO, 2020) (Tab. 1). In summary, for low value applications such as roadbase and foundations a maximum of 2 % glass is allowed. For recycling of concrete granulate in concrete (high value concrete aggregate/concrete granulate A+) a more stringent limit of 0.5 % for all impurities, including glass, is imposed.

Tab. 1: Glass limitation in aggregates

Standard	Aggregate quality	Limitation (*)
NBN EN 206-1	Type A recycled aggregates	$XRg \leq 1 \%$
	Type B recycled aggregates	$XRg \leq 2 \%$
NBN B 15-001:2018	High value Concrete granulate Type A+	$XRg \leq 0.5 \%$
	High value mixed granulate Type B+	$XRg \leq 2 \%$
PTV 406	Concrete granulate	$Rg \leq 2 \%$
	Asphalt granulate	$Rg \leq 2 \%$
	Mixed granulate	$Rg \leq 2 \%$
	High value concrete granulate	$XRg \leq 0.5 \%$
	High value mixed granulate	$XRg \leq 2 \%$

(\*)  $Rg$  = fraction glass,  $XRg$  = fraction glass + other contaminants such as gypsum, organics etc.

Based on Suez historical data, the mineral fraction contains approximately 3.6 m % glass (ranging from 0.9 m % up to 23.4 m %), which exceeds the limit values. Additional glass removal is therefore required for valorisation.

In a first step, feasibility tests on 25-75 kg of material of size 4-8 mm and 8-20 mm were done in the TOMRA testing facility at Mülheim-Kärlich (Germany), using different sensor-based sorting equipment, namely:

- Autosort Laser, which combines laser technology, to distinguish glass from other mineral phases such as ceramic, stones and porcelain (CSP), with NIR to separate transparent polymers from glass (Fig. 3).

- Combisense, that uses a colour line scan camera to sort according to colour, brightness, shape and size. This method distinguishes glass based on its lustre. The Combisense was used in two different setups: a belt system for the 8-20 mm fraction, and a chute for the 4-8 mm fraction (Fig. 4).
- Prototype Laser Unit, that sorts based on laser illumination (Fig. 4).

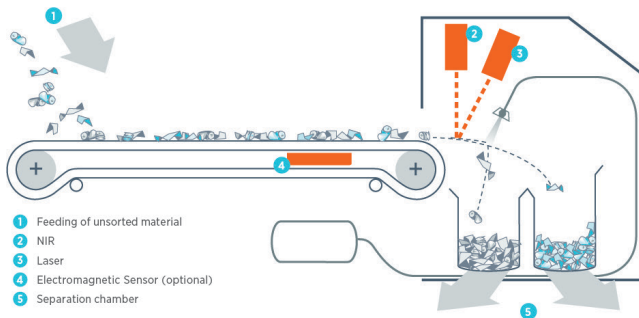


Fig. 3: Principle of Autosort laser

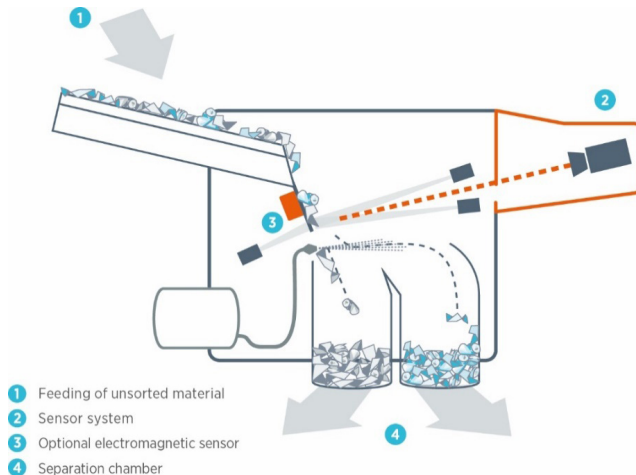


Fig. 4: Principle of Combisense chute and Prototype Laser

The feasibility test results (Tab. 2) show that the Combisense chute performed best for both glass and aggregates. Therefore, this method was chosen for further optimisation in larger scale tests on the 4-8 mm sample, which was found to contain the most glass.

Tab. 2: Performance of glass sorting techniques

	<b>Glass purity</b>	<b>Glass recovery</b>	<b>Aggregate purity</b>	<b>Aggregate recovery</b>
<b>4-8 mm</b>				
Autosort Laser	16.4 %	82.1 %	95.3 %	57.0 %
Combisense chute	81.9 %	94.3 %	94.9 %	98.6 %
<b>8-20 mm</b>				
Autosort Laser	11.9 %	51.5 %	94.2 %	86.7 %
Combisense belt	6.0 %	72.3 %	96.5 %	72.1 %
Prototype Laser	24.6 %	81.6 %	97.8 %	90.1 %

In the optimization trials, glass purity could be increased from 9.6 % to 81.9 % in one step, with a 94.3 % recovery. It is expected that the purity can be further increased by adding treatment steps. However, the inherent quality of the glass is low as it is a mix of various colours, shapes and chemical compositions.

The purity of the aggregate fraction could be increased to > 99 %. The glass content in the aggregate fraction was determined according to the Flemish standard for analysis CMA/2/II/A.22, which is based on EN 933-11 (EN, 2009). Approximately 10 kg of sample was dried at 105°C and sieved at 4 mm to remove fine particles. Contaminants are visually removed from the sieved fraction by handpicking. The sample is then submerged in water, and a separation is made between floating and non-floating particles. Finally, a second handpicking is done on the washed samples. The test results showed a presence of 0.35 % glass (Rg), and 0.44 % other contaminants (X). As such, the requirements for low value application of the aggregates ( $XRg \leq 2\%$ ) are met. The glass fraction is also in line with the requirements for high value concrete application. However, the combination of contaminants (XRg) is slightly above 0.5 % and warrants further investigation.

## 4 Conclusion

In the INSTAnT project, a bottom ash classification model was developed based on DE-XRT and 3D Laser images. The model achieved an overall accuracy of 90 % for 6 classes of materials (slag, glass, ceramic, ferrous, aluminium, copper). Preparation of long-term representative and pure training fractions is the main challenge for further improvement of the accuracy towards industrial implementation.

The sensor-based sorting technology CombiSense Chute was able to separate glass from other mineral components, achieving a high (> 99 %) purity of the aggregate fraction.

## Acknowledgement

The INSTAnT project was funded by the ERA-MIN2 research and innovation programme on raw materials to foster the circular economy, co-funded by the Horizon 2020 programme of the European Union. National funding was obtained from the VLAIO/Hermesfonds (Flanders) and BMBF (Germany).

## References

- CEWEP (The Confederation of European Waste-to-Energy plants), 2018. Waste-to-Energy plants in Europe in 2018, <https://www.cewep.eu/waste-to-energy-plants-in-europe-in-2018/>.
- CEWEP, 2017. Bottom ash fact sheet, <https://www.cewep.eu/wp-content/uploads/2017/09/FINAL-Bottom-Ash-factsheet.pdf>.
- NBN, 2016. NBN EN 206:2013+A1:2016. Concrete – Specification, performance, production and conformity
- BNB, 2018. BNB B15-001:2018. Beton – Specificatie, eigenschappen, vervaardiging en conformiteit – Nationale aanvulling bij NBN EN 206:2013+A1:2016.
- COPRO, 2020. PTV 406 (9.0) – Technische voorschriften voor gerecycleerde granulaten (<https://www.copro.eu/nl/ptv-406>).

EN, 2009. EN 933-11:2009. Reference method for the examination of coarse recycled aggregates for the purpose of identifying and estimating the relative proportions of constituent materials. The related CMA (compendium for sampling and analysis of waste materials and soil) procedures can be found at <https://emis.vito.be/nl/erkende-laboratoria/bodem-en-afvalstoffen-ovam/compendium-cma>.



# Deep-Learning-based Aluminum Sorting on Dual Energy X-Ray Transmission Data

Steffen Rüger<sup>1\*</sup>, Jann Goschenhofer<sup>1,2</sup>, Ayush Nath<sup>1</sup>,  
Markus Firsching<sup>1</sup>, Alexander Ennen<sup>1</sup>, Bernd Bischl<sup>1,2</sup>

<sup>1</sup>Fraunhofer IIS, Fraunhofer Institute for Integrated Circuits IIS, Erlangen, Germany

<sup>2</sup>Department of Statistics, LMU Munich, Munich, Germany

\* Corresponding Author: Flugplatzstraße 75, 90768 Fürth, Germany, steffen.rueger@iis.fraunhofer.de

---

Keywords: recycling, aluminum sorting, dual energy X-ray transmission, deep learning, data augmentation, cross validation, explainable AI

## Abstract

Sorting systems in the recycling industry are crucial for an efficient and sustainable reuse of used materials. This requires robust and precise sorting systems to distinguish between different materials. Current systems mainly rely on rule-based methods that need to be parametrized by human experts. In this work, we propose a deep-learning-based sorting system that learns important features for the sorting decisions from the acquired data from scratch. In the context of major household appliance (MHA) recycling, we acquired an application-oriented database from shredded MHA on a conveyor belt with an integrated dual energy X-ray scanner. These dual energy X-ray images of the flakes were then processed with a convolutional neural network model to enable an automated separation and to distinguish high-grade aluminum flakes from low-grade residual flakes. In the recycling context, one often faces the trade-off between optimizing precision and recall as a performance metric. In this context, we describe the use of a customized performance metric to account for the specific purity requirements that are present in such recycling tasks. Our work shows promising results for automated aluminum sorting via deep learning yielding an  $F_{\beta=0.2}$  of 91.74 % and a resulting precision of 93.08 %. Further, we provide local explanations of the model decision via Attribution Maps to foster trust of practitioners in the proposed solution.



# 1 Introduction

## 1.1 Motivation

The finite nature of primary raw materials and the increase in the global consumption of raw materials are placing greater focus on the use of secondary raw materials, as the industry is dependent on the availability of raw materials. This substantiates the goals of the circular economy in which the recycling industry plays an important role, making it possible to process end-of-life materials efficiently and sustainably for reuse and to secure the availability of secondary raw materials.

This requires robust and accurate sorting systems that can distinguish different materials. Currently deployed systems mainly use rule-based methods that need to be parameterized by human experts and provide hardly any information about the actual sorting decision which would be valuable for the recycler itself and the downstream industries. This parametrization is a labour-intense task and scarcity of experts is a bottleneck in this context. In this work, we propose a deep learning based pipeline to automate this process and learn the sorting decisions in a data driven way.

## 1.2 Literature

The progress made in the past in the field of computer vision has also translated into sensor-based visual sorting systems used in material sorting and recycling.

In this context, (Bircanoglu, 2018) introduced the RecycleNet architecture and trained it on an annotated dataset of 2527 RGB images to separate waste from six different classes including metal, trash, plastic, glass, and cardboard. Despite an opaque evaluation strategy, they showed strong predictive performance of an InceptionNet-based architecture with a test accuracy of 95 %. (Bobulski, 2019) used a similar RGB-based system for the separation of plastic waste in four different classes leveraging different data augmentation techniques. In their recent work on ScrapNet, (Masand, 2021) experimented with different model architectures for visual waste separation on a collection of four open-source datasets with RGB images for trash sorting annotated with varying amounts of classes. Next to the successful use of pretrained model weights, they investigate the trade-off between model inference time and model performance under a realistic model evaluation scheme. They found an EfficientNetB3 architecture to yield the best performance of

92.87 % test accuracy on a combined dataset containing 8100 annotated samples over seven trash categories.

Next to visual sorting of waste from a broad range of sources, there also exists research on the use of deep learning for sorting of metal waste. (Diaz-Romero, 2021) investigated CNN-based architectures to distinguish cast from wrought aluminum samples from a proprietary dataset consisting of 548 annotated RGB images. The focus of their work lies on different representations of the image flakes, the fusion of various sensor inputs and the applicability of transfer learning in such settings. They further built upon the work of (Dang, 2019) that proposed a computer vision pipeline for the separation of aluminum from copper samples (4769 samples) as well as a three-class sorting task of brass, copper, and a rest class (7608 samples) with reported test accuracies of 99.93 % and 97.15 %, respectively. The proposed pipeline consists of a camera module to capture RGB images of samples on a conveyor belt followed by a Region of Interest (ROI) extraction module after which the preprocessed ROI boxes are fed into a deep learning module for the sorting task.

### **1.3 Contribution**

Our contributions are the following: 1) we investigate the applicability of different deep learning architectures of varying complexity and size for automated trash sorting of high-grade aluminum from low-grade residual flakes based on dual energy Xray scans of shredded major household appliance (MHA) flakes. Thereby, we 2) propose a multi-rater annotation scheme for data collection in such complex settings and 3) focus on a realistic model evaluation scheme throughout the experiments. We further explore the usage of explainable AI methods to 4) foster trust of the practitioners in such an automated system, which is crucial for its adoption in practice.

## 2 Data and Label Collection

A representative database is crucial for successful training of deep learning models as well as reliable model evaluation. Consequently, our data was collected in a real world environment in the recycling industry and measured via an X-ray system. In particular, the data used in this work consists of major household appliance recycling scrap. In the following, we describe the preprocessing steps for the acquired sensor data and their use for supervised training of different deep learning architectures.

### 2.1 X-Ray System

X-ray systems are established as robust devices to acquire information that is relevant for the sorting of used materials. Those systems integrate well in a processing line with additional systems and can handle tough and dirty surroundings. Such X-ray systems are usually preceded by shredding and vibrating modules which enables better handling of the material flow and subsequently sorting with a higher purity.

The used measurement system includes an X-ray source set to 160 kV acceleration voltage and 2 mA tube current, a dual energy line detector with 896 pixels at pixel pitch of 1.6 mm and a conveyor belt on that the material stream is transported. The two information per pixels are then processed with conventional image processing methods such as filtering and morphological operations. Further, the dual energy information was processed within consideration of physical properties of the underlying measurement setup and the law of attenuation of X-rays. This allows to utilize the *basis material decomposition* (BMD) which is used to distinguish between different basis materials (Firsching, Nachtrab, Uhlmann, & Hanke, 2011). One benefit of the BMD is the representation of the data in a way that facilitates human annotation.

### 2.2 Data Preprocessing

The preprocessing steps are illustrated in the Fig. 1. Starting with the measured pixel lines in step 1 that shows the low energy information of a few pixel lines. Step 2 illustrates the merging of those pixel lines into an image where only low energy information is shown in this a grayscale image. In step 3, the region of interest for each individual flake is marked in which the relevant information is present. The last step shows the extracted flake and its location in a  $224 \times 224 \times 2$  shaped dual energy data sample.

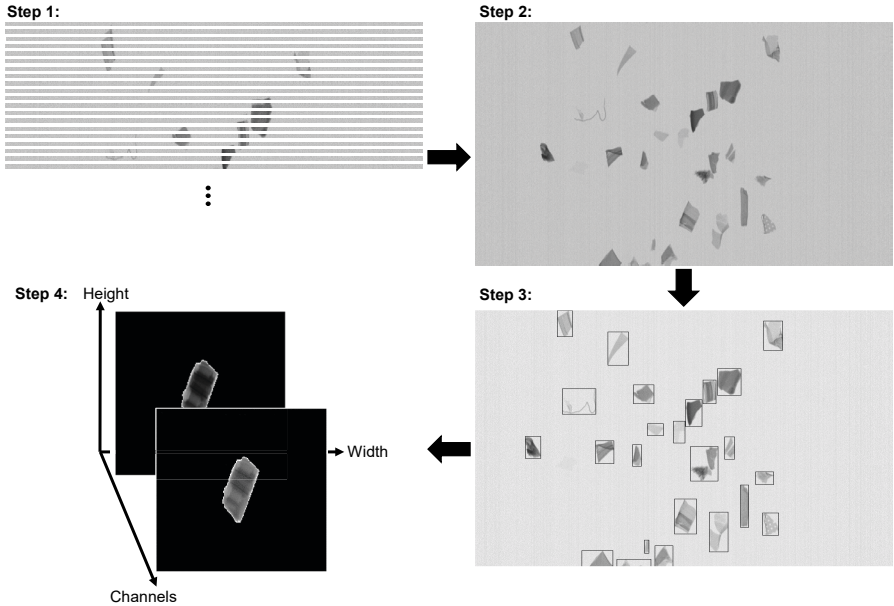


Fig. 1: Overview of the applied steps to preprocess the measured dual energy information

Those steps ensure that the entire spatial information for each energy channel per sample (flake) is captured in one individual resulting data sample. This procedure enables the further application of the proposed deep learning model which operates on a two-dimensional spatial image domain. The energy information per pixel for each flake are centred in a  $224 \times 224$  sized image to ensure a fixed input dimension for the deep learning model. This size was chosen for the extracted flakes to not exceed the maximum height and width which lies between 10 to 120 mm of the shredded flakes. Further, a filter checks if the extracted flakes exceed 224 pixels in height or width and removes larger flakes accordingly. In summary we process single dual energy pixel lines to a data stream and extract individual flake images with related spatial information prior to feeding it to the model.

### 2.3 Annotation Scheme

As shown in Fig. 1, the resulting data information of one shredded and scanned flake can be illustrated as a grayscale image. That shows energy  $E$  dependent attenuation  $\mu$  and material dependent areal density  $\rho$  of intensities  $I(E)$  in terms of Lambert-Beer's law (Firsching, Nachtrab, Uhlmann, & Hanke, 2011):

$$I(E) = I_0(E)e^{-\mu(E)\rho} \quad (1)$$

For the human visible system, this grayscale information is hard to distinguish especially for differentiation between two materials. Therefore, we use a different colour scheme and the processing of the dual energy information with the BMD for annotation. As shown in Fig. 2, this facilitates the data annotation where experts are tasked to separate flakes into a high-grade pure aluminium or a low-grade residual class.

For the annotation process, three human annotators were briefed by two human experts with a strong background in recycling and physics. We measured the agreement level among each other of the experts and the non-experts regarding their votes of the annotation task on 100 randomly chosen flake samples as a proxy for the annotation quality of the non-expert annotators. Therefore, we measure the inter-rater reliability via Cohens Kappa  $\kappa \in [0;1]$  where  $\kappa = 1$  represents complete agreement and  $\kappa = 0$  means that there is no agreement among annotators. A further interpretation of the resulting Kappa scores are: 0.01–0.20 as slight, 0.21–0.40 as fair, 0.41–0.60 as moderate, 0.61–0.80 as substantial, and 0.81–1.00 as almost perfect agreement (Cohen, 1960), (Artstein & Poesio, 2008), (McHugh, 2012).

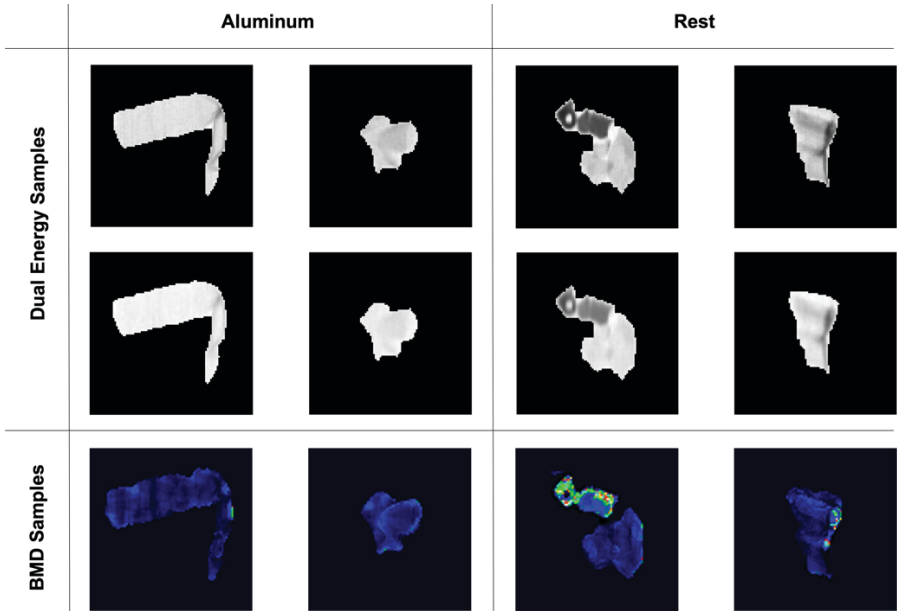


Fig. 2: Illustration of two flake examples per class of the extracted dual energy X-ray data and the processed results of the images that are used for annotation (BMD samples). It can easily be observed, that the BMD representation facilitates the data annotation process as it helps visualizing the structural properties of the residual waste class.

The Kappa scores among annotators from Tab. 1 shows substantial agreement for the mutual comparison of experts. This holds for two of three non-expert human annotators according to the agreement to expert number one. Interestingly, we measure a moderate to substantial inter-rater agreement among both experts and non-experts. This leads us to two conclusions: 1) the task at hand is not trivial and 2) non-experts that were instructed accordingly by experts in the field can annotate these flakes with a considerable quality. As a result, 3000 flakes were randomly selected from the total set of 7346 flakes. These selected samples were then annotated via the trained non-experts were each flake received three annotations to account for the potential annotation uncertainty introduced by the hardness of the task.

Tab. 1: The Cohens Kappa scores between two recycling and X-ray physics experts and three non-expert annotators

	Expert 1	Expert 2	Non-Expert 1	Non-Expert 2	Non-Expert 3
Expert 1	1.00	0.62	0.58	0.72	0.68
Expert 2	0.62	1.00	0.40	0.47	0.53
Non-Expert 1	0.58	0.40	1.00	0.59	0.69
Non-Expert 2	0.72	0.47	0.59	1.00	0.76
Non-Expert 3	0.68	0.53	0.69	0.76	1.00

## 2.4 Final Database

The available database consists of 7346 single flakes of major household appliance recycling scrap. The appliances are shredded previously that leads to resulting flake sizes between 10 to 120 mm. As described, 3000 flakes  $x_i$  were randomly selected and annotated with our proposed annotation scheme into two classes  $Y \in \{0,1\}$ : where pure aluminium = 0 and low-grade residuals = 1. The resulting class distribution follows a 1:2 ratio of pure aluminum to residual flakes. Out of the 3000 annotated flakes, the three annotators assigned 2172 the same class label, later referred to as the *certain dataset*. The validation and test datasets, sampled with a test and validation split of 20 % respectively, were generated from this certain dataset. The remaining 828 samples, termed *noisy dataset*, were used in further experiments as described in Section 3.3. We leave the use of the remaining 4346 unlabelled samples for un- and semi-supervised learning model training open for future research.

### 3 Methods

Fig. 3 illustrated the proposed pipeline starting from the measurement of recycling data and its acquisition over the preprocessing steps to the final classification of the individual flakes via a machine learning (ML) unit. In the following subsections, we provide a detailed description of this ML unit and its underlying methods.

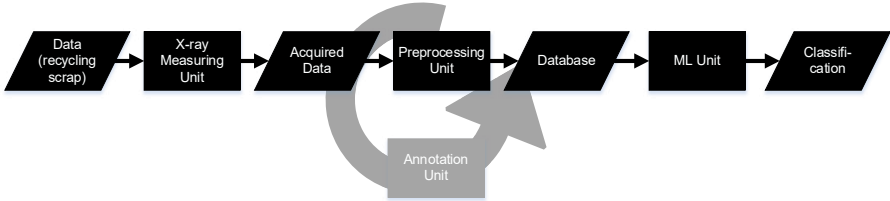


*Fig. 3: Proposed pipeline for the deep learning based sorting of MHA trash flakes into aluminum and residual waste where ML Unit describes the actual Machine Learning model*

#### 3.1 Architectures

We experimented with different backbone architectures that were established for image classification tasks. Next to the Resnet18 model architecture (He, Zhang, Ren, & Sun, 2016), we ran experiments with different versions of the EfficientNet architecture (Tan & Le, 2019). This latter architecture class offers a methodology to scale the complexity and size of a modular basic architecture and was introduced with the rationale to provide a scalable choice for the trade-off between the architecture size and the required inference time as expressed in model complexity. In particular, we employed the B0, B1, B2 and B4 versions of the EfficientNet in our experiments. The use of this model architecture allowed us to evaluate the effect of the model complexity on predictive performance. All those model architectures were initially designed to work with 3-channel RGB images, whereas our data has a 2-channel dual energy format as outlined in Section „2 Data and Label Collection“. Therefore, we added a learnable linear layer to the beginning of the model architecture that projects the input data from a  $224 \times 224 \times 2$  to a  $224 \times 224 \times 3$  format to train above mentioned architectures with our dual energy data.



### 3.2 Data Augmentation

Data augmentation strategies are a crucial component of modern deep learning training strategies. Especially in scenarios with a limited amount of labelled data it helps regularizing the model and avoid overfitting. We used a set of data augmentation procedures and wrapped them via the RandAugment procedure to facilitate the tuning towards our use case.

The following data augmentation procedures were applied to the individual flakes within the 224×224 grid: 1) Random rotation, 2) Horizontal flipping, 3) the addition of Gaussian noise and 4) The addition of salt and pepper noise. Refer to Fig. 4 for an illustration of the procedures.

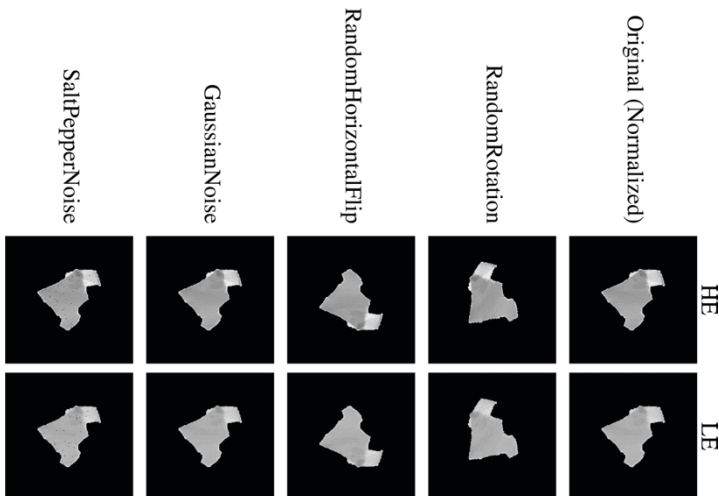


Fig. 4: Illustration of the data augmentation strategies applied on the Dual Energy Data

Each of these procedures were parametrized with a magnitude parameter  $mag \in [0; 1]$  that controls the strength of the augmentation. For 1) random rotation,  $mag$  controls the degree of the rotation, for 2) it refers to the probability of a flip for 3) it refers to the standard deviation of the Gaussian noise distribution and for 4) it controls the ratio of salt and pepper pixels (white and black) as well as the amount of those noisy pixels. The RandAugment strategy (Cubuk, Zoph, Shlens, & Le, 2020) serves as a wrapper for different data augmentation procedures to allow an elegant tuning of those individual procedures towards the task by introducing

two hyperparameters  $n$  and  $mag$ . Therein,  $n$  controls the amount of procedure that are randomly selected at each training step and  $mag$  controls their strength as described above. Next to the facilitation of the tuning procedure, RandAugment follows the rationale that potentially detrimental data augmentation procedures would be averaged out in the training process, reducing their potential harm.

### 3.3 Annotation Noise

As described in Section „2 Data and Label Collection“ and motivated by the complexity of the annotation task, we mined annotations from three human annotators in the data labelling process. Thus, for each annotated flake  $x_i$ , there are three annotations  $y_{i1}, y_{i2}, y_{i3}$  with  $y_{ij} \in \{0; 1\}$ . This allows for different schemes to aggregate the individual annotations to one global annotation  $y_i^*$  used as target in model training.

1. **Clean Annotations:** only those flakes for which all three annotators align in their annotation decision are selected as training data. Practically, this means that “unconfident” flakes e.g., where  $y_{i1}=0, y_{i2}=1, y_{i3}=0$ , are excluded to guarantee a noise-free training data set at the cost of reducing the amount of training samples.
2. **Majority Vote:** the majority of the three annotations is selected as global annotation  $y_i^*$ . This procedure allows the use of all annotated samples in model training at the cost of ignoring the uncertainty in data annotations (Tanno, Saeedi, Sankaranarayanan, Alexander, & Silberman, 2019).
3. **Soft Annotations:** the three annotations are averaged to a continuous score as global annotation  $y_i^* \in \{0.0, 0.33, 0.67, 1.0\}$  i.e., soft labels (Szegedy, 2016). This scheme allows the use of the whole training data set while reflecting the annotation noise in model training.

As part of our experiments, we empirically compared those three aggregation schemes and describe the results in more detail in Section „Results“.

Conceptually, we distinguish *Label Noise* from *Annotator Noise*. The former describes label noise on the macro level of the task and can, for instance, be modelled via noise transition matrices with estimated probabilities for the mis-annotation of the true label into other labels (Song, 2020). These approaches try to

estimate the inherent noise of the task annotations. On the other hand, *Annotator Noise* describes the disagreement of multiple observers on annotations on a micro level of individual samples (Tanno, Saeedi, Sankaranarayanan, Alexander, & Silberman, 2019). As we mined annotations from three different annotators, this setting of *Annotator Noise* fits our task at hand. While there exists a multitude of different approaches to modelling annotator noise, we restricted ourselves to the three above-described settings and leave the application of more advanced methods open for future research.

### 3.4 Model Explainability

High trust of practitioners in the model decisions are crucial for its adoption in practice. Next to a sound evaluation of its predictive performance, trust can be fostered by making the model decisions explainable to the user. Such explainable AI (XAI) solutions also allow debugging of the models and ensure it is not performing shortcut learning but learns features from the data that are relevant for real world deployment (Geirhos, 2020).

We focus on local interpretation methods, which allow us to assess the attribution of each input feature towards the model prediction (Molnar, 2019), that is the contribution of each pixel in this setting. Attribution maps based on the concept of Shapley Values (Shapley, 1952) allow the calculation of pixelwise attribution scores that describe the attribution of said pixel to the respective classes. Shapley values satisfy axioms of interpretability, theoretically backing the model explanation (Molnar, 2019). While these are computationally expensive for high-dimensional data, the Integrated Gradients method approximates the Shapley value to an infinite number of input features (Sundararajan, Taly, & Yan, 2017). This makes Integrated Gradients more tractable than the sampling of Shapley values for each input. Expected Gradients further extend Integrated Gradients to approximate SHAP values based on its differentiation from a baseline that is sampled from a subset of the dataset. The resulting attribution maps are illustrated in Section „Results“.

## 4 Experimental Section

### 4.1 Performance Metric

The main objective of this work is the training of a model that allows the separation of aluminum and residual flakes where aluminum recyclate is more valuable. As the value of recycled aluminum in downstream re-use is heavily dependent on the purity of the resulting recyclate, we needed to employ a performance metric that reflects this purity requirement. Specifically, this performance metric had to reflect our interest in a high Precision at the potential cost of a low Recall for the aluminum class. The  $F_\beta$ -Score allows for the adjustment of this trade-off via the  $\beta$ -parameter via its definition:

$$F_\beta = (1 + \beta^2) \frac{\text{Precision} \cdot \text{Recall}}{(\beta^2 \cdot \text{Precision}) + \text{Recall}} \quad (2)$$

Discussions with the domain experts involved in this project revealed that a False Positive is 5 times as costly as a False Negative given a positive label corresponds to the aluminum class. Practically speaking, the misclassification of a true residual flake as aluminum incurs a cost that is 5 times higher than the misclassification of a true aluminum flake as residual. We integrated this requirement in the performance metric via a  $\beta=0.2$ -Score attributing Precision a relative weight of 5 over the Recall for the aluminum class.

### 4.2 Evaluation Protocol

The limited size of the annotated dataset left us with a small test data set. To yield a realistic estimation of the generalization performance of the final model, we used a 5-fold Cross Validation scheme as an outer loop in the model validation step (Hastie, 2009). Further, we included an inner loop with a holdout validation split to tune the hyperparameters of the different model architectures and backbones. For hyperparameter tuning, we used the Hyperband algorithm with an equal tuning budget across folds (Li, 2017). A test and validation split ratio of 20 % was used respectively and the validation and test data were sampled from the certain dataset only. The tuning budget was set to 100 GPU hours while the performance metric from Section „4.1 Performance Metric“ was used. We report the mean and standard deviation of model performance across folds in the results section.

### 4.3 Results

The experimental results are illustrated in Tab. 2 and structured following the structure of the methods Section: 3.1 Architectures, 3.2 Data Augmentation Strategies and 3.3 Annotation Noise.

Tab. 2: Final results of the proposed methods and their experimental setups

	Backbone:	Strategies		Score	
		Augmentation:	Annotation:	$F_{\beta=0.2}$	
Methods	3.1	ResNet18	$mag = 0.5$	Clean	87.60 % +/- 3.80 %
		EffNet-B0	$mag = 0.5$	Clean	88.36 % +/- 2.08 %
		EffNet-B2	$mag = 0.5$	Clean	89.56 % +/- 3.10 %
		EffNet-B4	$mag = 0.5$	Clean	<b>91.74 %</b> + /- 1.39 %
		ResNet18	None	Clean	87.12 % +/- 2.61 %
	3.2	ResNet18	$mag = 0.5$	Clean	87.60 % +/- 3.80 %
		ResNet18	RandAugment	Clean	<u>87.88 %</u> +/- 1.80 %
		ResNet18	RandAugment	Clean	87.88 % +/- 1.80 %
	3.3	ResNet18	RandAugment	Majority	<u>88.72 %</u> +/- 1.50 %
		ResNet18	RandAugment	Soft	86.98 % +/- 1.10 %

The experiments on the use of different backbone architectures reveal that stronger model performances can be achieved with an increase in parameters and therefore an increase in complexity of the investigated backbone architectures (ResNet18, EffNetB0, EffNetB2, or EffNetB4). This is observed in terms of our proposed performance score  $F_{\beta=0.2}$  which was used as a criterion for the tuning procedure

of the architectures, as well. EffNetB4 shows the best results in this comparison where the certain dataset was used as training dataset.

Regarding data augmentation strategy, we found RandAugment to yield a slight performance increase over regular data augmentation with  $mag = 0.5$  ( $F_{\beta=0.2} = 87.60\%$ ), resulting in a  $F_{\beta=0.2}$  score of 87.88 % given a Resnet18 backbone. Both data augmentation strategies increase model performance over the use of no data augmentation ( $F_{\beta=0.2} = 87.12\%$ ).

The experiments on the use of different schemes to deal with annotation noise revealed the majority vote scheme to outperform the clean and soft annotation strategies with a model performance of  $F_{\beta=0.2} = 88.72\%$  given a Resnet18 backbone. Surprisingly, the use of clean annotations, i.e., the certain dataset, yields stronger model performance ( $F_{\beta=0.2} = 87.88\%$ ) than the explicit modelling of annotator noise via soft labels ( $F_{\beta=0.2} = 86.98\%$ ) in this specific application.

Overall, best model performance across experiments was achieved using the EffNetB4 architecture as backbone trained with clean annotations resulting in a  $F_{\beta=0.2}$  of 91.74 %.

Next to the predictive model performance, we wanted to shed light on the decision making of the model on individual input flakes. As motivated in Section 3.4, we therefore applied SHAP Expected Gradient as postprocessing step on the trained model to enable an interpretation of the single pixels attribution towards the model prediction. These attribution maps obtained for a subset of test examples are illustrated in Fig. 5 jointly with the BMD representations that were used for data annotation samples. For the present binary task, we visualized the attribution of the individual pixels towards the model prediction on a scale [-1; 1] where -1 indicates a respective pixel as being attributive towards the aluminum class and, vice versa, +1 towards the residual class while an attribution value of 0 signifies the model did not rely on that respective pixel for its prediction. Further, taking the absolute value of these class attributions allows the creation of absolute attribution maps which indicate regions of interest for the model.

Interestingly, we found the model to focus pixel regions such as the edges of the flakes, elevated regions, or regions with heterogeneous structure. These areas were also crucial in the data annotators' decision making based on the BMD samples. For instance, the model shows high attribution for the rest class within

the elevated area on the middle-right edge in sample 4 as well as the elevated are in the top left region of sample 3. Furthermore, we find the model to show high absolute attribution towards the edges of the aluminum flakes 1 and 2, and while it does integrate the elevated are in the top right of sample 1 in its decision making it finds this area of being indicative of the aluminum class, which is also revealed by the BMD representation.

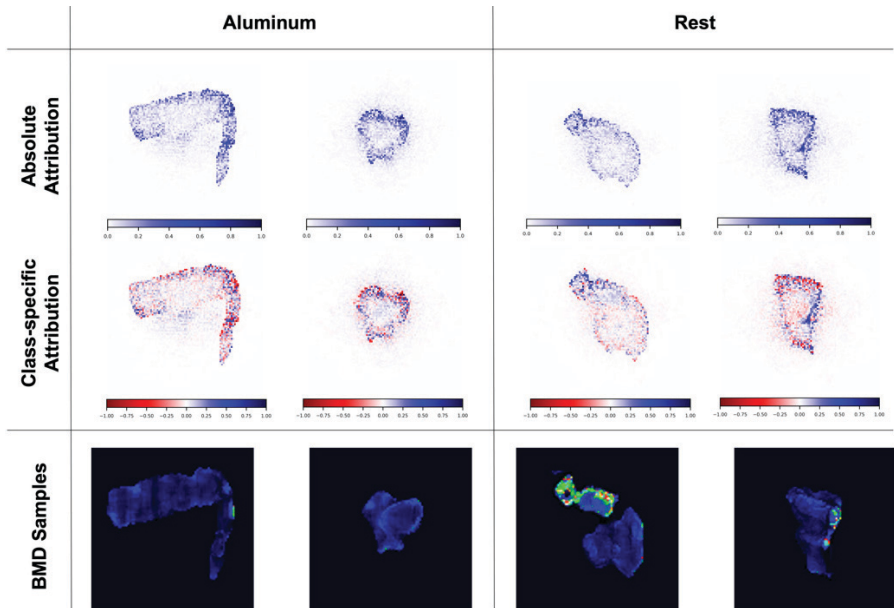


Fig. 5: Attribution Maps obtained via SHAP Expected Gradients on test samples for both classes combined with the BMD representations that were used to annotate those samples

In general, these findings confirm our hypothesis that the developed models learn to make use of the subtle features and structure of the flakes that are also revealed by the time- and labour-intensive BMD for its prediction and do not rely on shortcut learning. While the quality of local attribution maps is hard to quantify and should be taken with caution, we believe that the use of XAI methods can contribute to the acceptance of such deep learning based pipelines in sensor based sorting systems.

## 5 Conclusion

We propose a pipeline for the distinction of high-value aluminum flakes from low-value trash flakes that are acquired as dual energy X-ray data via a material stream of recycling scrap on a conveyor belt. The core of the pipeline is a deep learning module based on state-of-the-art deep learning architectures. Further, we integrated the high purity requirements for the aluminum flakes into the model selection process via a weighted  $F_{\beta=0.2}$  – Score. Within our experiments, we found an EfficientNet-based architecture to achieve a strong test performance of  $F_{\beta=0.2}$  of 91.74%.

In this context, we overcame common challenges in the application of machine learning in such settings: the collection of sufficient annotated data, a crucial component especially for the training of supervised learning models. We provide a detailed description of our data annotation scheme via three human annotators and the integration of expert knowledge from the recycling domain to compile a representative labeled dataset. Therein, we paid special attention to the handling of annotator noise that stems from the use of three human annotators during model training and explore different suitable model architectures for this problem. We further used a set of data augmentation strategies that were tailored towards dual energy X-ray data to prevent the model from overfitting to the relatively small amount of training data.

A small amount of labeled data also renders model evaluation a difficult problem. Thus, we employed a 5-fold nested cross validation scheme with a holdout validation set for hyperparameter tuning to ensure a realistic and comparable performance estimate of the final model.

Next to sufficiently strong model performance, the final deployment of such deep learning approaches depends on the acceptance by the practitioners and their trust in such models. We therefore employ state-of-the-art local explainable AI methods to open these black box models and provide insights into how the model makes its predictions over different flakes. This can foster trust amongst practitioners, which is an important step towards the final deployment of such automated sorting systems.



## Acknowledgments

This work was supported by the Bavarian Ministry of Economic Affairs, Regional Development and Energy through the Center for Analytics – Data – Applications (ADA-Center) within the framework of BAYERN DIG-ITAL II (20-3410-2- 9-8) as well as the German Federal Ministry of Education and Research (BMBF) under Grant No. 01IS18036A.

## References

- Ancona, M., Ceolinj, E., Öztireli, C., & Gross, M. (2018). Towards better understanding of gradient-based attribution methods for Deep Neural Networks. Retrieved from <https://arxiv.org/abs/1711.06104>
- Ancona, M., Oztireli, C., & Gross, M. (2019). Explaining Deep Neural Networks with a Polynomial Time Algorithm for Shapley Value Approximation. *Proceedings of Machine Learning Research*, 97, pp. 272-281. International Conference on Machine Learning.
- Artstein, R., & Poesio, M. (2008). Inter-coder agreement for computational linguistics. *Computational Linguistics*, 34, pp. 555-596.
- Bircanoglu, C. a. (2018). RecycleNet: Intelligent waste sorting using deep neural networks. *Innovations in Intelligent Systems and Applications (INISTA)*, pp. 1-7.
- Bobulski, J. a. (2019). Waste classification system using image processing and convolutional neural networks. *International Work-Conference on Artificial Neural Networks*, pp. 350-361.
- Cohen, J. (1960). A coefficient of agreement for nominal scales. *Educational and Psychological Measurement*, 20, pp. 37-46. doi:doi:10.1177/001316446002000104
- Cubuk, E. D., Zoph, B., Shlens, J., & Le, Q. V. (2020). RandAugment: Practical automated data augmentation with a reduced search space. *Neural Information Processing Systems*, 34, pp. 18613-18624.
- Dang, T. L. (2019). Classification of metal objects using deep neural networks in waste processing line. *International Journal of Innovative Computing, Information and Control*, pp. 1901-1912.

- Diaz-Romero, D. a. (2021). Deep learning computer vision for the separation of Cast-and Wrought-Aluminum scrap. *Resources, Conservation and Recycling*.
- Firsching, M., Nachtrab, F., Uhlmann, N., & Hanke, R. (2011). Multi-Energy X-ray Imaging as a Quantitative Method for Materials Characterization. *Advanced Materials*, 23, pp. 2655-2656.
- Geirhos, R. a.-H. (2020). Shortcut learning in deep neural networks. *Nature Machine Intelligence*, 2(11), 665--673.
- Gruber, A., & Weiss, Y. (2003). Factorization with Uncertainty and Missing Data: Exploiting Temporal Coherence. *Advances in Neural Information Processing Systems*.
- Hastie, T. a. (2009). *The elements of statistical learning*. Springer Series in Statistics.
- He, K. (2016, 07). test. *cvpr*.
- He, K., Zhang, X., Ren, S., & Sun, J. (2016). Deep residual learning for image recognition. *IEEE Conference on Computer Vision and Pattern Recognition*, (pp. 770-778).
- Hwanjun, S., Minseok, K., Dongmin, P., Yooju, S., & Jae-Gil, L. (2021). Learning from Noisy Labels with Deep Neural Networks: A Survey. Retrieved from <https://arxiv.org/abs/2007.08199>
- Li, L. a. (2017). Hyperband: A novel bandit-based approach to hyperparameter optimization. *The Journal of Machine Learning Research*, pp. 6765-6816.
- Lundberg, S. M., & Lee, S.-I. (2017). A Unified Approach to Interpreting Model Predictions. *International Conference on Neural Information Processing Systems*, (pp. 4768–4777).
- Masand, A. a. (2021). ScrapNet: An Efficient Approach to Trash Classification. *IEEE Access*.
- McHugh, M. L. (2012). Interrater reliability: the kappa statistic. *Biochemia medica*, 22, pp. 276–282.
- Molnar, C. (2019). *Interpretable Machine Learning*.

- Shapley, L. S. (1952). *A Value for N-Person Games*. Santa Monica, CA: RAND Corporation.
- Song, H. a.-G. (2020). Learning from noisy labels with deep neural networks: A survey. *Arxiv*.
- Štrumbelj, E., & Kononenko, I. (2014). Explaining prediction models and individual predictions with feature contributions. *Knowledge and Information Systems*, 41, pp. 647–665. doi:<https://doi.org/10.1007/s10115-013-0679-x>
- Sturmfels, P., Lundberg, S., & Lee, S.-I. (2020). Visualizing the Impact of Feature Attribution Baselines. *Distill*. doi:10.23915/distill.00022
- Sundararajan, M., Taly, A., & Yan, Q. (2017). Axiomatic Attribution for Deep Networks. *Proceedings of Machine Learning Research*. 70, pp. 3319-3328. International Conference on Machine Learning.
- Szegedy, C. a. (2016). Rethinking the inception architecture for computer vision. *Proceedings of the IEEE conference on computer vision and pattern recognition*, pp. 2818-2826.
- Tan, M., & Le, Q. (2019). EfficientNet: Rethinking model scaling for convolutional neural networks. *International Conference on Machine Learning*, 97, pp. 6105-6114.
- Tanno, R., Saeedi, A., Sankaranarayanan, D., Alexander, D. C., & Silberman, N. (2019). Learning From Noisy Labels by Regularized Estimation of Annotator Confusion. *IEEE/CVF Conference on Computer Vision and Pattern Recognition*, (pp. 11236-11245). doi:10.1109/CVPR.2019.01150
- Zhang, Q. a. (2021). Recyclable waste image recognition based on deep learning. *Resources, Conservation and Recycling*.

# Rapid GEOSCAN fully penetrative analysis enabling bulk diversion

Luke Balzan<sup>1\*</sup>, Henry Kurth<sup>2</sup>

<sup>1</sup>Scantech International, Chief Technology Officer, Adelaide, Australia

<sup>2</sup>Scantech International, Chief Marketing Officer, Brisbane, Australia

\* Corresponding Author: 143 Mooringe Ave, Camden Park, SA, Australia, l.balzan@scantech.com.au

---

*Keywords: analysis, online, real time, bulk diversion, PGNAA*

## Abstract

Sorting of material streams in mining and mineral processing has always been a fundamental process for productivity and efficiency improvements. As technology has developed over the years, various techniques to enhance sorting capabilities have been adopted to assist in achieving these goals of various improvements. Bulk ore sorting or bulk diversion has become an area of particular interest in recent times, where capability for diversion of full material streams based on measurements of the input material has become a reality. A variety of technologies are capable of measurement of different properties and aspects of the material stream, with some measuring a single or limited set of qualities, some measuring only on the surface, and some being able to provide fully penetrative analysis. Coupled with advances in the signal processing of prompt gamma neutron activation analysis measurements, fully penetrative analysis for bulk ore sorting has become a reality using the GEOSCAN to analyse material streams in real time, allowing for true bulk diversion based on representative analysis of short measured increments. This paper outlines the underlying technology and advances that have made this possible, as well as detailing examples from a series of successful installations around the world.

# **1 Introduction**

Advances in technology have enabled many efficiency gains across the mining and mineral processing value chain. An area of significant interest has been incorporating sensors to provide representative analysis to enable decisions to be made to keep or divert material based on grade or other economic properties. In the past, sensors have been fast but not able to provide representative data, or have been representative but have given data too slowly for use with diversion systems. Many optical systems provide analysis very quickly, but the sensors are not able to sufficiently penetrate the material to provide representative analysis, and are also susceptible to variations in particle size and weathering, and even the presence of dust. By contrast, analysis techniques like prompt gamma neutron activation analysis (PGNAA) utilise radioactive interactions and are fully penetrative of material flows, but rely heavily on measurement statistics to build confidence in results, and thus have had relatively long integration periods in the past before producing a result (Keeney et al, 2020, Scott et al, 2020).

Recent developments with Scantech's GEOSCAN PGNAA elemental analyser has allowed for analysis to be both fast and representative, essentially acting as an enabler of bulk diversion (Balzan, 2017). A number of GEOSCANs have been successfully implemented around the world, with significant economic impacts for the sites in question. Typically, the first phase of an installation is to characterise the material, where the extent of material variability can be observed and is often found to be more than first expected, and then diversion systems can be established to lead to material handling, processing and economic gains (Nadolski, 2018, Kurth, 2019). This paper describes the underlying analysis system and the enhancements that have been made to allow for rapid and accurate analysis, and describes case studies in a number of installations including copper, nickel and platinum across multiple continents. Examples of feed ore variation in each case are provided, together with data demonstrating the effects of being able to differentiate and sort on small tonnage increments. The gains are shown both in tonnage and economic terms. Examples making comparisons for different performance and sorting increment bases are provided.

## **2 GEOSCAN analysis technology**

In order to enable diversion of material in real time, it is necessary to have both accurate representative analysis of the material and to have rapid access to this data. Traditionally, data about material flows was obtained via laboratory analysis of samples collected from the material stream. While such analysis could be considered representative, assuming a finite sampling error, analysis data is available only after significant delays for handling and assaying. Additionally, sampling of primary streams, typically comprising either large material throughputs or large particle top size, or both, is challenging. The development of online analysis techniques has allowed for the measurement of material streams in real time, removing the delays associated with sampling and laboratory analysis. Obtaining representative analysis however remains challenging, as many analysis techniques are optical and therefore only measure the surface of the flow, or are only able to observe a small portion of the material flow. Prompt gamma neutron activation analysis (PGNAA) overcomes the issue of analysis data being representative, as it is a fully penetrative technique, and when combined with the correct physics of measurement and appropriate signal processing and calibration techniques, a PGNAA system such as Scantech's GEOSCAN is able to supply truly representative analysis of the entire belt load and full bed depth of material, and it can supply this accurate and representative data rapidly to allow timely process control decisions to be made.

Originally developing the GEOSCAN for use in the coal and cement industries (Butel et al, 1993; Ortiz & Harris, 2002; Harris et al, 2005), Scantech recognised the potential for applying the GEOSCAN on belt analyser to the minerals sector, with great success across many commodities in the minerals industry. The GEOSCAN became the first successful application in minerals in the early 2000s when it was applied to iron ore (Matthews & du Toit, 2011; Balzan et al, 2015), and developments and learnings obtained through experience in other industries continue to yield benefits in this sector (Balzan & Nieuwenhuys, 2021). The benefits of GEOSCAN elemental analysis were also able to be exploited in other commodities, including copper (Arena & McTiernan, 2011; Balzan et al, 2016 a), lead-zinc (Patel, 2014), manganese (Balzan & Harris, 2015), iron sinter for steel making (Balzan et al, 2016 b), phosphate (Balzan & Kalicinski, 2019), bauxite, and many more. In each commodity, different applications and motivations for use of the technology apply, from varying suites of elements for analysis, different elemental ranges, and different analysis periods, though similar gains are obtainable by accessing accurate data

about the material stream and its composition in real time. The remainder of this section gives a brief overview of how the GEOSCAN works to provide real time analysis, how it can be adapted to give rapid results to enable bulk diversion, and a summary of the bulk diversion process.

## **2.1 How GEOSCAN works**

The GEOSCAN on belt analyser utilises thermal neutron capture technology to determine the elemental composition of conveyed bulk materials in real time. A Californium-252 radioactive source located within the instrument below the belt generates a flux of neutrons, which are then absorbed by the conveyed material as it passes through the tunnel of the GEOSCAN. The neutrons are captured by the nuclei of the atoms in the material flowing on the belt, and gamma-rays are instantaneously produced at specific energies for each element. The gamma-ray spectrum is captured by an array of high performance detectors located at the top of the GEOSCAN, where Scantech's signal processing algorithms resolve the signal into a set of individual elemental results.

The measurement technique is completely penetrative allowing for analysis of the full material stream, and entire bed-depth and belt-width. It is also independent of ore mineralogy, particle size, and belt speed, thereby allowing for fully representative analysis of the conveyed material. Since all material is analysed continuously, the GEOSCAN does not suffer from sampling errors, such as if any of the top surface only measurement techniques were used. Results are produced for a suite of elements calibrated for the specific requirements of the particular application, which can vary from installation to installation, and is tailored to account for variation due to changes in the belt load and material composition.

Additionally, through-belt moisture (TBM) analysis systems, utilising a microwave transmission measurement technique to directly measure the moisture content of the conveyed material, are installed alongside the majority of GEOSCANs providing both elemental and moisture results. The TBM has undergone scrutiny for use within the iron ore industry, and has become widely accepted for its high level of accuracy (Balzan & Harris, 2015) in this and the majority of commodities in the minerals industry.

Results from the GEOSCAN and TBM are output to the plant control system typically every two minutes in the majority of installations. This analysis period has been

traditionally selected as it allows sufficient time for reliable and repeatable results while minimising inherent randomness from radioactive decay. In the majority of cases, this analysis period is also fast enough to provide results that can be acted upon in downstream process control (feed-forward control) or upstream material management (feedback control) as required.

Unfortunately, while two-minute analyses have proven to be sufficient for a majority of applications, it has given rise to the idea that PGNAA analysis is too slow for bulk diversion (Valery et al, 2016). Other PGNAA configurations from other manufacturers utilise alternative physics of measurement, which also may necessitate slower analysis in order to yield sufficient confidence in individual results. As a result of this perception, adoption of PGNAA for bulk diversion has not been as readily accepted as its adaptation to varying mineral commodities. In 2016, Scantech recognised a need to increase the speed of analysis so that the GEOSCAN data could be used to determine process control decisions on small material flow increments, and thus to enable the concept of bulk sorting based on representative and accurate analysis. Scantech undertook research to satisfy this requirement, and has since been able to have analysis performed rapidly in as short as 30-seconds while maintaining the repeatability statistics (precision) expected over longer integration periods. This is discussed further in the following section.

## **2.2 Rapid analysis enabler**

As discussed above, the vast majority of GEOSCAN installations in the minerals sector utilise a two-minute analysis increment. Two minutes has been found to be sufficient for a majority of process control purposes. In some cases, such as where GEOSCAN data has been used to control mill feed based on grade variation, even longer periods such as up to 30-minutes of analysis are used to enact process control (Arena & McTiernan, 2011). Similarly, GEOSCANs in iron ore are used to instigate process control using analysis periods and accumulated data over 2, 10, 30 and 60-minute integration times. Bulk sorting has been implemented using such data, as described by Matthews & du Toit (2011), where two-minute data was used to sort ore from separate mines on an overland conveyor into different grade stockpiles. Product quality ore bypassed the beneficiation circuit and this saved significant processing cost and ensured plant capacity was utilised for only the ore that required upgrading. For density control of a heavy medium plant in lead-zinc, 10-minute analyses were utilised to update controller parameters hourly



(Patel, 2014). In feedback and feed-forward control applications, such as in cement raw mill recipe control, sinter basicity control and phosphate acid reactor control, variously two and five-minute results have been utilised successfully. In each of these cases, the GEOSCAN has been specified with components to enable a high degree of accuracy across the calibrated range for elements of interest, as well as maintaining sufficient measurement repeatability (precision) to enable a high degree of confidence in individual results.

As described above, a need for shorter analysis was recognised to enable the use of PGNAAs representative and penetrative analysis for bulk diversion.

The PGNAAs technique is a statistical analysis technique that is based on a number of inherently random processes. The decay of neutrons is random, the interaction of neutrons with elements is random, the production of gamma rays is random, and the detection of gamma rays is random. Additionally, gamma rays are produced at different energies and distributed as a unique spectrum for each element. In order to produce accurate analysis and have a high degree of confidence in results, it is necessary to integrate a sufficient amount of data on which to base the analysis. This sufficient amount of data, often referred to as counting statistics, can be controlled either by changing the integration period or by changing the volume of observations. These may be traded off against each other, such that a doubling of observations can enable a halving of the integration period.

There is nuance to increasing the observations, and it is not sufficient to increase detector area or volume (such as described by Noble & Ferguson (2020)), as the detection random process is fundamentally non-linear and this does not consider either detection efficiency, pile-up (simultaneous incidence of detection), or analogue-to-digital-conversion (ADC) speed. These non-linearities are outside the scope of this paper, but this remains an important consideration since different PGNAAs analysers have different physics of measurement and different specifications (and different economics associated with these). This paper instead presents a quantitative summary obtained empirically by varying analysis time and the number of observations by varying the number of detectors used for analysis. The summary is therefore relative specifically to the GEOSCAN's physics of measurement, which may already exceed other specifications.

Following the approach of Balzan, et al (2017), and to continue to utilise existing infrastructure and systems, the minimum analysis period has been selected as

30-seconds. An outline of variation in measurement repeatability (precision) over 30-seconds, 1-minute, 2-minute, and 5-minute integration periods is shown for varying detector numbers in Table 1. The longer measurement increments are shown as a baseline on what is already considered widely acceptable, and demonstrate that the achieved 30-second results are also acceptable in successful applications (described in the following section).

Measurement repeatability (precision) is calculated as the standard deviation of repeated results for an unchanging sample presentation. To determine the measurement repeatability, a series of eight typical copper samples was statically analysed repeatedly in a production GEOSCAN over a period of three hours each. Multiple repeated analyses of each sample were obtained, and the standard deviation in calibrated results for each element calculated for each sample. The standard deviations across the eight samples were averaged to yield the average repeatability for each element across the typical range under a variety of scenarios of different analysis periods and different detector configurations. The repeatability results for copper across the range of 0.2% to 1.6% Cu are shown in Table 1 below.

*Tab. 1: Average GEOSCAN repeatability performance for copper*

<b>Analysis Period</b>	<b>Number of detectors</b>			
	<b>4</b>	<b>6</b>	<b>8</b>	<b>12</b>
<b>5 minutes</b>	0.022	0.018	0.016	0.013
<b>2 minutes</b>	0.035	0.029	0.025	0.020
<b>1 minute</b>	0.050	0.041	0.035	0.029
<b>30 seconds</b>	0.070	0.057	0.050	0.041

The results here demonstrate the relationship between result repeatability and both the number of detectors and the analysis period. As shown, it is possible to achieve a similarly acceptable level of result repeatability in a short analysis period by increasing the number of detectors. The work shows how analysis time can be traded off against the equipment specification, and that to achieve a short analysis time, a high specification is required. This is important to consider in specifying equipment, since an increase in the specification has a direct relationship to the cost of equipment, and there is no merit in obtaining a short analysis period if the

frequency of data is faster than any action that can be implemented based on the results.

Importantly, the results seen in Table 1 dispel the myth that analysis using PGNAA is necessarily slow, and a range of installations where 30-second analysis has been utilised for bulk diversion are proof of this concept. The following section describes the bulk diversion process and how GEOSCAN analysis is fundamental to the approach.

### **2.3 Bulk diversion explanation**

The concept of bulk diversion is fundamentally different to the more common particle sorting, and is in many ways is complementary and does not suffer from limitations in throughput. At the most basic level, both bulk diversion and particle sorting seek to achieve the same objectives of increasing economic grade and discarding waste, particle sorting does this with a resolution of the individual particle and thus requires careful analysis of each particle in the material stream. By contrast, bulk diversion makes its assessment on the entire flow of material, producing an average elemental composition for the complete parcel of material in each analysis increment. The two approaches yield significantly different measurement resolution and sorting sensitivity and thus can be considered as complementary approaches with similar but different objectives and different set points.

In a typical bulk diversion system, the desired sorting increment is an important consideration. Since the minimum analysis time is currently a 30-second analysis period, the sorting increment will depend on the tonnage throughput at the location of the GEOSCAN installation. For a 500 tonnes-per-hour (tph) flow, 30-seconds corresponds to approximately 4 tonnes of material, for 1000 tph it is 8 tonnes, and for 2500 tph, it would be approximately 21 tonnes. In many cases, this level of resolution is less than a shovel or haul truck and certainly less than a typical mining block. An important advantage over other measurement techniques on similar increments, such as an XRF sensor on a shovel, is that PGNAA offers a truly representative analysis by being fully penetrative of the entire flow, and not just observing the surface of the material. This has led to bulk diversion using the GEOSCAN to be a favoured approach by a number of users (Keeney et al, 2020, Rutter et al, 2020).

A bulk diversion system has the GEOSCAN analysis close to the start of the process, usually after some crushing and/or hopper-buffer, to ensure a steady throughput not exceeding the amount of material or particle size that can fit within the GEOSCAN's analysis tunnel. The GEOSCAN variously allows for bed depths of 280mm, 380mm, 530mm or 1200mm depending on frame size. Following the GEOSCAN analysis, the analysis period needs to be considered such that the diversion mechanism is at least 30-seconds of belt travel time downstream from the GEOSCAN location. This allows the GEOSCAN's analysis to be completed and the entire 30-second plot to be fully diverted.

A variety of diversion mechanisms have been employed by different end users. These have included diversion using a plough, where the belt is lifted into a diversion plough or cutter to divert material from the main stream. Another mechanism involves a diversion gate or flop gate at the head of the conveyor, where the gate can allow material to transfer in two or more directions in a transfer chute. Screens may also be incorporated into such a system to allow fines to pass, but larger particles to be diverted. Grade by size analysis is used to determine whether a screen or gate is appropriate as in many cases the fines fractions have proportionally higher metal concentrations than coarser material. A range of suppliers have systems capable of bulk diversion, and these can even be implemented on a semi-mobile basis (for example, Keeney et al, 2020 b, Scott et al, 2020). An important consideration is the activation time for the system to physically divert material. Delays associated with diverting the stream can be a source of error and need to be taken into account in the control system. Similarly, employing good control paradigms incorporating hysteresis and state-based models for changing material path need to be considered in light of mechanical movement and potential wear and tear versus the economics of diversion. Cut points for diversion can be modified dynamically, with the GEOSCAN having provision for this, so any dynamic and changing economic factors can be considered as part of any diversion regime. In all cases, the GEOSCAN is able to send both the estimates of any and all elements of interest, as well as providing a signal recommendation to divert or not based on user inputs. The plant can then utilise this signal to implement control as required. The GEOSCAN maintains a running total of tonnes and grade of material above and below the diversion threshold value/s.

### **3 Case Studies**

Scantech has had a long history with over 35 years of experience in bulk sorting (Kurth & Balzan 2020). The earliest examples involve measurements in coal and diversion based on ash measurement using a flop-gate diverter, and longer analysis increment diversion has been implemented successfully in iron ore. In more recent times, the approach has focused on rapid analysis in base and precious metals commodities, with some results outlined below. It has been observed at multiple sites that high precision measurement provides a significant reduction in misallocation of material than lower precision measurement, even when the latter measurement occurs over shorter time increments.

#### **3.1 Base Metals**

The largest area of interest in bulk sorting has come from base metals commodities such as copper and nickel. Scantech has implemented a large number of copper bulk diversion projects around the world, including two in Canada, two in Chile, one in Peru, and two in Australia. For nickel, two projects have been successful in measuring nickel in Brazil and Australia respectively. Each site has taken a different approach depending on local requirements, but in all cases, a similar process has been undertaken in the development of successful bulk diversion.

The first steps involve a successful and reliable calibration of the GEOSCAN, calibrated against samples collected and subsequently verified using the same method. The next step involved characterisation of the material variability by collecting 30-second GEOSCAN analyses over a period of time and evaluating the variability considering the economics of diversion. From this study, suitable analysis periods have been selected (usually 30-seconds, but in some cases, 1 minute or 2 minutes), and the bulk diversion regime implemented accordingly. Customer feedback has suggested improvements from 10% to 30%. Paramount to this success is the GEOSCAN's analysis performance, with Figures 1 and 2 below showing results for copper and nickel respectively.

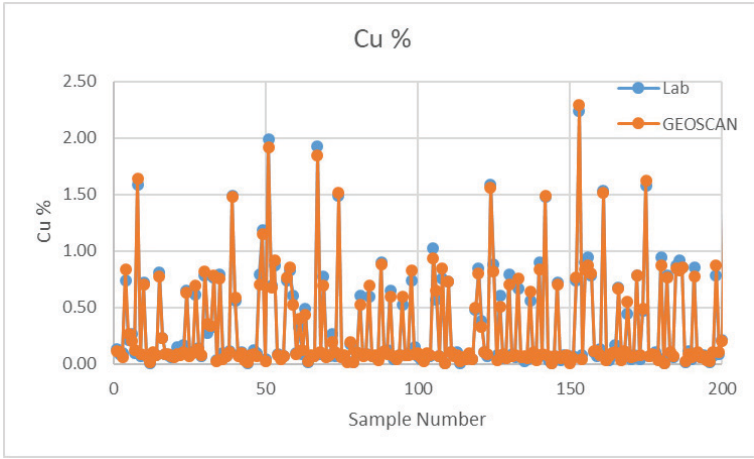


Fig. 1: GEOSCAN and laboratory results for Cu %

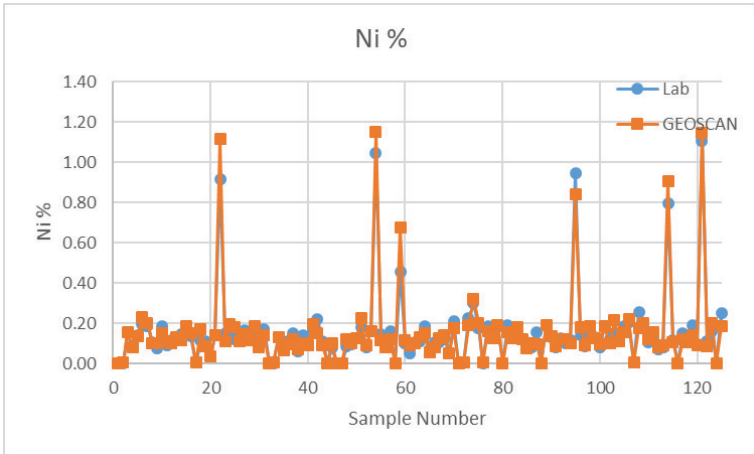


Fig. 2: GEOSCAN and Laboratory results for Ni %

### 3.2 Precious Metals

In recent times, Scantech has led developments in the direct measurement of precious metals in ore using PGNAA (Balzan et al, 2022). However, due to the typically low concentration of precious metals in ore, the direct measurement analysis of these elements is typically significantly slower than for other elements, such that direct measurement of elements like gold, silver, and platinum cannot be used in a typical bulk diversion system, where 30-second analysis is usually required. However, for many sites, there are strong correlations between elements like gold or platinum and other elements that can be readily measured on a 30-second basis. This has formed the basis for a number of installations of bulk diversion for precious metals, including two in Africa, one in Canada, and three in Australia where precious metals are reported by proxy measurement of other elements including sulphur, copper, and nickel. Figures 3 and 4 below highlight the GEOSCAN's performance in such proxy measurements for gold and platinum respectively.

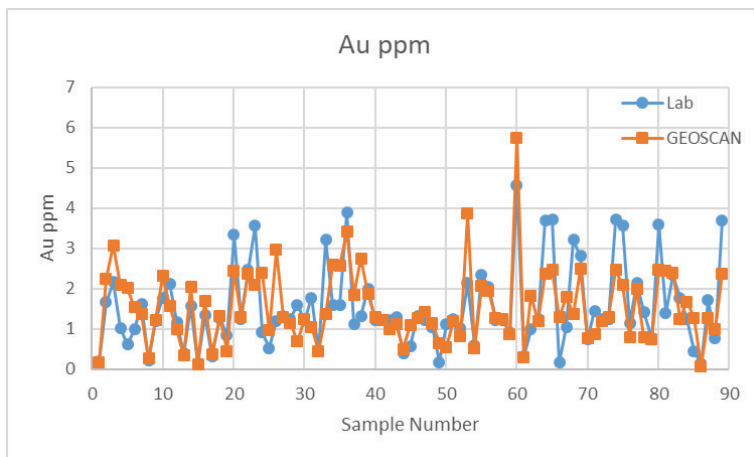


Fig. 3: GEOSCAN and laboratory results for Au ppm

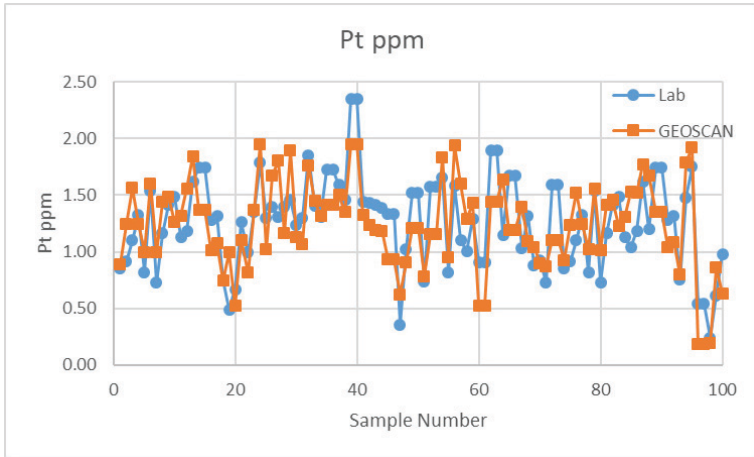


Fig. 4: GEOSCAN and laboratory results for Pt ppm

It is important to note that it remains a possibility to measure the precious metal directly on a longer time basis and report this on a longer time interval. This can be done on the same system that is otherwise set up for bulk diversion. While such data may not be useful in the bulk diversion control, particularly where longer conveyors are absent, it can still be valuable for operations and can verify the bulk diversion approaches. The GEOSCAN is simultaneously able to output results of direct elemental analysis and proxy measurement on a 30-second basis, and direct precious metal measurement on a longer time basis with less frequent results.

## 4 Conclusion

This paper has provided an outline of the concept of bulk diversion for a variety of mineral commodities. It has provided a basis for technology that has enabled the practice of bulk diversion, focused on elemental analysis from Scantech's GEOSCAN PGNAA elemental analyser. It has discussed the technology and principles of analysis, including advances that have allowed for rapid analysis to enable bulk diversion. It has provided an overview of bulk diversion systems and provided case studies where such systems have been implemented in a number of commodities. The examples provided demonstrate the case for using such a system for bulk diversion, providing performance results and a demonstration of the



effectiveness. The successful implementations show that the GEOSCAN's PGNAA analysis is an effective tool enabling true representative analysis for bulk diversion of conveyed flows that can be implemented in real time.

## References

- Arena, T. and McTiernan, J. (2011). On-belt analysis at Sepon copper operation. *Proceedings MetPlant 2011*. Australasian Institute of Mining and Metallurgy, pp 527—535.
- Balzan, L., Beven, B.J. and Harris, A. (2015). GEOSCAN online analyser use for process control at Fortescue Metals Group sites in Western Australia. *Proceedings Iron Ore 2015*. Australasian Institute of Mining and Metallurgy, pp 99—105.
- Balzan, L. and Harris, A. (2015). Adaptation and performance of GEOSCAN on-belt analysers for manganese ore at Assmang Black Rock. *Proceedings Africa Australia Technical Mining Conference 2015*. The Australasian Institute of Mining and Metallurgy, pp 125—130.
- Balzan, L., Jolly, T., Harris, A. and Bauk, Z. (2016 a). Greater use of GEOSCAN on-belt analysis for process control at Sepon copper operation. *Proceedings XXVIII International Mineral Processing Congress 2016*. Canadian Institute of Mining, Metallurgy and Petroleum.
- Balzan L. A., Harris A. R., and Bauk Z. (2016 b). Process improvement through real-time analysis. *Proceedings of the 46th Ironmaking, 17th Iron Ore and 4th Agglomeration Conference 2016*. Rio de Janeiro, Brazil: Associação Brasileira de Metalurgia, Materiais e Mineração
- Balzan, L. A., Harris, A. R., and Bauk, Z. (2017). Faster analysis: recent advances in GEOSCAN on-belt analysis techniques allowing for rapid real-time measurement of minerals. *Proceedings of COM2017 Conference of Metallurgists*. Canadian Institute of Mining, Metallurgy and Petroleum.
- Balzan, L.A., and Kalicinski, M. (2019). GEOSCAN-M Use For Process Improvement in Phosphate Plants. "SYMPHOS 2019", *5th International Symposium on Innovation and Technology in the Phosphate Industry*. Procedia Engineering.

- Balzan, L.A., and Nieuwenhuys, F. (2021). Real time phosphorus analysis using GEOSCAN on belt analysers at Assmang Khumani Mine in the Northern Cape. *Proceedings Iron Ore 2021*. Australasian Institute of Mining and Metallurgy, pp 342—350.
- Balzan, L.A., A. de Paor, A. Doorgapershad and W. Futcher (2022). The end of the rainbow: real time direct gold analysis in run of mine ore at Newcrest's Telfer mine using GEOSCAN analysis. *Proceedings of International Mineral Processing Conference 2022*, Australasian Institute of Mining and Metallurgy, in preparation.
- Butel, D., Howarth, W.J., Rogis, J., and Smith, K.G. (1993). Coal sorting. *Coal Preparation*, vol 12. Gordon and Breach Science Publishers, pp 203—214.
- Harris, A., Smith, K., and Rossi, F. (2005). On-belt analysis breakthrough. *International Cement Review*. October 2005, pp 62—66.
- Keeney, L., La Rosa, D., Walters, P., Rutter, J., and Scott, M. (2020 a). Evaluation and operationalisation of bulk sensing technologies: insights from real world case studies. *Proceedings of Preconcentration Digital Conference 2020*. Australasian Institute of Mining and Metallurgy, pp 52—65.
- Keeney, L., Beaton, N., Scott, M., La Rosa, D., Amini, E., Rutter, J., and Faramarzi F. (2020 b). The integration of mine-to-mill and grade engineering at Anglo American's Los Bronces Mine using IES. *Proceedings of Preconcentration Digital Conference 2020*. Australasian Institute of Mining and Metallurgy, pp 116—129.
- Kurth, H. (2019). Sampling or on-line analysis – which to use when. *Proceedings of Ninth World Conference on Sampling and Blending*. Beijing General Research Institute of Mining and Metallurgy, pp 737—745.
- Kurth, H., and Balzan, L. (2020). Bulk sensing for effective ore sorting – learnings over 35 years. *Proceedings of Preconcentration Digital Conference 2020*. Australasian Institute of Mining and Metallurgy, pp 238—247.
- Matthews, D, and du Toit, T. (2011). Real-time online analysis of iron, validation of material stockpiles and roll out for overall elemental balance as observed in the Khumani Iron Ore Mine South Africa. *Proceedings Iron Ore 2011* Australasian Institute of Mining and Metallurgy, pp 297—305.

- Nadolski, S, Samuels, M, Klein, B and Hart, D, (2018). Evaluation of bulk and particle sensor-based sorting strategies for the New Afton block caving operation. *Proceedings 8th International Conference, Sensor-Based Sorting & Control*. RWTH: Aachen, Germany.
- Noble, G., and Ferguson, S. (2020). Understanding ore heterogeneity and effective bulk ore sorting using PGNAA/PFTNA. *Proceedings of Preconcentration Digital Conference 2020*. Australasian Institute of Mining and Metallurgy, pp 260—265.
- Ortiz, C. and Harris, A. (2002). Raw mix control. *World Cement*. February 2005, pp 46—49.
- Patel, M. (2014). On-belt elemental analysis of lead-zinc ores using prompt gamma neutron activation analysis. *Proceedings XXVII International Mineral Processing Congress 2014*. Gecamin: Santiago, Chile, chapter 17.
- Rutter, J., Scott, M., Odiar, N., Federov, M., and Francois-Bongarcon, D. (2020). Quantification of surface sensor representivity of primary crushed ore for bulk ore sorting. *Proceedings of Preconcentration Digital Conference 2020*. Australasian Institute of Mining and Metallurgy, pp 275—286.
- Scott, M., Rutter, J., du Plessis, J., and Alexander, D. (2020). Operational deployment of sensor technologies for bulk ore sorting at Mogalakwena PGE Mine. *Proceedings of Preconcentration Digital Conference 2020*. Australasian Institute of Mining and Metallurgy, pp 169—181.
- Valery, W., Duffy, K., Holtham, P., Reple, A., Walker, P., and Rosario, P. (2016). Techno-economic evaluation of bulk ore sorting for copper ore at the PanAust Phu Kham operation. *Proceedings of XXVIII International Mineral Processing Congress*. Canadian Institute of Mining, Metallurgy and Petroleum.

# The impact of mixing and scale on the bulk ore sorting potential of a panel cave mine

Mahir Can Cetin<sup>1\*</sup>, Bern Klein<sup>1</sup>, Stefan Nadolski<sup>2</sup>

<sup>1</sup>University of British Columbia, Norman B. Keevil Institute of Mining Engineering, Vancouver BC, Canada

<sup>2</sup>Minpraxis Solutions Ltd. Vancouver, BC, Canada

\* Corresponding Author: [mcetin@mail.ubc.ca](mailto:mcetin@mail.ubc.ca)

---

Keywords: Sensor-based bulk ore sorting, grade heterogeneity, sorting potential, block caving, mixing of ore, sorting scale

## Abstract

Cave mining methods, principally block and panel caving, have become the main underground bulk mining methods of choice as a result of the exhaustion of near-surface high-grade ore deposits. Mining companies are looking into the application of caving methods to extend the life of their open-pit operations as well as to develop new mines for large and deeply situated low-grade ore deposits. Despite that cave mining can offer comparably high production rates with low operating costs, it inherently suffers from a lack of grade selectivity due to various blending and size reduction events that take place in draw columns and during the handling of the ore underground (Nadolski et al., 2016). Therefore, caving run-of-mine grades often trend towards the orebody average (Moss et al., 2018)

As a pre-concentration method, sensor-based bulk ore sorting can potentially address the limited grade selectivity associated with cave mining methods by rejecting the barren or low-grade material ahead of processing, providing the mill with more consistent and higher-grade feed. The potential of a bulk ore sorting application is dependent on the grade heterogeneity of the ore and the ability of sensors to detect the heterogeneity (Klein and Bamber, 2019). Though the former is usually present in different ore types at varying amounts, mixing in cave mining methods decreases the grade variability naturally present in the ore. The latter

is usually limited for the elements present in trace amounts such that longer integration times of sensors are needed for more accurate grade predictions. However, prolonged measurement times of sensors obscure the grade variability in the ore due to the increase in the sorting scale.

To assess the impact of mixing and scale on the bulk ore sorting potential, a quantitative assessment was carried out for the Cadia East panel cave mine, where two of the bulk ore sorting technologies – Prompt Gamma Neutron Activation Analysis (PGNAA) and Magnetic Resonance (MR) are in use. Heterogeneity analyses were conducted using the drill core assay data, draw point sampling data, and real-time sensor data to show the change in sorting potential of the ore as it caves and flows to the extraction level and is subsequently being crushed underground and conveyed to the surface. The results of the study showed that both mixing and scale have a negative impact on heterogeneity, thus on the sorting potential, such that:

1. Mixing in the cave columns and during the material handling decreases copper and gold variability in the ore, although retained to a certain extent.
2. Larger ore pods due to the increase in mining and sorting scale obscure the grade heterogeneity, which results in the decrease of the bulk ore sorting potential.

## **References**

- Klein, B., & Bamber, A. (2019). Mineral Sorting. In R. C. Dunne, S. K. Kawatra, & C. A. Young, *Mineral Processing and Extractive Metallurgy Handbook* (pp. 763-786). Englewood, CO: Society for Mining, Metallurgy & Exploration (SME).
- Moss, A., Klein, B., & Nadolski, S. (2018). Cave to mill: improving value of caving operations. *Caving 2018* (pp. 119-132). Vancouver, British Columbia: Australian Centre for Geomechanics.
- Nadolski, S., Klein, B., Elmo, D., Scoble, M., Liu, Y., & Scholar, J. (2016). Investigation into the Implementation of Sensor-based Ore Sorting Systems at a Block Caving Operation. *Seventh International Conference & Exhibition on Mass Mining* (pp. 393-399). Sydney, NSW: AusIMM.

# **Mineral process sampling and analysis using X-ray computed tomography – a feasibility test results on cassiterite ore**

Christopher Robben <sup>1\*</sup>, Pedro Condori<sup>2</sup>, Gerhard Zacher<sup>3</sup>,  
Andreas Staude<sup>4</sup>, Aysa Moslemiyekan<sup>1</sup>, Kim Esbensen<sup>5</sup>

<sup>1</sup>SIX-S Consulting, Wedel, Germany

<sup>2</sup>Minsur SA, San Borja, Lima, Peru

<sup>3</sup>Waygate Technologies, Wunstorf, Germany

<sup>4</sup>Thermo Fisher Scientific, Dreieich, Germany

<sup>5</sup>KHE Consulting, Copenhagen, Denmark

\* Corresponding Author: Hinter der Kirche 1A, 22880 Wedel, Germany,  
chris.robben@six-s.com

---

Keywords: X-ray tomography, assaying, particle size analysis, process sampling, Theory of Sampling, grade-frequency distribution

## **Abstract**

Process control decisions in mineral processing rely on real-time information about the composition of particulate material streams. While process control in the minerals industry is done with techniques that report the chemical composition of an aggregate sample, little information is known about the intrinsic heterogeneity. As all physical separation processes, including flotation, depend on the exploitation of heterogeneity, it is evident that appropriate sampling protocols must be combined with a laboratory technique that captures this relevant property, such as X-ray computed tomography (XCT).

With the recent developments in XCT equipment and software processing capabilities, an entry barrier would appear to be overcome. We here present results from a first technical and financial feasibility study conducted on a 117 g

cassiterite ore sample in the size range 1-4 mm. We focus on the information that can be derived for process monitoring and control, i.e. particle size distribution, grade frequency distribution and upgrade potential – while emphasising relevant demands for primary ore sampling validity.

## **1 Introduction**

About ten years ago, the author conducted a series of measurements on various X-ray tomographs from different suppliers on different base-, precious- and ferrous metal ores as well as industrial minerals.

It was evident, that X-ray computed tomography (XCT) already showed the following advantages over other available technologies, such as mineral liberation analysis with the scanning electron microscope:

- Fast and easy sample preparation
- Reduction of Total Sampling Error
- Safe to operate, no reagents are required
- Content as well as shape information can be derived
- Relatively short measurement times
- Non-invasive
- Non-destructive
- Ability to automate

The XCT technology therefore offers several advantages for sample characterisation in mineral processing and metallurgy. Waygate Technologies, Thermo Fisher Scientific and SIX-S have teamed up to demonstrate the capabilities and value add for different applications along the mineral process value chain. One application identified as being of high value is the combination of process sampling and XCT analyses.

What information, and what potential added value can be gained from optimizing the generic sampling/analysis process?

Primarily, the approach exemplified here will allow the assessment of the Total Analytical Error uncertainty (TAE) in relation to the observable Total Process Variability (TPV). This will further illustrate the potential economic value-added information available at more frequent intervals (essentially in real-time), potentially allowing plant process decisions to be made with less uncertainty. How can increased sampling resolution and increased in-sight in the mineral processing variations be used to optimise the control of the process?

Reliable quantitative information of real-time variability within a particulate process will enable analysis, understanding, and subsequently opportunities, to be better controlled, when matched with the TPV and the economic drivers of the operations. Equipment control and optimization must be data-driven and process-focused, using fit-for-purpose sampling procedures and equipment to optimise the mineral process value chain.

The quality of primary samples is crucial for reliable calibration of complex process analytical systems, XCT no exception. There is a universal demand for being able to conduct a fully representative primary ore sampling process; this has to be governed by the Theory of Sampling (TOS), Esbensen (2020).

## **2 Introduction of X-ray Computed Tomography**

X-ray computed tomography falls under the umbrella of non-destructive testing (NDT); and XCT is a method that examines the target sample by penetrating it with X-rays (wavelength 1 nm to 1 pm), measuring the levels of radiation that is scattered and absorbed, and collecting projection images during one full rotation of the sample. Computed tomography then provides a three-dimensional, spatial image of the object, or in this case, the bulk particulate sample, under inspection.

The CT-image shows different material attenuation effects which appear as different shades of grey. To generate a three-dimensional image, a high number of two-dimensional X-ray images (projections) are taken around a single axis of rotation (360 °). These X-ray images - containing different grey values according to material properties and thicknesses - are then reformatted as volumetric representations of structures (3D) using a complex reconstruction algorithm.

Mineral phase differentiation in the three dimensional is therefore possible based on differences in X-ray attenuation coefficients of the matter in each voxel in the



volume inspected. Differences of X-ray attenuation measured, which are usually displayed in grey scale, can therefore be related to the mineral phases present in each voxel respectively.

Applications of XCT in the geosciences have developed over three decades and correlate with steadily increasing computing power, allowing to render in-creasing large image data sets to volume models, with the main application for petrologic characterisation of drill cores to define permeability and pore volume (Kyle & Ketcham, 2015). Fractures can be analysed as well for different scales to study deformation processes (Kaufhold et al., 2016). Also, the scientific fundamentals of XCT of minerals are well developed, allowing determination of particle size, shape, and damage, as well as porosity and pore network structure of packed particle beds used to determine permeability, mineral composition, coal-washability, mineral liberation, and exposed grain surface area (Wang & Miller, 2020).

### **3 Aim of the Test Work**

The present test campaign is designed to assess the state-of-the-art of micro X-ray computed tomography with regards to its application in the context of characterisation of particulate assemblies in mineral processing. The aim of the work is to define the optimum equipment and measurement parameters, as well as sample preparation requirements as basis for developing standard procedures for assaying and sample characterisation in mineral processing.

#### **3.1 Sample Description**

For this study, a sample of cassiterite ore was selected. This ore is a suitable starting point as it represents two discrete mineral phases, a quartz dominated host rock with the ore mineral cassiterite. Cassiterite mineralisation occurs in high grade along quartz veins; the cassiterite size can be described as rather coarse (Mlynarczyk, Sherlock, & William-Jones, 2003). Since 2015, XRT-based particle ore sorting has been applied for coarse waste rejection which is based on 2-dimensional X-ray imaging of the ore, determining the presence or absence of Cassiterite as basis for physical separation (Robben, Condori, Pinto, Ronald, & Takala, 2020). It is therefore expected to be well suited for the present purpose, as different sized mineralisation can be expected at scales easy to be detected with XCT.

The sample was extracted from the primary screen feed to the sorting plant at San Rafael using stratified random extraction of 100 kg parallel increment belt cuts per day. Increments were alternately discharged into three plastic one cubic meter big-bags, thereby combining them to a composite sample of 3 t, sized 0-70 mm. Geometric lot transformation was not possible, so a 25 kg sub-sample had to be extracted from the top of the big-bags in a stratified-random manner, attempting to penetrate as deeply as possible into the bag. This is a violation of the Fundamental Sampling Principle (TOS), but is considered acceptable here because the objective of the present study is to determine the technical and financial feasibility of the XCT approach only, not yet implementing this for routine process monitoring and control. Multiple size fractions were then separated using laboratory wire mesh screens. This paper here describes the test program and results obtained on the 1-4 mm size fraction. A total of 7 kg in the size range 1-4 mm is then split five times with a 16-slot riffle splitter to 117 g of the sample is and filled into a cylindrical PE container with 50 mm outer diameter, as shown in Figure 1.



*Fig. 1: Cassiterite ore sample*

### **3.2 Test Equipment**

The tests are conducted with a Phoenix V|tome|x M from Waygate Technologies at their premises. The tomograph is a powerful industrial computer tomography (CT) system, designed for 3D metrology and analysis, provides industry-leading magnification up to 300 kV. It applies a so-called Scatter|correct technology, to automatically removing scatter artifacts for higher image quality. With a variety of proprietary CT technologies, the Phoenix V|tome|x M delivers faster scans and higher throughputs without compromising image quality, which is an important driver in reducing specific costs per scan in an industrial environment.



Fig. 2: XCT scanner used for measurement

The Phoenix V|tome|x M, as seen in Figure 2, comes standard with the so-called 4 MP Dynamic 41|200 next-generation industrial X-ray detector. It provides a 10 times increased sensitivity relative to the state-of-the-art 200  $\mu\text{m}$  pixel-size DXR detectors producing a 2-3 times cycle time increase without image quality impact, making inspections and measurements more efficient and productive.

### 3.3 Test Procedure

The test procedure is two-staged, starting with the measurement within the instrument itself, followed by image pre-processing and construction of the volume model. The second stage includes processing of the image volume model.

### 3.4 Measurement

The sample container is loaded into the tomograph and mounted on the sample manipulator between the X-ray source and the detector. The manipulator is articulated with three translatory and one rotational degrees of freedom. The three translatory movements allow the sample to be placed in the position that delivers the desired projection on the detector. The sample rotates stepwise around the

vertical axis. At each step, a single or multiple images are recorded. Table 1 shows the main parameters of the measurement.

Tab. 1: XCT scan parameters

Parameter	Value
Tube	xs 300 d
Tube voltage	270 kV
Current	80 $\mu$ A
Filter	0.5 Cu + 0.5 Sn
Recording time	18 min
Voxel resolution	25.32 $\mu$ m

The final result of a measurement is a reconstructed and pre-processed volume model with grey-scale classification. The volume model has the dimensions: 46 mm cylinder diameter, 38 mm cylinder height. Figure 2 shows three cross-sections along the centre x, y and z planes of the volume model. High density voxels are displayed in brighter shades relative to low(er) density voxels. The fourth image shows a three-dimensional representation of the pre-processed density model, in which low-density voxels representing air, as well as sample holder voxels have been repressed (hidden).

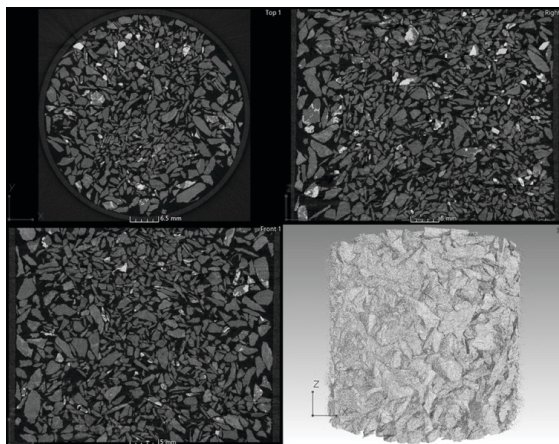


Fig. 3: Four views of the pre-processed density model; Sample plug dimensions are: diameter 36 mm and height 46 mm respectively

### 3.5 Volume Image Processing

The volume model is then further processed applying Thermo Scientific's Avizo software, which allows analysis and visualization of the volume imaging data. The following images describe the software process flow as applied to the volume model.

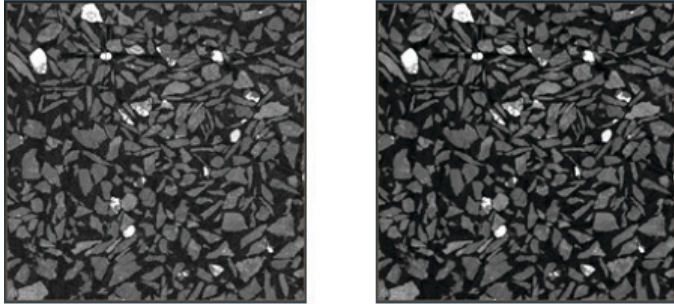


Fig. 4: Pre-processed volume file as input (a) and filtering applied (b)



Fig. 5: Particle segmentation (a) and particle separation and rejection of particle touching the border (b)

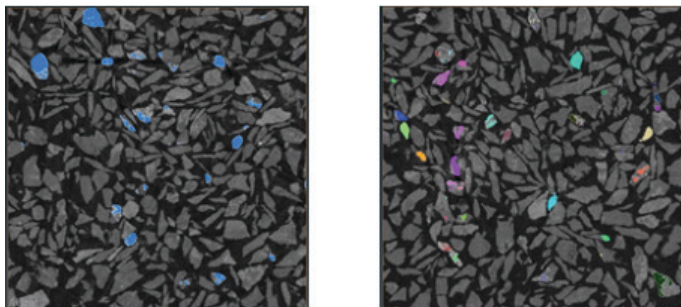


Fig. 6: Cassiterite particle segmentation (a) and separation of Cassiterite particles (b)

The information on segmented grains and cassiterite – particles can be combined to calculate the cassiterite content in each particle.

## 4 Results and Discussion

A total of 7,222 particles are segmented from the volume model. 2,275 are in contact with the outer borders and are excluded from further analysis. Therefore, a data set containing 4,947 particles is further analysed and the results are presented in the following paragraphs.

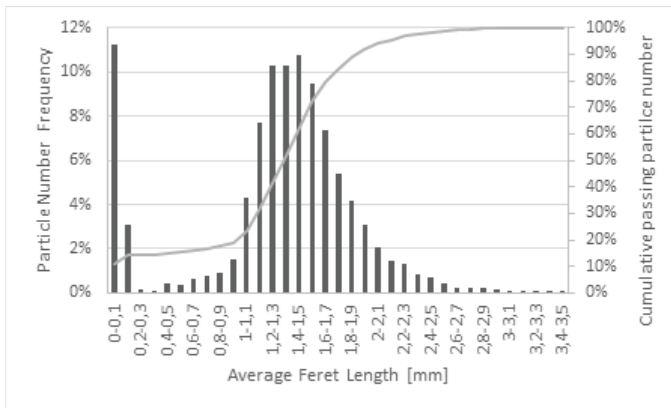


Fig. 7: Particle Number Frequency Distribution

A first assessment is done based on the frequency distribution of the particles in different particle size ranges. The industry standard is still sieve analysis, measuring the shape with the probability, that a particle will pass a certain square mesh opening. To relate particle volume properties to the probability of passing a square mesh opening, it was decided to apply the calculated average between the measured maximum and minimum Feret diameter per particle as a measure of particle size. The following figure shows the frequency distribution of the particles in bins of 0.1 mm intervals.

Understandably, the number of particles per size fraction distorts the potential information, as it is disproportional to the weight. Therefore, the weight per particle is calculated, applying i) a matrix density of 2.8 g/cm<sup>3</sup> and ii) Cassiterite density

of 6.98 g/cm<sup>3</sup> to the volume proportions of each particle. These results are shown in Figure 11. The particle sizing derived from the calculated average Feret length corresponds well with the sieve size applied for preparation of the sample (1-4 mm square mesh). The  $d_3$  value derived from the volume image analysis is 1 mm,  $d_{50}$  is 1.7 mm and  $d_{97}$  is 2.9 mm average ferret length respectively.

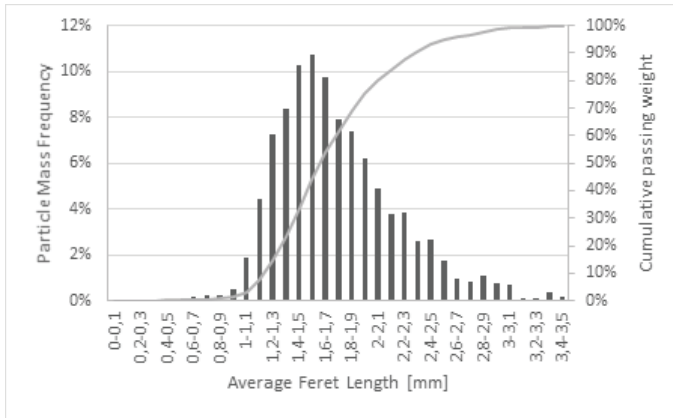


Fig. 8: Particle size distribution

The average Sn grade of the sample is 6.06%. Further analysis is done on the grade distribution per size fraction. The grade distribution per size fraction, displayed in Figure 12, shows a relatively steady grade between 3% and 10% Sn up to 3 mm size. Above this particle size, it increases to 50% Sn.

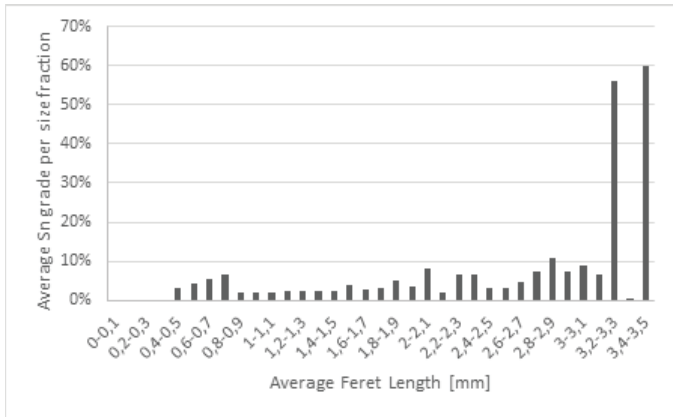


Fig. 9: Tin grade distribution per size fraction

This is to be explained by the nugget effect. In the two size intervals in question, only one particle each is found with a high grade. This *may* mean that competent Cassiterite minerals are accumulating in this size fraction but could also be introduced by a sampling error. This result underlines the need for impeccable primary sampling in order that all samples used for calibration are defensible as representing the mineralisation in its full features; the mineral top-size is a well-known victim of non-representativity.

A further analysis reveals the liberation characteristics of the sample. It is done by applying the grade versus mass frequency distribution of the particles, which can be seen in Figure 13. About 85% of the particles do not contain any Cassiterite. For this reason, the y-axis is displayed with logarithmic scale.



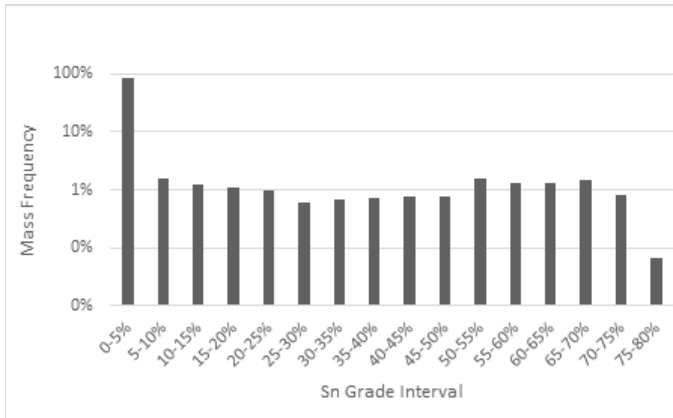


Fig. 10: Grade frequency distribution

A resulting Mayer-I diagram displaying the yield-recovery- and grade-recovery functions is shown in the next figure. Figure 14 shows the maximum possible separation efficiency fully exploiting the heterogeneity of the sample. For example, when product specification is 60% Sn, the maximum possible yield is 7% with a waste grade of 2% Sn and a recovery of 73% respectively.

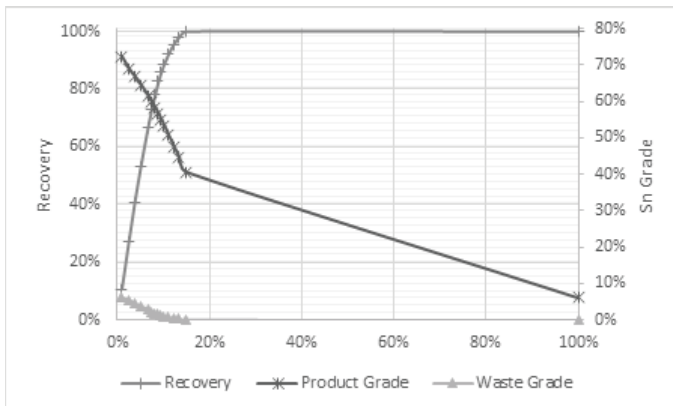


Fig. 11: Mayer-I grade recovery function

## 5 Discussion

It appears that the screen mesh size used for sample preparation corresponds well with the average Feret length, considering a brittle ore phase with a right-skewed normal distribution. Due to geometrical calibration of the equipment, high image quality and discrete particle boundaries, it is expected that the actual particle shape corresponds accurately with the reported volumes by the software. It *may* be necessary to further calibrate the analysis to the standard of square mesh sieve analysis for specific ores, which may show *specific* shapes and mass distributions. Efforts necessary for this are estimated to be low to moderate.

It needs to be further assessed, if the accumulation of grade is due to insufficient sample size and a nugget effect - or if it indeed correlates well to ore mineral crystallisation grain size. These are issues related to the validity of the primary ore sampling, issues which are governed by the Theory of Sampling (TOS), Esbensen (2020). One may take advantage of such sampling effects in process technology design when better understood.

## 6 Conclusion and Outlook

It has been demonstrated that state-of-the-art XCT equipment can deliver a volume model with the quality needed for measuring particulate systems in dimensions necessary to render relevant sample information at sufficient voxel resolution for minerals processing and acceptable speed. Costs per scan are relatively low, considering the low measurement time, the degree of automation possible and the significant reduction of manual sample preparation. Contrary to surface-based analytical methods, e.g. electron scanning microscope or microscope spectroscopy, the volume-based measurement of XCT captures a significantly larger sample volume. With the option to scan relatively high sample volumes, XCT contributes significantly to minimising the Total Sampling Error (TSE).

It was demonstrated that state-of-the-art volume image processing software is available to extract the information necessary for relevant economic management decisions for the ore mineral processing pathway, such total tin grade, particle size distribution and grade frequency distribution.

XCT volume imaging and image processing allow a detailed analysis of particulate systems, which are the basis of mineral raw materials processing systems. In

addition to averages of components delivered by laboratory chemical analyses (e.g. X-ray fluorescence, ICP-OES), it can deliver statistically relevant information on density class ratios per particle, shape information, contact surfaces and more.

Further work must be done on matching samples size requirements to the specific heterogeneity of the ore in question, but this is a standard demand from TOS, which also delivers all necessary means for execution, (Esbensen 2020). Even though 4,947 particles are reported in the data set, there are not enough particles in each size interval for countering the Fundamental Sampling Error (FSE) across all scales. Future developments will likely include multiple XCT measurements to be combined (scan acquisition composite sampling) to achieve statistically more substantiated data sets. Considering the moderate unit costs per measurement with an automated system, this is an economically feasible option that could find wide application.

It will be beneficial to conduct further work on ore-specific calibration for developing more automated laboratory procedures; there is a vast industrial calibration scope in front of the successful XCT technology, but everything needed is now available in the sufficient-and-necessary toolkit as presented here.

## References

- Hubbell, J. H., & Seltzer, S. E. (2019, Dec 11). X-Ray Mass Attenuation Coefficients. Retrieved from US National Institute of Standards and Technology: <https://www.nist.gov/pml/x-ray-mass-attenuation-coefficients>
- Kyle, R., & Ketcham, R. (March 2015). Application of high resolution X-ray computed tomography to mineral deposit origin, evaluation, and processing. *Ore Geology Reviews*.
- Mlynarczyk, M., Sherlock, R., & William-Jones, A. (18. January 2003). San Rafael, Peru: geology and structure of the worlds richest tin lode. *Mineralium Deposita*, 38.
- Kaufhold, A., Halisch, M., Zacher, G., and Kaufhold, S.: X-ray computed tomography investigation of structures in Opalinus Clay from large-scale to small-scale after mechanical testing, *Solid Earth*, 7, 1171-1183, doi:10.5194/se-7-1171-2016, 2016.

Okrusch, M., & Matthes, S. (2005). *Mineralogie*. Würzburg: Springer.

Robben, C., Condori, P., Pinto, A., Ronald, M., & Takala, A. (1. January 2020). X-ray-transmission based ore sorting at the San Rafael tin mine. *Minerals Engineering*, 145.

Wang, & Miller, J. D. (11. October 2020). Current developments and applications in micro-CT for the 3D analysis of multiphase mineral systems in geometallurgy. *Earth-Science Reviews*.

Esbensen, K.H. (2020) *Introduction to the theory and practice of sampling* ISBN: 978-1-906715-29-8, DOI: 10.1255/978-1-906715-29-8



# **New Protocols for Pre-Concentration Sampling and Testing**

Bob McCarthy<sup>1\*</sup>, Adrian Dance<sup>2</sup>

<sup>1</sup>SRK Consulting (Canada), Vancouver, Canada

<sup>2</sup>SRK Consulting (Canada), Vancouver, Canada

\* Corresponding Author: [bmccarthy@srk.com](mailto:bmccarthy@srk.com)

---

Keywords: heterogeneity, particle sorting, sampling, representative

## **Abstract**

Common challenges for metallurgical testing are to gather samples representative of the orebody and to conduct testing in a cost-effective manner; this is especially true for pre-concentration evaluations. The authors have developed processes that answer these challenges, including new lab protocols that can be applied across a range of projects, particularly those considering particle-based ore sorting.

Heterogeneity is assessed from exploration drill hole data to determine waste and ore distributions in both ore and marginal waste zones. Drill core intervals are targeted for sampling as being representative of these distributions, as well as ore types. These samples are commonly 50 kg of half core – similar to current comminution test requirements as part of a metallurgical testwork program.

Samples are sent to an independent laboratory for assay by size testing as well as sample preparation for mineral sensing testing. Presently, mineral sensor testing samples are sent to specialty research centres or particle sorting equipment suppliers. The new protocol adopts a more cost-effective approach than the current rock by rock, sensor testing which incurs considerable assay costs.

The paper will describe the heterogeneity techniques, sample selection process, and new protocol for pre-concentration testing. Real projects will be presented that have followed these processes.

## **1 Introduction**

Critical to the evaluation of any mining project is having a good understanding of the relevant metallurgical processes and how different materials respond to these processes. This includes being able to estimate metal recovery and mass pull (i.e. concentrate grade) of milled material at any point in the ore deposit or mine plan. Pre-concentration is no different, but unlike established metallurgical processes, there is little consensus or standards on how to conduct testing for pre-concentration.

For the purposes of this paper, pre-concentration is defined as “methods to reject waste from mill feed when still coarse, dry and transportable”. This typically means any combination of screening, bulk sorting and particle sorting (McCarthy & Dance, 2021). Screening, required in any case in advance of particle sorting, can segregate material based on the deportment of mineralization to different size fractions (Burn & Grimes, 1986; Dupont, 2016). Bulk sorting can be accomplished with mineral sensing and diversion of conveyed materials or bucket/truck sensing and sorting (Henning, 2018). Particle sorting, applied to material 12 mm to 250 mm in size, accomplishes separation with targeted air bursts applied to either accepted or rejected particles.

To date, most sampling and testing for pre-concentration has focused on particle sorting as the expected process. Either large samples of hundreds of individual rocks (or core pieces) are taken for bench scale mineral sensor testing and assaying or several hundred-kilogram bulk samples are taken for pilot testing (Robben et al, 2017; Assis et al, 2021). Both are challenged to ensure that the sampling is representative of what sorting systems may see at any point in the life-of-mine (LOM) plan; and both can be expensive.

The authors have developed processes that answer these challenges, including new lab protocols that can be applied across a range of projects, particularly those considering particle-based ore sorting. The objective in developing these processes

was to address not only representativeness, but also the costly nature of early testing.

This paper describes new analytical and testing processes and describes two case studies where elements of these processes were deployed.

## **2 Heterogeneity Analyses**

### **2.1 Heterogeneity and Scale**

The authors have developed two heterogeneity analyses. The first is referred to as “Heterogeneity and Scale”, which assesses how heterogeneity varies with scale, particularly mining scale. It is effective in assessing the bench height in open pit mining but also projects how pre-concentration can be effective at different scales.

Fig. 1 shows the results of a Heterogeneity and Scale analysis for the project referred later in the case studies as “Company B”. The analysis is based on drill hole data whereby, for each sample interval, adjacent samples in the same drill hole are aggregated over increasing distance from that sample. Statistical measures can then be run against these aggregations; two of which are shown in Fig. 1



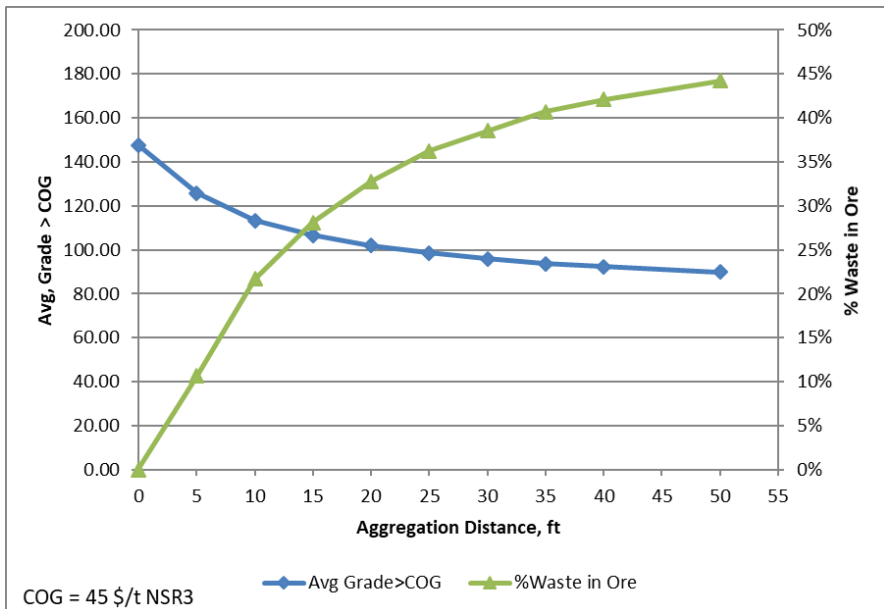


Fig. 1: Company B Sample Heterogeneity and Scale

The blue line in Fig. 4 is the average grade (in this case, net smelter return or NSR) of material above the cut-off grade (COG), which is \$45/ton here. It shows that the average grade of aggregations decreases as the aggregation distance (mining scale) increases. The decrease is more pronounced at shorter aggregations, eventually levelling off. Similarly, with the other measure, “waste in ore” (W/O), which is the portion of below-COG material in an aggregation that is above-COG, the rate of increase in W/O at shorter aggregations is quite high, tailing off at longer aggregations. Both these suggest that the smaller the mining or sampling scale, the greater the heterogeneity and potential to exclude waste.

## 2.2 Composite-Sample Relationship

The other heterogeneity analysis, called “Composite-Sample Relationship”, uses grade or NSR for each of the sample intervals in the drill hole dataset as well as those calculated for bench (or underground sub-level) composites. The sample interval grades are then compared to the composite grades. Fig. 2 shows the Composite-Sample Relationship for select 20-ft composites, again for case study, Company B, described later in the paper.

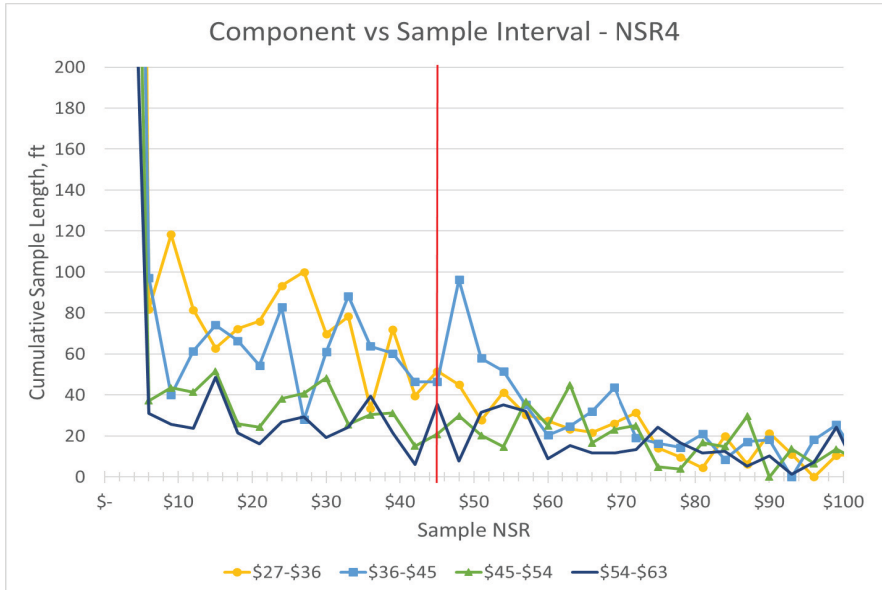


Fig. 2: Company B Composite-Sample Relationship

In Fig. 2, four composite ranges are shown, two above the NSR COG and two below the COG. The composite ranges are each \$9/t in size. The chart shows the cumulative length of samples (y-axis) against the grade or NSR values of those samples (x-axis). The red vertical line is drawn at the COG.

The dataset is limited in these grade ranges and thus the erratic nature of the plots. However, two phenomena can be seen. For composites above the NSR COG, which represent “ore” (the \$45-\$54 and \$54-\$63 lines), there are sample intervals left of the COG line. These samples represent “waste in ore” (W/O). Similarly, for composites below the COG, which represent waste (the \$27-\$36 and \$36-\$45

lines), there are sample intervals right of the COG. These samples represent “ore in waste” (O/W). By quantifying these heterogeneity measures, W/O and O/W, one can make predictions of preconcentration.

### **2.3 Heterogeneity Visualization**

The heterogeneity described here can be visualized by plotting parameters such as W/O and O/W against drill holes in 3D. This gives the most direct visualization of spatial relationships of these parameters.

Fig. 3 shows three drill holes for a gold property. The top image shows the sample intervals with their varying grades colour coded. Purple, red and orange are above-COG intervals ( $\geq 0.25$  ppm Au), while other interval colours are below-COG (0-0.25 ppm Au). The middle image shows composites that are below-COG, and these are colour coded by O/W percentages. The bottom image has composites that are above-COG, coloured by W/O percentage.

While all the holes in the image have either waste or ore composite intervals, the far-right hole is of particular interest. In close proximity, there are long contiguous intervals of both ore (above) and waste (below), with elevated W/O and O/W respectively. These can be targeted for sampling and further testing.

3D visualizations such as this, as well as elevation plans of bench composites, can be used to identify holes of interest for sampling. Ore types and areas of the deposit representative of the LOM plan can be targeted.

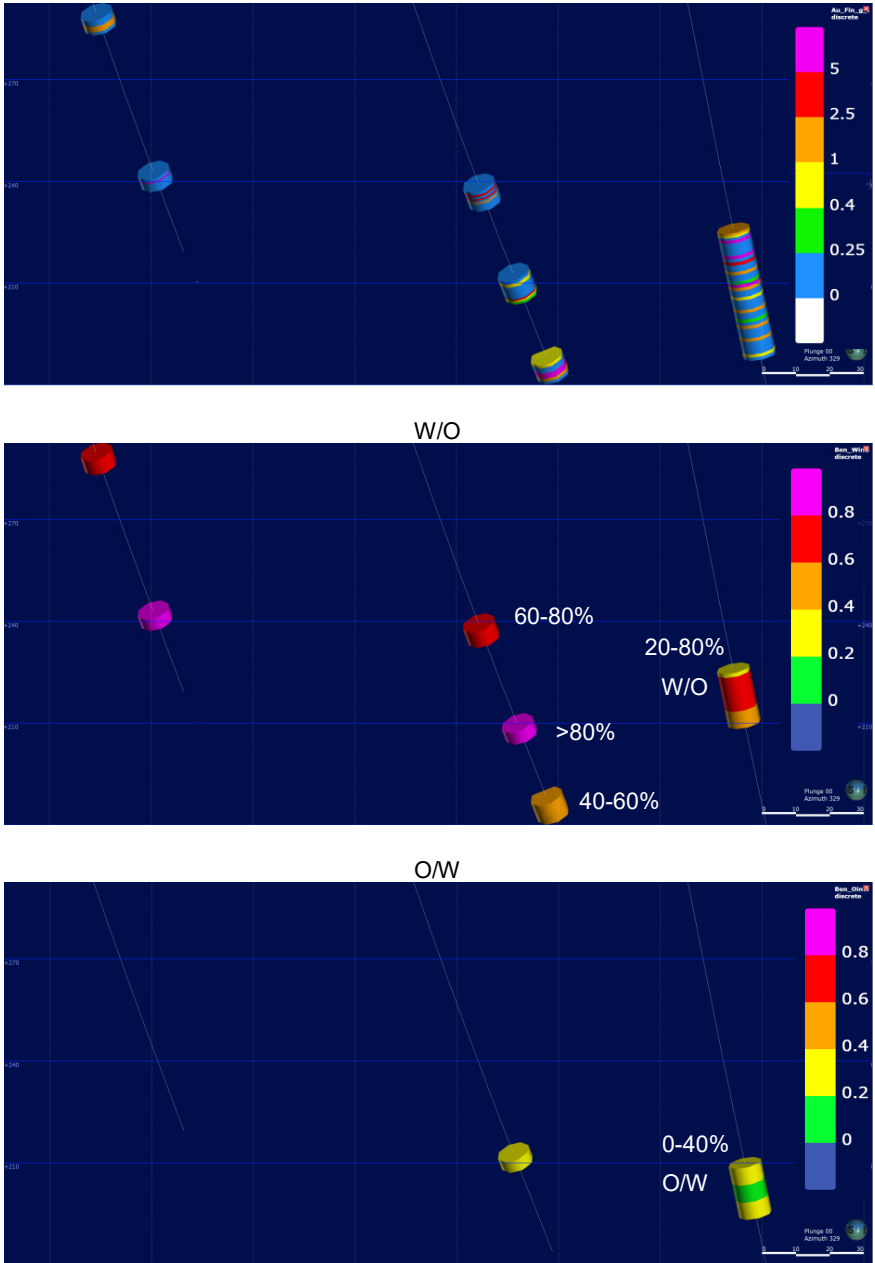


Fig. 3: Drillhole visualization

## **3 Sample Selection**

### **3.1 Bulk Sampling**

Four types of sampling are defined in this report: bulk sampling, composite sampling, contiguous interval sampling, and rock-by-rock sampling.

Bulk sampling, in a preconcentration context, is generally done for performance testing of sorting technology whether this is particle sorting or bulk sorting. It involves gathering hundreds of kilograms of material from excavations (surface, underground) or from one or more drillholes. The former is a good test of what a sorting technology might see at a moment in time, while the latter (drill holes) is mostly a procedure to get a large enough sample for testing. Neither bulk sampling method results in testing outcomes that are fully representative of what can be expected throughout a LOM plan.

### **3.2 Composite Sampling**

Composite sampling is when drill core is sampled in a length long enough to provide a sample of sufficient mass for testing. Specifically, the SRK Protocol introduced in this paper requires about 50 kg of sample. These samples can be of variable composition, including above- and below-COG sample intervals, though generally ore zones are targeted.

Composite samples can be used to perform variability testing. Samples can be targeted for differing ore types or regions of the deposit that are representative of the LOM plan.

### **3.3 Contiguous Interval Sampling**

Contiguous interval sampling is a subset of composite sampling. After observing in heterogeneity studies that ore zones can contain extended lengths of below-COG material, the authors developed a sampling procedure that targets both above-COG and below-COG material independently in the same ore or marginal material zones. In testing these samples independently, it is believed that this better represents the variation in feed that might be encountered by sorting technologies.

Contiguous samples of above and below-COG core are taken in sufficient lengths to make up 50 kg samples. Samples are gathered within a single bench composite where possible, but, if necessary, adjacent bench composites are included.

Per composite sampling, smaller samples taken in this way (as opposed to bulk samples) allow cost effective variability testing that best represents different ore types and time frames of the LOM plan.

### **3.4 Rock-by-Rock Sampling**

This form of sampling has been common for bench scale testing for particle sorting. It relies on taking 200 to 400 grab samples that are then subject to bench scale mineral sensing testing. The testing responses can be used to project the performance of particle sorting.

However, the challenge with this form of sampling and testing is ensuring that samples are representative. The authors contend that the nature of such grab sampling makes it quite difficult to ensure representativeness.

So, in the end, the authors have used and will continue to use composite sampling or contiguous interval sampling in assessing projects for pre-concentration.

## **4 SRK Laboratory Procedure**

The protocol used for pre-concentration assessment, shown schematically in Fig. 4, was originally developed to estimate metal upgrading following crushing and screening. The sample mass and size was established to also meet current comminution (size reduction) testing requirements – namely, 30 kg to 50 kg of half drill core. This is typically the only source of samples available during the early study phases of a mineral project.

### 4.1 Assay By Size

Metal deportment estimates are done by comparing the size fractions grades (assayed for both metals of interest as well as waste elements) after lab crushing as well as comminution testing. The comminution test subjects narrow size fractions (typically 32 x 27 mm) to a range of specific energy (in kWh/t). These energies reflect those occurring during blasting and first/ second-stage crushing – processes needed to prepare material for particle sorting.

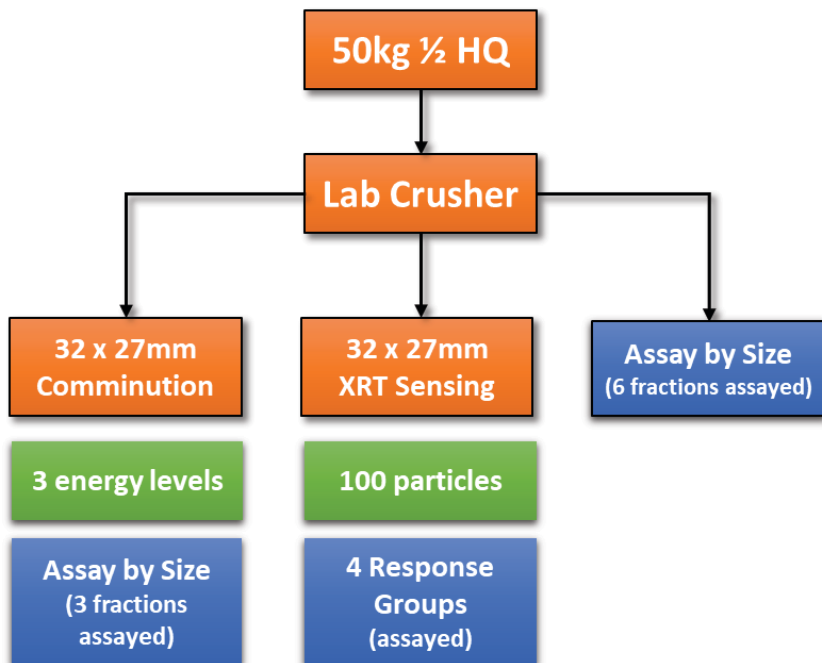


Fig. 4: SRK Protocol sample processing flowsheet (simplified)

Measuring material response to these specific energies allows the actual grade-by-size distribution following primary and secondary crushing to be estimated. In the authors’ opinion, this overcomes a significant deficiency in current particle sorting studies – the ability to estimate the amount of fines bypassing particle sorting (typically, all crushed material finer than 10 mm or 15 mm).

## **4.2 Mineral Sensing Testing**

In addition to measuring metal deportment following crushing, the test also provides a sub-sample for mineral sensing. A representative set of specimens (typically 100 particles) are submitted to either equipment suppliers and/or independent research centres which have an assortment of mineral sensing equipment. The particle responses to sensors are ranked and grouped into typically four categories. Only these groups are assayed to measure the metal recovery versus mass pull relationship. In other words, the mineral sensor(s) estimates grade and the assays confirm if the metal of interest deports accordingly. This saves a considerable amount of time and money processing each sample. As SRK's Protocol uses much smaller sample masses and can be done quickly and cheaply, a much larger number of samples can be tested – allowing orebody variability to be determined.

SRK's Protocol is to assess half drill core samples of both waste and ore, specifically, intervals of above and below COG material. As the sample mass is relatively small, only a few metres or half core is required, making assessments possible on different lithologies, spatial locations and structural intercepts.

## **5 Laboratory Data Interpretation**

### **5.1 Particle Size Distribution Prediction**

An example output of the grade-by-size information gathered from the comminution test results is shown in Fig. 5 for a copper porphyry sample. Note that both the mass and metal deportment can be estimated following primary crushing, screening at 100 mm and 50 mm as well as secondary crushing. For example, the -50 mm fraction after primary crushing is 63% of the mass at 0.30% copper. The +100 mm fraction is 17% of the mass at 0.19% copper – a measure of the metal deportment between these sizes.



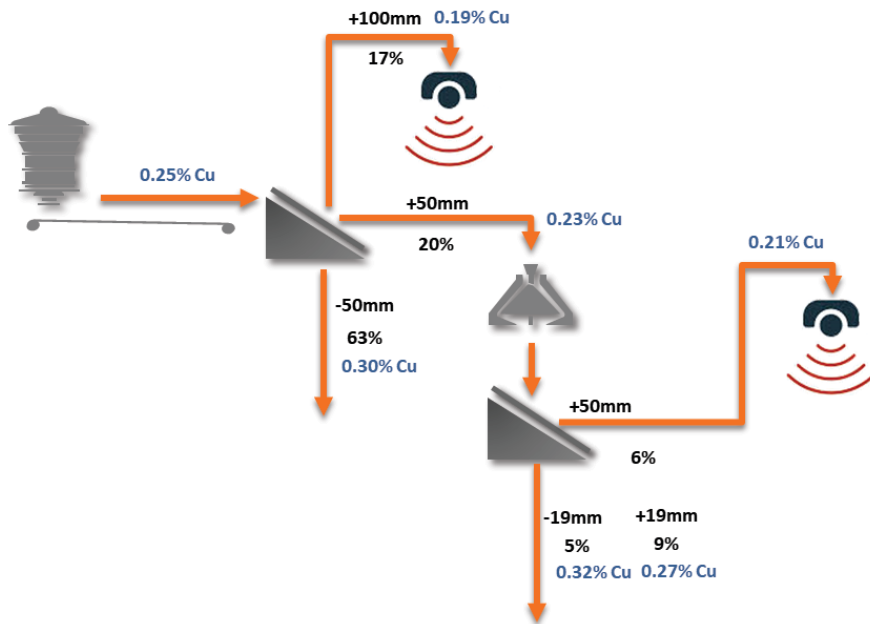


Fig. 5: Example flowsheet showing size and grade department (SRK test output)

## 5.2 Mass Pull and Metal Recovery

Using the SRK Protocol, specimens are grouped according to their mineral sensor responses. At least four response groups are suggested per test, and these typically can be referred to as “High”, “Medium”, “Low”, and “Waste”. The specimens in these groups are weighed and then combined and prepared as group samples for assaying. So instead of dozens of specimen assays, only four assays per sample are needed.

Using ranking of sample groups by sensor responses, cumulative distributions of mass pull and metal recovery are developed for the samples. The resulting metal recovery – mass pull curve represents a range of outcomes for particle sorting. Since the SRK Protocol tests above-COG (ore) and below-COG material (waste) separately, this results in two sets of curves.

The case study for Company A produced the recovery curves shown in Fig. 6 for gold and silver. Eight ore samples and ten waste samples of four to five response groups each are plotted on the respective charts.

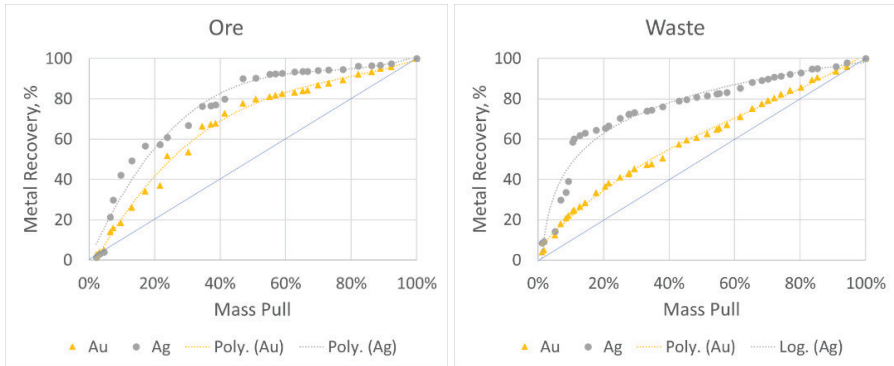


Fig. 6: Metal Recovery versus Mass Pull (samples above COG and below COG)

### 5.3 Pre-Concentration Predictions

The W/O and O/W heterogeneity measures can lead to pre-concentration predictions. W/O can be representative of waste rejection in above-COG feed, while O/W can predict above-COG material recovery in marginal feed. However, owing to the source data scale (one to three metres), such predictions would be more indicative of bulk sorting outcomes – not particle sorting. Nonetheless, the authors suggest that variations in composition at the drill core sample interval scale are indicative of variations in particle sorter feed.

Consequently, the authors have developed methods to integrate the W/O and O/W measures with the metal recovery and mass pull relationships from lab testing. In a mine plan, W/O can be used to estimate the portion of below-COG material in ore sort feed, and with this, the recovery modelled from testing ore samples would apply. O/W estimates the above-COG portion of marginal material, and recoveries from testing waste would apply.

If mineral sensor testing has resulted in optimization of sensor settings and algorithms, the resulting deterministic mass pull and metal recovery predictions can be applied directly to the W/O and O/W portions in the mine plan. However, if

testing generates more stochastic recovery curves, such as for the SRK Protocol, an alternate approach is required.

The suggested approach is to consider multiple scenarios across several mass pulls. Metal recoveries are determined for a minimum of three selected mass pulls per ore and marginal material. These then are applied to the mine plan in an economic analysis for evaluation. By studying the range of results, one can determine which mass pulls for ore and marginal material work best. These can be related back to appropriate sorter settings.

## 6 Case Studies

### 6.1 Company A

The authors were asked by Company A to conduct a pre-concentration evaluation on its gold property in North America. Original drill hole assays and half core were available for investigation.

Unlike the methodology outlined in this paper, the heterogeneity study and lab testing were not conducted sequentially; the lab testwork was done in advance of the heterogeneity study. Nonetheless, these two activities were conducted in accordance with the processes described herein, and it was possible to integrate the work to drive some conclusions for the project.

Heterogeneity analyses were conducted on the deposit resulting in the Composite-Sample Relationship plots for ore and waste in Fig. 7. The analysis was constrained to data within the reserve pit of the time.

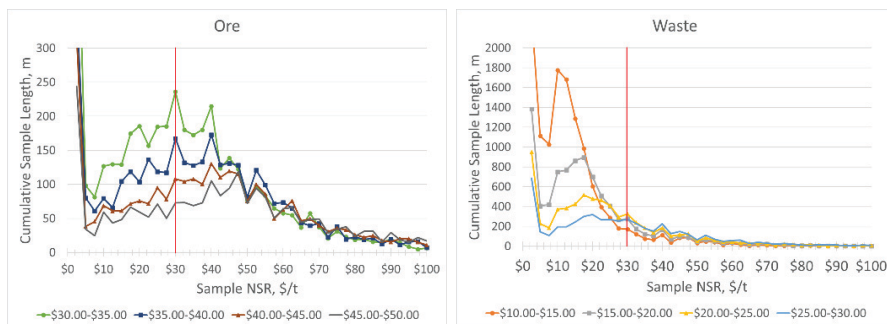


Fig. 7: Company A Composite-Sample Relationships

The underlying data to Fig. 7 provides the following heterogeneity results:

- Using an upper limit of \$60/t for ore to be sorted, the W/O was 36%.
- Using a lower limit of \$20/t for marginal material, only 4% additional material (beyond the above-COG ore) was available, with O/W of 15%.

The above suggests that the opportunity for sorting marginal material may be limited and that the real opportunity might be in rejecting waste from the ore feed. For further analyses, these W/O and O/W values were applied to the LOM plan to derive quantities that were subject to the recovery curves generated from sensor testing at both Tomra and Steinert (refer back to Fig. 6).

Subsequently, economic analyses were run at different mass pulls. The analyses showed that at no mass pull was it worth sorting the above-COG ore. This is understood by looking at the ore recovery curve in Fig. 6. The authors find that for precious metals projects, metal recovery needs to stay in the high 90%+ range; otherwise, metal losses negate any benefits of waste rejection. Here, achieving this level of metal recovery required pulling almost the entire sorter feed into accepted product. And while there was some additional revenue provided by processing marginal material, it did not sufficiently cover additional costs to make this option truly attractive.

## **6.2 Company B**

Company B holds a copper-nickel-platinum group metal (gold, platinum, palladium) project in North America. The authors were engaged to evaluate the pre-concentration potential for a restart of this historic mine.

Extensive exploration drill hole data was available for heterogeneity analysis, as was drill core from recently drilled holes for core testing.

The two heterogeneity analyses (Heterogeneity and Scale and Composite-Sample Relationship) were conducted on the drill core data (refer back to *Fig. 1* and *Fig. 2*). The analyses showed potential to reject waste, with the Homogeneity and Scale analysis showing W/O of over 30% at mining scales of 20 ft. As well, the underlying data for the Composite-Sample Relationship in *Fig. 2* result in the heterogeneity analysis outcomes in *Tab. 1*.

Tab. 1: Heterogeneity parameters for pre-concentration evaluation

Parameter	Ore Material	Marginal Material
Target Ore Sort	>\$45/ton, no upper limit	N/A
% Waste in Ore (W/O)	49.3%	N/A
Target Marginal Sort	N/A	\$36/ton < Sort < \$45/ton
Additional Marginal Material	N/A	8.7%
% Ore in Waste (O/W)	N/A	34.6%
Sorter Feed Grades		
Cu	0.34%	0.18%
Ni	0.24%	0.11%
Au	0.90 ppm	0.23 ppm
Pt	2.79 ppm	0.79 ppm
Pd	1.57 ppm	0.37 ppm
% Reporting to Waste		
Cu	13.9%	41.4%
Ni	9.9%	27.4%
Au	6.1%	27.2%
Pt	5.4%	17.3%
Pd	5.5%	22.0%

Based on the distribution of W/O and O/W values among all drill hole composites, two drillholes were selected for sampling and testing. Six lengths of contiguous sample intervals were selected for testing. Two were considered “ore” (>COG), while four were “waste” (<COG). The half drill core samples were sent to a commercial laboratory for preparation. After light crushing, specimens were randomly selected: 20 from each of the ore samples and 30 from each of the waste samples. These specimens were mounted and sent to Steinert for mineral sensing testing. Following sensor testing, the samples were returned for assaying. In this case, the individual specimens were assayed as opposed to the suggested methodology to assay whole groups defined by sensor response.

Steinert conducted tests with various sensors arriving at an optimized combination of XRT, laser and induction sensors. This resulted in accept or reject simulations for each specimen. Aggregating these results across all specimens provides the

mass pull portion of the recovery curve, while the specimen assays helped build the metal recoveries.

The results are presented in Tab. 2. They indicate that upwards of 70% of contained metal in marginal material can be recovered in 34% of the feed (66% waste rejection). And for ore feed, upwards of 97% of the metal is recovered in 70% of the sort feed (30% waste rejection).

*Tab. 2: Mass pull and metal recoveries derived from Steinert test results*

	<b>Waste Material</b>	<b>Ore Material</b>
Product Mass Pull	34.2%	70.0%
Metal Recoveries		
Cu	74.2%	98.2%
Ni	63.6%	97.1%
Au	81.1%	97.5%
Pt	87.1%	96.6%
Pd	81.7%	98.7%

The authors integrated the results in Tab. 1 and Tab. 2 and fed these into mine plans for the project. As well, there was a grade recovery relationship, which meant with the sorter-upgraded feed, higher mill recoveries resulted.

In applying the W/O to the ore fraction ( $\geq \$45/\text{ton}$  NSR) and the O/W to the marginal fraction ( $\$36/\text{ton} < \text{NSR} < \$45/\text{ton}$ ), an overall 49% waste rejection was estimated. And with the recovery-mass pull projections, metal recoveries were estimated at 98% Cu, 94% Ni, 92% Au, 93% Pt, and 97% Pd. With these inputs, the economic evaluation of implementing particle sorting showed a positive outcome.

## 7 Conclusions

Up until now, there have been different procedures developed to sample and test materials for pre-concentration investigations. For particle sorting, these have largely involved gathering grab samples for bench scale testing or much larger, several hundred-kilogram samples for performance testing of sorting machines. There are two challenges in such approaches: (1) cost effectiveness and (2) ensuring sampling and study outcomes are representative of LOM plans. The authors have

developed and presented herein a methodology that combines heterogeneity analyses with bench scale testing of drill core to answer these challenges.

Heterogeneity analysis assesses the potential for segregating ore zones and marginal zones into their above- and below-COG constituents. It is applied to drill hole datasets and thus is flexible enough to evaluate ore types and regions that are representative of a project's LOM plan. The analysis can also aid in the selection of samples for pre-concentration testing, targeting for instance, contiguous intervals of above- and below-COG drill core within ore types.

For lab testing, the authors have developed the SRK Protocol, which can be readily included in a metallurgical test program as the sample requirements follow that for comminution (hardness) testing – namely, 30 kg to 50 kg of half drill core. The Protocol can generate estimates of metal department by size, following multiple stages of crushing. This includes the amount of fines that bypass particle sorting – an important factor in assessing coarse pre-concentration.

By providing a consistent method for assessing both size upgrading and mineral sensing of coarse particles, the SRK Protocol can be adopted by the mineral industry as an early-stage assessment tool. Once mining projects have confirmed their material is suitable for pre-concentration, current 'performance testing' methods used by sorter suppliers should also be conducted on larger sample masses.

An end objective of heterogeneity analyses and the SRK Protocol is to be able to integrate their outcomes in economic evaluations. This is possible by assessing potential sorter feed as a combination of above- and below-COG materials, each with their own recovery, mass-pull relationships.

Case studies have been presented that adopted elements of the methodologies described herein. They have jointly demonstrated the efficacy of the approaches, allowing mining companies to assess at an early stage, and without significant expense, whether their projects have pre-concentration potential.

Investigations are being proposed which adopt the full methodology described herein, giving proponents the full benefit of a comprehensive, representative and cost-effective approach to pre-concentration evaluations. The focus of the paper has been around particle sorting; however, the methods can be extended for the other pre-concentration strategies of screening and bulk sorting.

## **References**

- Assis V.M., Henriques, A.B., Lemos, M.G., Dumont, J.A. (2021, Jan-Mar). Technological Innovation in Córrego do Sítio Mineração – A Study of Technical and Economic Aspects By Using Sensor-Based Sorting For Refractory Gold Ore, REM International Engineering Journal, Ouro Preto, 74(1), pp 117-125.
- Burns R., Grimes A. (1986, June). The Application of Pre-Concentration by Screening at B.C.L, Papua New Guinea Mineral Development Symposium.
- Dupont J.F., (2016, January). Beneficiation of Low Grade Ore at the Detour Lake Mine. 48th Canadian Mineral Processors Conference, Ottawa ONT, Canada.
- Henning M.G., (2018, October). Grade Control and Segregation at New Gold's New Afton Block Cave Operation, Kamloops, British Columbia. Caving 2018, Vancouver BC, Canada.
- McCarthy R.J., Dance A.D. (2021, October). Integration Opportunities for Particle Sorting and Bulk Sorting [Conference presentation]. TOMRA Sensor-Based Sorting Seminar, Toronto ON, Canada.
- Robben C., Girard, D., Cline, H., Takala, A. (2017, August). X-ray Transmission Sorting at the Kensington Gold Mine. Conference of Metallurgists, Vancouver BC, Canada.





# **Laser sensors enable robotic sorting for tool alloys recycling**

Cord Fricke-Begemann<sup>1\*</sup>, Frederik Schreckenber<sup>1</sup>, Martin Geisler<sup>2</sup>,  
Michaela Lindemann<sup>2</sup>

<sup>1</sup>Fraunhofer institute for laser technology ILT, Aachen, Germany

<sup>2</sup>Cronimet Ferrole<sup>g</sup>. GmbH, Karlsruhe, Germany

\* Corresponding Author: Cord Fricke-Begemann, Fraunhofer ILT, Steinbachstr. 15, 52074 Aachen, E-mail: cord.fricke-begemann@ilt.fraunhofer.de

---

Keywords: alloys, scrap, laser, LIBS, robots, material identification

## **Abstract**

Due to the high variability of alloys in industrial use, it is desirable to sort input material automatically into a high number of target fractions for an economic industrial sorting application. Instantaneous multi-element measurements by laser-induced breakdown spectroscopy (LIBS) are used for classification of individual scrap pieces. Since a high number of different alloys can be classified by LIBS, the best use of this technology is obtained in combination with a sorting approach, which is capable of discharging individual pieces into a large number of fractions in a single pass. For the treatment of input material distributed on a belt conveyor, the concept of combined 3D laser imaging and scanning LIBS is extended to include now also image-based robotic picking and sorting of the scrap pieces.

## **1 Introduction**

An increasingly broad range of metals is used industrially on a large scale, and the supply of numerous raw materials is critical for European industry (EC, 2020). The recovery of raw materials from scrap metal plays an important role in the supply, and the re-melting of used alloys directly in the target composition generates the highest value and the highest impact for a sustainable economy. There is a need for industrial equipment, which is able to generate a variety of well-defined alloy fractions out of an input stream of mixed materials.

## **2 Approach**

In many established sorting applications, the incoming material stream is separated into one or two value fractions and a residual fraction. If the residual fraction is not classified as waste, then it is sorted again in subsequent processes or run through the same machine again with another parameterisation. However, when a larger number of output fractions is desired, it has clear economic advantages to sort the material directly into all fractions in a single process step.

A large number of chemical elements is used in the metals industry to produce an even larger number of different alloys for specific applications. The value of metal scrap is determined by both the value of the individual chemical constituents contained and the precision to which its composition is determined and can be used to provide the composition required for recycling.

A system has been developed to demonstrate in an industrial environment the interlinked metal identification by laser-induced breakdown spectroscopy (LIBS) and robotic sorting of the classified pieces of tool steel and carbide metal. LIBS measurements are carried out remotely over a scanner-guided beam path based on a patented approach. The targeted measurement spots are calculated beforehand on the basis of 3D images, taking into account the often highly structured surface geometry. Since tool steel parts for recycling are often covered by hardening surface coatings, such as TiC and TaC, their local removal prior to material analysis is inevitable for correct identification. Here, it is realised by a single laser in tailored operation mode. A classification algorithm has been worked out which evaluates multiple chemical elements simultaneously to identify individual scrap pieces correctly within a hierarchy of material classes and subclasses. The geometry information is also evaluated to determine handling positions for gripping the

individual pieces and allowing a robotic transfer into the alloy fraction defined by the end-users selection.

## **2.1 3D laser imaging**

Scrap pieces are fed into the sorting machine onto a belt conveyor. A combination of vibration feeders is used for singularisation of the scrap pieces. Careful parameterisation allows to obtain for different types of mixed scrap a high loading of the belt with still sufficient separation of individual pieces. After the pieces have come to rest relative to the moving belt, they are first imaged by a colour camera and a laser line section system. The projected laser line enables to determine the height of the surface in each position. From the 3D contour, not only the position of each piece on the belt is determined. The geometry is also used to calculate automatically the surface locations, which are best suited for the following LIBS measurements. The selection of flat surface regions, for example, can increase the quality of the chemical classification. Furthermore, the geometrical structure contains also the required information for picking the pieces by the robot for sorting.

## **2.2 LIBS classification**

LIBS is a method for fast and remote multi-element analysis of materials of any constitution. A pulsed laser beam is focussed onto the surface of each piece and ablates a small amount of material. The laser further excites this material until it emits an element specific radiation, which is detected by a spectrometer and evaluated to determine the chemical composition of the material.

In our configuration, fast adjustable scanning mirrors guide the laser beam to the position of the piece to be classified and the location selected on its surface for analysis while it is moving on the belt conveyor. The laser beam is steered in three dimensions what allows to reach pieces at any position on the belt, to measure subsequently at several selected spots on one piece, and to measure two or more pieces lying beneath each other and passing the detector at the same time. Thereby, a continuous use of the laser operation without temporal gaps is achieved, which allows an economic use of the LIBS sensor with high throughput.

Figure 1 exemplifies the scanning LIBS processes. While the measuring object (MO) moves on the belt, a series of individual measurements is carried out at

times  $t_1$  to  $t_4$ . At pre-defined positions the laser induces the material ablation and excitation of the plasma (LP), which is visible in white on the photography and spectroscopically analysed in the system. For the subsequent measurement, another position is selected which is independent of the previous measurement position (MP). For composed objects it is important to acquire chemical information from each part, e.g., in the case of a drill bit from the shaft and the cutting part, as depicted in Fig. 1. Since the beam steering is executed in parallel and perpendicular to the direction of the belt movement, the measurement positions can be reached independently of the position and orientation of the object on the belt.

Beyond laboratory use, LIBS sensors have been introduced in the past years into several industrial applications (Noll et al., 2014). For metal recycling, we have previously demonstrated the separation of two classes of aluminium scrap (Aydin et al., 2006) and realised the first classification of a range of different aluminium wrought alloys in an automated sorting machine (Werheit et al., 2011). Furthermore, it has been demonstrated that LIBS can be successfully applied to improve material recovery in e-waste recycling (Noll et al., 2021).

For the classification of tool steel, a high-resolution spectrometer is applied and up to 14 chemical elements are detected and evaluated in a multivariate calculation. For example, the cobalt content plays a major role in valuation of scrap and appears in a broad range of concentrations. It is therefore not only classified into a high and a low Co fraction, but into several degrees of different Co concentration. By measuring scrap pieces at several spots, it is also possible to identify and sort pieces that are composed of different alloys. This is often the case for drill bits or milling cutters.

As in many scrap sorting applications, dirt or oxidation layers usually cover the surface of the pieces. In addition, tool parts are partly protected by hardening coating, for example TiC and TaC. Direct LIBS measurements of such surface contaminations would result in a misclassification since the bulk material is of interest. Therefore, at each measurement location, the surface is first locally cleaned by a part of the laser light, which is specifically formed to provide efficient ablation of the contamination, before it is analysed by the second part of the laser pulse train applied to the same spot.

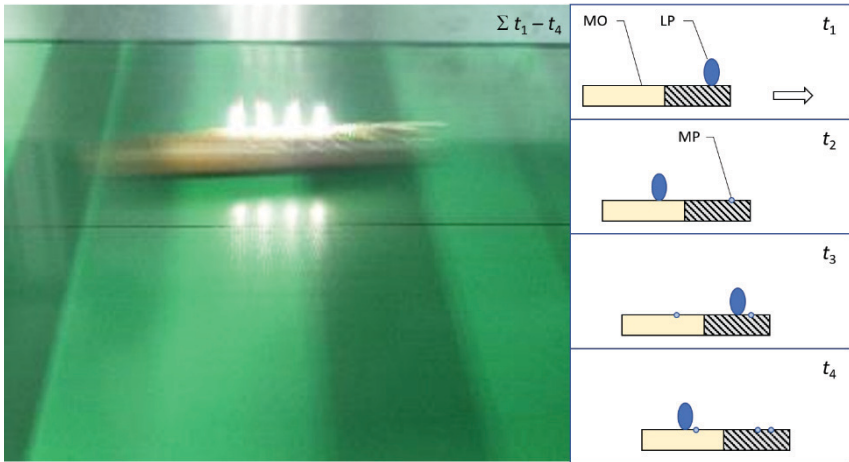


Fig. 1: A series of LIBS measurements on a drill bit moving on a belt conveyor from left to right; left: long-exposure photography; right: schematic of the scanning LIBS measurement process, MO – measuring object, LP – laser-induced plasma, MP – measurement position, see text for further explanation [property: Fraunhofer ILT]

### 2.3 Robotic sorting

Downstream of the LIBS sensor, the scrap pieces are sorted individually. An ABB “FlexPicker” is employed here, which is used in several automated production and packaging lines. For each piece, the handling procedure is determined from the images. When using a finger type gripper, as shown in Fig. 2, the most suitable positions at two opposite sides of a piece are calculated using a pre-trained algorithm. For reliable picking, it is necessary to achieve a tight contact, as well as to balance the mass of the piece. With this type of gripper, structures in any orientation as small as 2 mm are taken from the moving belt. Alternatively, other gripper types can be used, for example a suction gripper for flat pieces.

Once the robot has picked a scrap piece, it is free to transport it to any location next to the belt conveyor. In our configuration, six slots are located on both sides of the belt, in which the pieces are dropped according to the classification calculated from the LIBS measurement. With a single “FlexPicker”, up to sixty pieces per minute are sorted into any of these fractions. Throughput can be increased by employing additional robotic stations down the belt.

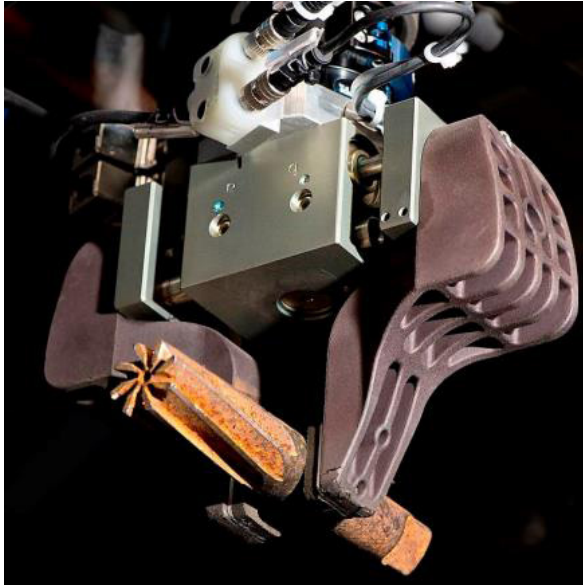


Fig. 2: A drill bit is picked by a robot gripper [property: Cronimet Ferroleg.]

### 3 Conclusion

A system was developed and implemented, which is to our knowledge the first realisation of a LIBS sensor with robotic sorting for metal recycling. The system is installed in an industrial scrap sorting plant. Sorting trials have demonstrated the ability of the system to classify and separate tool steels of various grades into a high number of sorting fractions. For example, high speed steel is sorted into fractions with different levels of cobalt as alloying element and at the same time other alloying elements are also regarded. The multi-element classification by LIBS is obtained in spite of surface contaminations encountered on the scrap pieces by using an integrated optical surface cleaning process. Optical acquisition of location and geometrical structure of each scrap piece is proven to provide a common basis for both multi-fraction classification and sorting in fully automated operation.

The sorting system is in preparation for the routine operation in a recycling plant of CRONIMET Ferroleg. GmbH in variable applications, in which up to 6 simultaneous

sorting fractions are defined by assignment of 20 sensor-identified alloys for extraction.

The work presented was supported by funding from the German ministry of education and research (BMBF).

## **References**

- EC (2020): COMMUNICATION FROM THE COMMISSION TO THE EUROPEAN PARLIAMENT, THE COUNCIL, THE EUROPEAN ECONOMIC AND SOCIAL COMMITTEE AND THE COMMITTEE OF THE REGIONS Critical Raw Materials Resilience: Charting a Path towards greater Security and Sustainability; COM/2020/474 final; <https://eur-lex.europa.eu/>
- Noll, R., Fricke-Begemann, C., Brunk, M., Connemann, S., Meinhardt, C., Scharun, M., Sturm, V., Makowe J., Gehlen, C. (2014). Laser-induced breakdown spectroscopy expands into industrial applications. *Spectrochimica Acta Part B: Atomic Spectroscopy*, 93, 41-51.
- Aydin, Ü., Noll, R., Makowe, J. (2006). Automatic sorting of aluminium alloys by fast LIBS identification. In *Proceedings of the 7 Intl. Workshop in Progress in Analytical Chemistry in the Steel and Metal Industries*, 2006.
- Werheit, P., Fricke-Begemann, C., Gesing, M., Noll, R. (2011). Fast single piece identification with a 3D scanning LIBS for aluminium cast and wrought alloys recycling. *Journal of Analytical Atomic Spectrometry*, 26(11), 2166-2174.
- Noll, R., C. Fricke-Begemann, F. Schreckenberger (2021). Laser-induced breakdown spectroscopy as enabling key methodology for inverse production of end-of-life electronics. *Spectrochimica Acta Part B: Atomic Spectroscopy*, 181, 106213.





# Importance of Sensor Based Sorting to Sound Metals Recycling

Shuji Owada<sup>1\*</sup>

<sup>1</sup>Waseda University, Resources and Environmental Engineering, Tokyo, Japan

\* Corresponding Author: address, E-mail: owadas@waseda.jp

---

Keywords: Sensor Based Sorting, Metal, Recycling, XRT, XRF, LIBS

## Abstract

Sensor based sorting (SBS) is one of the powerful unit operations to achieve highly efficient separation for example to realize mutual separation of metal alloys which was impossible with conventional sorting technologies. Our laboratory has intensively investigated novel metal recycling processes using the SBS for the last ten years, such as removal of stainless steels from shredder magnetic products, mutual separation of aluminium alloys and iron alloys, by using existing and newly developed visible light, X-ray transmission (XRT), X-ray fluorescence (XRF), and laser induced breakdown spectroscopy (LIBS) sorters. This paper introduces the outline of the above results and proposes a next generation metal recycling process by combining high performance comminution (liberation) technology and the above SBS technologies.

We are investigating the application of the LIBS sorter to the mutual separation of iron alloys, and here introduces one of the results, in which we removed stainless steel from carbon steel by detecting LIBS Cr/Fe peak ratio and realized complete removal of Cr bearing stainless steels.

We developed, in 2012, a novel process to separate high purity (over 99 wt%) 6063 aluminium alloy from the other aluminium alloys by applying XRT and XRF sorters, and we improved, in 2015, this kind of sorting by applying newly developed LIBS sorter, to achieve mutual separation of most of the aluminium alloys, involving

1000 to 7000 series and casting alloys, with the efficiency of approx. 100 %. The high purity aluminium alloys obtained by this process are currently used as interior materials for “Shinkansen” trains.

Finally, we would like to propose a super energy saving metal recycling process by combining the above “intelligent comminution (liberation)” and “intelligent sorting (SBS)”.

## **1 Introduction**

Sensor based sorting is usually assumed to be one of the most innovative sorting technologies in this 40 years in sorting engineering because of their high sensing accuracy, possibility of various sensing systems combination and applicability to recent digital transformation systems. Our laboratory has developed and applied various sorting processes to achieve horizontal recycling systems which could not be realized by conventional sorting technologies.

This paper introduces such results involving (i) Removal of stainless steels from magnetic products in shredder plant, (ii) Mutual separation of aluminium alloys by combining X-ray transmission (XRT) and X-ray fluorescence (XRF) sortings, (iii) Mutual separation of aluminium alloys by laser induced breakdown spectroscopy (LIBS) sorting.

We would like to create, near in the future, super energy saving recycling processes by developing novel sorters and applying various kinds of sorting systems and hereby propose one of the future metal recycling processes as an example.

## **2 Removal of Stainless Steels from Magnetic Products in Shredder Plant**

In most of the shredder plants, various kinds of scraps, involving automobiles, home appliances, etc., are finely shredded and iron components are recovered in the first step by magnetic separation. But the magnetic product usually involves not only carbon steel but also Cr bearing magnetic stainless (ferrite and martensite) steels, and their removal should be important to reutilize the magnetic products for raw materials of iron and steel making. Since LIBS could detect the Cr components sharply, we detected optimum conditions for the removal by using the LIBS sorter

which was originally developed in 2015 by our laboratory in corporation with the German company, Secopta, Japanese AIST, National Institute of Advanced Industrial Science and Technology, and several Japanese companies.

First of all, we determined the optimum Cr and Fe peaks for the LIBS sorting, as “Cr II 286.573 nm” and “Fe I 366.974 nm”, considering their strength, linearity of the calibration curve, effect of self-absorption, etc.

Figure 1 shows the LIBS detection results for the real scrap materials and also standard samples. The linearity between Cr contents and peak intensities for the stainless steel particles is not so high, and the separation efficiency (SE) of stainless steel from carbon steel, as a function of threshold Cr peak intensity, was not so high (see Figure 2). On the other hand, as showing in Figure 3, the linearity between Cr/Fe contents ratio and Cr/Fe peak intensities ratio quite high, almost the same as that for standard samples, and the SE of stainless steel from carbon steel could be kept high values in wide range of threshold Cr/Fe ratio. We could conclude that magnetic stainless steels could be removed from shredder magnetic products completely with a SE of 100 %.

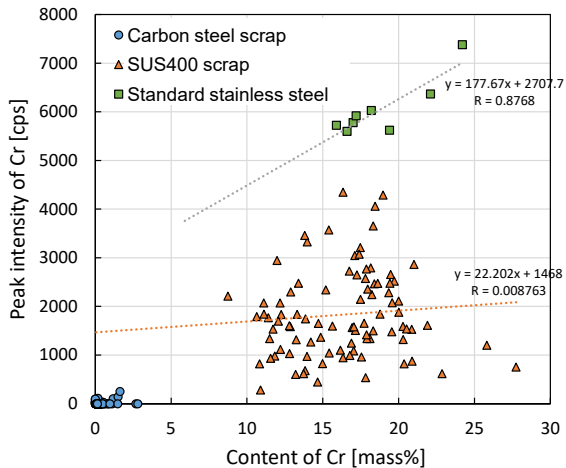


Fig. 1: Relation between content and LIBS peak intensity of chromium in the shredder magnetic product

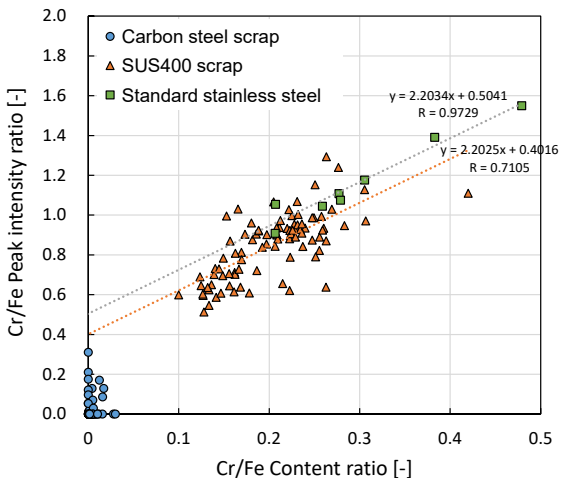


Fig. 2: Relation between content ratio and LIBS peak intensity ratio of chromium/iron in the shredder magnetic product

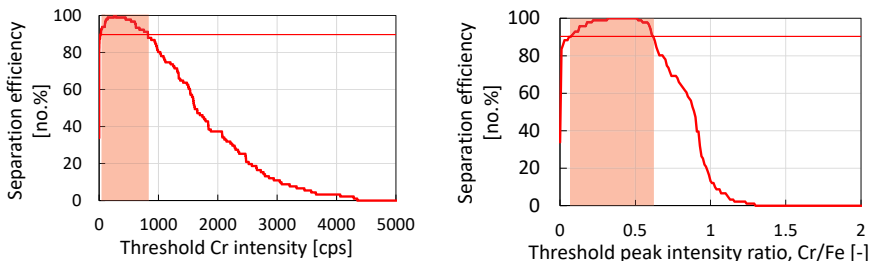


Fig. 3: Separation efficiency of Stainless steels from carbon steels by LIBS sorting

### 3 Mutual Separation of Aluminium Alloys

#### 3.1 Combination of XRT and XRF sorting

Most of the scrap aluminum alloys are usually mixed at wholesalers and the mixed alloys are used as raw material of automobile gasoline engine. This process is just a cascade recycling and the mixed alloys should be separated from each other and utilize them as each wrought materials to establish a horizontal recycling (see Figure 4).

We applied two kinds of sensing technologies, XRT and XRF, to achieve mutual separation of such aluminium alloys (Owada, 2014), which could not be done with any conventional physical separation technologies. In the NEDO project (2010-2012), our target to be recovered was 6063 alloys, which was the raw material of window sash, from scrap aluminums. We have finally made a novel recycling flow as shown in Figure 5 and constructed a pilot plant (Figure 6) in which over 99 mass% of 6063 aluminium alloys could be produced from the mixed scrap aluminium alloys with the recovery of approx. 95 %, and was now operating as a commercial scale.

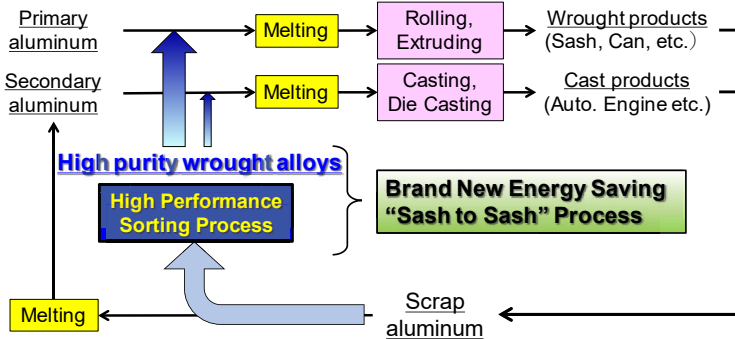


Fig. 4: Typical aluminium circulation flow

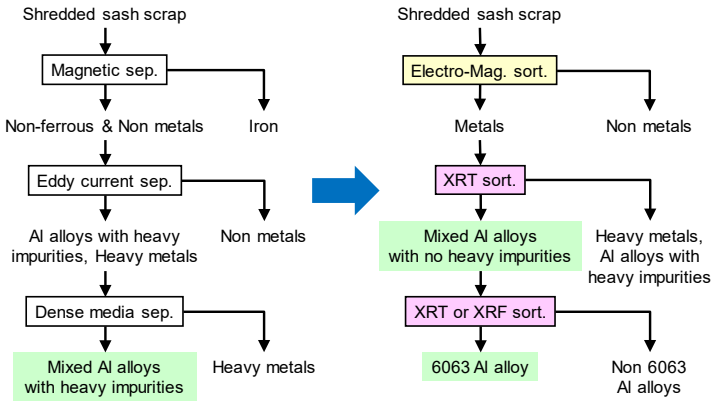


Fig. 5: Novel and conventional aluminium recycling flow



Fig. 6: Pilot plant to realize horizontal recycling for aluminium in the NEDO project (2010-2012)

### 3.2 Application of LIBS Sorter

We recognized in the above project that the XRT and XRF sorters have had quite a good performance, but XRF sorter could not detect light elements, such as Si, Mg, etc., then, we adopted the LIBS sensor and assembled as a LIBS sorter to identify them. Conceptual diagram of the LIBS sorter and the appearance are shown in Figures 7 and 8, respectively. Typical separation result for various kinds of aluminium alloys are shown in Table 1 (Togawa, et.al., 2016), in which we understood that high purity aluminium alloys could be recovered from each other with relatively high recoveries. If we apply this process to 70 % of all the aluminium scraps generated in Japan, we could save 1.63 billion L in oil base energy per year. Now several projects are running by using the LIBS sorters in order to realize the horizontal aluminium alloy recycling.

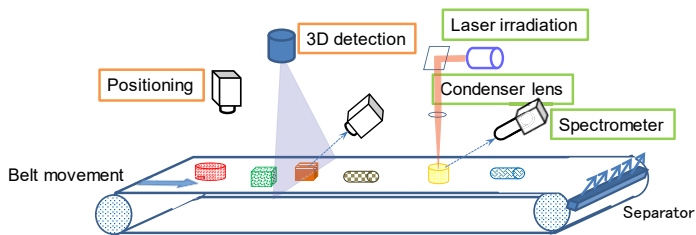


Fig. 7: Conceptual diagram of LIBS sorting

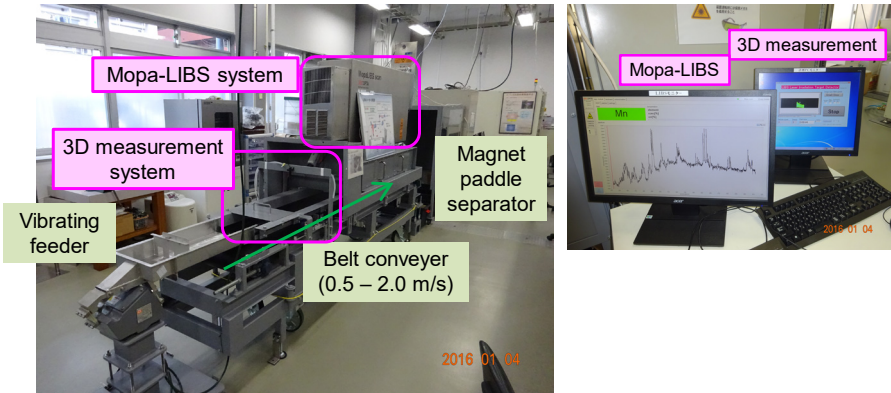


Fig. 8: LIBS sorter developed by our laboratory in the project of “High Efficiency Rare Elements Extraction Technology Area, Tohoku Univ.”

Tab. 1: Typical separation result in case of mutual separation of various aluminium alloys

	2000 series	3000 series	4000 series	5000 series	6000 series	7000 series	Casting alloys
Grade (wt%)	100	100	100	100	100	100	100
Recovery (%)	99.9	99.2	100	100	100	99.5	100

## 4 Conclusion -Proposal of Next Generation Metal Recycling Process

We have many kinds of sensors which could be applied to sorting technology and we will be able to establish a super energy saving and more economically feasible metal recycling process by utilizing these technologies near in the future. For example, if we develop novel copper recycling process as shown in Figure 9, huge amount of energy could be saved compared with the conventional process as shown in Figure 10 and 11, because physical, in other words solid base, separation requires much less energy and cost compared with pyro- and hydro-metallurgical, liquid base, processes.

But one other key technology must be the liberation. Conventionally, comminution technologies were developed to reduce particle size, but important in recycling



engineering is not the reduction but liberation of compositional elements in the scraps. If we can realize the liberation in coarse size ranges, such as over 10 mm, we can apply the high performance sensor based sorting technologies. Figure 12 shows the comminution technologies, “Intelligent Comminution”, expected to be developed and sensor based sorting, “Intelligent sorting”.

It is possible that these “intelligent comminution/sorting” technologies could contribute much to improve recycling process from the viewpoint of energy saving and economic feasibility, and thus, could establish a sound material cycle society.

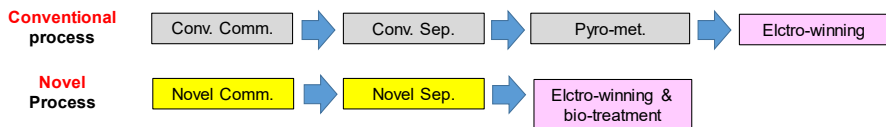


Fig. 9: Conventional and novel metal recycling processes

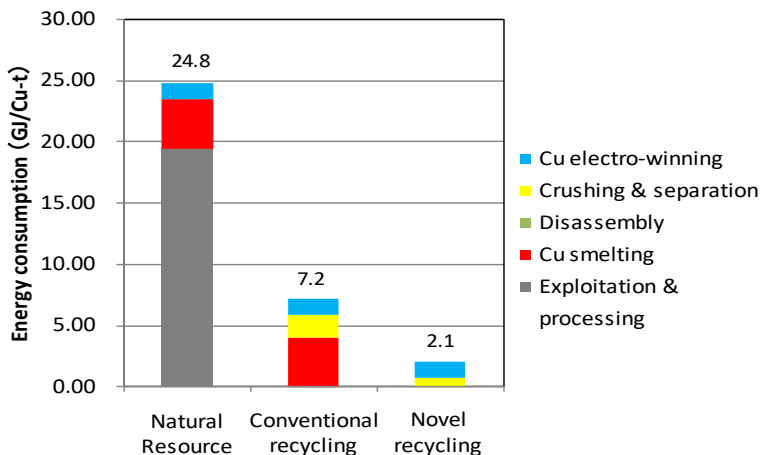


Fig. 10: Results of the LCA compared several scenarios of Cu manufacturing processes

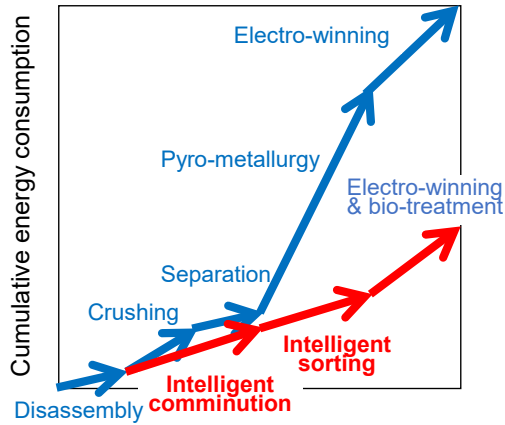


Fig. 11: Image of energy consumption comparing conventional and novel processes

**Liberation in coarse size range by selective comminution, “Intelligent Comminution”**



- Pre-treatment
  - ✓ Microwave Irradiation
  - ✓ Heating-Quenching
- AG / SAG
- Electrical Disintegration
- Underwater Explosion
- Surface Grinding

**High-performance SBS combination, “Intelligent Sorting”**

- Size, Shape, Color, Roughness, Hardness, Electro-mag., Luster, Wave Absorption, Density, XRT, XRF, LIBS,,,,,

Fig. 12: “Intelligent Comminution” and “Intelligent Sorting” expected to be developed

## **References**

- Owada,S.: SBS Technology for Creating Environment Friendly Process of Various Metals Recycling --Advances and problems to be solved--, Sensor Based Sorting, Aachen, (2014), 11-2.
- Togawa,R, Sato,K, Owada,S, and Nakamura,T: Fundamental Study on sintered Ta recovery from PCBs and Al alloys mutual separation by LIBS sorting, Spring meeting, MMIJ, (2016), 1-6.

# Sorting of post-consumer aluminium scrap using Laser-Induced Breakdown Spectroscopy (LIBS) and machine learning

Simon Van den Eynde<sup>1\*</sup>, Dillam Jossue Diaz-Romero<sup>1,2</sup>, Bart Engelen<sup>1,3</sup>, Alexander Eckert<sup>4</sup>, Luc Waignein<sup>5</sup>, Jörn Vandewalle<sup>5</sup>, Isiah Zaplana<sup>1</sup>, Jef Peeters<sup>1</sup>

<sup>1</sup>Department of Mechanical Engineering – KU Leuven, Celestijnenlaan 300A, Box 2422, 3001, Leuven, Belgium

<sup>2</sup>PSI-EAVISE – KU Leuven, Jan Pieter De Nayerlaan 5, 2860, Sint-Katelijne-Waver, Belgium

<sup>3</sup>Technology Campus Diepenbeek – KU Leuven, Agoralaan Gebouw B, 3590, Diepenbeek, Belgium

<sup>4</sup>Redwave – Wolfgang Binder Str. 4, 8200, Eggersdorf bei Graz, Austria

<sup>5</sup>Galoo – Wervikstraat 320, 8930, Menen - België

\* Corresponding Author: Celestijnenlaan 300A, Box 2422, 3001, Leuven, Belgium, [simon.vandeneynde@kuleuven.be](mailto:simon.vandeneynde@kuleuven.be)

---

Keywords: Aluminium, Post-consumer scrap, Sorting, Laser-Induced Breakdown Spectroscopy, Classification

## Abstract

To prevent the emergence of a scrap surplus, it is essential to implement alloy based sorting of post-consumer aluminium scrap on an industrial scale. This can be achieved by integrating Laser-Induced Breakdown Spectroscopy (LIBS) in sorting systems. The presented research evaluates the performance of machine learning methods that classify post-consumer aluminium scrap samples based on the spectral data collected by a LIBS system. The classification performance is assessed with X-Ray Fluorescence (XRF) reference measurements on 834 aluminium scrap pieces, demonstrating that an accuracy of up to 60.76%, a precision of 60.8%, a recall of 60.7%, and an f1 score of 57.9% can be achieved. Furthermore, composition measurements indicate that the desired concentration thresholds for alloying elements can be met by implementing the developed methods.

# **1 Introduction**

Sorting post-consumer aluminium scrap into different qualities is of commercial interest for recycling companies, as aluminium with lower concentrations of alloying elements can today be sold at a higher price due to its broader applicability compared to mixed aluminium scrap. In addition, it is of strategic importance to prevent the emergence of an aluminium scrap surplus, which is expected to occur in the coming decade (Van den Eynde et al., 2021). Therefore, this research investigates the opportunities of LIBS based aluminium sorting for a large Belgian recycling facility.

## **2 Materials and Methods**

### **2.1 Selection of sorting targets**

The output fraction of the aluminium recycling facility in this case study is a mix of shredded post-consumer aluminium scrap containing wrought and cast alloys from electric and electronic equipment, automotive and construction waste. The selection of the sorting targets of the LIBS sorting step in this case study is based on discussions with the involved recycling company. The first of the three target fractions is the “Premium” class. The purpose of separating a Premium fraction from the rest of the scrap is to sell it at a significantly higher price than that of the current output fraction, either to refiners for diluting low purity scrap for the production of cast alloys or to remelters for the production of secondary wrought alloys. This class has strict limits to the concentrations of the most common alloying elements. The most severe concentration thresholds are for copper (0.04 wt%), zinc (0.05 wt%) and manganese (0.06 wt%). The second class is called “Desox”. It stands for “deoxidation aluminium” which, according to the EAA definition, is aluminium consisting of alloys with a high concentration of metallic aluminium (usually exceeding 95%) used to remove free oxygen from liquid steel (European Aluminium Association, 2016). This class has specific thresholds on the concentrations of alloying elements as well, but they are less severe than those for the Premium class. The last target fraction is the “Secondary” class. This fraction is meant to be sold to refiners at a similar price as the current output fraction for the production of cast alloys.

## 2.2 Sampling and measuring procedure

A representative sample of the existing output fraction, consisting of 834 pieces weighing 39.28 kg in total, has been collected by adopting a systematic sub-sampling procedure. Subsequently, each metal piece in the acquired material library has been labelled with a unique number. A small part of each piece's surface has been cleaned, after which the composition of each piece is measured with an Olympus Vanta handheld XRF device on the cleaned surface. Based on the results of the XRF analysis, every piece in the dataset is assigned to one of the target classes. The Premium, Desox, and Secondary classes constitute 28.3%, 28.8%, and 42.9% of the mass of the total sample, respectively. Next, the LIBS experiment is conducted. The gated LIBS system has a pulse energy of 80 mJ and a frequency of 10 Hz. The Echelle type spectrometer has a spectral range of 180 - 800 nm. The exposure time is 85  $\mu$ s. Ten LIBS measurements are conducted for each piece in the dataset on the uncleaned part of the surface.

## 2.3 Classification method

Various classification algorithms, such as Random Forest (RF) (Zhan et al., 2019), Support Vector Machine (SVM) (Dai et al., 2021) and Logistic Regression (LR) (Menking-Hoggatt et al., 2019), have been investigated in recent research. These three methods are implemented in this research with 217 custom designed features. The performance of these methods is expressed with four metrics: accuracy, weighted average precision, weighted average recall, and weighted average f1 score. 80% of the samples are used to train the classifiers, while 20% is used as a test set to evaluate the performance. As an additional way to evaluate the classification performance, the composition of the sorting outputs is calculated considering the mass and composition of all sorted test set samples.

## 3 Results

In terms of accuracy, the SVM classifier (60.76%) slightly outperforms the RF (59.49%) and LR (55.10%) classifiers. The other metrics are close to the accuracy score and indicate the same ranking between the classifiers, as shown in Table 1.

Tab. 1: Performance metrics classifier algorithms

<b>Classifier</b>	<b>Metric</b>	<b>Score</b>
Logistic Regression	Accuracy	55.10%
	Precision	0.560
	Recall	0.551
	f1 score	0.525
Support Vector Machine	Accuracy	<b>60.76%</b>
	Precision	<b>0.608</b>
	Recall	<b>0.607</b>
	f1 score	<b>0.579</b>
Random Forest	Accuracy	59.49%
	Precision	0.583
	Recall	0.595
	f1 score	0.585

Table 2 shows the composition of the sorted output fractions when the test set samples are classified with the SVM method. This composition is calculated based on the XRF composition measurements and the mass of the test set samples. The concentration limits are met for all elements in the Desox and Secondary class. In the Premium class, only the concentrations of copper and manganese slightly exceed the specified thresholds (0.04 and 0.06 wt% respectively).

Tab. 2: Composition of the output fractions when classified with SVM (concentrations in wt%)

Element	Premium	Desox	Secondary
Al	97.975	98.400	94.054
Cu	<b>0.079</b>	0.125	0.860
Zn	0.023	0.054	0.564
Fe	0.358	0.299	0.521
Mn	<b>0.134</b>	0.075	0.293
Mg	0.957	0.271	0.308
Si	0.281	0.740	3.228

## 4 Conclusion

A novel method is presented to evaluate spectroscopic sorting systems for metal recycling and shows that the use of classification algorithms on LIBS spectra is highly promising for sorting post-consumer scrap. The SVM classifier shows the best results. While the accuracy of the classifiers is rather limited, the presented results demonstrate that the thresholds on the desired output fractions are almost reached. Therefore, ongoing research investigates opportunities to further tune and improve the classification and to adopt data fusion techniques to enhance the performances while increasing the throughput. In addition, melting experiments are ongoing to validate the sorting performance.



## References

- Dai, Y., Zhao, S., Song, C., & Gao, X. (2021). Identification of aluminum alloy by laser-induced breakdown spectroscopy combined with machine algorithm. *Microwave and Optical Technology Letters*, 63(6), 1629-1634. <https://doi.org/10.1002/mop.32810>
- European Aluminium Association. 2016. *Ea Recycling Brochure 2016*. [https://european-aluminium.eu/media/1712/ea\\_recycling-brochure-2016.pdf](https://european-aluminium.eu/media/1712/ea_recycling-brochure-2016.pdf)
- Menking-Hoggatt, K., Arroyo, L., Curran, J., & Trejos, T. Novel LIBS method for micro-spatial chemical analysis of inorganic gunshot residues. *Journal of Chemometrics*, 35(1), 1-13. <https://doi.org/10.1002/cem.3208>
- Van den Eynde, S., Bracquen e, E., Diaz-Romero, D., Zaplana, I., Engelen, B., R. Dufflou, J., & R. Peeters, J. (2022). Forecasting global aluminium flows to demonstrate the need for improved sorting and recycling methods. *Waste Management*, 137, 231-240. <https://doi.org/10.1016/j.wasman.2021.11.019>
- Zhan, L., Ma, X., Fang, W., Wang, R., Liu, Z., Song, Y., & Zhao, H. (2019). A rapid classification method of aluminum alloy based on laser-induced breakdown spectroscopy and random forest algorithm. *Plasma Science and Technology*, 21(3), 1-7. <http://dx.doi.org/10.1088/2058-6272/aaf7bf>

We would like to thank the following sponsors for their support:



MAGNETIC + SENSOR **SORTING SOLUTIONS**

